

**A PERSPECTIVE ON THE STATUS OF COAL RESEARCH  
FROM SHIPMENTS OF SAMPLES**

Karl S. Vorres\*, Carl W. Kruse\*\*, Koen A. Nater\*\*\*,  
David C. Glick\*\*\*\* and Alan Davis\*\*\*\*

\* CHM/211, Argonne National Laboratory, Argonne, IL 60439

\*\* Illinois State Geological Survey, 615 E. Peabody Dr., Champaign, IL 61820

\*\*\* deGrote Vos, Zeeweg 37, 1753 BB St. Martenzee, Netherlands

\*\*\*\* Coal and Organic Petrology Laboratories, 105 Academic Projects Bldg., Pennsylvania State University, University Park, PA 16802

**INTRODUCTION**

Research on all aspects of coal research, at least for more small scale work, involves the use of samples at the beginning of experimental work. Most research workers for smaller scale work do not collect their own coal samples, but rather order them from a group of sample suppliers. The number of suppliers meeting the major needs in the US, as well as for the world, is not very large. An examination of the shipments of samples from each of these suppliers will give an interesting insight into the general trends in volume of work in the field.

The suppliers involved in this study include the Argonne Premium Coal Sample Program, the Illinois Basin Coal Sample Program, the SBN and the several groups of samples from the Pennsylvania State University Coal Sample Bank. Each of these supplies a different number of samples in varying quantities. The quantities and variety of samples is important to the individual worker in selecting a supplier. The type of work to be done frequently affects the quantities and choice of sample, which in turn affects the choice of supplier. Some suppliers tend to ship samples to smaller scale users who tend to do more fundamental work, while other suppliers tend to ship to larger scale users who tend to do both fundamental and the beginnings of applied work. The number of samples shipped from each supplier over a period of years would indicate something of the relative amounts of work done over that period. This paper provides some insight into this measure of work. Individually the trends would speak only for the experience of one sample supplier. If all suppliers have similar experience, then sample shipments may be a useful measure of coal research in the areas that they serve.

The Argonne Premium Coal Sample Program (APCSP).

This program (1) provides samples of 8 coals from the US in two sample container sizes. Either 5 grams of -100 mesh or 10 grams of -20 mesh are available in individual borosilicate glass ampules. Orders may request as many of the ampules as needed for a research program. There is currently a charge of \$1.60 per gram of sample regardless of the sample amount. This program began in late 1982. Samples are processed in a large nitrogen-filled glove box in one ton lots. The samples have been sent to about 350 users in most of the major nations in which coal research is done. Records are kept of the individual shipments, and have been tabulated in terms of the total shipments of ampules on a monthly basis since shipments began. A plot of the cumulative totals of ampule shipments, and also the numbers of -100 and -20 mesh samples shipped is shown in Figure 1. It can be seen that the number of ampules shipped increases in a generally linear fashion at a rate of about 3000 per year. In mid 1987 a number of samples were shipped and appear to have been used in programs until mid 1988 when a more uniform series of orders began. The slope of the plot is consistent to about mid 1991. The slope then decreases through mid 1992, and may be decreasing again. An examination of the relative numbers indicates a greater interest in the finer -100 mesh and smaller sized samples used for the small scale experiments.

An examination of the most popular samples as shown in Figure 2 indicates that the Illinois #6 (IL) is most requested, indicating an interest in the samples with high sulfur content. The second most requested sample, Wyodak (WY), is reactive, large reserves are available at relatively low cost, and is of interest for syn-

thetic fuel production. The other samples in decreasing order of requests are: Beulah-Zap lignite (ND), Pittsburgh (PITT), Upper Freeport (UF) and Pocahontas #3 (POC). Not shown, and less requested are the Blind Canyon and Lewiston-Stockton.

#### The Illinois Basin Coal Sample Program (IBCSMP)

The goal of this program is to provide reproducible samples of various Illinois Basin coals. The program was initiated in 1983 and currently provides samples of 12 different lots of coal. Most of the lots are mine-washed coals. Samples are available in two sizes, a nominal 1-pound sample (8 mesh by zero particle size) and a nominal 20 pound sample (3/8" by zero) that are 1/256th and 1/16th riffled splits of a barrel of coal, respectively. Samples are provided free of charge to most researchers on request. The ICCI reserves the right to limit the quantities. Distribution of samples from nearly depleted lots is restricted to previous users. Two distinguishing characteristics of the IBCSP are the large sizes of the samples relative to other programs and the focus on Illinois Basin coals.

The time the coal is exposed to air while processing is as short as practical, but the samples (IBC-105 excepted) show minor amounts of sulfatic sulfur and traces of elemental sulfur that are products of air oxidation. Lots are stored under a nitrogen atmosphere to enable users to obtain samples for several years without significant exposure to air.

Analytical historical data and user data are also available. These data include results of semiannual tests of Btu, FSI, forms of sulfur, and chlorine contents, proximate and ultimate analyses and the names, addresses, project titles and research objectives of users of each lot are available. Two hundred investigators made a total of 688 requests and received 2100 samples totaling 25,500 pounds in the ten years of operation through August 1993. Most investigators have requested more than one coal and many have received several shipments. All told, 96 of the investigators were from Illinois, 97 from other states, and 7 from outside the United States; 105 of them were from academic laboratories, 49 from industrial laboratories and 46 from government laboratories. The origins of the 688 requests were: Illinois, 393; other states, 277; outside the United States, 18. The distribution of requests was 327 academic, 250 governmental, and 111 industrial.

The pattern of the distribution for the ten years of operation shows the activity peaked in 1988-90 (Figure 3). Reasons include a peak of activity on laboratory-scale, coal cleaning projects funded by the Illinois Coal Cleaning Institute, Carterville, Illinois. Scale-up of successful projects required quantities larger than those offered by the IBCSP. The program assisted a number of researchers in making arrangements for multi-ton quantities of coal directly from the mines. The pattern of distribution for eight of the 12 lots by year is shown in Figure 4. Not shown are IBC-105, a lot prepared by Argonne National Laboratory from an a block of Illinois #6 coal adjacent to that used in the Premium Coal Sample Program; IBC-107, an  $^{34}\text{S}/^{32}\text{S}$  isotopically characterized Herrin (Illinois #6) recommended for researchers who wish to follow the fate of forms of sulfur in chemical reactions of coal by monitoring the ratio of sulfur isotopes in the products; IBC-108, a state-of-the-art, physically-cleaned, micron-sized blend of Herrin (#6) and Springfield (#5) coal (80% and 20% respectively) that now has a very low pyrite and ash; IBC-111, a Danville (Indiana VII) coal.

An ideal projected ten year life for each lot was not reached with IBC-103, IBC-104 and IBC-106. It was not possible to obtain the desired lot of Illinois No. 5 seam in 1983. The compromise was IBC-103, an 80:20 mixture of Illinois #5 and Illinois #6. Its inventory was purposely drawn down in 1986 by use of IBC-103 for mild gasification tests at the time requests for a typical-sulfur coal were shifted to a single-seam lot, IBC-106. Requests for a coal with forms of sulfur typical of Illinois and Indiana coals (about 50:50 pyritic and organic forms) continued high and it was necessary to plan for IBC-106 replacement before 10 years. That replacement is IBC-112. The projected interest in a run-of-mine coal was also underestimated in 1983. The 1500 pounds of IBC-104 lasted only 7 years.

### The Pennsylvania State University Coal Sample Bank

Since its inception in 1967, 1457 samples have been collected for this sample bank; 1176 remain available for distribution (2). Thirty more samples will be collected over the next four years as part of the DOE (U. S. Department of Energy) Coal Sample Bank, a subset of the larger Penn State Coal Sample Bank. Samples from all coal provinces of the U. S. are available, representing a wide variety of ranks, organic and inorganic compositions, petrographic constituents and behavior in liquefaction, carbonization and combustion processes.

Typically, whole-seam channel samples of 200 to 300 kg are collected from fresh exposures in active mines. Samples are crushed to -6 mm, homogenized, and subsampled. A portion is crushed to -20 mesh and further subdivided. The typical subsample supplied to researchers is 300 g of coal at -20 mesh, available for \$20.00; larger quantities of -6 mm or -25 mm (for older samples) coal are also available. Samples collected since 1989 in the DECS (Department of Energy Coal Sample) series have been packaged under argon in heat-sealed foil/polyethylene multilaminate bags which preserve initial sample properties (3). Earlier samples in the PSOC series were sealed under argon in steel cans. Analyses are performed on each sample and the resulting data comprise the Penn State Coal Data Base. Computer printouts of analytical data are available for every sample.

The most recent program of sample collection and distribution began in 1988. Since then, over 700 requests for samples and/or data printouts (usually for several samples per request) have been received from more than 250 agencies. Universities accounted for 63% of the requests, government agencies 12 %, and industry 25%. Ninety-five percent of the requests were from the U. S.

Figure 5 shows that in 5 1/2 years, 3270 kg of samples were distributed, 510 kg at -20 or -60 mesh in 300 g bags or cans and the remainder in larger quantities at larger particle sizes. Sharp jumps in the cumulative amount distributed represent occasional shipments of entire 100 kg drums of coal; the increase in May, 1992, represents distribution of 4 drums totaling 400 kg.

The trends in amounts of samples distributed over time are similar to those of the Argonne program. The highest rate of distribution occurred in the first year, followed by four years with a somewhat lower rate which nevertheless represents large quantities of coal samples distributed on a consistent basis. Although a further decrease in rate of distribution occurred late in 1992, periodic variations of 6 to 12 months duration make long term predictions from short term trends inadvisable, and very recent data indicate an increase.

The most requested samples have been those of the Pittsburgh seam (DECS-12, PSOC-1451, -1519, -1528, -1529, 1531), the Illinois #6 seam (DECS-2, PSOC-1493), and the Wyodak (Smith-Roland) seam (DECS-8, PSOC-1520). Recently, U. S. Department of Energy research projects investigating the use of dispersed catalysts for liquefaction have been conducted on the Blind Canyon coal (DECS-6, -16, -17, PSOC-1503). This activity has significantly increased the demand for these samples. Figure 6 illustrates the trends in distribution of these samples. These four seams alone account for over 20% of the samples distributed since 1988, although samples of over 300 other seams with a wide variety of properties are available.

### The SBN

The European Center for Coal Specimens, SBN, has collected a large number of coal samples from important mines of the world. These have been prepared in a variety of sizes. A number of these samples have been prepared with special consideration for protection from the atmosphere. A coal catalog is available which indicates source and type of sample as well as analytical information.

It has been observed that the number of requests for general samples from the main collection has been decreasing, but there is a growing interest in production of a certified series of samples dedicated to multi-laboratory research projects as are being sponsored by the European Community's and European Coal and Steel Community's research programs. There is also an interest in samples of coal fly and bottom ashes and of building materials based on secondary resources.

#### CONCLUSIONS

There are both similarities and differences. There are periodic periods of extensive sample orders that tend to alter some long term trends. The APCSP has seen a period of consistent shipments from late 1988 to late 1991. Since that time there has been a decline to a lower but persistent level of shipments. The most popular coals for the APCSP are the Illinois #6 and Wyodak, reflecting concerns about sulfur in coal, and converting coal into synthetic liquids. The small size of these samples may be an indicator of the level of activity in the most fundamental studies.

The pattern of the Penn State Coal Sample Bank total shipments is similar to that for the APCSP. The most popular coal is from the Pittsburgh seam reflecting interests in liquefaction of this Eastern U. S. high volatile A bituminous coal. The Illinois #6 is second most popular, followed by Wyodak and Blind Canyon seams. The intermediate size of the available samples reflects interests in both basic and somewhat larger scale work.

The IBCSP shipped the largest quantities of coal in 1987 and has shipped declining total amounts since then. The number of researchers requesting samples has declined more slowly than the quantities shipped, reflecting smaller quantities per shipment. The emphasis on coal cleaning at the time of maximum quantities reflects a change in type of work away from coal cleaning. The samples are larger than the APCSP and reflect interests in both basic and applied work.

Overall the distribution curves for the samples reflect a number of rather strong and continuing programs in coal research despite recent difficulties in funding. For all of the programs most of the requests come from academic institutions. Clearly much work is done there, primarily with government funding. Industry and government organizations make similar but fewer requests, reflecting the smaller number of organizations involved in this work. Relatively few requests come from overseas, presumably because their sponsors are outside of the U.S. These workers need to use their domestic sample sources, but want to be able to compare with well-known external samples.

In general these data indicate that researchers realize the advantages of acquiring samples from centralized sample banks. These advantages include a lower cost than would be incurred from individual sampling and preparation; availability of analyzed samples; preservation of samples and the possibility of comparing results with others who have worked on the same samples.

#### ACKNOWLEDGMENTS

KSV gratefully acknowledges support from the US Department of Energy, Office of Basic Energy Sciences, Chemical Sciences Division under contract no. W-31-109-ENG-38. DCG and AD acknowledge support from the U. S. Department of Energy, Pittsburgh Energy Technology Center, Liquid Fuels Division. CWK acknowledges that the IBCSP has been sponsored by the Illinois Department of Energy and Natural Resources through its Coal Development Board and Illinois Clean Coal Institute, and by the State of Indiana through the Indiana Energy Development Board (IEB) and the Indiana Geological Survey (IGS).

#### REFERENCES

1. Vorres, K. S.; Energy Fuels 1990 4 420-426
2. Glick, D. C.; Davis, A. Org. Geochem. 1991 17 421-430

Figure 4.

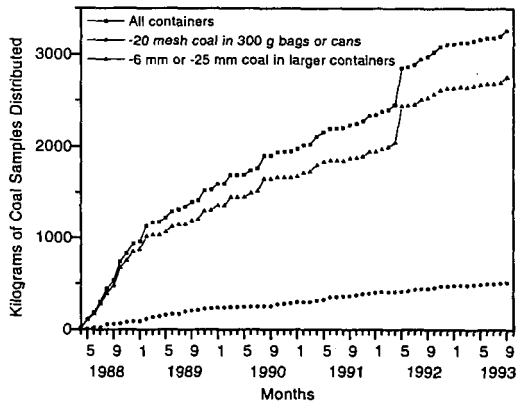
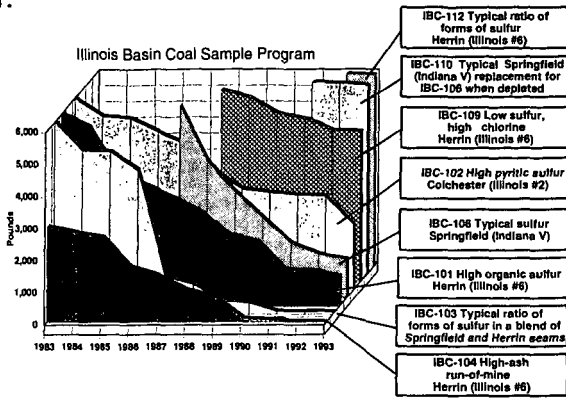


Figure 5. Cumulative weights of samples distributed from the Penn State Coal Sample Bank, -20 mesh (cans and small bags) and -6 mm or -25 mm (buckets, drums and large bags)

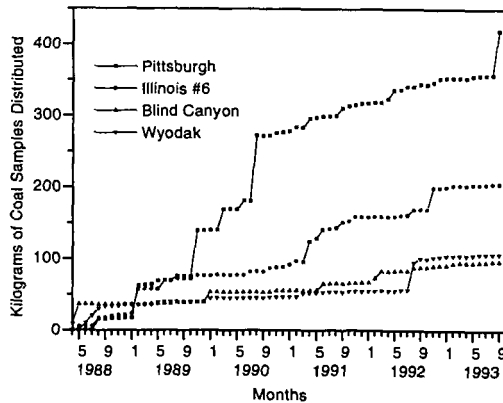
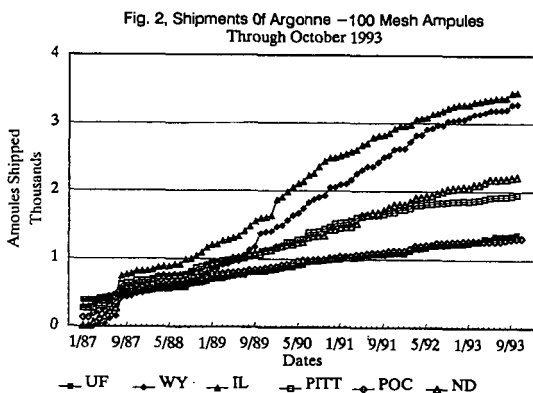
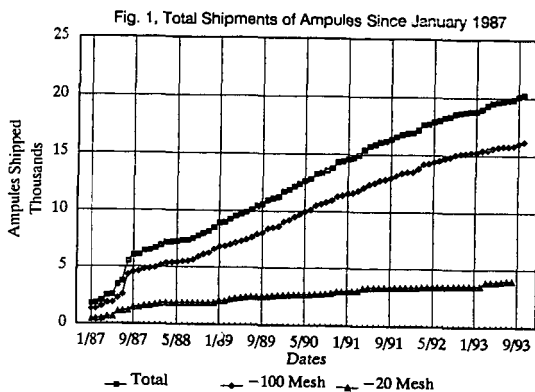


Figure 6. Cumulative weights of most frequently requested samples (Pittsburgh, Illinois #6, Blind Canyon and Wyodak seams) distributed from the Penn State Coal Sample Bank

3. Glick, D. C.; Mitchell, G. D.; Davis, A., Am. Chem. Soc., Fuel Chem. Prepr. 1991 36:3 861-868

4. Harvey, R. D.; Kruse, C. W. 1988. The Illinois Basin Coal Sample Program: Status and Sample Characterization. J. Coal Quality, 7 (4) 109-113. Illinois State Geological Survey Reprint Series 1989-A.



Illinois Basin Coal Sample Program

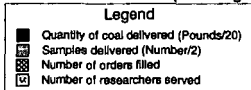
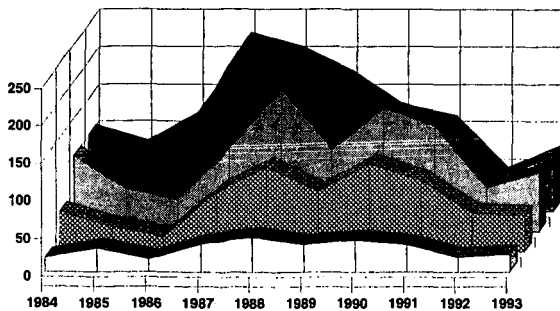


Figure 3.



# COALIFICATION OF LIGNIN TO FORM VITRINITE: A NEW STRUCTURAL TEMPLATE BASED ON AN HELICAL STRUCTURE.

Patrick G. Hatcher<sup>1</sup>

and

Jean-Loup Faulon<sup>2</sup>

<sup>1</sup> Fuel Science Program  
The Pennsylvania State University  
University Park, PA 16802

<sup>2</sup> Fuel Science Department  
Sandia National Laboratories  
Albuquerque, NM 87185

Keywords: vitrinite, coal structure, lignin, molecular modeling

## INTRODUCTION

The structural evolution of vitrinite has been previously studied in our group through detailed characterization of coalified wood which spans the entire coalification range (1-6). The use of coalified logs was demonstrated to be especially useful as it removes the superposed problem of maceral scale heterogeneities from the problem of identifying fundamental transformations which delineate the coal's chemical structural evolution. The net result of these detailed studies using <sup>13</sup>C NMR and pyrolysis/gas chromatography/ mass spectrometric (py/gc/ms) methods is the identification of several key chemical structural transformations which typify the coalification of woody material into high volatile bituminous coal. By comparisons of the chemical compositions of wood at various stages of coalification, one can infer specific reactions responsible for coalification.

Although, the coalification series represents a continuum of parallel and serial processes; several principle stages of coalification are clearly evident. The initial, biochemical, stage of coalification is characterized by a complete loss in hemicellulose, a significant reduction in cellulose, and selective preservation, with minimal alteration, of lignin derived material (2, 7). Early diagenetic changes accompanying the transformation from brown coal into lignite result in a near complete removal of cellulose and some modification of the lignin, a macromolecular material composed of methoxyphenols with a polyhydroxypropanol side-chain as basic building blocks. These modifications are, dominantly, rearrangement of alkyl-aryl ether bond that links the methoxyphenols together to yield methoxyphenols linked by an aryl-alkyl bond between the structural units, as well as some demethylation of methoxy groups yielding catechol-like structures (4). The transformation of coalified wood from lignite through the subbituminous rank range to high volatile C rank bituminous coal is characterized by transformations which result in complete demethylation of methoxyphenols to catechols and a subsequent reduction of the catechol-like structures, presumably through reaction, to form phenol-like structures (6, 8, 9). The focus of this paper is to review our current understanding of the evidence for these aforementioned chemical transformations and to present these reactions within the context of a new three-dimensional helical model that has been developed for lignin (10).

## PEATIFICATION

It was made especially clear from studies of fresh wood and peatified wood (1, 7, 9) that cellulosic components of wood, the ones contributing more than 60% of the structure, essentially are mineralized or degraded and lost within a short span of time geologically. Thus, the cellulosic components do not play a significant role in the structural make-up of coalified wood. The lignin, however, is selectively preserved in a relatively unaltered state during peatification and is the substance which eventually forms the coalified wood's vitrinitic component.

Perhaps the most astounding aspect of this degradative process is the selectivity and structural precision with which it occurs. Essentially all of the major mass component of wood, the cellulose, is lost. One might infer that tremendous physical destruction ensues; however, peatified wood remarkably retains its morphology. This can clearly be seen in SEM photomicrographs of degraded wood in peat (11). Delicate wood structures such as bordered pits and cell wall tracheids appear physically intact even though all the cellulose has been degraded. Apparently, the wood has been degraded by bacteria which use extracellular enzymes to enable destruction of the cellulosic materials. This process apparently does not involve physical maceration.

Framed within the context of the helical model of lignin, the degradation of cellulose affects the three-dimensional extension of the helical chain if one considers the cellulose microfibrils on wood to be hydrogen bonded or even covalently bonded to the cellulose (10, 11). The pitch of the helix under such circumstances can be viewed to at a low angle relative to the axial dimension, depending upon how many hydrogen or covalent bonds are formed with the cellulose. In the middle lamellar region of wood cells, the general depletion of cellulose renders lignin helices with

high angle pitches. In the secondary cell wall, the high amount of cellulose provides many bonding sites, allowing the helix to be extended at a low angle pitch.

The loss of the cellulose backbone allows collapse of the helix to its most condensed configuration. This condensed configuration brings into relatively close proximity some important reaction centers for reactions that have been postulated to occur during coalification (11).

#### COALIFICATION TO BROWN COAL AND LIGNITE

The lignin which survives this initial degradative process relatively unscathed, is eventually altered over the course of geological time as wood in peat is buried in sedimentary systems. We know this from studies of coalified wood in brown coals and lignites (3, 4, 8, 9). By comparing the chemistries of peatified wood, mainly lignin, with brown coal or lignitic woods of the same family (e.g., gymnosperms, angiosperms), we can decipher reactions which might be responsible for observed changes. We certainly can identify the nature of chemical changes which occurred. These are depicted in Figure 1.

Perhaps the most chemically and microbiologically labile bond in lignin is the bond linking the methoxyphenolic aromatic monomers together, the  $\beta$ -O-4 bond. Evidence that this bond is cleaved during coalification was provided by Hatcher (3), from an examination of the NMR spectra of brown coal woods. If we consider that all such bonds in lignin are broken and the fact that approximately 60% of the bonds in lignin are of this type, then we might expect the lignin, or the peatified wood, to be completely macerated because rupture of this bond would release molecular fragments which are likely to be soluble in water. Examination of SEM photomicrographs of brown coal wood in which such bond ruptures have occurred shows that physical disruption of the wood anatomy does not occur to any great extent. Delicate structures such as bordered pits would not physically survive a maceration. Also, the SEM photos do not provide any evidence for dissolution or even partial dissolution of cell walls. This must imply that another reaction maintains the macromolecular integrity of the lignin.

The reaction most likely responsible for maintaining structural integrity must be one which allows connectivity between methoxyphenolic structures in lignin. Thus, we must maintain some bond between the aromatic units. Alkylation following  $\beta$ -O-4 bond rupture is the likely reaction. Botto (12) has shown that such an alkylation is possible when lignin labeled at the  $\beta$  carbon is subjected to artificial coalification in the presence of clays. In essence, the rupture of the  $\beta$ -O-4 bond releases a carbocation, the  $\beta$  carbon on the sidechain, which is a good electrophile and will attack positions on the aromatic ring of adjacent phenolic structures which are susceptible to electrophilic substitution (e.g., the C-5 predominantly). The most likely aromatic ring to be alkylated is the one from which the  $\beta$ -O-4 bond rupture occurred. The rupture of the  $\beta$ -O-4 bond would produce a phenol which would likely activate the C-5 site to alkylation. Evidence that such a reaction occurs in brown coal wood comes from the NMR data which show increased aromatic ring substitution (2, 4). Dipolar dephasing NMR studies indicate that brown coal wood samples have fewer protons per ring than their respective counterparts in peat, indicating that, on the average, one of the ring sites has become covalently bound to an atom other than hydrogen. The NMR data also indicate that the additional substituent atom is not an oxygen but a carbon atom. It is clear that the data all point to the fact that cleavage of the  $\beta$ -O-4 bond during coalification of the lignin in peatified wood leads to an alkylation of an adjacent ring by the resulting carbocation, and this overall process leads to a maintenance of the physical integrity of the wood.

To maintain this integrity observed unambiguously from SEM data it is necessary that the above reaction occur without much structural rearrangement of the lignin. In other words, the reaction must proceed rapidly and must occur at a relatively proximal site to the  $\beta$ -O-4 cleavage. If one considers a lignin model as one which is random in the connectivity between methoxyphenolic units (13, 14), then the likelihood that structural order will be maintained with the above-mentioned transformation is minimal. In a random model, distances between aromatic reaction centers are variable and some significant physical disruptions will ensue if the carbocations formed from  $\beta$ -O-4 bond rupture have to link up with aromatic centers which are more than just local.

The recently proposed ordered model for lignin (10) would overcome this problem. The order is believed to derive from the fact that the methoxyphenolic units linked by the  $\beta$ -O-4 bonds in lignin exist in a helical conformation. With such a configuration, cleavage of this bond releases a carbocation which is in relatively close proximity to the C-5 site on the aromatic ring. The alkylation of this site causes minimum disruption of the helical order as a  $\beta$ -C-5 bond is formed. Thus, we might also expect minimum disruption of the physical integrity of the sample, consistent with what is observed in brown coal wood.

Another important coalification reaction which is observed to occur through the lignite stage of coalification is the cleavage of other aryl-O bonds in lignin. The specific bonds are those of

# DIVISION OF FUEL CHEMISTRY, AMERICAN CHEMICAL SOCIETY

FEDERAL I.D. 52 6054150

Make Check Payable in U. S. Dollars

to: Division of Fuel Chemistry, ACS

MAIL PAYMENT TO:

Professor Gerald P. Huffman

Room 233, Mining & Minerals Resources Bldg.

University of Kentucky

Lexington, KY 40506-0107

For Publication Information and Orders contact:

Professor John C. Crelling

Director of Preprint Subscriptions

ACS Division of Fuel Chemistry

Department of Geology

Southern Illinois University at Carbondale

Carbondale, Illinois 62901-4324

Bill DIVISION OF FUEL CHEMISTRY  
 To: M. D. SCHLESINGER  
 4766 WALLINGFORD STREET  
 PITTSBURGH PA 15213

Ship DIVISION OF FUEL CHEMISTRY  
 To: M. D. SCHLESINGER  
 4766 WALLINGFORD STREET  
 PITTSBURGH PA 15213

Original

BALANCE DUE: 0.00

Date	Invoice
2 Feb 94	94018

PO Number	Terms	Rep	Ship Date	Ship Via	F.O.B.	Project
	NO CHARGE		18 Feb 94	US MAIL		
Quantity	Item Code	Description			Price Each	Amount
1	1-1	VOLUME 39, NUMBER 1			0.00	0.00
1	1-2	VOLUME 39, NUMBER 2			0.00	0.00
NO CHARGE. DIVISION OF FUEL CHEMISTRY, ACS					TOTAL:	0.00

methoxyl groups attached to the aromatic ring. Both NMR and py/gc/ms data show that this is happening (2, 9). The chemical degradative data of Ohta and Venkatesan (8) also show this reaction. All these studies indicate that the loss of methoxyl is through a demethylation process whereby the bond between the methyl carbons and the oxygen attached to the ring is cleaved. The molecular modeling studies show that the helical configuration is not affected by such a reaction (11). The resulting structure of the coal contains a phenol where there once was a methoxyl group, and the structure is now said to have one similar to that of catechols, if one considers that the cleavage of the  $\beta$ -O-4 bond has already occurred.

Additional changes in lignin structure are more subtle, but somewhat evident from NMR data. In lignin and peatified wood, the sidechains are hydroxylated at both the  $\alpha$  and  $\gamma$  sites. Loss of hydroxyl groups from the sidechains is another reaction resulting from coalification of the lignin. NMR resonances attributable to these hydroxyls diminish substantially during coalification through to the rank of subbituminous coal. Simple loss of the sidechain units by a pyrolytic process would explain the loss of these resonances, but this would lead to a significant increase in aromaticity. Because aromaticities of coalified wood samples do not increase over the course of the observed loss of hydroxyls, it is likely that simple reduction of the hydroxyls to alkyl groups is the preferred pathway. This would shift the NMR resonances into the alkyl region of the spectra and preserve carbon aromaticities. Such a reaction would also be consistent with the physical structural data, because reduction of hydroxyls would maintain the presumed helical conformation and would cause minimum disruption of the helical macromolecular structure. Pyrolytic loss of the sidechain carbons would likely macerate the structures beyond recognition. Clearly, to preserve physical integrity to the rank of brown coal or even lignite, the side chains must not be lost.

The eventual structural model which can be drafted based on the helical lignin template and altered by the coalification processes mentioned above is shown in Figure 2. It is difficult to display and to describe all the features of such a model in two dimensional space, but one can discern readily that an helical configuration is apparent, even though some significant chemical changes have ensued.

#### COALIFICATION TO SUBBITUMINOUS AND BITUMINOUS COAL

The transformations of brown coal and lignitic woods to higher rank involve some significant changes in chemical structure. This is perhaps the primary cause for the change in physical morphology often observed as coal becomes more lustrous and the vitrinite becomes more homogeneous. This transformation has often been referred to as gelification (15). The wood cells have become deformed significantly, presumably due to increased burial pressure, and some cells actually become annealed to a homogeneous mass.

While structures in brown coal and lignite are dominated by the catechol-like rings arranged in an helical conformation perhaps, the major components of subbituminous and bituminous woods are phenol-like structures. Evidence for the transformation of catechol-like structures to phenol-like structures as shown in Figure 3 comes from both NMR and py/gc/ms data (4, 6). The NMR data clearly indicate a loss of aryl-O carbon. In lignite, aryl-O carbons account for approximately 2 of the six aromatic carbons on the ring, whereas in subbituminous and bituminous coal, only 1 of six aromatic carbons is an aryl-O carbon. Pyrolysis data demonstrate the same observation, with lignitic wood samples being rich in catechols and subbituminous wood samples being rich only in phenols and alkylated phenols. Elemental data show that a significant diminution of oxygen content can explain these transformations.

Coalification to the rank of high-volatile bituminous coal leads to further reductions in oxygen contents for coalified wood. Considering the fact that the amounts of aryl-O do not change significantly, it is likely that the changes imply a further condensation of phenols to aryl ethers or dibenzofuran-like structures as shown in Figure 4 (6). The py/gc/ms data confirm this as more alkylbenzenes and dibenzofurans are observed. The alkylbenzenes in pyrolyzates could arise from thermal cracking of dibenzofuran or diaryl ethers during flash pyrolysis. Also, the increased quantities of condensed aromatic rings, naphthalenes and fluorenes, in pyrolyzates suggests that aromatic ring condensation is occurring. It is likely that this condensation will disrupt the helical structure proposed. At this time we have little to offer in the way of a mechanism for this condensation. Aromaticity of coalified wood appears to increase at this rank (2), suggesting that one possible route for the formation of condensed rings is ring closure and aromatization of the alkyl sidechains. Further studies are needed to verify such a pathway.

Perhaps the next most apparent difference between woods coalified to the rank of subbituminous / bituminous coal and those at the rank of lignite or lower rank is the lack of oxygenated alkyl structures (i.e., hydroxyls or alkyl ethers). The NMR data for subbituminous and bituminous coalified woods show essentially baseline in this region of the spectra, evidence that such functional groups are not significant. Thus what were originally hydroxylated lignin sidechains have been altered. As discussed above, it is most likely that the lignin-derived hydroxyl groups have been reduced rather than lost by pyrolysis of the sidechain. The reduction of hydroxyls is essentially complete at the rank of subbituminous coal.

Consequently, the structural composition of subbituminous coal is that of a lignin structure which has lost its methoxyl groups (via demethylation and dehydroxylation) and all its hydroxyls and alkyl ethers. Presumably, all these reactions can occur with minimal disruption of the three dimensional helical network inherited from lignin. Indeed, some semblance of cellular morphology still remains at the rank of subbituminous coal (11). Pressure and temperature begin to combine at these and higher ranks to have a significant effect on physical morphology of wood. Thus, it becomes less clear whether loss of morphology is purely a physical or chemical phenomenon or both. With such a disruption in the macromolecular structure of wood brought on by the formation of condensed ring systems, it seems reasonable that cellular morphology which persists well up to the rank of bituminous coal begins to degrade into a homogeneous glassy appearance with little semblance of cell wall boundaries at ranks of bituminous coal or higher.

The helical structure is less apparent for wood coalified to bituminous coal (Figure 5) because some significant disruptions of the helix are induced by the reactions at this rank level. Condensations of phenols to diaryl ethers and dibenzofurans are primarily responsible for these disruptions of the helix which are likely to be manifested by physical disruptions in the coalified wood.

#### REFERENCES

1. Hatcher, P.G., Breger, I.A., Earl, W.L., *Organic Geochemistry*, 3,49, 1981.
2. Hatcher, P.G., *Energy and Fuels*, 2, 48, 1988.
3. Hatcher, P.G., Lerch, H.E., III, and Verheyen, T.V., *Int. J. Coal Geol.*, 13, 65, 1989.
4. Hatcher, P. G., *Organic Geochemistry*, 16, 959, 1990.
5. Hatcher, P.G., Lerch, H.E., III, Kotra, R.K., and Verheyen, T.V., *Fuel*, 67, 1069, 1988.
6. Hatcher, P. G., Faulon, J.-L., Wenzel, K. A. and Cody, G. D., *Energy & Fuels*, 6, 813, 1992
7. Hedges, J.J., Cowie, G.L., Ertel, J.R., Barbour, R.J., and Hatcher, P.G., *Geochimica et Cosmochimica Acta*, 49, 701, 1985.
8. Ohta, K. and Venkatesan, M. I., *Energy & Fuels*, 6, 271, 1992.
9. Stout, S. A., Boon, J. J. and Spackman, W., *Geochim. Cosmochim. Acta*, 52, 405, 1988.
10. Faulon, J. L. and Hatcher, P. G., *Energy & Fuels* (in press).
11. Hatcher, P. G., Wenzel, K. A. and Faulon, J.-L., Preprints, American Chemical Society Fuel Division, 38, 1270, 1993.
12. Botto, R. E. *Energy & Fuels* 1, 228, 1987.
13. Adler E., *Wood Sci. Technol.* 11, 169, 1977.
14. Simz H., *Angew. Chem Int. Ed. Engl.* 13, 313, 1974.
15. Stach, E., Taylor, G. H., Mackowski, M-Th., Chandra, D., Teichmüller, M. and Teichmüller, R. *Stach's Textbook of Coal Petrology*, Gebrüder Bornträger, Berlin, 428pp.

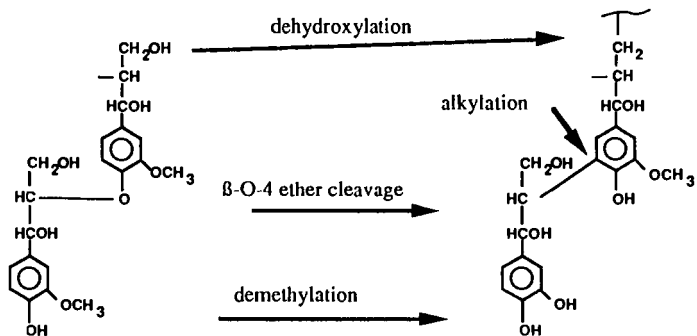


Figure 1. Reactions responsible for the transformation of lignin in peatified gymnospermous wood to brown coal and lignitic wood.

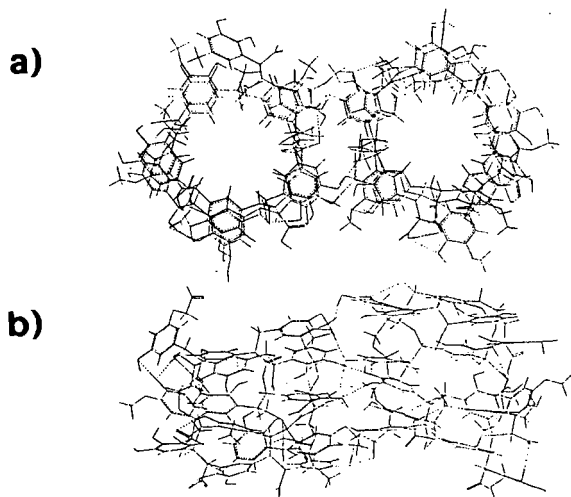


Figure 2. Two dimensional projections of the three dimensional helical model for brown coal and lignitic gymnospermous wood. a) Plan view of the structure and b) elevation view.

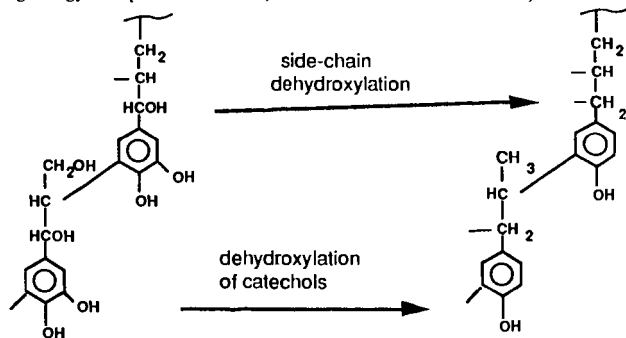


Figure 3. Reactions proposed for the transformation of lignitic gymnospermous wood to subbituminous coal wood.

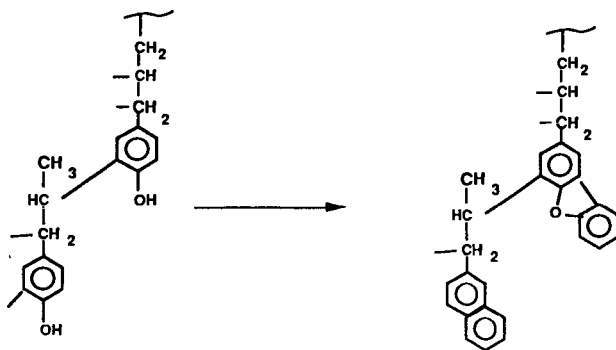


Figure 4. Reactions proposed for the transformation of subbituminous wood to bituminous wood.

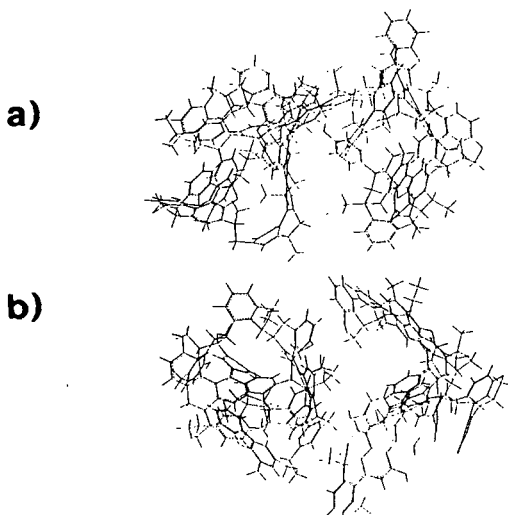


Figure 5. Structural model for bituminous coalified wood built from the helical lignin template and showing a) plan and b) elevation views of the three dimensional structure which has been energy minimized by methods outlined in Faulon and Hatcher ().

REVIEW OF SOME RECENT RESEARCH ON THE COMBUSTION  
PROPERTIES OF COAL MACERALS

John C. Crelling  
Department of Geology  
Southern Illinois University  
Carbondale, IL 62901 USA

K. Mark Thomas  
Northern Carbon Research Laboratories  
University of Newcastle upon Tyne  
Newcastle upon Tyne, NE1 7RU, United Kingdom

Keywords: Macerals, Coal Combustion, Reactivity

INTRODUCTION

The work reviewed here deals with combustion studies on coal macerals, the individual plant derived substances that make up coal, and lithotypes which are associations of macerals. Studies on these components are important for two reasons. One is that broad industrial experience in pulverized fuel combustion has shown that independently of both coal rank and ash type and content, maceral composition has a significant effect on combustion. A Gondwana coal with an high inertinite content will burn differently from a similar rank Illinois Basin coal dominated by vitrinite. The particle size in pulverized fuel combustion is  $70\% < 75$  micrometers. This is a size range where the particles are becoming very heterogeneous and can cover the broad range of maceral and lithotype properties. This may be a factor in carbon burn-out which is especially important in low "NOx" burners. The other reason is that the bulk of the work done on coal combustion has dealt with whole coals only and is, thus, not very informative on maceral effects.

The major difficulty in carrying out maceral and lithotype combustion work is obtaining well characterized samples. Lithotypes must be obtained in the field and usually require some further processing or cleaning up. The collection of large quantities (greater than a kilogram) is sometimes very difficult. While some vitrinite and fusinite maceral-enriched fractions can be hand-picked, the most reliable way of obtaining good concentrates of maceral groups and single macerals is by Density Gradient Centrifugation (DGC) [1-6]. For example, a typical density profile for a vitrinite-rich Herrin No. 6 coal from the Illinois Basin has a main peak in the center of the profile that represents the vitrinite group macerals while the lower and higher density tails respectively represent the liptinite and inertinite maceral groups. To get concentrates of these maceral groups, the sample is further centrifuged at two petrographically determined cut points at the maceral group boundaries. To get concentrates of single macerals, the separated maceral group samples are further subdivided in a similar manner. An easier way to get the single maceral concentrates is to separate lithotypes collected in the field. A typical example of the density profile of a fusain lithotype has two main peaks that are natural concentrations of semifusinite (lower density) and fusinite (higher density). Fractions taken from the center portion of each peak prove to be very homogeneous semifusinite and fusinite.

In using DGC techniques to obtain samples for combustion studies, three factors which need to be considered are the possible effects of the CsCl separation medium, the particle size vs. maceral liberation problem, and the representativeness of the single maceral concentrates. Although the trace amounts of the alkali metal salt (CsCl) that remain on the samples after washing might be expected to act as a catalyst during combustion, no significant effects have been found in combustion experiments [7]. In experiments dealing with pulverized boiler fuel, the particle size is still too coarse to liberate most of the liptinite and some inertinite macerals, and the product will, therefore, contain a large number of mixed phase particles. In the case of the inertinite macerals, this problem can be greatly reduced by using fusain lithotype samples as the feed. In regard to the question of how well the maceral samples represent a pulverized fuel that may have a significant proportion of mixed phase particles, it was found in a series of coal combustion profile experiments [7] that the individual maceral group profiles could be proportionally combined to match the combustion profile of the whole coal sample.

#### COAL COMBUSTION PROFILE EXPERIMENTS

Maceral group concentrates from a rank series of Oklahoma coals were used in a set of experiments in which the samples were combusted in air in a TGA at a heating rate of 15°C per minute [7]. Compared to the whole coals, the maceral concentrates showed similar rank trends e.g., the temperatures of combustion onset, maximum combustion rate, 50% burn-off, and char burn-out all increased with rank, but were more reproducible, more linear, and less variable. Of the maceral groups the vitrinite began combustion at a slightly higher temperature than the other macerals, but it burned significantly faster and more intensely. Semifusinite temperatures, excluding combustion onset, were generally higher and the maximum rate of weight loss was lower than that of the coexisting vitrinite. The few sporinite samples that were studied were initially more reactive than the other macerals, but they became less so at higher temperatures. They had the highest char burn-out temperatures and the lowest maximum rate of weight loss. It should also be noted that the variation in combustion properties due to maceral effects are of the same order of magnitude as the rank effect. This observation confirms earlier work [8].

#### COAL AND CHAR EXPERIMENTS

In another recent set of experiments the combustion properties of a channel sample of the Herrin No. 6 coal, its selected lithotypes, single maceral concentrates, and associated chars were studied [9-10]. The chars were made in an Entrained Flow Reactor at 1000°C in a nitrogen atmosphere at heating rates comparable to pulverized fuel conditions ( $10^4$  to  $10^5$  °C second<sup>-1</sup>). The chars were then combusted in a TGA in an atmosphere of 80% argon and 20% oxygen and the combustion gases were analyzed in a mass spectrometer.

The results of ultimate analyses show that compared to the whole coal channel sample the DGC vitrinite had slightly less carbon and about half the sulfur content, while the DGC fusinite had slightly more carbon and about two-thirds less hydrogen and nitrogen. In the corresponding chars, the nitrogen increased by almost one-third in the vitrinite and by about two-thirds in the fusinite.

The morphology of the chars were strikingly different. The extremes were the uniform open thin-walled cenospheres of the DGC vitrinite and the totally unfused and unchanged forms of the fusinite. The semifusinite showed a mix of thick-walled open cenospheres, thick-walled honeycombed cenospheres, and unfused particles. The char from the whole coal showed a proportional mix of all these forms.

The differences in reactivity (rate of weight loss) in temperature programmed experiments are also striking. While the DGC vitrinite is just slightly more reactive than the whole coal which has about 85% vitrinite, the DGC fusinite was only about half as reactive. The DGC semifusinite is intermediate between these two extremes. Thus, there can be a wide variation in reactivity between different coal particles from the same sample.

The gas evolution profiles of these samples also show some strong similarities and differences. The temperature programmed TGA runs of the chars all show a dominant CO<sub>2</sub> peak with a lower intensity CO peak of the same shape and position (see Figure 1. a,b,c). The SO<sub>2</sub> release is bimodal with a peak before the start of CO<sub>2</sub> evolution related to inorganic sulfur and one just after the CO<sub>2</sub> maximum related to organic sulfur. The peak of nitrogen evolution consistently occurs well after the main CO<sub>2</sub> peak although there is a lower temperature shoulder suggesting two release mechanisms or two types of nitrogen functionality. Work on model compounds of nitrogen suggests that the pyrrolic and pyridinic functionality may be responsible [11-12]. The results on the combustion of the coal samples were generally similar except for a low temperature shoulder in all the curves representing volatile release (Figure 2. a,b,c).

The biggest differences between the vitrinite and fusinite DGC maceral profiles were that both the vitrinite coal and char were more reactive than the fusinite. For example, the temperature of 50% and 100% burnout for the vitrinite coal samples were 443°C and 549°C respectively, while for the fusinite they were 558°C and 705°C. For the chars the same temperatures for the DGC vitrinite were 489°C and 565°C respectively, while for the fusinite they were

557°C and 720°C. However, a higher proportion of the inherent nitrogen in the fusinite was converted to NO. For example, in the coal combustion the ratio of NO/N for the DGC vitrinite was 0.19 while for the fusinite it was 0.29. The same figures for the char combustion were 0.08 for the vitrinite and 0.19 for the fusinite.

This variation in conversion of fuel nitrogen to nitric oxide can be explained by differences in reactivity leading to varying degrees of NO reduction on the carbon. A higher percentage of the nitrogen content in the fusinite maceral is converted to nitric oxide. Thus, while the nitrogen contents of the macerals decrease in the order: vitrinite > semifusinite > fusinite, the conversion of the coal and char nitrogen to NO shows the reverse order. Therefore, there appears to be a compensation effect whereby the amount of NO evolved from the macerals is similar.

#### REFERENCES CITED

1. Dyrkacz, G.R. and Horowitz, P.E. Fuel 1982, 60, 3
2. Dyrkacz, G.R., Bloomquist, C.A.A., Ruscic, L., and Horowitz, E.P. Fuel 1984, 1166
3. Dyrkacz, G.R., Bloomquist, C.A.A., Ruscic, L. and Horowitz, E.P. 1984, in Chemistry and Characterization of Coal Macerals, eds. R.R. Winans and J.C. Crelling, American Chemical Society Symposium Series 252. Washington D.C., 67-77
4. Dyrkacz, G.R., Bloomquist, C.A.A. and Soloman, P.R. Fuel 1984, 63, 536
5. Karas, J., Pugmire, R.J., Woolfenden, W., Grant, D.M. and Blair, S. International Journal of Coal Geology 1985, 5 315
6. Crelling, John C., Ironmaking Proceedings-AIME, 1988, 43, 351
7. Crelling, John C., Hippo, Edwin J., Woerner, Bruce A., and West Jr., David P., Fuel, 1992, 71, 151
8. Crelling, J.C., Skorupska, N.M. and Marsh, H. Fuel 1988, 67, 781
9. Crelling, John C., Thomas, K. Mark, and Marsh, Harry, Fuel, 1993, 72, 339
10. Hindmarsh, Christopher J., Wang, Wanxing, Thomas, K. Mark, and Crelling, John C., Fuel, (in press)
11. Wang, W. and Thomas, K. M., Fuel, 1992, 71, 871
12. Spracklin, C. J., Stanczyk, K., Thomas, K.M., Marsh, H., Edwards, I. A. S., and Skorupska, N.M., Proceedings of the 1990 International Carbon Conference, 1990, p.330

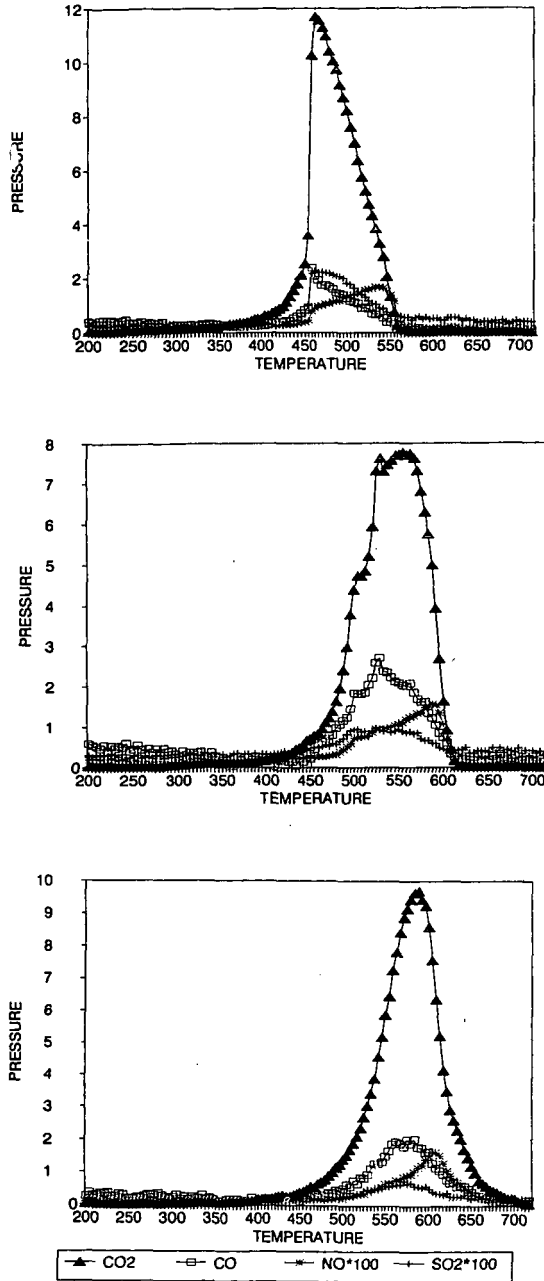


FIGURE 1. Gas evolution profiles of maceral chars combusted in an atmosphere of 80% Argon and 20% Oxygen, 1a (top) vitrinite, 1b (middle) semifusinite, 1c (bottom) fusinite. Note the shift in the peaks from top to bottom indicating decreasing reactivity.

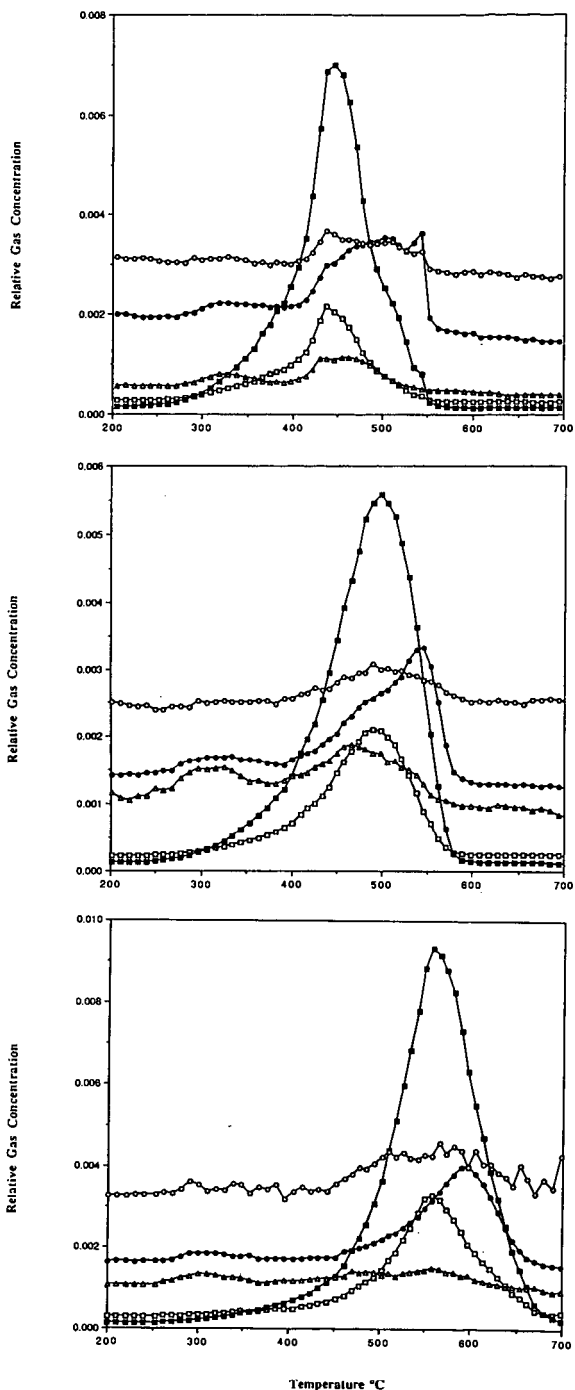


FIGURE 2. Gas evolution profiles of coal macerals combusted in an atmosphere of 80% Argon and 20% Oxygen, 1a (top) vitrinite, 1b (middle) semifusinite, 1c (bottom) fusinite. Note the shift in the peaks from top to bottom indicating decreasing reactivity. KEY: (□) CO, (■) CO<sub>2</sub>, (●) NO x100, (△) HCN x100, (○) N<sub>2</sub><sup>+</sup> x70.

## APPLICATIONS OF MOLECULAR MODELING IN COAL RESEARCH

Gary A. Carlson and Jean-Ioup Faulon  
Fuel Science Department  
Sandia National Laboratories  
Albuquerque, N.M. 87185-0710

Keywords: molecular modeling, computer modeling, coal structure

Over the past several years, molecular modeling has been applied to study various characteristics of coal molecular structures. Powerful workstations coupled with molecular force-field-based software packages have been used to study coal and coal-related molecules. Early work involved determination of the minimum-energy three-dimensional conformations of various published coal structures (Given, Wiser, Solomon and Shinn), and the dominant role of van der Waals and hydrogen bonding forces in defining the energy-minimized structures. These studies have been extended to explore various physical properties of coal structures, including density, microporosity, surface area, and fractal dimension. Other studies have related structural characteristics to cross-link density and have explored small molecule interactions with coal. Finally, recent studies using a structural elucidation (molecular builder) technique have constructed statistically diverse coal structures based on quantitative and qualitative data on coal and its decomposition products. This technique is also being applied to study coalification processes based on postulated coalification chemistry.

The three-dimensional molecular structure of coal is of considerable interest because of the relationship between structure and reactivity (especially as related to coal liquefaction). Recently, a new technique, computer-aided molecular design (CAMD), or computer-aided molecular modeling (hereafter called simply molecular modeling), has been developed and used to study the structural characteristics of complex molecular systems (1). Initially used to aid in the design of pharmaceutical molecules, the technique is now being applied in many fields such as biochemistry, materials science, polymer science, and fuel science. In the area of coal research, molecular modeling has been used to study coal and coal-related molecules and the interactions of coal with solvents and other molecular species. This paper reviews the use of the molecular modeling technique for this latter application.

The molecular modeling methods used for most coal-related studies are molecular mechanics and molecular dynamics calculations. These use a classical force field approximation to simulate the interactions of atoms within and between molecules (2). With these techniques, the minimum-energy three-dimensional structures of molecules can be determined, as well as a number of other physical properties. There are a number of commercial software packages that include energy-minimization capabilities based on force field calculations, coupled with graphical interfaces for visualization of molecules in three dimensions. These packages are described in the various papers that form the basis for this review, and will not be discussed in more detail here.

The earliest use of molecular modeling for fossil fuel applications that the authors are aware of was a structural elucidation study by Oka, Chang and Gavallas in the 1970s directed at coal-derived compounds (3). Their method used analytical data to determine appropriate combinations of structural groups that were then combined to build molecules. Ten years later, Robinson published a study of heavy coal liquids (4), in which the three-dimensional structures were explored but not the energetics. Soon after, Faulon and coworkers (5) constructed molecular representations of kerogen macromolecules, utilizing a structural elucidation technique to build the macromolecules.

The first use of molecular modeling to study coal structures was by Carlson and Granoff (6, 7), who studied a series of previously-postulated bituminous coal structures (Given, Wiser, Solomon and Shinn) and compared their minimum energy structures, physical densities and hydrogen bond interactions. Good agreement with

experimental data was obtained for density and hydrogen bonding. Carlson also explored the specific interactions that define the tertiary structure of coal (hydrogen bonding and van der Waals interactions), finding that the much weaker (but ubiquitous) van der Waals interactions actually dominated the energy-minimization driving force for coals of bituminous rank (8, 9). A method of calculating porosities as well as physical densities from the computer modeling data utilizing a grid system was presented (9), and microporosities were determined for the coal structures studied.

Carlson also addressed the concept of coal as a three-dimensionally cross-linked (network) solid, attempting to compare results with the experimental and theoretical relationships found between coal cross-link density and degree of solvent swelling (10). Previous coal molecular models (Given, Shinn, etc.) did not include cross-linking explicitly. In unpublished work (11), Carlson found that structures constructed with widely-varying cross-link densities showed no significant variations in energy, physical density or microporosity, suggesting that cross-links were not important sources of rigidity in coal structures.

In 1992, Faulon *et al.* published an extension of his original molecular builder program (12), and applied the method to build representative structures for vitrinite from bituminous coal (13, 14). In this work, the analytical data on which the structures were based were derived from elemental analysis, NMR studies and flash pyrolysis/gc/ms data from coalified wood of bituminous rank. It was found that constraints had to be introduced into the builder program to develop models with reasonable energy and physical properties (the builder had to be constrained to generate models with the maximum number of new five and six membered rings—i.e., hydroaromatic structures); otherwise, the energies were much too high, and the degree of cross-linking was excessive. In extensions of this work (15, 16), Faulon *et al.* showed that, although the number of possible coal structures that could be generated from analytical data was very high (over 300,000 for a structure of 650 total atoms), a statistical sampling of 15 structures was sufficient to provide representative results for vitrinite macerals of bituminous coal. Minimized energies, physical densities and micropore volumes for the 15 structures were essentially the same, within the statistical uncertainty. Since the cross-link densities of the 15 structures varied ten-fold, but the physical characteristics of the structures did not appreciably change, these results confirmed the previous observations by Carlson (11) that cross-link density is not a strong driver for rigidity in coal structures.

Faulon and coworkers have extended the post-modeling analysis of three-dimensional coal molecular structures, exploring porosity, surface area and fractal dimension at a molecular level for vitrinite maceral models. Results consistent with experimental measurements of microporosity and CO<sub>2</sub> and N<sub>2</sub> surface areas have been obtained. Additionally, fractal dimensions of 2.7 for coal structures, in agreement with experiment, were observed (17).

Hatcher and Faulon have also used the builder methodology to study the coalification process (18), beginning with a lignin structure and proceeding stepwise through brown coal, to lignite coal, to subbituminous coal and finally to bituminous coal structure. At each step appropriate chemical transformations of the molecular structure were used and computer results were matched to experimental data. In this study and a more extensive companion study (19), it was determined that the most probable tertiary structure for lignin in wood, as well as for isolated lignin following degradation of the cellulosic component of wood, is a helical structure.

Recently, Nakamura, Murata *et al.*, have developed a new method to simulate the physical density of coal structures using molecular modeling (20-22). The method, which involves utilizing the periodic boundary conditions available in certain modeling packages, allows a coal macromolecule to be replicated in adjacent physical locations and thus to interact with its replicates. By shrinking the size of the periodic boundaries, it is possible to estimate the optimal packing arrangement for the structure, and from this, the density. The technique has been used to study model polymers and simulated structures of four Japanese coals of varying carbon content (72-87%). The densities determined for the coal structures to date are somewhat lower (4-20%) than experimental values. For one of the coals, several

structural modifications were made in the links between molecular clusters and the effects on density determined (23). In contrast to the studies referenced earlier, cross-linked structures were found to have a significant influence (reduction of ~10%) on density.

Takanohashi *et al.* have investigated the association of coal soluble constituents using molecular modeling (24). Molecules typical of pyridine soluble and pyridine insoluble fractions were simulated and found to form relatively stable three-dimensional structures, held together by non-covalent interactions, perhaps similar to the structures and interactions in the parent coal.

Kumagai and coworkers have studied the interactions of a lignite molecular model with water molecules (25). By adding water to the lignite structure before and after energy minimization, they were able to simulate the native coal-water interactions as well as the heat of desorption of water from the lignite and the tendency of the lignite structures not to reverse the conformational changes that occurred upon drying.

In other rather different applications of molecular modeling, Vorpagel and Lavin utilized molecular mechanics calculations to explore the most stable geometric arrangements of associated polynuclear aromatic hydrocarbons (26). These studies, with a focus on the behavior of pitches, could have relevance to the stacking of polynuclear aromatic structures within coal structures as well. In another study, Budzinski *et al.* modeled the enthalpies of formation of alkylnaphthalenes using several modeling methods (27). These results are cited because of the similarity of the studied molecules to components of coal structure. Finally, as the power of available computers grows, the application of semi-empirical and even quantum mechanical methods to coal research has become more practical. For example, Ades and coworkers have recently used a molecular orbital method to study cleavage mechanisms of model compounds related to direct coal liquefaction (28). Currently, Li *et al.* are studying small molecule adsorption on nanocluster metal catalysts utilizing density functional quantum mechanical methods adapted to massively parallel computers (29). It appears likely that within the next few years, significant advances in catalysis modeling will be made utilizing these powerful new techniques.

In summary, molecular modeling has become a valuable technique for the investigation of the three-dimensional conformations and physical properties of coal molecular structures, coal-small molecule interactions and coal soluble constituents. Modeling results generally agree with experimental results, and provide additional insight beyond that from experiments alone. With the advent of new high-speed massively parallel computers, it will be possible to model significantly larger macromolecular structures, as well as to begin to utilize quantum chemical methods more effectively.

#### References

1. Bajorath, J.; Kraut, J.; Li, Z.; Kitson, D. H.; Hagler, A. T., *Proc. Natl. Acad. Sci.* **1991**, *88*, 6423-6426.
2. Fruhbeis, H.; Klein, R.; Wallmeir, H., *Angew. Chem. Intl. Ed. Engl.* **1987**, *26*, 403-418.
3. Oka, M.; Chang, H.; Gavalas, G. R., *Fuel* **1977**, *56*, 3-8.
4. Robinson, K. K., *Proc. Electric Power Res. Inst. Conf. on Coal Structure* **1987**, 3.1-3.11.
5. Faulon, J. L.; Vandenbroucke, M.; Drappier, J. M.; Behar, F.; Romero, M., *Adv. Org. Geochem.* **1990**, *16*, 981-993.
6. Carlson, G. A.; Granoff, B., *Am. Chem. Soc. Div. Fuel Chem. Preprints* **1989**, *34(3)*, 780-786.
7. Carlson, G. A.; Granoff, B., "Modeling of Coal Structure Using Computer-Aided Molecular Design," *Coal Science II*, Ed. H. H. Schobert, K. D. Bartle and L. J. Lynch, *ACS Symposium Series* **1991**, *461*, 159-170.
8. Carlson, G. A., *Am. Chem. Soc. Div. Fuel Chem. Preprints* **1991**, *36(1)*, 398-404.
9. Carlson, G. A., *Energy and Fuels* **1992**, *6*, 771-778.

10. Carlson, G. A., *Proc. 1991 Intl. Conf. Coal Science* **1991**, 24-27.
11. Carlson, G. A., unpublished work (1992).
12. Faulon, J. L., *J. Chem. Info. Comput. Sci.* **1992**, 32, 338-348.
13. Faulon, J. L.; Hatcher, P. G.; Wenzel, K. A., *Am. Chem. Soc. Div. Fuel Chem. Preprints* **1992**, 37(2), 900-907.
14. Faulon, J. L.; Hatcher, P. G.; Carlson, G. A.; Wenzel, K. A., *Fuel Processing Technology* **1993**, 34, 277-293.
15. Faulon, J. L.; Carlson, G. A.; Mathews, J. P.; Hatcher, P. G., *Am. Chem. Soc. Div. Fuel Chem. Preprints* **1993**, 38(4), 1275-1280.
16. Faulon, J. L.; Carlson, G. A.; Hatcher, P. G., "Statistical Models for Bituminous Coal: A Three-Dimensional Evaluation of Structural and Physical Properties Based on Computer-Generated Structures," to be published in *Energy and Fuels*, 1994.
17. Faulon, J. L.; Mathews, J. P.; Carlson, G. A.; Hatcher, P. G., "Correlation between Microporosity and Fractal Dimension of Bituminous Coal Based on Computer, Generated Models," unpublished data (1993).
18. Hatcher, P. G.; Wenzel, K. A.; Faulon, J. L., *Am. Chem. Soc. Div. Fuel Chem. Preprints* **1993**, 38(4), 1270-1274.
19. Faulon, J. L.; Carlson, G. A.; Hatcher, P. G., "A Three-Dimensional Model for Lignocellulose," unpublished data (1993).
20. Nakamura, K.; Murata, S.; Nomura, M., *Energy & Fuels* **1993**, 7, 347-350.
21. Murata, S.; Nomura, M.; Nakamura, K.; Kumagai, H.; Sanada, Y., *Energy & Fuels* **1993**, 7, 469-472.
22. Nakamura, K.; Murata, S.; Nomura, M.; Kumagai, H.; Sanada, Y., *Proc. 7th Intl. Conf. Coal Science* **1993**, 1, 385-388.
23. Dong, T.; Murata, S.; Miura, M.; Nomura, M.; Nakamura, K., "Computer-Aided Molecular Design Study of Coal Model Molecules. 3. Density Simulation for Model Structures of Bituminous Akabira Coal," unpublished data (1993).
24. Takanoashi, M.; Iino, M.; Nakamura, K.; Murata, S.; Nomura, M., *Proc. 7th Intl. Conf. Coal Science* **1993**, II, 593-596.
25. Kumagai, H.; Nakamura, K.; Sasaki, M.; Yoneda, J.; Sanada, Y., *Proc. 7th Intl. Conf. Coal Science* **1993**, I, 136-139.
26. Vorpagel, E. R.; Lavin, J. G., *Carbon* **1992**, 7, 1033-1040.
27. Budzinski, H.; Garrigues, P., *Energy & Fuels* **1993**, 7, 505-511.
28. Ades, H. F.; Companion, A. L.; Subbaswamy, K. R., *J. Phys. Chem.* **1991**, 95, 6502-6507.
29. Li, Y. S., unpublished data (1993).

Acknowledgements Funding was provided by the U. S. Department of Energy at Sandia National laboratories under contract DE-AC04-94AL85000.

## THE ROLE OF MODEL COMPOUND STUDIES IN COAL RESEARCH

A. C. Buchanan, III and Phillip F. Britt  
Chemical and Analytical Sciences Division  
Oak Ridge National Laboratory  
P. O. Box 2008  
Oak Ridge, Tennessee 37831-6197

**Keywords:** Model compounds, retrogressive, interfaces, hydrogen transfer

### INTRODUCTION

The extraordinarily complex chemical and physical structure of coals continues to present coal scientists with major challenges in advancing the base of scientific knowledge required for the development of substantially improved coal utilization technologies. As a consequence, model compound studies play a foundational role in advancing coal science. Model compounds are employed in studies for: (a) determination of kinetic and mechanistic information relevant to coal pyrolysis and liquefaction chemistry, and to computational modeling of these processes; (b) development of new catalysts for coal conversion or upgrading of coal-derived liquids; (c) development and benchmarking of various spectroscopic methods for analysis of coal structure and constitution by NMR, FTIR, mass spectrometry, X-ray techniques (XPS, XANES), etc.; and, (d) exploration and development of new chemical reactions for coal such as depolymerization under mild conditions, selective heteroatom removal, etc.

The choice of a model compound should not be prescribed, and the rationale for the selection can vary with the goal of the research. In general, compounds are selected as substructures, or surrogates for a range of related substructures, in coal. The goal of these studies is to understand the behavior of a well-defined chemical system. Once a system is precisely understood then complexities found in coal can be added systematically, such as restricted mass transport, functional group interactions, medium and interfacial effects, etc. Whereas most early studies of model compounds involved simple molecular systems in homogeneous phases, current model compound studies include a substantial contribution from more complicated systems such as reporter molecules in multiphase media under coal conversion conditions<sup>1</sup>, chemically and isotopically labeled coal derivatives<sup>2</sup>, silica-immobilized organics<sup>3-5</sup>, and polymers<sup>6-9</sup>.

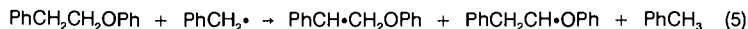
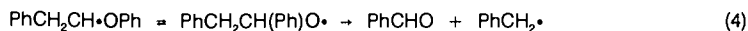
The breadth of use of model compounds in coal research precludes a thorough examination in this report. Instead, we will focus on the use of model compound studies to reveal kinetic and mechanistic details underlying coal pyrolysis and liquefaction. We will limit our examination of this topic to the presentation of four areas that we feel are prominent in current research, and that will continue to be significant in the near future. The aim is to illustrate where model compound studies can and do contribute to coal research, along with the presentation of an occasional brief example. The topics are arbitrarily categorized and, clearly, there exists a substantial degree of overlap among them.

### Model Compounds Containing Heteroatoms

There has been substantial progress in obtaining detailed knowledge of the thermal chemistry of hydrocarbon models including aromatics, alkylaromatics,  $\alpha,\omega$ -diarylalkanes, and hydroaromatics, which has recently been reviewed by Poutsma<sup>10-11</sup> and Stein<sup>12</sup>. The depth of our understanding for molecules containing heteroatoms (O, S, N) is not as advanced (for example, PhSCH<sub>2</sub>Ph vs. the well-understood PhCH<sub>2</sub>CH<sub>2</sub>Ph)<sup>11</sup>. Recent mass spectrometry studies by Winans and coworkers have demonstrated the abundance of heteroatom-containing molecules in coals, macerals, and extracts.<sup>13</sup> For example, it is well-known that oxygen functionalities are particularly abundant in low rank coals and lignites. Furthermore, oxygen-containing functional groups have been implicated in the difficulty found in processing low rank coals.<sup>14</sup> A more detailed understanding of the chemistry of oxygen-containing model compounds is needed.

We have recently reinvestigated the thermolysis of phenethyl phenyl ether (PhCH<sub>2</sub>CH<sub>2</sub>OPh, PPE),<sup>15</sup> which is the simplest model for the  $\beta$ -aryl ether units that are

key constituents of lignin and which are also present in low-rank coals. This research has revealed a previously undetected reaction pathway that accounts for ca. 25% of the conversion of PPE, and which may account for some of the products previously observed in the pyrolyses of lignins. The standard chain propagation steps for free radical decomposition of PPE (Eqs. 1 & 2) must now be augmented by the chain propagation steps shown in Eqs. 3-5, which includes a step involving a neophyl-like rearrangement for an aliphatic radical  $\alpha$  to oxygen prior to  $\beta$ -scission (Eq. 4).



We are in the process of examining substituent effects (relevant to lignin substructures) on the thermolysis of PPE. Our initial findings indicate that the additional reaction pathway is general, but that the selectivity for this pathway (and the rate of decomposition of PPE) is sensitive to the substitution pattern.

This research also revealed a general need for better defined rate constants and Arrhenius parameters for many of the individual reaction steps, which are important in unraveling reaction mechanisms, global reaction kinetics, and substituent effects for complex reactions. This data can be very difficult to extract from complex reactions such as observed for PPE, particularly when secondary reactions become important at low conversions. Franz and coworkers, for example, have been able to design experiments to directly measure such absolute rate data for the  $\beta$ -scission of  $\text{PhCH}^\bullet\text{CH}(\text{CH}_3)\text{O}^\bullet$ <sup>16</sup>, which provides key information relevant to Eq. 2 above. A particularly visible gap in our knowledge is the lack of absolute rate constants and Arrhenius parameters for hydrogen abstractions by phenoxy (and other aryloxy) radicals. Given the apparent importance of such reaction steps in the processing of lignins and low rank coals, kinetic information of this type would be very valuable.

The effect of a heteroatom substituent on a thermolysis reaction is not always easy to predict, and the results can range from subtle to dramatic. For example, we have found that pyrolysis of *p*-Me<sub>2</sub>SiOPh(CH<sub>2</sub>)<sub>3</sub>Ph proceeds similarly to Ph(CH<sub>2</sub>)<sub>3</sub>Ph with little influence of the oxygen substituent on the reaction.<sup>4</sup> Similarly, *m*-HOPhCH<sub>2</sub>Ph is stable at 400°C as is the unsubstituted analog, PhCH<sub>2</sub>Ph.<sup>17</sup> On the other hand, McMillen and coworkers have shown that *o*- and *p*-HOPhCH<sub>2</sub>Ph decay readily at 400°C, because an initial enol-keto tautomerization generates an intermediate with a thermally labile bond.<sup>17</sup> The presence of the ortho-hydroxy group in guaiacol (*o*-HOPhOCH<sub>3</sub>) has been shown to decrease the O-C bond dissociation energy of the methoxy group by 7 kcal/mol, suggesting that hydrogen bonding interactions are important in the radical formed.<sup>18</sup> Finally, thermolysis of 1-naphthol has been shown to proceed by C-C ring coupling prior to condensation (loss of water),<sup>19</sup> while 1,3-dihydroxynaphthalene undergoes condensation first.<sup>20</sup> These few selected examples illustrate that there is much work to be done to understand the impact of oxygen in thermal reaction chemistry related to coal conversion, and a similar status exists for sulfur- and nitrogen-containing organic structures.

### Retrogressive Reaction Pathways

The majority of previous model compound studies have been designed to learn about the cleavage of bonds during coal pyrolysis and liquefaction, and ways of altering reaction media and conditions to promote these reactions. There is now considerable interest in learning more about bond forming reactions and the conditions where they become kinetically competitive. Of particular interest are processes that form more refractory bonds since these reactions are the essence of retrogressive chemistry in coal processing. Malhotra and McMillen have discussed this chemistry with respect to hydrogen transfer reactions in a recent review.<sup>21</sup>

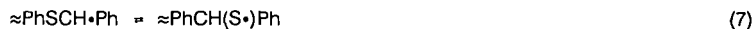
A current topic is the retrogressive chemistry that is prominent in the processing of low rank coals. This chemistry has been documented most completely by Solomon,

Serio, and coworkers who have proposed that the formation of new crosslinks in the coal network is associated with the loss of CO<sub>2</sub> and water from oxygen-containing functional groups. A recent review of this pyrolysis research has been published.<sup>22</sup> These authors have also obtained substantial information recently on the effects of demineralization, aqueous pretreatments, introduction of ion-exchanged catalysts, etc. on the liquefaction behavior of low rank coals, techniques which are designed to reduce retrogressive reactions.<sup>23</sup> However, a clear definition of the actual chemical reactions underlying these processes remains elusive. Ring coupling following decarboxylation of acids has been presumed to be involved. However, there is surprisingly little relevant information available in the literature on such reactions, and McMillen and coworkers have recently shown that, under liquefaction conditions, decarboxylation of model aromatic carboxylic acids is not accompanied by significant ring coupling.<sup>24</sup> Hence, if CO<sub>2</sub> evolution is a signature of the cross-linking event, additional studies are required to determine the nature of the cross-linking reactions associated with decarboxylation. We have recently initiated a project to prepare polymeric model systems containing carboxylic acids to examine the impact of a polymeric network on the thermolysis chemistry.<sup>25</sup> The diffusional constraints imposed by such a polymer system may alter the reactivity pattern for the decarboxylation process, as we have occasionally observed previously in the pyrolysis pathways for silica-immobilized model compounds.

There are other types of retrogressive reactions that may be involved in coal processing that need to be studied in more detail. These include ring growth through a sequence of cyclization and aromatization, and radical recombinations and skeletal rearrangements that form strong bonds.<sup>21</sup> We have found that restricted mass transport (induced by immobilization on silica) promotes retrogressive reactions for bibenzyl by both skeletal rearrangement (to PhCH(CH<sub>2</sub>)Ph) and ring growth (to phenanthrene).<sup>3</sup> We recently found that a similar rearrangement process appears to occur at 300°C for the structurally related silica-immobilized phenyl benzyl sulfide (≈PhSCH<sub>2</sub>Ph), which accounts for 10-15% of the reaction. This process converts a



very labile linkage into a much more refractory diphenylmethane-type linkage. Our current hypothesis is that Eqs. 7-8 are the key chain propagation steps in this



process analogous to bibenzyl. The sulfur to carbon neophyl-like rearrangement for the fluid-phase analog of Eq. 7 has recently been directly observed by Alnajjar and Franz.<sup>26</sup> Coal science would benefit from an improved molecular level understanding of retrogressive reaction types, and the impact that coal physical properties and coal processing media may have on them.

### Interfacial Chemistry

Coal is of course not a homogeneous material. It is a complex, heterogeneous solid that includes interdispersed mineral matter. Yet knowledge of organic-mineral matter interactions, and how they effect the reactivity of coal is only rudimentary. There is also growing evidence that water can play a significant role in affecting the course of chemical reactions during coal processing, which needs to be investigated in more detail.<sup>23</sup> A more complete description of coal reactivity under pyrolysis or liquefaction conditions requires a better molecular level understanding of the effect of minerals on coal reactivity in the solid state. Clays such as montmorillonite, for example, are known to be effective catalysts for organic reactions. They have also been proposed as key catalysts for the thermal alteration of lignin during the coalification process.<sup>27</sup> This suggests that catalytic interactions at the solid-solid interface are important. Recently, we were able to demonstrate that montmorillonite, and other small particle size silica-aluminas, can induce acid-catalyzed reactions in the solid state for several silica-immobilized model compounds including phenethyl phenyl ether.<sup>28</sup>

The catalytic liquefaction of coal constitutes a truly multiphase system, involving solid coal and catalyst, hydrogen gas, and a hydrogen donor "solvent", where interfacial interactions are obviously important. Recently Malhotra and McMillen have

summarized the potential role of the reaction medium in transferring hydrogen atom activity from the catalyst to the coal reactive site.<sup>21</sup> A very active area of research on coal conversion is the search for new nanoscale dispersed catalysts, which could improve the direct interaction of solid coal particles with catalyst.<sup>29</sup> Only recently has evidence begun to emerge that such solid state interactions might be important in affecting the outcome of coal conversion. For example, Bockrath and coworkers used a pulse-flow microreactor to show that organic hydrogen in coal can be exchanged with D<sub>2</sub> gas at low temperatures as a result of MoS<sub>2</sub> catalyst-coal interactions.<sup>30</sup> In collaboration with Snape and coworkers, we have made a preliminary investigation of the catalyzed hydrocracking of silica-immobilized diphenylmethane in the solid state using temperature programmed reduction (TPR) under high pressures of hydrogen with mass spectrometric detection of volatile products.<sup>31</sup> We gained evidence, from the substantially lowered temperatures for benzene and toluene evolution, that a dispersed sulfided Mo catalyst can significantly promote the hydrogenolysis reaction (Eq. 9) in the solid state. The degree to which coal conversion can be modified

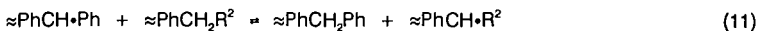
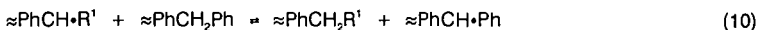


by dispersed catalysts, and the factors controlling such interactions, have only begun to be explored and are a frontier area for model compound research.

### Hydrogen Transfer Chemistry

Despite the longstanding interest and the wealth of information available, improved knowledge of the mechanisms of hydrogen transfer remains a crucial area for the attention of model compound researchers. Hydrogen transfer reactions are important in both bond breaking and bond forming reactions. Of particular current interest are medium effects (solvent systems, catalysts, restricted mass transport, etc.) on hydrogen transfer processes. An array of hydrogen transfer steps have been invoked as being involved including hydrogen abstraction by radicals, transfer of free hydrogen atoms, reverse radical disproportionation (RRD), and radical hydrogen transfer (RHT). RHT involves hydrogen transfer from a cyclohexadienyl-type carrier radical to a substrate in a single step, and has gained significant attention in recent coal and model compound studies.<sup>21,32</sup> However, contrary opinions on the importance of RHT have been recently presented.<sup>33</sup> The exact details aside, it appears that the presence of polycyclic aromatic hydrocarbons in solvent systems can mediate hydrogenolysis activity in coal liquefaction. Given the importance of controlling hydrogen utilization in the development of economically competitive coal utilization technologies, additional model compound research in this area is needed.

We have been actively investigating the effects of restricted mass transport, which may be important in coal chemistry, on thermolysis reactions through the study of silica-immobilized model compounds.<sup>35</sup> By employing two-component surfaces, one can begin to explore the effects of diffusionally constrained environments on hydrogen transfer processes. We have acquired evidence that a mechanism involving rapid serial hydrogen transfer steps on the surface can provide an alternative, non diffusional pathway for free-radical centers to "migrate" as illustrated below.<sup>34</sup>



Moreover, we have recently found that the retrogressive radical chain rearrangement path for silica-immobilized bibenzyl (analogous to Eqs. 7-8 above) is more effectively inhibited by naphthalene spacers (hydrogen transfer barricades) than by hydrogen donor spacers such as tetralin (radical relay centers).<sup>35</sup> These results have important implications for the transfer of reactive sites in the cross-linked network structure of coal which must be explored in more detail.

### Summary

Model compound studies have made and continue to make important contributions in advancing coal science, ranging from determination of quantitative kinetic information for elementary reaction steps to unravelling the effects of restricted diffusion or interfacial phenomena on chemical processes. Constant interactions between model compound and coal researchers will enhance the prospects that the model compound

researcher is performing work of relevance to coal science, and that the coal researcher is employing the appropriate scientific basis in interpretation of coal results. Research that reveals new information on the chemical reactions associated with heteroatom-containing model compounds, retrogressive reaction pathways, organic-mineral interactions and other interfacial effects, and details of hydrogen transfer processes is of particular current interest.

### Acknowledgement

This research was sponsored by the Division of Chemical Sciences, Office of Basic Energy Sciences, U.S. Department of Energy, under Contract DE-AC05-84OR21400 with Martin Marietta Energy Systems, Inc.

### References

1. Bockrath, B. C.; Schroeder, K. T.; Smith, M. R. *Energy and Fuels* **1989**, *3*, 268.
2. Stock, L. M. *Acc. Chem. Res.* **1989**, *22*, 427.
3. Buchanan, III, A. C.; Dunstan, T. D. J.; Douglas, E. C.; Poutsma, M. L. *J. Am. Chem. Soc.* **1986**, *108*, 7703.
4. Buchanan, III, A. C.; Biggs, C. A. *J. Org. Chem.* **1989**, *54*, 517.
5. Britt, P. F.; Buchanan, III, A. C. *J. Org. Chem.* **1991**, *56*, 6132.
6. Malhotra, R.; McMillen, D. F.; Tse, D. S.; St. John, G. A. *Energy Fuels* **1989**, *3*, 465.
7. McMillen, D. F.; Satyam, A.; Malhotra, R. *Proc., 7<sup>th</sup> Int. Conf. Coal Sci., Banff, Alberta, Canada*, **1993**, Vol. II, 163.
8. Squire, K. R.; Solomon, P. R.; Carangelo, R. M.; DiTaranto, M. B. *Fuel* **1986**, *65*, 833.
9. Winans, R. E.; Hayatsu, R.; Squires, T. G.; Carrado, K. A.; Botto, R. E. *Prepr. Pap.-Am. Chem. Soc., Div. Fuel Chem.* **1990**, *35(2)*, 423.
10. Poutsma, M. L. *Energy Fuels* **1990**, *4*, 113.
11. Poutsma, M. L. "A Review of Thermolysis Studies of Model Compounds Relevant to Processing of Coal," Oak Ridge National Laboratory, ORNL/TM-10637, November, 1987.
12. Stein, S. E. *Acc. Chem. Res.* **1991**, *24*, 350.
13. Winans, R. E. "Mass Spectrometric Studies of Coals and Coal Macerals," In *Advances In Coal Spectroscopy*, Muezelaar, H. L. C., Ed.; Plenum Press: New York, **1992**, 255.
14. Solomon, P. R.; Serio, M. A.; Despande, G. V.; Kroo, E. *Energy Fuels* **1990**, *4*, 42.
15. Britt, P. F.; Buchanan, III, A. C.; Hitsman, V. M. *Proc., 6<sup>th</sup> Int. Conf. Coal Sci., Newcastle-upon-Tyne, United Kingdom*, **1991**, 207.
16. Autrey, S. T.; Alnajjar, M. S.; Nelson, D. A.; Franz, J. A. *J. Org. Chem.* **1991**, *56*, 2197.
17. McMillen, D. F.; Ogier, W. C.; Ross, D. S. *J. Org. Chem.* **1981**, *46*, 3322.
18. Suryan, M. M.; Kafafi, S. A.; Stein, S. E. *J. Am. Chem. Soc.* **1989**, *111*, 1423.
19. Poutsma, M. L.; Dyer, C. W. *J. Org. Chem.* **1982**, *47*, 3367.
20. McMillen, D. F.; Chang, S. -J.; Nigenda, S. E.; Malhotra, R. *Prepr. Pap.-Am. Chem. Soc., Div. Fuel Chem.* **1985**, *30(4)*, 414.
21. Malhotra, R.; McMillen, D. F. *Energy Fuels* **1993**, *7*, 227.
22. Solomon, P. R.; Fletcher, T. H.; Pugmire, R. J. *Fuel* **1993**, *72*, 587.
23. Serio, M. A.; Kroo, E.; Charpenay, S.; Solomon, P. R. *Prepr. Pap.-Am. Chem. Soc., Div. Fuel Chem.* **1993**, *38(3)*, 1021.
24. Manion, J. A.; McMillen, D. F.; Malhotra, R. *Prepr. Pap.-Am. Chem. Soc., Div. Fuel Chem.* **1992**, *37(4)*, 1720.
25. Britt, P. F.; Buchanan, III, A. C. *Proc., 7<sup>th</sup> Int. Conf. Coal Sci., Banff, Alberta, Canada*, **1993**, Vol. II, 297.
26. Alnajjar, M. S.; Franz, J. A. *J. Am. Chem. Soc.* **1992**, *114*, 1052.
27. Hayatsu, R.; McBeth, R. L.; Scott, R. G.; Botto, R. E.; Winans, R. E. *Org. Geochem.* **1984**, *6*, 463.
28. Buchanan, III, A. C.; Britt, P. F.; Thomas, K. B.; Biggs, C. A. *Energy Fuels* **1993**, *7*, 373.
29. Derbyshire, F. J. *Energy Fuels* **1989**, *3*, 273.
30. Bockrath, B. C.; Finseth, D. H.; Hough, M. R. *Fuel* **1992**, *71*, 767.
31. Mitchell, S. C.; Lafferty, C. J.; Garcia, R.; Snape, C. E.; Buchanan, III, A. C.; Britt, P. F.; Klavetter, E. *Energy Fuels* **1993**, *7*, 331.
32. Smith, C. M.; Savage, P. E. *Energy Fuels* **1992**, *6*, 195.
33. Autrey, S. T.; Camaioni, D. M.; Ferris, K. F.; Franz, J. A. *Proc., 7<sup>th</sup> Int. Conf. Coal Sci., Banff, Alberta, Canada*, **1993**, Vol. I, 336.
34. Buchanan, III, A. C.; Britt, P. F.; Biggs, C. A. *Energy Fuels* **1990**, *4*, 415.
35. Buchanan, III, A. C.; Britt, P. F.; Thomas, K. B. *Proc., 7<sup>th</sup> Int. Conf. Coal Sci., Banff, Alberta, Canada*, **1993**, Vol. I, 627.

## ORGANIC STRUCTURE COMPONENTS WITHIN THE ARGONNE PREMIUM COAL SAMPLES\*

Randall E. Winans  
Chemistry Division, Building 200  
Argonne National Laboratory  
Argonne, IL 60439

Keywords: Coal Structure, Heteroatoms, Argonne Premium Coals

### INTRODUCTION

The nature of the major organic molecular types that make up the structures in the Argonne Premium Coals will be discussed. Data derived using a number of approaches from the literature and from our laboratory will be included to assemble statistical models for these coals. The nature and distribution of the heteroatoms will be emphasized. In addition, deficiencies in our information such as quantitation of linkages between stable clusters will be examined.

Elucidation of the important structural features in coals has been facilitated by the availability of the Argonne Premium Coal Samples. For the first time, differences between techniques and labs using the same techniques cannot be attributed to differences in the coal sample. Also, the method of storage of the samples, sealed in glass, ensures that studies started today can be compared to studies done on these samples a number of years ago. These samples are with one exception, vitrinite rich, and the discussion in this paper will focus on the organic structures in vitrinites. It is fairly clear that a majority of vitrinite is derived from lignin.<sup>1,2</sup> While the nature of the starting material is important in studying the "structure" of coal, there are ambiguities in our understanding of the structure of lignins.<sup>3</sup> The nature of the monomers is fairly well known, but it is not totally clear how they combine to make the biopolymer. Given the complexity of the starting materials, the severe reaction conditions, and the insolubility of the finished product, one can only hope to develop a statistical picture of coal structure. However, such a picture can be very useful in the development of new technology for coal utilization.

One objective of this paper is to examine what we now know about the structural features of the Argonne coals using information derived from a number of complementary approaches. The second objective is to determine what other information would be useful to better define a statistical picture of coal structure. It should be noted that the literature cited in this paper is not complete but is only representative. The broad topic of physical structure will not be discussed in this study.

Of all the direct techniques used to examine the Argonne Coals, solid <sup>13</sup>C NMR is the most popular.<sup>4,5</sup> A round-robin study focusing on the determination of aromaticity, involving thirteen groups, resulted in a book with a summary of all the results presented in the final chapter.<sup>4</sup> In addition, EPR studies are presented in this compilation. Both XPS<sup>6</sup> and XANES<sup>5,7</sup> have been used to speciate the main sulfur groups. This work has recently been reviewed.<sup>8</sup> Also recently, nitrogen compounds have been investigated by XPS.<sup>9</sup>

Most indirect methods use thermolysis to release smaller molecules, which can then be individually detected. These results are rich in information but are thought to be quantitatively less reliable than direct techniques. Various mass spectrometric methods are the most popular and those applied to the Argonne coals are listed in Table 1. Also, TG-FTIR has been used to quantify thermally released gases and tars.<sup>17</sup>

**Table 1**

Mass Spectrometric Techniques used to analyze the Argonne Premium Coals.

Ionization	Instrument	Resolution	Reference
Low voltage EI	Quadrupole	Low	10
Field Ionization	Sector	Low	11, 12
Fast Atom Bombardment	Sector	Low	13
Desorption Chemical Ionization	Sector	High	14
Desorption EI	Sector	High	15
TGA - LVEI	Quadrupole	Low	10
Laser Desorption	Time-of-flight	Low	16

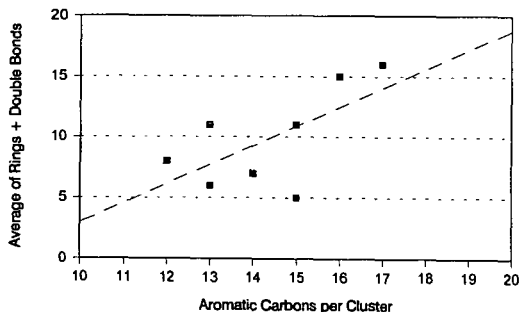
The use of coal extracts simplify some of the problems in coal structure studies and are being used by a number of researchers.<sup>5,14,15,16</sup> Some exotic solvent mixtures result in very high yields for some of the coals. In addition, chemical modification such as alkylation has been used in studies of these coals.

#### EXPERIMENTAL

The preparation and properties of the samples have been described.<sup>18</sup> The Desorption Electron Impact High Resolution Mass Spectrometry (DEIHRMS) experiments were performed using an HRMS EI source modified to take a desorption chemical ionization probe.<sup>15</sup> With this probe the sample is desorbed and pyrolysed directly in the source of the mass spectrometer which reduces the likelihood of secondary reactions such as recombinations and aromatizations. The pyridine extractions have been described elsewhere.<sup>14</sup>

#### RESULTS AND DISCUSSIONS

**Aromatic Structures.** The fraction of aromatic carbons in the Argonne Premium coals have been determined by NMR and it is apparent that the single pulse excitation is the best approach.<sup>4</sup> Molecular weight determinations are not nearly so well defined. Mass spectrometry of volatile extracts or pyrolysis products should provide fairly good numbers. However, the results are very technique dependent. If one examines all of the methods in Table 1 being applied to the same sample, the following trend for average molecular weight results are: lveI/Quad < DEI < DCI = LD < FAB < FI. The differences can be contributed to a combination of fragmentation, ionization technique sensitivity, mass analysis sensitivity, and secondary reactions. Even with these problems several trends are normally observed. Average molecular weight normally increases with rank specifically for aromatic molecules. With aliphatic molecules the trends depend on the biomarker content and types in the coal. The average molecular weights are relatively low, normally between 300 and 500. However, these methods will observe larger molecules if they exist.



HRMS results can be compared to NMR results for the extracts which are shown in Figure 1. Considering the assumptions and

**Figure 1.** Correlation of aromatic carbons from NMR<sup>5</sup> with hydrogen deficiencies from HRMS<sup>15</sup> data derived from extracts of the Argonne Premium Coals.

errors from both techniques, the correlation is quite good. The lignite is the most obvious outlier, but the yields from extraction were much different. A demineralized lignite which gave a greater yield was used in the MS experiment. The MS data shows a smooth increasing average size, while the NMR shows similar trends with a few discontinuities. The important result of all these studies is that the structures are not dominated by large polycyclic aromatic compounds.

**Heteroatoms.** Because of their large abundance, heteroatoms must dominate the chemistry of most coals. Figure 2 shows the average number of heteroatoms per aromatic carbon. Even for the high rank coals, the heteroatom content is significant, but they are likely to be involved as links. This is especially true for oxygen, as can be seen in Figure 3 which shows the amount of ethers or furans present, estimated from three different techniques. The methylation data is incomplete, but the available numbers agree very well with the HRMS estimates. A similar trend is seen for NMR results, but the numbers are much lower which is attributed to difficulties in separating overlapping resonances. All three approaches agree for the Pocahontas coal. The nature of this coal has been thoroughly discussed in a recent paper<sup>19</sup>. The most inconsistent results are for the lignite which has also been observed in the NMR study of extracts.<sup>5</sup> In summary, phenols derived from lignin dominate in the lower rank coals, while furans and ethers may be major links in the higher rank coals.

From XANES, XPS, DEIHMS, and TG-FTIR it is apparent that coals contain a significant amount of aliphatic sulfur. Data from all four techniques have been averaged and the result is shown in Figure 4. Although not shown here, a significant finding is that the indirect, thermal techniques agree very well with the direct methods. Also, there is a very distinct rank dependence with aliphatic sulfur becoming a very minor fraction in the high rank coals.

Nitrogen is found as pyrolic, pyridinic and quaternary by XPS with no evidence for free amines. Pyrolic content varies between

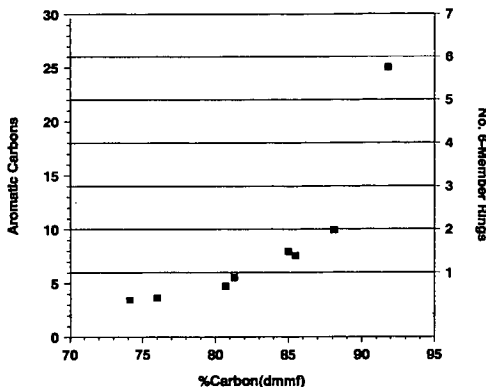


Figure 2. Number of aromatic carbons per heteroatom for the Argonne Premium Coals.

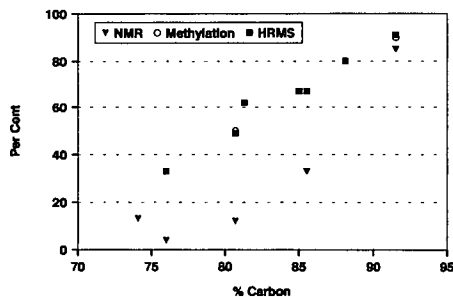


Figure 3. Estimates of the amounts of oxygen species as ethers or furans in the Argonne Premium Coals.

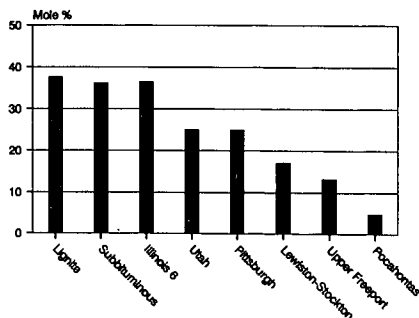
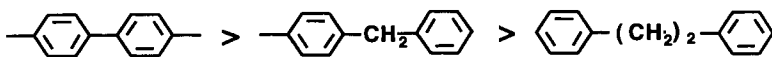


Figure 4. Averages of all available aliphatic sulfur data.

55% and 65% with little rank dependence while quaternary decreases with increasing rank. This species is probably protonated pyridinic nitrogen. DEIHMS indicates that a significant amount of the nitrogen compounds contain an additional heteroatom. This is not surprising if one considers the data in Figure 2.

**Linkages.** Generally, it is thought that aliphatics such as ethylene make up the links between aromatic clusters in coals. However, the evidence for this is not compelling. Biaryl links are thought to be important in the Pocahontas coal and could be significant contributors in many of the >85% carbon bituminous coals. Biaryl and methylene links also tend to be more thermodynamically stable as is shown in the series below.



Oxygen functionalities likely play an important role in linkages, especially in higher rank coals. The decreasing oxygen content is compensated for by an increasing percentage of ethers and furans and an increase in aromatic cluster size. More information is needed to quantitate the distribution of linkages which is critical to an understanding of coal reactivity.

#### SUMMARY

Several key features are evident from examining the data from the Argonne coals. First, the aromatic clusters are not very large. Second, heteroatoms are associated with a majority of the clusters. Finally, we need more quantitative information on the links between clusters.

#### ACKNOWLEDGEMENT

This work was performed under the auspices of the Office of Basic Energy Sciences, Division of Chemical Sciences, U. S. Department of Energy, under contract number W-31-109-ENG-38.

#### REFERENCES

1. Hayatsu, R.; Botto, R. E.; Scott, R. G.; McBeth, R. L.; Winans, R. E. *Fuel* **1986**, *65*, 821.
2. Hatcher, P. G.; Faulon, J. L.; Wenzel, K. A.; Cody, G. D. *Energy Fuels* **1992**, *6*, 813.
3. *Lignin: Properties and Materials*; Glasser, W. G.; Sarkanen, S., Eds; American Chemical Society: Washington D.C., 1989.
4. *Magnetic Resonance of Carbonaceous Solids*; Botto, R. E.; Sanada, Y., Eds.; American Chemical Society: Washington D.C., 1993.
5. Fletcher, T. H.; Bai, S.; Pugmire, R. J.; Solum, M. S.; Wood, S.; Grant, D. M. *Energy Fuels* **1993**, *7*, 734.
6. George, G. N.; Gorbaty, M. L.; Kelemen, S. R.; Sansone, M. *Energy Fuels*, **1991**, *5*, 93.
7. Huffman, G. P.; Mitra, S.; Huggins, F. E.; Shah, N.; Vaidya, S.; Lu, F. *Energy Fuels* **1991**, *5*, 574.
8. *Organic Sulfur in Coal*, Davidson R.; IEA Coal Research: London, 1993.
9. Kelemen, S. R.; Gorbaty, M. L.; Vaughn, S. N.; Kwiatek, P.J. *Prepr. Pap. - Am. Chem. Soc., Div. Fuel Chem.* **1993**, *38*(2), 384.
10. Yun, Y.; Meuzelaar, H. L. C.; Simmleit, N.; Schulten, H-R. *Energy Fuels*, **1991**, *5*, 22
11. Malhotra, R.; McMillen, D. F.; Huestis, D. L. *Prepr. Pap. - Am. Chem. Soc., Div. Fuel Chem.* **1991**, *36*(3), 1252.
12. Simmleit, N.; Schulten, H-R.; Yun, Y.; Meuzelaar, H.L.C. in *Advances in Coal Spectroscopy*, Meuzelaar, H. L.C., Ed.; Plenum Press: N.Y. 1992, 295.
13. Winans, R. E. *J. Anal. Appl. Pyrolysis*, **1991**, *120*, 1.
14. Winans, R. E.; McBeth, R. L.; Hunt, J. L.; Melnikov, P. E. *Proceeding, 1991 International Conf. Coal Sci.* **1991**, *44*.
15. Winans, R. E.; McBeth, R. L. ; Melnikov, P.E., Botto, R.E. *1993 International Conf. Coal Sci.* **1993**, 515.
16. Hunt, J. E.; Lykee, K. R.; Winans, R. E. *Prepr. Pap - Am. Chem. Soc. Div. Fuel Chem.* **1991**, *36*(3), 1325.
17. Bassilakis, R.; Zhao, Y.; Solomon, P. R.; Serio, M. A. *Energy Fuels* **1993**, *7*, 710.
18. Vorres, K. S. *Energy Fuels* **1990**, *4*, 420.
19. Stock, L. M.; Muntean, J. V. *Energy Fuels* **1993**, *7*, 704.

## Organic Oxygen and Nitrogen Transformations During Pyrolysis of Coal

S. R. Kelemen, M. L. Gorbaty and P. J. Kwiatek  
Exxon Research and Engineering Co.  
Annandale, NJ 08801, USA

Keywords: Argonne Premium Coals, Oxygen, Nitrogen

### Abstract

The chemical changes in organically bound oxygen and nitrogen forms have been studied using X-ray Photoelectron Spectroscopy (XPS) following mild pyrolysis of Argonne Premium coal. The evolution of CO<sub>2</sub>, CO and H<sub>2</sub>O during pyrolysis was quantified and their appearance was associated with the loss of hydroxyl and carboxyl functional groups present in coal. There is a corresponding loss of quaternary nitrogen species upon pyrolysis. This loss of quaternary nitrogen species is interpreted to result from broken associations between pyridinic nitrogen and hydroxyl groups from either carboxylic acids or aromatic hydroxyl moieties.

### I. Introduction

During the pyrolysis, hydrolysis and liquefaction of coal the thermolysis of labile chemical bonds is thought to initiate a complex series of reactions that can lead to either hydrogen addition reactions and lower molecular weight products or retrograde cross-linking reactions and heavier products [1-4]. The chemical reactions of organic oxygen functionalities initially present in coal have been implicated as important factors. However, there exists little detailed information about the transformations that take place early during coal conversion. The present work focuses on the chemical changes of organically bound oxygen and nitrogen forms in coal structure prior to the evolution of liquid-like products during coal pyrolysis.

### II. Experimental

X-Ray Photoelectron Spectroscopy was used to speciate and characterize the organic oxygen and nitrogen functional group distributions. An energy correction was made to the spectra due to sample charging based on a carbon (1s) peak position of 284.8 eV. The amount of organic oxygen was determined relative to carbon from the total area of the XPS peaks after accounting for inorganic contributions to the oxygen (1s) and sulfur (2p) peak intensities [5-7]. The inelastic background and shake-up emission features to the carbon (1s) spectra were subtracted prior to curve resolution [8]. The details of the carbon (1s) and nitrogen (1s) curve resolution process appear elsewhere [5,6,8,9]. Argonne Premium coals were used in this study [10]. Pyrolysis experiments were done in helium. The details of the pyrolysis reactor have been described previously [5]. Briefly, a linear (0.5 deg/sec) heat-up period from 160 to 400°C was followed by isothermal reaction at 400°C for 5 min. Analysis of the accumulated gas composition following the heat-up and isothermal period was made by GC analysis using a thermal conductivity detector.

### III. Results and Discussion

During the early stages of coal pyrolysis a substantial amount CO, CO<sub>2</sub>, H<sub>2</sub>O and other light gaseous products are formed. The amount of these gaseous products have been quantified. Table I shows the results of gas analyses following pyrolysis at 400°C for 5 min. The results are expressed as molecules per 100 carbons initially present in each coal sample. Included in Table I is the total amount of oxygen that can be accounted for by these gaseous products. For the lower rank coals the loss of oxygen is greater than for higher rank coals.

XPS has been used to follow the corresponding changes in total organic oxygen in the coal chars. Table II shows the results expressed as atoms of oxygen per 100 carbons initially present. Included in Table II are the corresponding results of the XPS analysis of fresh Argonne premium coals. All coals show a decrease in the level of organic oxygen upon pyrolysis but the effect is most evident with lower rank coal.

There are well known problems associated with different techniques for establishing the level of total organic oxygen and different oxygen functionalities present in coal. Fast neutron activation analysis (FNAA) for oxygen analysis [11,12] followed by correction for inorganic forms has been attempted as an alternate to ASTM oxygen-by-difference estimates and similar modified "by difference" formulas. Indirect chemical methods have been combined with these by-difference determinations for total oxygen to provide functional group information [13, 20, 21]. These results have been compared to indirect pyrolysis attempts at organic oxygen analysis [13, 22].  $^{13}\text{C}$  NMR analysis of Argonne Premium coal has yielded insight into the kinds of organic functionalities present [14]. XPS has also been used to evaluate organic oxygen [5, 15-19].

With the emergence of more reliable methods for determining XPS shake-up and inelastic loss processes, the XPS carbon (1s) line shape can provide quantitative information about the kinds of organic oxygen functionalities initially present in coal [8]. XPS was used in the present work to determine the kinds of organic oxygen functionalities initially present in Argonne Premium coals and those that remain after pyrolysis. Figure 1 shows the XPS carbon (1s) spectrum following background subtraction of the initial Wyodak. Included in this figure are the results of a curve resolution analysis. For the starting Wyodak coal, the main peak is due to unoxidized carbon. There is also a strong peak due to carbon with a single bond to oxygen. Carbonyl and carboxyl peaks show up with less intensity. After pyrolysis, only singly bonded carbon oxygen functionalities are observed and with less relative intensity to unoxidized carbon species. The digital results of the detailed XPS analysis for oxygen functionality for Wyodak and the other Argonne Premium coals are shown in Table II. Low rank coals contain much more carbonyl and carboxyl species. After pyrolysis, low rank coals show a loss of carboxyl and carbonyl species. For low rank coals, much of the lost carboxyl and carbonyl oxygen functionalities can be accounted for in the evolution of light gaseous products. The loss of hydroxyls, mostly from acid functional groups, is thought to occur and explains the appearance of  $\text{H}_2\text{O}$  as a major pyrolysis product of low rank coal.

The changes in the XPS nitrogen (1s) line shape following mild pyrolysis of Argonne Premium coal have been studied. These results are shown in Table III. In contrast to oxygen, the total level of nitrogen remains nearly constant relative to carbon after pyrolysis [9]. The retention of nitrogen in the pyrolysis char is expected, based on lack of gaseous evolution of nitrogen containing pyrolysis products. The results of curve resolution analysis of the nitrogen (1s) spectra for fresh Argonne Premium coals have been previously reported [9] and these results are included in Table III for comparison. In all cases the level of quaternary nitrogen decreases upon pyrolysis, while a corresponding increase in pyridinic nitrogen is observed. The level of pyrrolic nitrogen remains almost constant. These observations, taken together with the results for organic oxygen, suggest that the quaternary nitrogen species are pyridinic forms associated with hydroxyls and that the association is broken as a result of thermal reactions [9].

#### IV. References

- 1) Wiser, W. H., *Fuel*, **1969**, *47*, 475.
- 2) Gorin, E, *Chemistry of Coal Utilization*; Wiley Interscience: N. Y. 1981 Supp. Vol. 2, Chapter 27.
- 3) Whitehurst, D. D.; Mitchell, T. O.; Farcasiu, M., *Coal Liquefaction*; Academic Press: NY 1980.
- 4) Neavel, R. C., *Fuel* **1976**, *55*, 237.
- 5) Kelemen, S. R.; Freund, H., *Energy & Fuels*, **1989**, *3*, 498; **1990**, *4*, 165.
- 6) Kelemen, S. R.; George, G. N.; Gorbaty, M. L., *Fuel*, **1990**, *69*, 939.
- 7) Kelemen, S. R.; Gorbaty, M. L.; George, G. N.; Kwiatek, P. J., *Energy & Fuels*, **1991**, *5*, 720.

- 8) Kelemen, S. R.; Rose, K. D.; Kwiatek, P. J., *App. Surface Science*, **1993**, 64, 167.
- 9) Kelemen, S. R.; Gorbaty, M. L.; Vaughn, S. N.; Kwiatek, P. J., *Prepr. Pap. ACS Fuel Div.*, **1993**, 38, 384.
- 10) Vorres, K. S., *Energy & Fuels*, **1990**, 4, 420.
- 11) Ehmman, W. D.; Koppenall, D. W.; Hamrin Jr., C. E.; Jones, W. C.; Prasad, M. N.; Tian, W. Z., *Fuel*, **1986**, 65, 1563.
- 12) Mahajan, O. P., *Fuel*, **1985**, 64, 973.
- 13) Jung, B.; Stachel, S. J.; Calkins, W. H., *Prep. Pap. ACS Fuel Div.*, **1991**, 36, 869.
- 14) Solum, M. S.; Pugmire, R. J.; Grant, D. M., *Energy & Fuels*, **1989**, 3, 187.
- 15) Clark, D. T.; Wilson, R., *Fuel*, **1983**, 62, 1034.
- 16) Grint, A.; Perry, D. L., *Fuel*, **1983**, 1029.
- 17) Wu, M. M.; Robbins, G. A.; Winschel, R. A.; Burke, F. P., *Energy & Fuels*, **1988**, 2, 150.
- 18) Gonzalez-Elope, A. R.; Martinez-Alonso, A.; Tascon, J. M. D., *Surf. Inter. Anal.*, **1988**, 12, 565.
- 19) Weitzsacker, C. L.; Gardella Jr., J. A., *Anal. Chem.*, **1992**, 64, 1068.
- 20) Liotta, R.; *Am. Chem. Soc.*, **1981**, 103, 1735.
- 21) Liotta, R.; *Fuel*, **1981**, 60, 453.
- 22) Winans, R. E.; McBeth, R. L.; Meinikov, P. E.; Botto, R. E., *Proc. 7th Int. Conf. Coal Sci. Vol. II*, **1993**, 515.

Table I

Coal	Molecules Per 100 Initial Carbons				
	CH <sub>4</sub>	CO <sub>2</sub>	H <sub>2</sub> O	CO	Total Oxygen in These Gases
Beulah Zap	0.26	1.58	4.07	0.21	7.44
Wyodak	0.20	0.84	3.30	0.40	5.38
Illinois #6	0.40	0.32	0.56	0.05	1.25
Blind Canyon	0.33	0.22	0.54	0.08	1.06
Pittsburgh #8	0.44	0.56	0.34	<0.05	1.46
Lewiston	0.46	0.11	0.19	<0.05	0.41
Upper Freeport	0.09	0.06	0.12	<0.05	0.24
Pocahontas	0.05	0.05	0.10	<0.05	0.20

Table II

Coal		Atoms Per 100 Initial Carbons			
		Total Org. Oxygen	-O	C=O	O-C=O
Beulah Zap	Fresh	18.8	11.2	1.4	6.2
	Char	10.7	9.2	0.5	1.0
Wyodak	Fresh	16.9	10.4	1.3	5.2
	Char	10.8	9.3	0.5	1.0
Illinois #6	Fresh	10.9	9.9	0.4	0.6
	Char	8.2	8.2	0.0	0.0
Blind Canyon	Fresh	10.0	9.6	0.4	0.0
	Char	8.5	8.5	0.0	0.0
Pittsburgh #8	Fresh	7.8	6.8	0.9	0.0
	Char	6.2	6.2	0.0	0.0
Lewiston	Fresh	8.0	6.8	1.2	0.0
	Char	6.5	6.5	0.0	0.0
Upper Freeport	Fresh	4.5	3.9	0.6	0.0
	Char	3.8	3.8	0.0	0.0
Pocahontas	Fresh	3.2	3.2	0.0	0.0
	Char	3.0	3.0	0.0	0.0

Table III

Coal		XPS Mole Percent ( $\pm 3.0$ )		
		Pyridinic	Pyrrolic	Quaternary
Beulah Zap	Fresh	26	58	16
	Char	29	60	11
Wyodak	Fresh	25	60	15
	Char	30	61	9
Illinois #6	Fresh	26	62	12
	Char	30	63	7
Blind Canyon	Fresh	31	55	14
	Char	39	57	4
Pittsburgh #8	Fresh	32	61	7
	Char	35	63	2
Lewiston	Fresh	31	60	9
	Char	34	63	3
Upper Freeport	Fresh	28	65	7
	Char	35	63	2
Pocahontas	Fresh	33	64	3
	Char	34	65	1

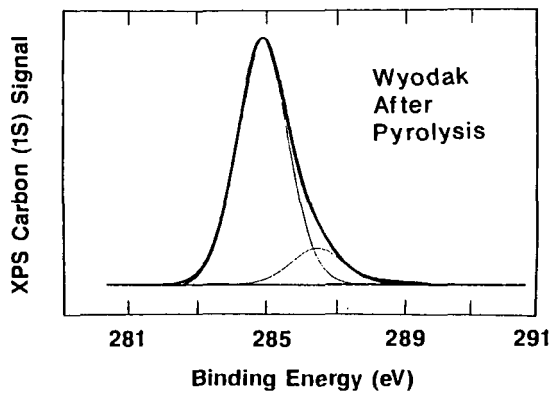
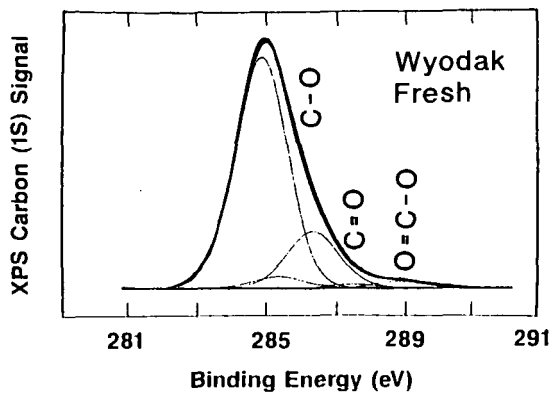


Figure 1

Top) XPS carbon (1s) spectrum of fresh Wyodak coal after background subtraction. Included in the figure are the results of the curve resolution analysis. Bottom) XPS carbon (1s) spectrum after background subtraction of Wyodak coal pyrolyzed at 400 Celcius. Included in the figure are the results of curve resolution analysis.

# ROLE OF ON-LINE MASS SPECTROMETRY FOR STUDYING THE STRUCTURE/REACTIVITY RELATIONSHIPS AND CONVERSION PROCESSES OF COAL

Henk L.C. Meuzelaar, Center for Micro Analysis & Reaction Chemistry  
University of Utah, Salt Lake City, UT 84112

**KEYWORDS:** on-line mass spectrometry techniques; coal structure/reactivity studies; coal conversion process monitoring

## INTRODUCTION

Less than two decades ago a typical mass spectrometer was an extremely expensive and delicate instrument that would completely take up a moderately sized laboratory room. Few coal scientists or engineers had access to such an instrument and even fewer mass spectrometrists were willing to "contaminate" their instrument with something as complex and dirty as coal and its tar. Against this historic background it is nothing less than amazing that as early as 1966 Vastola et al. [1] at Penn State University, using a finely focussed ruby laser and a time of flight (TOF) mass spectrometer, already carried out laser pyrolysis experiments on coal samples inside the ion source. Their example was soon followed by Joy et al., [2]. However, since Vastola's experiment was too far ahead of the state-of-the-art in signal processing electronics it would take more than 15 years before his group was able to obtain reproducible pyrolysis mass spectrometry (Py-MS) patterns from a series of PSOC coal samples [3].

In the meantime, the same coal samples had already been studied by Curie-point pyrolysis mass spectrometry (Py-MS) in our own laboratory [4] as part of a series of 104 Rocky Mountain Province coals. The latter study demonstrated the reproducibility of carefully designed, dedicated Py-MS instruments, as well as the power of multivariate statistical analysis techniques, for reducing the voluminous MS data and bringing out the most significant chemical components and trends.

Already during the late seventies and early eighties several organic geochemistry groups, e.g., at the Technical University Delft (DeLeeuw et al. [5]) at Chevron (Gallegos [6]) and at the University of Bartlesville (Philp et al. [7]) had started to use pyrolysis-gas chromatography/mass spectrometry to characterize a broad range of different coals and coal macerals. Yet another promising instrumental approach, namely thermogravimetry (TG) in direct combination with MS (also reported by Gallegos [6]) was being developed further by Szekely's laboratory in Budapest [8] followed by the development of a vacuum TG/MS system in our own laboratory (Yun [9]). In the mid eighties further advances in TG/MS techniques were reported by Ohrbaeh and Kettrup [10] using a commercially available molecular beam type interface. Most recently, a homebuilt TG/MS system based on similar principles was successfully tested in our own laboratory [11]. Finally, the promising results of the various TG/MS combinations prompted us to pursue more sophisticated analytical configurations such as TG/IR/MS [12] and TG/GC/MS [13], with the latter method eventually being adapted to on-line analysis of high pressure reactions, as reported by Kui et al. [14].

In the mid eighties, Schulten's laboratory in West Germany started pursuing an entirely different approach involving direct probe type pyrolysis of coal directly in the ion source of a high resolution magnetic sector MS system with field ionization (FI) and field desorption (FD) capabilities [15]. Related FIMS work was reported at SRI by Malhotra et al. [16]. That a wealth of information on coal conversion processes and reaction products could also be obtained by high resolution MS in combination with other ionization methods, such as low voltage electron ionization (LVEI) and fast atom bombardment (FAB) was elegantly demonstrated by Winans et al. [17] at Argonne National Laboratory. Last year, a collaborative comparison between different desorption/ionization methods capable of producing ion signals up to several thousand Dalton was performed by two different research groups [18]. Barely was their report submitted or one of the authors (Herod, et al.) published several articles raising the upper mass limit of detected ion species to 4,000 and 270,000 Dalton for FAB [19] and matrix assisted laser desorption/ionization (MALDI [20]), respectively.

Obviously, high mass MS techniques are presently a hot topic in coal science. However, in order to keep the scope of this article within the limitations posed by the ACS Fuel Chemistry Division preprint format, only techniques and applications of MS methods involving direct coupling to micro-scale or upscale coal conversion reactors will be discussed.

## METHODOLOGY

Figure 1 depicts six basic configurations that have found application in coal science and technology. Sequentially progressing from configuration I to configuration VI we notice an increasing spatial and temporal separation between reaction and ionization zones. Configurations I-III involve vacuum pyrolysis. However, whereas in configuration I reaction and ionization zones overlap more or less completely, configurations II and III require some vapor transport mechanism. Configurations IV and V feature (near)ambient pressure reactors whereas configuration VI depicts a high pressure reactor. The degree of separation between reaction and ionization regions in configurations IV and V progresses from a molecular beam or leak type inlet (IV) to a capillary transfer line or full fledged chromatographic column (V). The final configuration (VI) shows a high pressure reactor region with a two stage coupling (involving an intermediate ambient pressure step) to the mass spectrometer vacuum.

Configuration I - Integral Pyrolysis/Ionization Zones - Examples include the LAMMA (Laser Microprobe Mass Analyzer) experiments (Dutta and Talmi [21]) and the pyrolysis field desorption MS studies (Schulten [22]) reported in 1982. Also some of the early laser ionization MS experiments reported by Vastola et al. [23] and Joy et al. [2] fall into this category. More recently, FAB studies were described by Winans et al. [24] and by Herod et al. [19] whereas laser desorption/ionization experiments were reported by Herod et al. [25] and by John et al. [20]. Generally speaking, the interpretation of the results obtained by the integral degradation/desorption/ionization methods have two things in common: (1) very large ions (ranging from  $10^3$  to over  $10^5$  Daltons) are observed, and (2) chemical interpretation of the results has not yet been very successful.

Configuration II - Direct Probe Inlets - Much of the published on-line MS work falls under this broad category, which includes direct probe Py-FIMS, as well as Curie-point Py-MS and vacuum TG/MS studies. Also, the newer work reported by Vastola's group, involving LVEIMS of neutral laser pyrolysis products, falls under this category. As shown in Figure 2 results obtained by the various techniques can be surprisingly similar in spite of the large differences in pyrolysis, ionization and mass spectrometry methods used. This demonstrates that the underlying pyrolysis chemistry is quite constant and that a satisfactory degree of interlaboratory reproducibility is attainable when operating under chemically controlled, conditions (as is readily achievable in Configuration II experiments). Among these techniques, the pyrolysis field ionization MS results reported by the German [26] and US groups [16] stand out with regard to mass range covered (up to approx. 1200 amu) and the absence of confusing fragmentation processes such as produced by conventional (70 eV) electron ionization. However, the upper mass range limit in Py-FIMS is determined by vapor transport limitations and ion transmission characteristics of the mass spectrometer. Remarkably similar spectra can be obtained by electron ionization at 12 eV, as reported by Taghizadeh et al. [27] and Yun et al. [28] and illustrated in Figure 2. As illustrated in Figure 3, the work performed with configuration II instruments has distinguished itself with regard to the application of advanced data reduction and pattern recognition methods [4, 29], especially when combined with time- and temperature-resolved MS data [30, 31].

Configuration III - Vacuum Manifold Inlets - The use of vacuum manifold type transfer lines between pyrolysis and ionization regions is generally the result of MS instruments equipped with batch (vapor) inlets being adapted to pyrolysis studies. Some of the work reported by Winans et al. [32] and by Burnham et al. [33] falls into this category. Also, Curie-point Py-MS studies using a so-called "expansion chamber" [34,35] could be included here. With properly heated, inactivated lines and short residence times results of vacuum manifold type inlets may become "nearly indistinguishable from category II direct probe inlet results. However, the risk of desorption losses and/or secondary reactions requires careful attention to experimental procedures.

Configuration IV - Molecular Beam Type Interfaces - The commercial TG/MS system used by Ohrbach and Ketttrup [10] has an inlet consisting of two nested quartz tubes with carefully aligned centerline pinholes, affording direct access of volatile products into the ion source of a quadrupole mass spectrometer. Nonetheless, the largest coal pyrolysis product ions reported by these authors appear to consist of relatively low MW phenols. A more recent inlet of this type developed by Nie et al. [11] features special flow arrangements designed to minimize condensation losses and the low voltage EI MS patterns obtained closely resemble the corresponding Py-FIMS profiles produced with configuration II type inlets, with peak intensities well into the  $m/z$  400-500 range.

Configuration V - Transfer Line and GC Column Interfaces - Configurations falling into this category feature a narrow bore capillary transfer line which may or may not function as a GC column, depending on temperature and sample injection method used. A broad variety of Py-GC/MS type inlets have been used to study the organic geochemistry of coal and coal macerals

[36]. Closely related is the so-called transfer line GC (TLGC) interface between reaction and pyrolysis zone described by Maswadeh et al [37] for CO<sub>2</sub> laser pyrolysis studies of single coal particles (see GC/MS profiles in Figure 4). Furthermore, the capillary TG/MS interface used by Blaszo et al. [8] and the TG/IR/MS interface reported by our laboratory [12] could be included here, as well as the recent ruby laser Py-GC/MS studies reported by Greenwood et al. [38].

Configuration VI - High Pressure Transfer Line GC Interfaces - Most recently, Kiu et al. [14] described a two stage TLGC interface between a high pressure PG system and a quadrupole mass spectrometer permitting on-line monitoring of high pressure (hydro) pyrolysis reactions in coal under thermally and catalytically controlled conditions. Currently, work is underway in our laboratory to extend this approach to high pressure liquid flow-through reactors [39], thus permitting monitoring of coal hydroliquefaction processes, as illustrated in Figure 5.

## APPLICATIONS

Fortunately, the bewildering array of techniques described appears to conceal a limited number of experimental objectives, namely: (A) elucidation of coal composition and structure as well as structure/reactivity relationships; (B) mechanistic and kinetic studies of coal reactions and (C) optimization of coal conversion processes as well as a characterization of conversion products.

(A) Structural Characterization - This includes many of the organic geochemistry studies using type V (Py-GC/MS) inlet configurations as well as the type I desorption/ionization experiments by means of laser, fast atom bombardment or field desorption techniques. Most recently John et al. reported the "identification" of molecular masses up to 270,000 Dalton by Matrix-Assisted laser desorption MS [20]. Major contributions in this area have also been made by direct probe type (Configuration II) pyrolysis FIMS and HRFIMS studies and by the vacuum manifold (Configuration III) type HREIMS work shown in Figure 6. It can be stated without exaggeration that our current understanding of the molecular composition and structure of coal and its structure/reactivity relationships, however incomplete, depends more strongly on mass spectrometry than on any other analytical methodology.

(B) Reaction Mechanisms and Kinetics - Particularly informative are the time- and temperature-resolved pyrolysis MS studies performed with category II (see Figure 7) as well as IV type experiments which combine the ability to detect labile, reactive species while permitting quantitative analysis of rates and yields. Combined thermogravimetry/mass spectrometry methods are especially well suited for such studies since knowledge of the precise weight loss rates and yields without knowing the chemical identity of the reactive species involved, and *vice versa*, does not fulfill the elementary criteria for kinetic and mechanistic studies. Nevertheless, useful information has been contributed by type III (e.g., HRMS) and type IV (e.g., laser Py-GC/MS) configurations, whereas type VI (high pressure TLGC/MS) methods are starting to open up a whole new field of study for catalytic reaction mechanisms and kinetics.

(C) Conversion Process and Product Characterization - Field Ionization MS techniques have gained an especially strong reputation in this area, although it should be pointed out that measurable vapor pressures are a strict requirement. Completely nonvolatile conversion products can only be analyzed by means of category I desorption/ionization techniques, although generally in an off-line mode. Sufficiently volatile conversion products can, of course, be analyzed by category V (or VI) on-line GC/MS techniques. Due to the availability of MS reference libraries containing over 200,000 standard spectra GC/MS techniques are likely to remain unparalleled in their ability to provide positive chemical identification of compounds in complex mixtures. For dynamic processes type IV molecular beam inlets offer a superior solution. However, if positive chemical identification is required short column "transfer line" GC methods may be the best compromise.

## ACKNOWLEDGEMENTS

This work was sponsored by the Advanced Combustion Engineering Research Center (funds for this Center are received from the National Science Foundation, the State of Utah, 23 industrial participants and the U.S. Department of Energy) and by the Consortium for Fossil Fuel Liquefaction Science (DOE grant no. UKRF-4-23576-90-10).

## REFERENCES

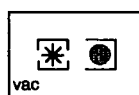
1. Vastola, F.J., et al. in *Advances in Organic Geochemistry*, 1966, 427.
2. Joy, W.K., et al., *Nature*, 217, 1968, 641.
3. McGahan, L.J., M.S. Thesis, Penn State University, May 1983.
4. Meuzelaar, H.L.C., et al. *Fuel*, 63(5), 1984, 640.

5. Van Graas, G., et al., in *Advances in Organic Geochemistry*, 1979, 485.
6. Gallegos, E.J., in *Analytical Chemistry of Liquid Fuel Sources, Advances in Chemistry*, #170, 1978, ACS (publ.), Washington D.C., 13.
7. Philp, R.P., et al., *J. Anal. Appl. Pyroly.*, 4, 1982, 143.
8. Blaszo, M., et al., *J. Anal. Appl. Pyroly.*, 8 1985, 255.
9. Yun, Y., et al., *ACS Preprints, Div. Fuel Chem.*, 33(3), 1988, 75.
10. Ohrbach, K.-H., et al., *J. Anal. Appl. Pyroly.*, 8, (1985), 195.
11. Nie, X. et al., *ACS Preprints, Div. Fuel Chem.*, 1994, San Diego, in press.
12. Dworzanski, J., et al., *ACS Preprints, Div. Fuel Chem.*, 37(2), 1992, 424.
13. McClennen, W.H., *Anal. Chem.*, 65, 1993, 2819.
14. Lui, K. X. et al., *ACS Preprints, Div. Fuel Chem.*, 1994, San Diego, in press.
15. Schulten, H.-R., Marzec, A., *Fuel*, 65, 1986, 855.
16. Malhotra, R., et al., *ACS Preprints, Div. Fuel Chem.*, 36(3), 1991, 1252.
17. Winans, W.E., in *Advances in Coal Spectroscopy*, 1992, Plenum Press, N.Y., 255.
18. Herod, A.A., et al., *Fuel*, 72, 1993, 31.
19. Herod, A.A., et al., *Fuel*, 72, 1993, 1317.
20. John, P., et al., *Rapid Comm. Mass Spectrom.*, 7, 1993, 795.
21. Dutta, R.K., Talmi, Y., *Fuel*, 61, 1982, 1241.
22. Schulten, H.-R., *Fuel*, 61, 1982, 670.
23. Vastola, F.J., et al., in *Spectrometry of Fuels*, 1970, Plenum Press, N.Y., 29.
24. Winans, R.E., *J. Anal. Appl. Pyroly.*, 20, 1991, 1.
25. Herod, A.A., *J. Chem. Soc., Chem. Commun.*, 9, 1993, 767.
26. Schulten, H.-R., et al., *Energy & Fuels*, 6, 1992, 103.
27. Taghizadeh, K., et al., *Fuel Processing Tech.*, 26, 1990, 181.
28. Yun, Y., Meuzelaar, H.L.C., *Energy & Fuels*, 5, 1991, 22.
29. Meuzelaar, H.L.C., et al., in *Computer-Enhanced Analytical Spectroscopy*, III, 1992, Plenum Press, N.Y.
30. Chakravarty, T., et al., *Energy & Fuels*, 2, 1988, 400.
31. Simmleit, N., et al., in *Advances in Coal Spectroscopy*, 1992, Plenum Press, N.Y., 295.
32. Winans, R.E., et al., *ACS Preprints, Div. Fuel Chem.*, 33(3), 1988, 85.
33. Burnham, A.K., et al., *Energy & Fuels*, 3, 1989, 42.
34. Tromp, P.J.J., et al., in *New Trends in Coal Science*, 1988, 241.
35. Meuzelaar, H.L.C., et al., *Curie-point Pyrolysis Mass Spectrometry of Recent and Fossil Biomaterials; Compendium and Atlas*, 1982, Elsevier, Amsterdam.
36. Vastola, F.J., McGahan, L.J., *Fuel*, 66, 1987, 886.
37. Maswadeh, W., et al., *Energy & Fuels*, 7, 1993, 1006.
38. Greenwood, P.F., *Anal. Chem.*, 65, 1993, 1937.
39. Gibbins, J.R., Kandiyoti, R., *Fuel*, 70, 1991, 909.
40. Maswadeh, W., et al., *ACS Preprints, Div. Fuel Chem.*, 37(2), 1992, 699.
41. Nie, X., et al., *ACS Preprints, Div. Fuel Chem.*, 38(4), 1993, 1147.
42. Yun, Y., et al., in *Advances in Coal Spectroscopy*, 1992, Plenum Press, N.Y., 275.

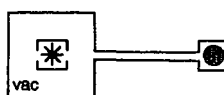
● = pyrolysis zone    \* = ionization zone    vac = vacuum    TLGC = transfer line GC



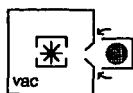
I) Integral zones



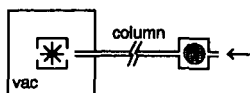
II) direct probe



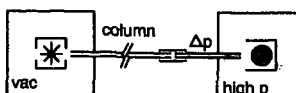
III) vacuum manifold



IV) molecular beam



V) GC & TLGC



VI) high pressure TLGC

Figure 1. Schematic representation of six different pyrolysis mass spectrometry interface configurations ordered according to degree of separation between pyrolysis and ionization zones.

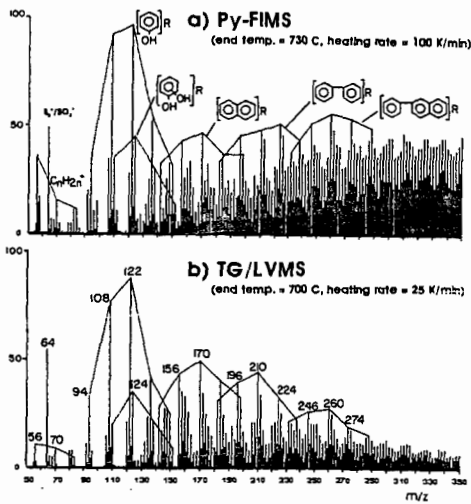


Figure 2. Comparison of mass pyrograms of hvAb Pittsburgh #8 coal obtained by (a) direct probe (100  $\mu$ g sample) Py-FIMS and (b) vacuum thermogravimetry (5 mg sample) in combination with low voltage (12 eV) EIMS (from ref. 28).

Figure 3. (a) Karhunen-Loeve ("factor") score plot for Curie-point pyrolysis mass spectra from 104 Rocky Mountain Province coals showing spontaneous separation by rank and depositional effects; (b) Chemical interpretation of the observed clustering trends (from ref. 4).

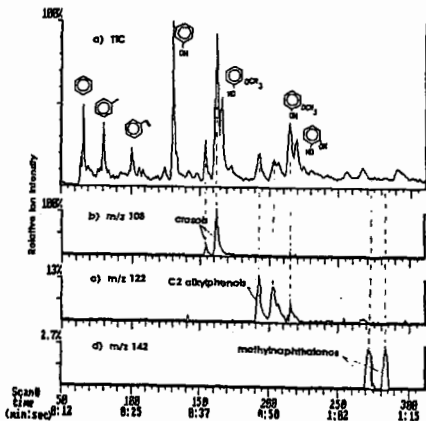
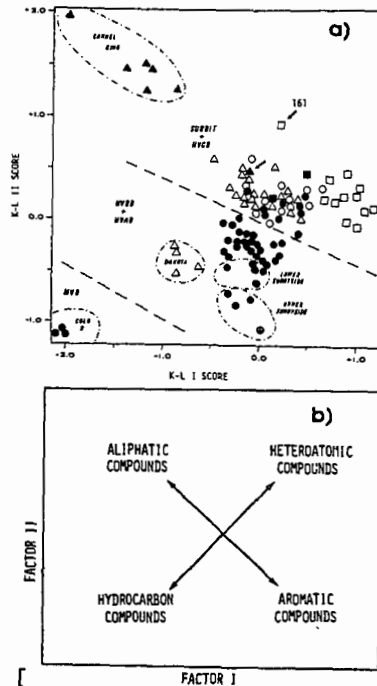


Figure 4. Typical  $\text{CO}_2$  laser pyrolysis GC/MS profile of a 100  $\mu\text{m}$  dia Beulah Zap lignite particle at 20 msec pulse duration showing effective GC separation within approx. 70 sec as well as dominant hydroxy- and methoxy-aromatic signals typical of low rank coal (from ref. 40).

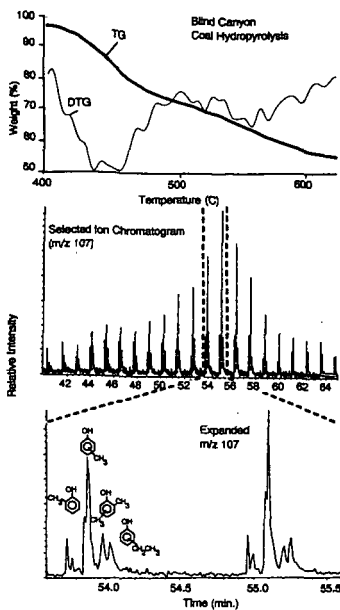


Figure 5. TG/GC/MS profiles of a 50 mg hvAb Blind Canyon coal sample in  $H_2$  at 900 psi obtained at a heating rate of 10 K/min, demonstrating feasibility of on-line GC/MS monitoring of high pressure coal conversion reactions (from ref. 41).

Figure 6. (a) Peaks containing one, two, or three oxygens from Py-HRMS of APCS #8 lignite; (b) area chart of the distribution of heteroatoms for the same coal (from ref. 17).

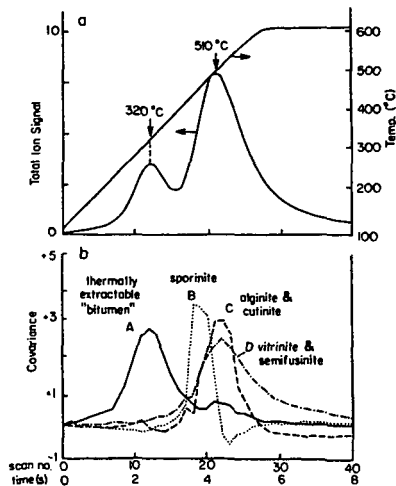
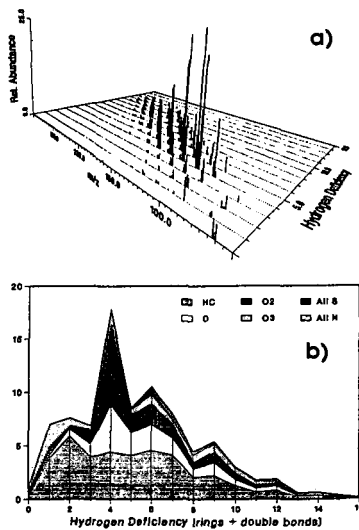


Figure 7. Time-resolved Curie-point pyrolysis MS profiles of a Pittsburgh #8 coal showing "deconvolution" of the total ion signal profile (a) into components A-D (b) by means of factor analysis techniques (from ref. 42).

THE MEASUREMENT OF  $^{13}\text{C}$  CHEMICAL SHIFT TENSORS IN COMPLEX  
POLYCYCLIC AROMATIC COMPOUNDS AND COALS BY AN EXTREMELY SLOW  
SPINNING MAS EXPERIMENT

R.J. Pugmire\*, J.Z. Hu+#, D.W. Alderman+, A.M. Orendt+, C. Ye#,  
and D.M. Grant+

Departments of Chemistry+ and Chemical and Fuels Engineering\*,  
University of Utah, Salt Lake City, Utah 84112 USA  
Wuhan Institute of Physics#, the Chinese Academy of Sciences, P.O.  
Box 71010, Wuhan 430071, China

NMR, Chemical Shift Anisotropy, Coal

#### INTRODUCTION

The  $^{13}\text{C}$  CP/MAS experiment has proven to be a powerful technique for obtaining high resolution spectra in complex solids such as coal (1). MAS narrows the chemical shift anisotropy (CSA) to its isotropic shift when the sample spinning speed is greater than the anisotropy. While the isotropic chemical shift is useful in characterizing chemical structure, the principal values of the chemical shift tensor provide even more information. These principal values are available from the powder pattern obtained from a stationary or slowly spinning sample. Unfortunately, the overlap of many broad powder patterns in a complex solid often prevents the measurement of the individual principal values.

In an effort to address this problem of spectral overlap, many 2D techniques have been developed to simultaneously obtain the dispersion by isotropic shift, such as produced by MAS, in one dimension and the tensorial information as separate powder patterns in the second dimension (2-6). A very successful technique is the slow spinning modification of the magic angle hopping experiment (2) recently proposed by Gan (5), which we call the Magic Angle Turning (MAT) experiment (6). This experiment has a number of advantages over earlier 2D methods. The use of very slow spinning speeds (<50 Hz) favors the quantitative polarization of all carbons and allows the use of a large volume sample rotor resulting in a typical 2D spectrum acquisition requiring less than 24 hours. The mechanical device for slow spinning is very stable and high resolution in the isotropic chemical shift dimension can be easily obtained. The MAT experiment could be done on a suitably stable MAS probe. The only disadvantage of the original MAT experiment is that data acquisition starts right after the last pulse, causing distortion in the evolution dimension (the second dimension) even if a delay as short as 20 $\mu\text{s}$  is used.

In this paper, a triple-echo MAT sequence, previously described (6,7), is employed which improves the 2D baseline. Two additional experiments, using short contact times and dipolar dephasing techniques, are also employed to further separate the powder patterns of protonated and nonprotonated carbons in complex compounds. Experimental results on representative model compounds as well as coals are presented in this paper.

#### EXPERIMENTAL DETAILS

The experiments were performed on a Varian VXR-200 NMR spectrometer. A large-sample-volume slow-spinning MAS probe was constructed for the experiment. The probe holds approximately 5  $\text{cm}^3$  of sample and has a very stable sample spinning rate ranging from 20 to 300 Hz. A spinning rate of 44 Hz was used for the experiments discussed below. 1,2,3-trimethoxybenzene (TMB) and 2,3-dimethylnaphthalene were used as received from Aldrich and the coal samples were obtained from Argonne Premium Coal Sample Bank.

#### RESULTS AND DISCUSSION

The triple-echo and dipolar dephased MAT sequences are given in Fig. 1. The 2D spectrum obtained in this manner and plotted in a square has the bands inclined relative to the acquisition dimension axis at an angle  $\arctan(\omega_2/(3\omega_1))$ , where  $\omega_1$  and  $\omega_2$  are the evolution and acquisition spectral widths, respectively. In order to obtain a 2D spectrum whose projection along one axis gives the isotropic shift spectrum, these data must be sheared through the inclination angle. For all experiments reported in this paper, the evolution-time increments are chosen to be three times the acquisition dwell times, so that the spectral widths for the acquisition dimensions are three times those for the evolution dimensions. This results in 2D spectra with bands inclined at an

angle of  $\arctan(1) = 45^\circ$ . After a  $45^\circ$  shearing operation, the isotropic shift spectrum is obtained from the projection on one axis, while the powder patterns are taken as the perpendicular slices at the isotropic shift positions. The resultant contour plot spectrum of 1,2,3-trimethoxybenzene (TMB) is shown in Fig. 2. The resolution achieved for the isotropic chemical shift dimension is about 1 ppm, as illustrated in Fig. 2, where the resonance for M1 and M3, separated by 1 ppm, are resolved (8). The flat baseline in the isotropic shift projection of Fig. 2 indicates the quality of the 2D baseline achieved, which is essential for the quantitative measurement of the aromaticity ( $f_a$ ) of coal. The individual powder patterns, from which the principal values of the chemical shift tensor can be extracted, are displayed in Fig. 3.

Results from a triple-echo MAT spectrum of 2,3-dimethylnaphthalene (2,3-DMN) are given in Fig. 4 and Table 1. The methyl carbon isotropic shift at 21 ppm is well-separated from those of the ring carbons, and is easily assigned. Assignment of the closely-spaced aromatic carbon shifts is more difficult. An expansion of the aromatic region of the MAT isotropic-shift projection and a similar portion of the MAS spectrum are shown in Figure 4(a). These spectra are interpreted as showing isotropic shift peaks at 124 ppm, 128 ppm, 133 ppm, and 134 ppm. The 128 ppm peak has double intensity, but it is no wider than the single intensity peak at 124 ppm, indicating that two pairs of chemically equivalent carbons have virtually identical isotropic shifts in the solid. A dipolar-dephasing MAS spectrum (not shown) indicates that the nonprotonated carbons are those with isotropic shifts of 133 ppm and 134 ppm. A tentative assignment of the aromatic carbons can be made by assuming that the order of the solid isotropic shifts is the same as that in solution. The chemical shift assignments for 2,3-DMN in solution reported by Wilson and Stothers (9) are given in Table 1. On the basis of the isotropic shift order the 124 ppm shift is assigned to C<sub>6,7</sub>, the 133 ppm shift to C<sub>4a,8a</sub>, and the 134 ppm shift to C<sub>2,3</sub>. These assignments are consistent with the dipolar-dephasing MAS data. The isotropic shifts of C<sub>1,4</sub> and C<sub>5,8</sub> have moved together in the solid to form the double-intensity peak at 128 ppm. Assignment of C<sub>1,4</sub> and C<sub>5,8</sub> requires examination of the principal values of the tensors and the details for the assignments of all carbons are given in reference 6. The important point of note from the example of 2,3-DMN is that the triple-echo MAT experiment provides sufficient resolution to deconvolute overlapping tensor principal values.

The combination of triple-echo MAT, dipolar dephasing triple-echo MAT, and short-contact-time triple-echo MAT experiments can be used as a basic technique for extracting  $^{13}\text{C}$  tensor information in complex powdered solids, e.g. coal. The flat 2D baseplanes produced by these modified sequences and the quantitative cross polarization of the MAT technique are especially important to this application. Shown in Figure 5(a) is the 2D contour plot of a spectrum of Pocahontas coal obtained with the triple-echo MAT pulse sequence; the projection onto the isotropic shift axis is given in Figure 5(b). The aromaticity ( $f_a$ ) obtained by a volume integration of the spectrum in the aliphatic and aromatic regions is 0.86, in good agreement with the value of 0.86 obtained by a variable contact time of  $^{13}\text{C}$  MAS experiment at a field of 2.35T (1). Pocahontas coal powder pattern slices are shown in Figure 6. The normal triple-echo MAT powder pattern at an isotropic shift of 20 ppm in Figure 6(a) corresponds to methyl carbons on aromatic rings. The dipolar dephasing triple-echo MAT powder pattern at 139 ppm in Figure 6(e) arises from the substituted aromatic carbons, some of which cluster in the 135-139 ppm range. Figure 6(b) shows the normal triple-echo MAT powder pattern from the overlapping protonated and nonprotonated aromatic carbons at 124 ppm. These overlapping patterns are successfully separated in Figures 6(c) and 6(d) by the short contact time and the dipolar dephasing experiments, respectively, into patterns characteristic of protonated and nonprotonated (bridgehead) carbons. Nonprotonated and protonated structural types can thus be distinguished in coal by these MAT techniques. The principal values of the tensors for different types of carbons obtained by measuring the shift at the peaks and half-heights of the breakpoints are given in Table 2. The principal values are in good agreement with those obtained by a 1D variable-angle spinning experiment (10). The extraction of the methyl powder pattern, difficult to see in a coal by any other technique, further demonstrates the power of the MAT experiment.

With the MAT experiment we have examined a number of anthracite coal as well as the coals from the Argonne Premium Sample Bank.

It is clear that a great deal of information is available in the experimental data and we are evaluating methods for analysis of the principal value data. The quantitative aspects of the MAT experiment on coals in portrayed in Fig. 7. The triple-echo MAT values of aromaticity correlate closely with those reported by Solum (1). A careful analysis of the quantitative nature of the experiment will be pursued in the future.

#### CONCLUSIONS

The data presented in this study demonstrate that the Magic Angle Turning experiment enables the measurement of  $^{13}\text{C}$  principal values in complex powdered solids by separating tensor powder patterns according to their isotropic shifts. Furthermore, the principal values of different types of tensors are recognizable even when the isotropic shifts overlap. The triple-echo MAT experiment produces 2D spectra with flat baseplanes which are well-adapted to quantitative analysis. Protonated and nonprotonated carbons may be separated by the short-contact-time and dipolar-dephasing variants of the triple-echo MAT experiment. The major problems associated with obtaining MAS spectra at high fields, the very high spinning speeds required to suppress or separate sidebands and the consequent difficulty in uniformly polarizing all spins, are eliminated by the MAT experiment. The triple-echo MAT experiment effectively suppresses spinning sidebands at low rotation frequencies, and the slowly rotating sample appears to promote the polarization of all spins. To date, none of the experiments performed in this laboratory on a wide range of model compounds exhibit recognizable magic angle holes. The MAT experiments described above are particularly promising for the investigation of complex solids such as coal at high fields. Hence, it appears that the MAT experiment will be very useful in the study of a wide range of complex materials. A particular advantage is found in the relatively high resolution features of the experiment. In the isotropic chemical shift dimension the spectral resolution is comparable to that of a traditional CP/MAS experiment, while the uncertainty in the principal values in the powder pattern projections is estimated at  $\pm 2$  ppm.

#### ACKNOWLEDGMENTS

This work was supported by the Pittsburgh Energy Technology Center through the Consortium for Fossil Fuel Liquefaction Science (Contract number DE-FC22-89PC89852) and by the Department of Energy Basic Energy Sciences (Contract number DE-FG02-86ER13510). The assistance of Yi Jin Jiang in building the probe and Dennis Edwards in constructing the optic sensor for detecting the rotation frequency is greatly appreciated. Julion Facelli and Mark Solum are gratefully acknowledged for their helpful discussions. Zhehong Gan, who invented the original MAT experiment, is particularly acknowledged for his cooperation.

#### REFERENCES

1. Solum, M.S., Pugmire, R.J., and Grant, D.M., *Energy & Fuel*, 1989, **3**, 187.
2. Bax, A., Szeverenyi, N.M., and Maciel, G.E., *J. Magn. Reson.*, 1983, **52**, 147.
3. Maciel, G.E., Szeverenyi, N.M., and Sardashti, M., *J. Magn. Reson.*, 1984, **64**, 365.
4. Kolbert, A.C. and Griffin, R.G., *Chem. Phys. Lett.*, 1990, **166**, 87.
5. Gan, Z., *J. Am. Chem. Soc.*, 1992, **114**, 8307.
6. Hu, J.Z., Orendt, A.M., Alderman, D.W., Pugmire, R.J., Ye, C., and Grant, D.M., submitted for publication.
7. Pugmire, R.J., Hu, J.Z., Alderman, D.W., Orendt, A.M., Ye, C., and Grant, D.M., *Proceedings, 7th International Conference on Coal Science*, Sept. 12-17, 1993, Banff, Alberta, Canada, p. 485.
8. Hu, J.Z., Alderman, D.W., Ye, C., Pugmire, R.J., and Grant, D.M., *Magn. Reson.*, 1993, **105**, 82.
9. N.K. Wilson and J.B. Strothers, *J. Magn. Reson*, 1974, **15**, 31.
10. Orendt, A.M., Solum, M.S., Sethi, N.K., Pugmire, R.J., and Grant, D.M., *Advances in Coal Spectroscopy*, Meuzelaar, H.L.C., Editor, Plenum Press, 1992, page 250.
11. Sherwood, M.H., Farelli, J.C., Alderman, D.W., and Grant, D.M., *J. Am. Chem. Soc.*, 1991, **113**, 750.

Table 1.  
Carbon-13 Chemical Shift Tensors in 2,3-Dimethylnaphthalene and Naphthalene.

Carbon	$\delta_{11}$	$\delta_{22}$	$\delta_{33}$	$\delta_{iso.}$	$\delta_{sol.}^b$
<b>2,3-Dimethylnaphthalene<sup>c</sup></b>					
Methyl	30	25	8	21	20.1
C1, 4	218 <sup>d</sup>	132	34	128	127.3
C2, 3	232	157	14	134	135.2
C5, 8	222 <sup>d</sup>	142	20	128	126.7
C6, 7	225	135	11	124	124.8
C4a, 8a	207	197	-4	133	132.3
<b>Naphthalene<sup>e</sup></b>					
C1, C4	224.7, 223.9	140.3, 145.6	22.8, 20.4	129.6	127.7
C2, C3	227.6, 227.6	139.3, 138.2	11.1, 10.4	125.7	125.6
C4a	208.5	202.2	-5.9	134.9	133.3

a. Shift obtained from isotropic projection and MAS spectrum.

b. Solution shifts from Reference 9.

c. Solid shifts in ppm from TMS. Estimated error in solid data is  $\pm 2$  ppm. The shifts are referenced via the methyl carbon of hexamethylbenzene at 17.3 ppm from TMS.

d. Calculated from  $\delta_{22}$ ,  $\delta_{33}$ , and  $\delta_{isotropic}$ .

e. Solid shifts taken from Reference 11; the single crystal environment exhibits  $C_i$  symmetry and has two values for the alpha and beta carbons.

Table 2. <sup>13</sup>C chemical shift tensors in Pocahontas coal.<sup>a</sup>

Carbon type	$\delta_1$	$\delta_2$	$\delta_3$	$\delta_{ave.}$	$\delta_{iso.}$
	1	2	3		
Methyl	35	22	5	20.7	20.3
Protonated	223	13	20	124.7	126.
Nonprotonated	197	18	-8	124.3	124.
Substituted	228	16	32	141.0	139.
		3			4

a. Shifts in ppm from TMS referenced via methyl carbon of hexamethylbenzene at 17.3 ppm from TMS.

b. Average of three principal value shifts.

c. Chemical shift of slice used.

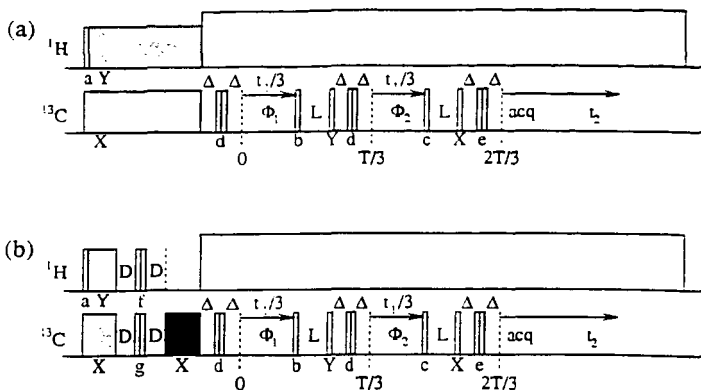


Figure 1. Pulse sequences for the 2D MAT experiments.  $90^\circ$  pulses are represented by single rectangles; two adjacent rectangles denote a  $180^\circ$  pulse. The cross-polarization pulses are shaded. The time  $T$  is an integral number of rotor periods (excluding a multiple of three rotor periods). The magnetization precesses in the transverse plane during the periods labeled  $f_1$  and  $f_2$ , and is along the longitudinal axis during the periods labeled  $L$ .

(a) Normal triple-echo MAT pulse sequence.  $\Delta$  is an echo delay time determined by the probe ring-down and receiver recovery time. The character above each pulse indicates the entry in the phase cycle table (reference 6) which gives the phase of the pulse.

(b) Dipolar dephasing triple-echo MAT pulse sequence. The spin-lock pulse is darkened. The character above each pulse indicates the entry in the phase cycle table (reference 6) which gives the phase of the pulse.

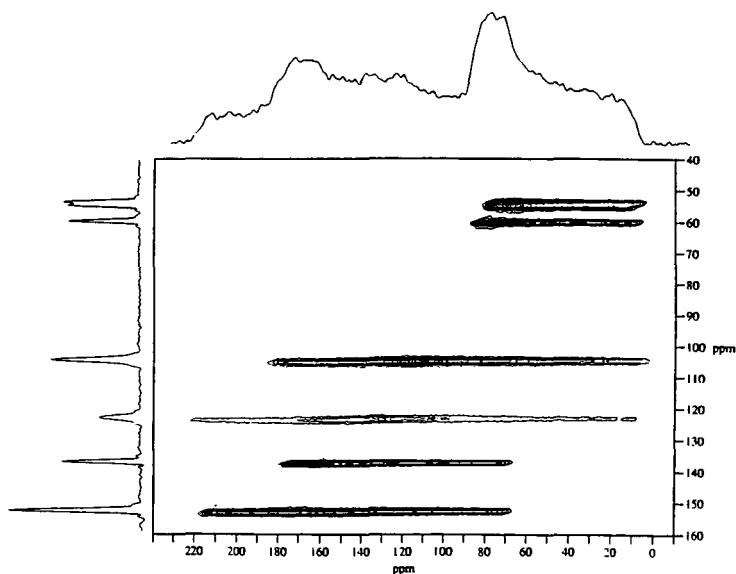


Figure 2. Contour plot of the central portion of the 1,2,3,-TMB 2D spectrum obtained by shearing the spectrum by  $45^\circ$ . The contour interval is 4% of the maximum peak height. The position of the breakpoints and peaks in the bands are given correctly by the ppm scale on the horizontal acquisition dimension axis. The isotropic shifts of the carbons can be read from ppm scale on the vertical axis. A 1.5 ppm Gaussian line broadening was applied in both dimensions, except that the isotropic shift projection was prepared from a 2D spectrum with no line broadening.

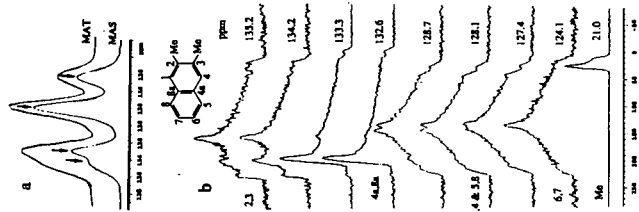


Figure 4. (a) The projection along the isotropic shift dimension and the CP/MAS spectrum of the aromatic carbons of 2,3-DMN with the isotropic shifts of the resolved resonances highlighted. (b) Powder pattern slices taken from normal triple-echo MAT spectrum of 2,3-DMN at indicated values of the isotropic chemical shift. The spectrum was obtained using a 4 ms contact time, spectral widths of  $\omega_2$ -3 $\omega_1$ -32000 Hz, a 12 s recycle delay, 32 scans for both real and imaginary FIDs, 120 evolution increments with a 93.75  $\mu$ s increment time, and 26 hours total experimental time.

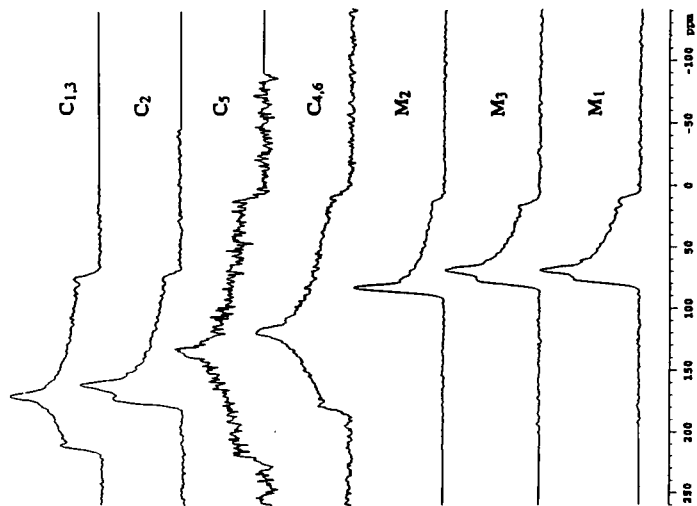


Figure 3. 1,2,3-TMB powder patterns from slices of the triple-echo MAT 2D spectrum in Figure 2.

## AROMATICITY VALUES IN ARGONNE PREMIUM COAL SAMPLES

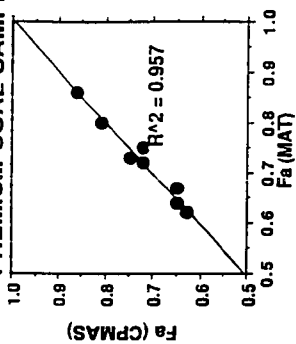


Figure 7. Comparison of the carbon aromaticity values ( $f_a$ ) for the Argonne Premium Coals as determined by the variable contact time CP/MAS technique (reference 1) and the triple echo MAT technique.

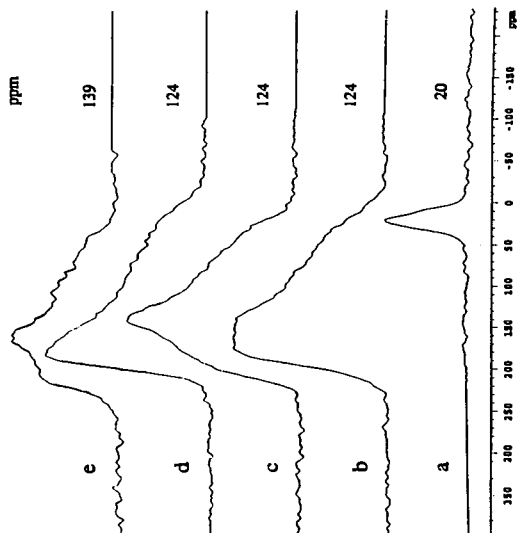


Figure 6. Pocahontas coal triple-echo MAT spectrum slices at selected isotropic shift values.  
 (a) Normal triple-echo MAT spectrum slice showing the aliphatic carbons centered at 20 ppm/  
 (b) Normal triple-echo MAT spectrum slice showing the overlapping protonated and nonprotonated (bridgehead) carbons centered at 124.0 ppm.  
 (c) 50  $\mu$ s contact time triple-echo MAT spectrum slice showing the protonated carbons centered at 124 ppm.  
 (d) Dipolar dephasing triple-echo MAT spectrum slice with  $D = 30$   $\mu$ s and a spin lock pulse of 1.5 ms showing the nonprotonated carbons centered at 124 ppm.  
 (e) Dipolar dephasing triple-echo MAT spectrum slice with  $D = 30$   $\mu$ s and a spin lock pulse of 1.5 MS showing the nonprotonated carbons centered at 139 ppm.

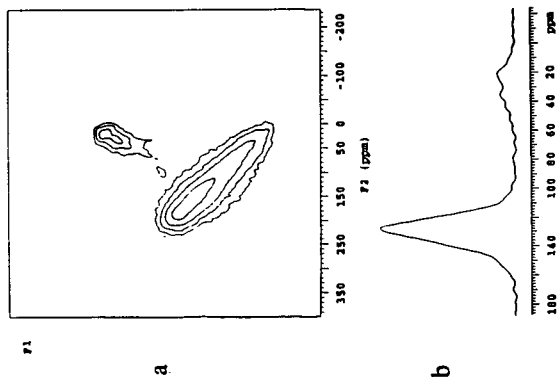


Figure 5. Pocahontas coal triple-echo MAT spectra.  
 (a) 2D spectrum obtained using a sample rotation rate of 4440.025 Hz, a  $\Delta$  of 60  $\mu$ s, a contact time of 2 ms, a recycle delay of 2 s, an acquisition dwell time of 31.25  $\mu$ s, a  $t_1$  increment of 93.75  $\mu$ s, and 25  $t_1$  increments. Data was acquired for 512 scans in the real data set and 512 scans in the imaginary data set for a total measuring time of approximately 8 hr. A 2 ppm full-width-at-half-maximum Gaussian line broadening was applied in both dimensions.  
 (b) Projection of the 2D spectrum in (a) onto the isotropic shift axis.

## CURRENT STATUS OF FTIR IN THE ANALYSIS OF COAL STRUCTURE

Paul Painter, Maria Sobkowiak, Shahrzad Heidary and Michael Coleman  
Polymer Science Program  
Penn State University  
University Park, PA 16802

### INTRODUCTION

Infrared spectroscopy has been a basic "workhorse" technique for coal characterization since the pioneering work of Brown nearly 40 years ago (1). The optical and data handling advantages of FTIR have allowed various advances, such as the introduction of "hyphenated" techniques (GC-FTIR, IR-Microscopy, etc.) and novel sampling methods (diffuse reflection, photo-acoustic measurement, etc.), but most of the problems in coal structural analysis remain the same; the quantitative determination of various functional groups in coal and how the concentration of these groups varies with, for example, oxidation or liquefaction.

In a short article of this type justice cannot be done to the range and scope of work reported by various groups. Accordingly, we will concentrate our attention on just one problem, but a problem that is of central importance in the analysis of coal structure; the determination of the aliphatic and aromatic CH content of coal and coal derived material.

### THE NATURE OF THE PROBLEM AND THE CURRENT STATE OF THE ART

Unlike nmr, band intensities in the infrared spectrum do not give a direct measure of the proportions of the functional groups giving rise to those bands. For spectra obtained in transmission the relationship depends on absorptivities or absorption coefficients through a Beers law relationship. Accordingly, it is the determination of these absorption coefficients for coal that is the central problem in applying FTIR to the analysis of coal structure. There are essentially three methods that in the past have been used to obtain these parameters;

- 1) calibration using model compounds
- 2) studies of solvent extracts, where calibration is provided by proton nmr measurements of the same samples.
- 3) equating band intensities to elemental hydrogen content and solving the simultaneous equations that can be written for a set of samples.

In one form or another all of these methods were used by the scientists who pioneered spectroscopic studies of coal (1-9), but most recent studies have used methods 2 and 3 to determine absorption coefficients. We will review this work first and in the following section indicate how some new work with polymeric models may contribute to solving various problems.

The seminal work on the application of FTIR to the quantitative measurement of the aromatic and aliphatic CH content of coals was performed by Solomon (10) and Solomon and co-workers (11-13). They employed the third calibration method listed above, setting up a set of simultaneous equations for a set of coals and coal derived materials, where the hydrogen contents determined by elemental analysis are equated to the OH and CH contents through equations involving band intensities and absorptivities. The principle problem with this approach is the ill-conditioned nature of the equations, which can result (depending on the sample set) in a range of almost equally valid solutions (14-16). In their most recent studies, Solomon and Carangelo (13) addressed this difficulty and obtained better defined solutions by broadening the range of their sample set. However, it is possible that the methodology used in this work introduces a systematic error, which we will discuss below.

In our studies we have employed a different methodology to that used by Solomon and co-workers. Our approach follows the general lines described in some older work (15), where absorption coefficients were determined by characterizing pyridine soluble coal extracts. The aromatic and aliphatic CH content of these materials can be established independently using proton nmr measurements. Naturally, if the extracts have a different average structure to the parent coal, then this procedure will not be of much use. This is only a problem with low rank coals, however. (See reference 17).

In early work (14) we studied only eleven samples. This is clearly inadequate if we are to accurately determine variations with rank, petrography, geological history, etc. Accordingly, in a recent study we characterized the extracts obtained from a very broad range of coals (17). The initial set of samples consists of 44 North American coals and 17 Polish coals. The use of such a large sample set has also allowed us to examine the effectiveness of various sample preparation

techniques (e.g., KBr pellets vs. diffuse reflectance) and methodologies. Space does not allow us to present the details of this work here, but our conclusion can be grouped into six separate areas;

1. Our first set of conclusions deals with sampling and curve resolving methodology. First, because relatively small amounts of material are required for analysis (1-2 mg), variations due to the inhomogeneous nature of coal are important. It is therefore necessary to average the results of a number of KBr pellets ( $\geq 5$ ) in order to obtain consistent results. Second, in applying curve resolving methods to the stretching region of the spectrum, allowance must be made for the different band shapes of the aromatic and aliphatic modes. Ignoring this factor leads predominantly to errors in the determination of the areas of the aromatic modes, the much more intense aliphatic modes are barely affected.
2. The absorption coefficients determined for the stretching modes vary not only with rank, the values for bituminous coals being distinctly different to those obtained for lignites and sub-bituminous coals, but also with the origin of the coal. We believe this is a particularly important result and to illustrate the type of data we obtained we have reproduced in figure 1 values of the ratio's of the intensities of the aromatic and phthalic CH stretching modes plotted against the ratio of aromatic to aliphatic CH content of the coal extracts determined by proton nmr. When the bituminous coals in our sample set are considered together then there is clearly a band of values, but when separated according to origin (U.S. Interior and Eastern Province Coals, U.S. Rocky mountain coals and Polish coals), good straight line correlations are obtained. The slopes of the lines are different, however, which translates into a difference in the ratio of the absorption coefficients (aromatic CH/aliphatic CH). Because the lines are straight it is reasonable to conclude that these absorption coefficients, which represent an average over the functional groups present, do not vary *within* each sample set. Variations in the relative proportion of such groups, and hence the average absorption coefficient, appear to be more significant between bituminous samples of different origin. [Also, an equivalent plot obtained for lignites and sub-bituminous coals has a very different slope to those shown in figure 1].
3. We have also demonstrated (see reference 17) that the use of the aromatic out-of-plane region of the spectrum ( $900-700\text{ cm}^{-1}$ ) must introduce a systematic error due to the presence of aliphatic rocking modes. This error depends on the absorption coefficient of such vibrations relative to the aromatic out-of-plane modes, but its size remains unknown at this point. This is important in that even though we have successfully obtained absorption coefficients for the stretching modes (see figure 1), the measurement of the area of the aromatic CH band is particularly prone to error because of its weak intensity. Measurements based on the out-of-plane modes are much easier to make and alleviate many problems associated with curve resolving the stretching modes. We will return to this point in the following section as we believe there is a set of experiments that can be performed that will allow us to assess the extent of any error in using the area of the bands between  $900$  and  $700\text{ cm}^{-1}$ . Preliminary experiments indicate that any error may be extremely small.
4. Similarities in the spectra and other considerations lead us to conclude that absorption coefficients for the pyridine extracts of bituminous coals can be applied to their parent material. This is not so for lignite and sub-bituminous coals, however, as the extracts are far more aliphatic than their parent material and appear to have very different absorption coefficients. A different procedure will have to be devised in order to determine absorption coefficients for these coals.
5. We have also characterized all of our samples using diffuse reflectance sampling methods. This technique is much easier to use and superficially less demanding than the preparation of KBr pellets and if we could establish appropriate procedures it would allow FTIR to be applied to coal characterization in a much more routine fashion. Unfortunately, the plots of the ratio of the intensities of the aromatic to aliphatic CH stretching modes show considerably more scatter than the equivalent plots for KBr pellets. The diffuse reflectance results are shown in figure 2. In part, this scatter may reflect a fundamental problem in the diffuse reflectance technique, in that weaker modes appear to be selectively enhanced in intensity (relative to absorption measurements) and this, in turn, depends on things such as packing (in the sampling cup) that are not easily controlled or reproducible.
6. Finally, how consistent are the results that have been obtained using different methodologies? The older work (compare refs 10-12 and 14-16) displayed some distinct differences, but there has been a remarkable convergence of values of the absorption coefficients obtained in more recent studies. Solomon and Carangelo(13) reported values for the absorption coefficients of the aliphatic CH stretching mode,  $a_{al}^{st}$ , and out-of-plane bending modes,  $a_{ar}^{op}$  of 744 and 684, respectively, for a Pittsburgh seam coal. These values are in remarkably good agreement with those reported in our work (17) for US bituminous coals from the Eastern and Interior Provinces (764 and 665, respectively, ref. 17). This agreement is truly extraordinary, considering the different methodologies employed in these studies. Clearly, as far as the stretching modes and the  $900-700\text{ cm}^{-1}$  region of the spectrum are concerned, the procedures used to prepare KBr pellets, measure band areas, etc. must be producing equivalent results. Furthermore, the absorption coefficients determined for extracts by calibration with proton nmr.

are apparently also in agreement with the results of the procedure applied to whole coals and char, indicating an equivalence in structure. There remains the question of the extent of the error that is introduced by the rocking modes that also appear in the 900-700  $\text{cm}^{-1}$  region of the spectrum, and this is where some new work sheds some light.

#### PHENOLIC RESINS AS MODELS FOR COAL

In order to determine the extent of any contribution of  $\text{CH}_2$  aliphatic rocking modes to the bands between 900 and 700  $\text{cm}^{-1}$  we have embarked on a study of various phenolic resins. Essentially, our plan is to prepare resins where the phenolic rings are protonated and the methylene linkages are deuterated (i.e., -  $\text{CD}_2$ -) and resins where this labeling is reversed. We have synthesized the first models and it appears from preliminary spectra that methylene vibrations contribute negligibly to the 900 - 700  $\text{cm}^{-1}$  region of the spectrum. This work will be completed in the next two months and a more complete discussion presented at the conference. The synthesis of these resins has also opened up what might become a new and intriguing area of study involving the near infrared region of the spectrum, and we will conclude this paper with a brief discussion of these initial results.

The near infrared region (~9000 - 4000  $\text{cm}^{-1}$ ) of the spectrum of coals (and many other materials) has not been studied in great detail, but appears to be very sensitive to aromatic and aliphatic CH content (because these modes are overtones and combinations and are a result of a breakdown of quantum mechanical selection rules, they usually involve vibrations of protons, which are "light" and therefore more likely to be anharmonic). A comparison of the spectrum of an all-protonated and  $\text{CD}_2$  linked resin is shown in figure 3. Coal has a similar spectrum, but with additional bands probably due to  $\text{CH}_3$  species as illustrated in figure 4. It is particularly interesting that the modes between about 6300  $\text{cm}^{-1}$  and 5500  $\text{cm}^{-1}$  have a band near 6000  $\text{cm}^{-1}$  which can be assigned to an overtone of aromatic CH stretching vibrations, that is much more intense than the aliphatic modes near 5700  $\text{cm}^{-1}$ , reversing the intensity ratio of the fundamentals. This may prove to be very useful in quantitative work.

#### CONCLUSIONS

The development of FTIR techniques for the quantitative determination of the functional groups present in coal has advanced considerably in the past few years. There has been particular progress in the measurement of aliphatic and aromatic CH content, with a pleasing convergence in the values of the absorption coefficients obtained by different groups using different methodologies. It appears that the use of phenolic resins as models should enable us to "sort out" the remaining problems and also allow band assignments in the near IR region of the spectrum, thus opening up a new means of analysis.

#### ACKNOWLEDGMENT

We gratefully acknowledge the support of the Office of Basic Energy Sciences, Division of Chemical Sciences, Department of Energy, under Grant no. DE-FG02-86ER 13537.

#### REFERENCES

1. Brown, J. K., p. 744, J. Chem. Soc., 1955.
2. Brown, J. K. and Ladner, W. R. Fuel, 1960, 39, 87.
3. von Tschamler, V. H. and de Ruiter, E., Grenst. - Chem., 1962, 43, 16.
4. Durie, R. A. and Sternhell, S., Aust. J. Chem., 1959, 12, 205.
5. Durie, R. A., Schewchyk, Y. and Sternhell, S., Fuel, 1966, 45, 99.
6. Fujii, S., Fuel, 1963, 42, 17, and 341.
7. Retcofsky, H. L. and Friedel, R. A., Fuel, 1968, 47, 487.
8. Retcofsky, H. L., Applied Spectroscopy, 1977, 31, 116.
9. Retcofsky, H. L. and Friedel, R. A. in "Spectrometry of Fuels" Editor, R. A. Friedel, Plenum Press, 1070, Chapter 6.
10. Solomon, P. R., Prepr. Pap.-Am. Chem. Soc. Div. Fuel Chem., 1979 24 (2), 185.
11. Solomon, P. R., and Carangelo, R. M. Fuel, 1982, 61, 663.
12. Solomon, P. R., Hamblen, D. G., and Carangelo, R. M., ACS Symp. Ser, 1982, 205, 77.
13. Solomon, P. R. and Carangelo, R.M., Fuel, 1988, 67, 949.
14. Sobkowiak, M., Riesser, B., Painter, P. C., and Given, P. H. Fuel 1984, 63, 1245.
15. Riesser, B., Starsinic, M., Squires, E., Davis A., and Painter, P. Fuel, 1984, 63, 1253.
16. Painter, P. C. Starsinic, M., and Coleman, M. M. in Fourier Transform Infrared Spectroscopy, 1985, Vol. 4, 169.
17. Sobkowiak, M. and Painter, P. C. Fuel 1992, 71, 1105.

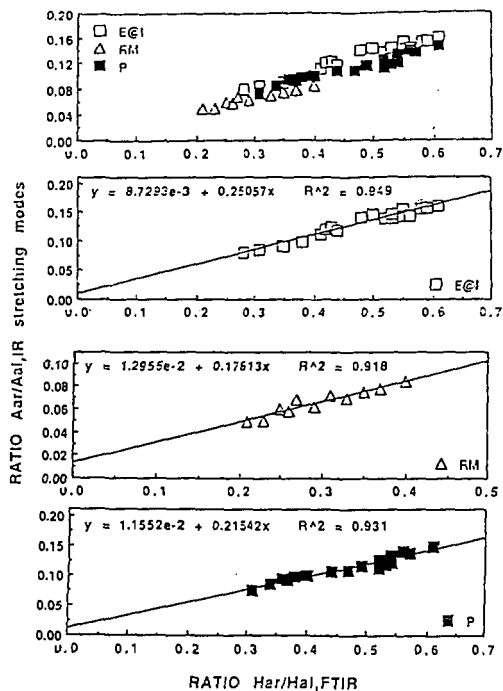


Figure 1. Plots of the ratio of the areas of the aromatic to phatialic CH stretching modes of KBr pellets of coal to aliphatic hydrogen determined by proton nmr.

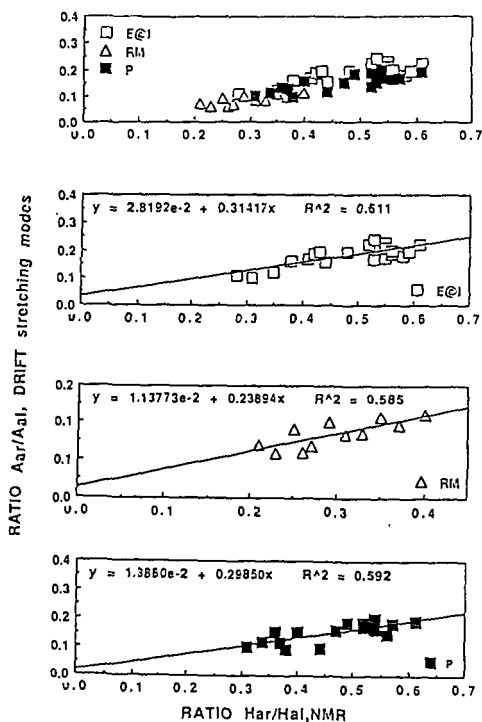


Figure 2. The same plots as Figure 1, but with the spectra of the extracts obtained by diffuse reflectance.

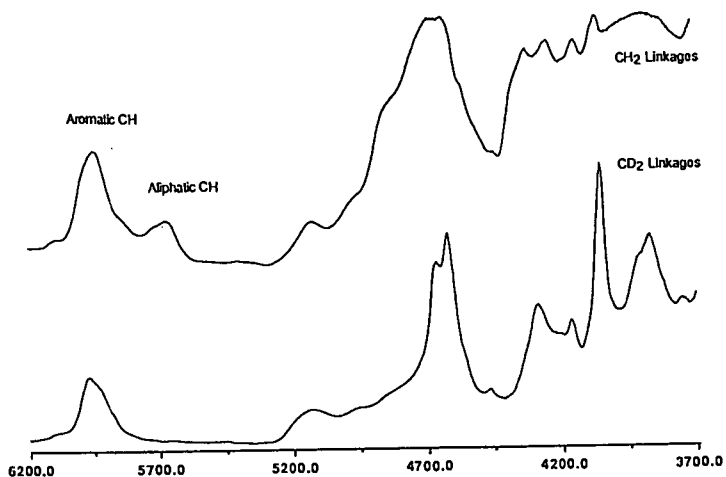


Figure 3. Near infrared spectrum of phenolic resins where the aromatic group are connected by CH<sub>2</sub> linkages (top) and CD<sub>2</sub> linkages (bottom).

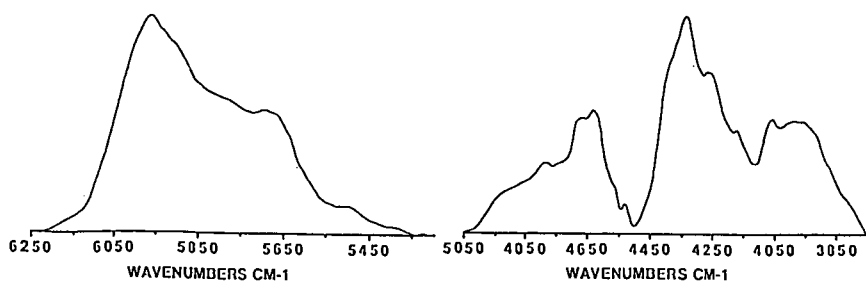


Figure 4. Near infrared spectrum of a coal extract.

# POROSITY OF APCS COALS: THE ACCESSIBLE NATURE OF COAL IN THE PRESENCE OF SWELLING SOLVENTS

Lowell D. Kispert, David Tucker and Wojciech Sady  
Department of Chemistry  
University of Alabama  
Tuscaloosa, Alabama 35487-0336

**KEYWORDS:** Coal, Porosity, Swelling Solvents, Accessibility

## ABSTRACT

A review will be given of the current status of spectroscopic techniques used to study the porous structure of coal with emphasis placed on the recent application of the EPR spin probe method to the study of Argonne Premium Coal Samples (APCS). The spin probe method has provided valuable insight into micropore size and shape characteristics during the swelling process. This technique also proved to be sensitive to changes in the coal structure brought about by variations in swelling solvent polarity, swelling temperature and other modifications of experimental conditions during the swelling process. Successive experiments showed that monitoring the accessibility of spin probes to the pore structure of coal could be used to follow the physical and chemical changes in coal during the weathering process, and to distinguish between the effects of dehydration and oxidation for periods as short as 30 seconds. Some of the results of long term weathering for periods upto six months of exposure to air will be discussed.

## INTRODUCTION

The porous structure of coal has been of concern for many decades. Catalysis in the conversion of coal is generally related to the surface area available to the catalyst. Since most of the surface area of coal lies in the micropore structure of the coal, the determination of this structure and its effect on catalyst accessibility are important in coal conversion.<sup>1,2</sup> The most popular and versatile method for determination of the porous structure of coal is the gas adsorption method. Although this method provides more information than Hg porosimetry or other physical methods, it does have some severe limitations.<sup>3</sup> Several studies have given contradictory data and it has been shown that micropore volumes can vary by more than an order of magnitude when different gases are used.<sup>4</sup> This leads naturally to spectroscopic or imaging methods.

SANS, SAXS and light scattering: In the mid 1980's, methods using small angle neutron diffraction and small angle x-ray diffraction were used with success to characterize the shape and size of the micropores in Illinois # 6 coal.<sup>5-11</sup> It was determined from these studies that the micropores in low-ranked coal had elongated cylindrical shapes which had diameters of about 5.2A. More recently, SAXS has been used to study the pore structure during fluid extraction.<sup>5</sup> It was shown that micropore dilation was an irreversible process, whereas swelling of the macropore system was a reversible process.<sup>5</sup> In 1981, Kalliat et. al. used small angle x-ray scattering to show that there were three classes of pore systems in coal.<sup>6</sup> These results were somewhat consistent with adsorption data interpretation at that time. Small angle x-ray scattering was used later on by Setek et. al. in 1983 to determine the micropore structure of brown coal.<sup>7</sup> SAXS has also been used by Nemmers et. al. in 1990 to study the porous structure of coal during fluid extraction.<sup>5</sup> During various stages of fluid extraction of coal with THF, small angle x-ray scattering experiments showed that the extensive micropore structure formed during fluid exposure played a key role in the interaction between the fluid and the coal matrix needed for substantial extraction yields.<sup>5</sup> It was determined by Tricker et. al. in 1983 that small angle neutron scattering could be used to effectively determine pore size distributions in various ranked coals.<sup>9</sup> They felt that since the data obtained were substantiated by gas adsorption techniques, SANS could be used to probe coal porosity under circumstances where gas adsorption techniques were either severely limited or not possible.<sup>9</sup> Likewise, in 1983, Kaiser and Gethner also used small angle neutron scattering to study pore distributions and pore accessibility in coal.<sup>10</sup> It was determined that D<sub>2</sub>O was not able to penetrate uniformly through dried coals.<sup>10</sup> Later, in 1986, Gethner used SANS to determine the void structure of Illinois #6 coal.<sup>3</sup> He determined that the microvoid volumes were elongated and possessed a well defined circular crosssection of about 25A.<sup>3</sup> Also by comparison of aqueous and non-aqueous solutions, it was determined that the surface of the microvoid volume was primarily aliphatic.<sup>3</sup> In 1987, Gethner used SANS and a combination of light scattering and absorption measurements to show that coal is a continuous distribution of voids rather than a well defined, discrete pore distribution, and to separate chemical changes from physical changes in coal during treatment and reactions.<sup>11</sup>

SEM and imaging techniques: Another technique used recently involves SEM analysis during liquid metal infiltration to provide direct imaging of the micropore system.<sup>12</sup> In 1991, Cody and Davis were able to directly image the pore space available to liquid metal (Wood's alloy) in a variety of coal ranks using SEM analysis.<sup>12</sup> They determined that the pores in the lowest rank coal were roughly cylindrical in shape, but that they constituted a rough particle surface and not an interconnected cylindrical pore network.<sup>12</sup> Pore space available to liquid metals in bituminous and higher ranked coals appeared to be made up entirely of microcracks.<sup>12</sup> Around this time, magnetic resonance imaging was also used to study pore structures during swelling.<sup>13</sup> It was shown that coal swells anisotropically; that is, solvents enter the bedding planes and thus the solvent is not distributed uniformly in the coal structure.<sup>13</sup>

#### NMR spin lattice relaxation and proton NMR

Glaves et. al. showed in 1988, that pore size distributions could be derived by deconvoluting measurements of the NMR relaxation spectra and applying a model to the pore fluid behavior.<sup>14</sup>

Xe129 NMR: Recently, Xe129 NMR studies have been used to determine average micropore volumes and diameters.<sup>15,16</sup> Xe-129 NMR was used in 1990 by Wernet et. al. to determine average micropore diameters in Illinois #6 bituminous coal.<sup>15</sup> After performing Xe-129 NMR experiments on spherocarb, which gave results very close to the manufacturer's specifications of microporosity, they found that the average micropore diameter of Illinois #6 coal was 5.2 Å.<sup>15</sup> More recently, in 1991, Tsiao and Botto use this technique to determine the average micropore size of APCS coals and to investigate the effect of weathering on the average micropore size of coals.<sup>16</sup> This information was then used to develop a model to approximate pore sizes and pore size swelling characteristics.<sup>16</sup>

EPR spin probe method: Finally, a technique using EPR to follow the inclusion of molecular probes in the micropore structure has been used to determine pore size and shape characteristics of a range of coals during the swelling process.<sup>17,18,23</sup> This technique has also been used to follow changes in the micropore structure during weathering, oxidation, dehydration and short term oxidation.<sup>24,26-30</sup> The EPR spin probe method was first used to study coal by Silbernagel et. al. in 1981.<sup>17</sup> Later, in 1985, Wu and Kispert expanded this technique to determine micropore size distributions in coal during swelling.<sup>18</sup> This EPR spin probe technique was further developed in this lab to study micropore size distributions and acid / base character of various ranked coals.<sup>19,21</sup> More recently, changes in pore structure and wall chemistry of APCS coals upon swelling at different temperatures and with solvents of various polarities were determined by following the retention characteristics of the coals.<sup>22,23</sup> The results showed that as the polarity of the solvent was increased, the shape of the micropores changed from spherical to cylindrical.<sup>22,23</sup> Additional studies employing EPR spin probe techniques were performed on the breaking up of the hydrogen bonding between bedding planes.<sup>24</sup> To gain insight into the accessible nature of the covalently cross-linked materials during swelling, the EPR spin probe method was used during the swelling of polystyrene-divinylbenzene copolymers which were cross-linked covalently to various extents (2% to 12%).<sup>25</sup> The study showed that hydrogen bonding in coal has a much greater impact than % cross-linking on the micropore structure and swelling character of coal. Despite this, significant amounts of guest molecules could be intercalated into the copolymer structure, even though the copolymers were relatively non-porous.<sup>25</sup> The effect of weathering on the structure and molecular accessibility of spin probes in coal was studied using the EPR spin probe technique.<sup>26</sup> It was shown that after seven days of exposure to air, coals of most ranks exhibited significant changes in spin probe retention.<sup>26</sup> The lower ranked coals (Beulah Zap and Wyodak Anderson), were observed to undergo structural collapse which precluded retention of even the smallest probes, while medium ranked coals actually exhibited improved retention.<sup>26</sup> A detailed analysis of the data collected from the swelling of coals oxidized in a moisture free environment was completed to differentiate between oxidation and the weathering process.<sup>27,28</sup> Eight vacuum dried APCS coals were oxidized in a pure O<sub>2</sub> environment and weathered in air, and the effects of oxidation alone on coal structure were determined by the intercalation of EPR spin probes.<sup>27,28</sup> It was shown that the removal of water was primarily responsible for the structural collapse observed in low ranked coals and for the increase in retention of polar spin probes in medium ranked coals.<sup>27</sup> Coals oxidized in a pure oxygen environment showed an increase in retention by as much as a factor of five.<sup>28</sup> Even the higher ranked coals showed significant retention of polar spin probes after four days of exposure to oxygen.<sup>28</sup> Studies of short term exposure of Illinois #6 to dry Argon and Oxygen were accomplished using the EPR spin probe technique.<sup>29</sup> It was determined that exposure to a dry gas could affect dramatic changes in the coal structure in as little as 30 seconds.<sup>29</sup> Currently, more detailed analyses of the effects of long term weathering for as long as six months have been carried out and will be discussed further in this paper.

## EXPERIMENTAL

Samples of eight APCS coals (Beulah Zap, Wyodak Anderson, Blind Canyon, Illinois #6, Lewis Stockton, Pittsburgh #8, Upper Freeport and Pocahontas #3, defined previously<sup>20</sup>) were stored in vials which were exposed to the air but protected from dust or other contaminants during the period of exposure. During the weathering period, the samples were agitated each day to insure complete exposure of the coal to the air. At various points during the weathering period of six months, samples were swelled in one millimolar solutions of each spin probe in the swelling solvents toluene and pyridine. The spin probes used for this study are shown in Figure 1, VI (3-carboxy-2,2,5,5-tetramethylpyrrolidine-1-oxyl), VII (TEMPAMINE) and VIII (TEMPO). 30 mg of each coal was mixed with 2mLs of the pyridine or toluene spin probe solution. The mixture was then stirred for 18 hours so that the swelling would reach an equilibrium. The coal was then filtered and vacuum dried for 2 hours. After this the samples were washed with cyclohexane, a non-swelling solvent, to remove any spin probes on the surface or any spin probes not trapped in the coal structure. The samples were again vacuum dried and then sealed in the evacuated EPR tubes. The concentration of spins in each sample was calculated from the EPR spectra as previously described.<sup>19</sup>

## RESULTS AND DISCUSSION

The concentration of spin probe VII retained in weathered APCS coals after swelling is shown as a function of rank and days of oxidation in Figure 2. The front edge at zero days of oxidation represents the retention of spin probe VII in fresh coals as a function of rank. Since toluene does not swell coal to a large extent, the data represents changes in structure and active site functionality during the weathering process which facilitate or inhibit interaction and retention of the polar amino spin probe. It can be seen at  $b_0$  that the retention of fresh Beulah Zap (74.05% carbon dmmf) is about  $2800 \times 10^{15}$  spins per gram. This concentration drops to about  $1000 \times 10^{15}$  spins per gram after 7 days of weathering. By comparing these data with the retention of spin probe VIII, it has been previously determined that this decrease is caused by a physical collapse of the structure brought about by water removal.<sup>26</sup> After 14 days of weathering, shown at  $b_{14}$ , Beulah Zap does not show much change. However, extending the weathering period out to 36 days and even further to 64 days shows a continuing drop in spin probe retention indicated at  $b_{36}$  and  $b_{64}$ . There is a slight increase as the period of exposure to air reaches 114 days, shown at  $b_{114}$ , but essentially the following changes are relatively small compared to the weathering period. It has been shown previously during exposure to pure oxygen in a dry environment, that oxidative changes in Beulah Zap will reopen the structure to polar spin probes. This clearly is not the case during exposure to air, and it can be inferred from this data that the presence of moisture in the air inhibits oxidation in Beulah Zap lignite.

The retention character of Illinois #6 (80.73% carbon dmmf) can be similarly tracked on the three dimensional plot shown in Figure 2. The retention of spin probe VII in fresh Illinois #6 is about  $750 \times 10^{15}$  spins per gram as shown at  $i_0$ . An increase in retention is observed after 7 days of exposure shown at  $i_7$  to about  $2800 \times 10^{15}$  spins per gram. This is followed at 14 days of exposure by a decrease in retention to about  $1200 \times 10^{15}$  spins per gram indicated at  $i_{14}$ . At 36 days of exposure, the retention of the spin probe is increased to  $2300 \times 10^{15}$  spins per gram as shown by  $i_{36}$ . It seems that an equilibrium is reached at 36 days, for further weathering has little effect on spin probe retention shown at  $i_{64}$ ,  $i_{114}$  and  $i_{180}$ . The initial increase in spin probe retention in Illinois #6 is attributed to removal of water from active sites with minimal collapse of the physical structure. Since the water loss in Illinois #6 has not reached an equilibrium by 14 days,<sup>27</sup> it can be asserted that a partial collapse inhibits the retention of spin probes at this point. The changes which bring about the increase in retention at 36 days must be primarily due to oxidative changes in the coal structure since the water loss has reached an equilibrium by this point.

It can be seen in Figure 2 that higher ranked coals are also affected by the weathering process. Fresh Upper Freeport coal (88.08% carbon dmmf) exhibits almost no retention of spin probe VII, as shown at  $u_0$ . As the coal is weathered for 7 days, an increase in retention is observed, shown at  $u_7$ . This increase reaches over an order of magnitude as the weathering period is extended to 14 days at  $u_{14}$ . This represents the maximum retention of Upper Freeport coal, for a decrease in retention is observed at 36 days and no further changes are observed after this. Like Illinois #6, the accessibility of Upper Freeport coal seems to reach an equilibrium at 36 days of exposure to air.

A two dimensional plot of the retention of spin probe VII is shown in Figure 3 for Beulah Zap, Illinois #6 and Upper Freeport coals. It can be more easily seen in this plot that little change is affected after a weathering period of 36 days. However the same is not true for Wyodak

Anderson (76.04% carbon dmmf), Blind Canyon (81.32% carbon dmmf) and Lewis Stockton (85.47% carbon dmmf) coals (shown in Figure 4), which undergo changes throughout the 6 month weathering period studied. This would indicate that oxidation does continue throughout this period. Some comparison to data collected for long term weathering of coals swelled in pyridine might provide additional insight into this process.

## CONCLUSION

It has been shown through the study of the collapse of the Beulah Zap structure, that the presence of moisture in air can inhibit oxidational changes. The structure of Illinois #6 is made much more accessible by long term weathering, and very little change of the structure is observed by monitoring the amino spin probe. Even the higher ranked coals are made more accessible during the weathering process, although this accessibility reaches a maximum after 14 days for Upper Freeport coal. Many of the coals do not exhibit continuing changes in retention of spin probe VII after 36 days.

## ACKNOWLEDGMENT

This work was supported by the U.S. Department of Energy, University Coal Grant Program, Grant No. DE-FG22-93PC93202.

## REFERENCES

1. Markova, K.; Radev, G.; Kostova, N. *Khim. Tverd. Topl. (Moscow)*, **1992**, *3*, 20-22
2. Itoh, M.; Demurs, A.; Oda, H.; Yokokawa, C. *Coal Sci. Technol.*, *11<sup>th</sup> (Int. Conf. Coal Sci., 1987)* **1987**, 527-530
3. Larsen, J. W.; Wernett, P. C. *Energy and Fuels* **1988**, *2*(5), 719-720
4. Larsen, J. W.; Wernett, P. C. *Prepr. Pap. Am. Chem. Soc., Div. Fuel Chem.* **1992**, *37*(2), 849-855
5. Nemmers, S.; Horne, D. K.; Bale, H. D. *J. Appl. Phys.* **1990**, *68*(7), 3178-3186
6. Kalliat, M.; Kwak, C. Y.; Schmidt, P. W. *ACS Symp. Ser.*, *169 (New Approaches Coal Chem.)* **1981**, 3-22
7. Setek, M.; Wagonfeld, H. K.; Stacy, W. O.; Kiss, L. T. *Fuel*, **1983**, *62*(4), 480-482
8. Gethner, J. S. *J. Appl. Phys.*, **1986**, *59*(4), 1068-1085
9. Tricker, M. J.; Grint, A.; Audley, G. J.; Church, S. M.; Rainy, V. S.; Wright, C. J. *Fuel* **1983**, *62*(9), 1092-1096
10. Kaiser, H.; Gethner, J. S. *Proc.-Inter. Conf. Coal Sci.* **1983**, 300-303
11. Gethner, J. S. *Prepr. Pap. Am. Chem. Soc., Div. Fuel Chem.* **1987**, *32*(1), 239-246
12. Cody, G. D.; Davis, A. *Energy and Fuels* **1991**, *5*(6), 776-781
13. Cody, G. D.; Larsen, J. W.; Siskin, M. *Energy and Fuels* **1988**, *2*, 340
14. Galves, C. L.; Davis, P. J.; Gallegos, D. P.; Smith D. M. *Energy and Fuels* **1988**, *2*(5), 662-668
15. Wernett, P. C.; Larsen, J. W.; Yamada, O.; Yue, H. J. *Energy and Fuels* **1990**, *4*(4), 412-413
16. Tsiao, C.; Botto, R. E. *Energy and Fuels* **1991**, *5*(1), 87-92
17. Silbernagel, B. G.; Ebert, L. B.; Schlosberg, R. H.; Long R. B. *Adv. Chem. Ser.* **1981**, *192*, 23-35
18. Wu, S. K.; Kispert, L. D. *Fuel* **1985**, *64*, 1681-1686
19. Goslar, J.; Kispert, L. D. *Energy and Fuels* **1989**, *3*, 589-594
20. Goslar, J.; Cooray, L. S.; Kispert, L. D. *Fuel* **1989**, *68*, 1402-1407
21. Goslar, J.; Kispert, L. D. *Fuel* **1990**, *69*, 564-569
22. Spears, D. R.; Kispert, L. D.; Piekara-Sady, L. *Fuel* **1992**, *71*, 1003-1014
23. Spears, D. R.; Sady, W.; Kispert, L. D. *Prepr. Pap. Am. Chem. Soc., Div. Fuel Chem.* **1991**, *36*, 1277
24. Spears, D. R.; Sady, W.; Kispert, L. D. *Fuel* **1993**, *72*, 1225-1233
25. Spears, D. R.; Sady, W.; Tucker, D.; Kispert, L. D. *Energy and Fuels In Press*
26. Sady, W.; Kispert, L. D.; Spears, D. R. *Prepr. Pap. Am. Chem. Soc., Div. Fuel Chem.* **1992**, *37*, 1151
27. Sady, W.; Tucker, D.; Kispert, L. D.; Spears, D. R. *Prepr. Pap. Am. Chem. Soc., Div. Fuel Chem.* **1993**, *38*, 1323
28. Tucker, D.; Kispert, L. D. *Prepr. Pap. Am. Chem. Soc., Div. Fuel Chem.* **1993**, *38*, 1330
29. Tucker, D.; Kispert, L. D. *Prepr. Pap. Am. Chem. Soc., Div. Fuel Chem.* **1993**, *38*, 1335
30. Vorres, K. S. *Energy and Fuels* **1990**, *4*, 420-426

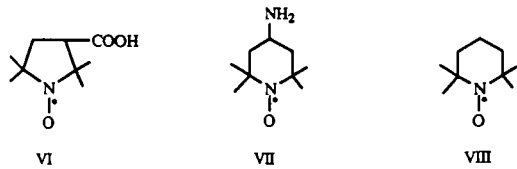


Figure 1. Spin probes VI, VII, and VIII.

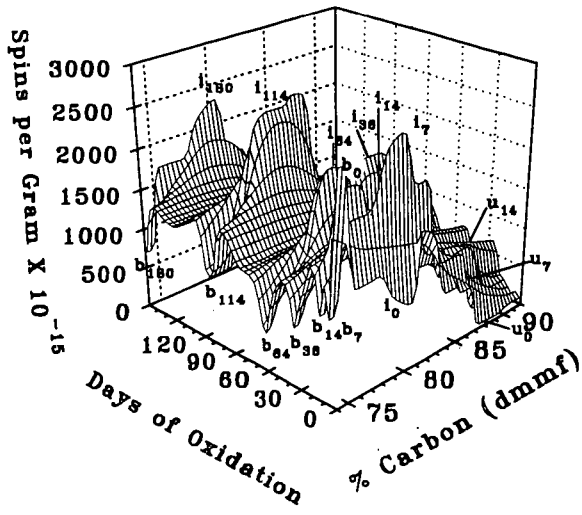


Fig.2 Spin probe VII concentration in fresh APCS coals weathered in air and swelled in toluene.

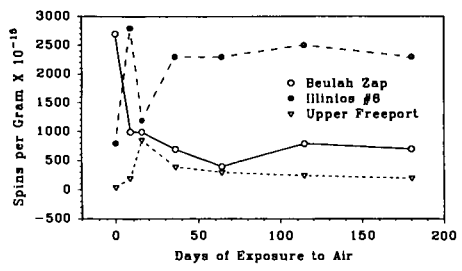


Fig.3 Spin probe VII concentration in fresh APCS Beulah Zap, Illinois #8 and Upper Freeport coals weathered in air and swelled in toluene

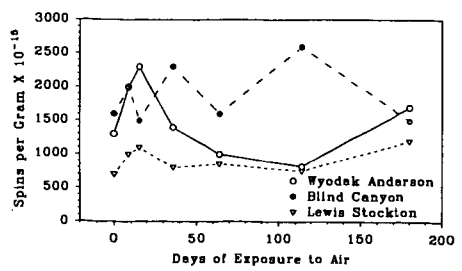


Fig.4 Spin probe VII concentration in fresh APCS Wyodak Anderson, Blind Canyon and Lewis Stockton coals weathered in air and swelled in toluene

# NMR Imaging of Heterogeneous Coal Macromolecular Networks

George D. Cody, David C. French and Robert E. Botto

Chemistry Division, Argonne National Laboratory, 9700 So. Cass Ave.  
Argonne, IL 60439

Keywords: Microscopy, NMR, Coal

## Introduction

Over the past few years, we have been developing new NMR imaging strategies for probing the chemical and physical structure of coal. Early experiments focused on proton NMR imaging techniques for spatially resolving individual macerals within a solid coal specimen.<sup>1</sup> Distinction of individual macerals was achieved by taking advantage of differences in proton density or in spin-lattice relaxation rates, which were shown to vary significantly between the two maceral types. With the implementation of multipulse proton line narrowing in the presence of large static magnetic field gradients, together with back-projection reconstruction NMR imaging methods<sup>2</sup>, we were able to image and distinguish macroscopic resinite and vitrinite regions within a 2-mm X 2-mm X 1.4-mm specimen of Utah Blind Canyon (APCS No. 6) coal to an in-plane resolution of about 150  $\mu\text{m}$ .

More recent efforts have focused on obtaining information concerning solvent accessibility in coals and maceral domains by proton NMR imaging of mobile proton distributions resulting from solvent swelling.<sup>3</sup> Imaging in the presence of deuterated solvents illuminated proton distributions of mobile phases within the coal macromolecular structure preferentially. Images with resolutions of 40 to 80  $\mu\text{m}$  were obtained using protic solvents, and showed the presence of different macerals, mineral cleats, and microfractures. Regions which differed with regard to pyridine accessibility were also contrasted in the images. We also were prompted by the initial investigation to elucidate the details of transport behavior of pyridine into coal during swelling. In that study,<sup>4</sup> time-resolved proton NMR images of pyridine penetrating a homogeneous sample of high volatile bituminous A rank vitrain (APCS No. 4) that had been pre-extracted with pyridine were used to describe the uptake behavior. In addition to coal swelling in pyridine, we investigated transient state imaging results from three polymer-solvent systems for comparison: polyethylmethacrylate swollen in methanol, polymethylsilicone swollen in hexafluorobenzene, and isobutyl rubber swollen in toluene. A model for case II transport in coals was described.

The purpose of this presentation is to review these earlier studies and to provide an overview of the present and future applications of NMR imaging for coal structure determination.

## Results and Discussion

### Solvent Swelling Studies.

Since the early work of Sanada and Honda, solvent swelling has been employed to probe the physical structure of coal.<sup>5</sup> The swelling behavior of bituminous coals in solvents such as pyridine has been used to assess different strengths or types of secondary interactions which determine the macromolecular structure of coal.<sup>5-9</sup> These include weak interactions of less than  $\sim 15 \text{ kcal mol}^{-1}$ , such as hydrogen bonding, van der Waals interactions, weak complexes, and  $\pi$ -electron intermolecular interactions.<sup>10-12</sup> The secondary interactions which can be broken by one solvent may be unaffected by a different solvent. A high degree of secondary interactions imparts rigidity to the macromolecular structure in coals, whereas disruption of these secondary interactions by a good swelling solvent mobilizes the structure. Pyridine has been found to effectively relax all of the secondary interactions in coal, leaving only covalent bonds intact.<sup>10,11</sup> It is known that the chemical heterogeneity of coal leads to anisotropic swelling.<sup>12</sup> Coal swelling has been found to be greater perpendicular to the bedding plane than parallel to it.<sup>13</sup> Cracking at mineral-organic interfaces is also expected due to differential swelling of the organic matrix relative to mineral matter.

Important information concerning solvent accessibility to the pore structure and maceral domains in coals also may be obtained by imaging mobile proton distributions resulting from solvent swelling. Images of coals swollen with perdeuterated solvents can be used to map mobile phases in the coal macromolecular structure, while images obtained with protic solvents map distributions of the ingressed solvent.

Here, we discuss the results from two different three-dimensional (3D) NMR imaging techniques for spatially mapping mobile proton distributions in coals that have been swollen with pyridine- $d_5$  or pyridine. Three-dimensional back-projection techniques

employing a 3D Radon transform inversion reconstruction algorithm were used to map mobile proton distributions on the basis of  $T_1$  (spin-lattice relaxation time) differences. Contrast based on differences in  $T_2$  (spin-spin relaxation time) was achieved employing 3D gradient recalled echo (GRE) pulse sequence for data acquisition, and image reconstruction by 3D Fourier transform (FT). Both techniques display proton distributions of mobile phases within the solid preferentially. Images with resolutions of 40 to 80 microns show the presence of different macerals, mineral cleats, microfractures, and the distribution of mobile macromolecular phases in solvent swollen coals. Regions which differ with regard to pyridine accessibility are also contrasted in the images.

The proton NMR spectrum of a specimen of Utah Blind Canyon coal swollen with pyridine- $d_5$  showed three distinct proton resonances. There was a broad resonance (ca. 27 kHz) arising from rigid protons, and there were two considerably narrower resonance lines discernable as aromatic and aliphatic signals arising from protons in environments of high molecular mobility. Analysis of the broad and narrow components revealed that 14% of the protons are found in regions of high mobility. The fraction aromaticity of mobile phase protons calculated from line simulation was 0.45 compared to a value of 0.24, obtained from proton CRAMPS analysis of the dried coal. The estimated contribution to the total proton signal from residual protons in the pyridine- $d_5$  was less than 0.1%, while the observed  $f_a^H$  increased nearly two-fold as a result of swelling. Clearly, there is a substantial enhancement in the amount of motionally narrowed aromatic proton signal due to swelling.

The 3D surface-rendered NMR image of the Utah coal swollen with pyridine- $d_5$  was a good representation of the general topology of the actual specimen. For example, a dark feature was found which is known to be a macroscopic crack from solvent swelling the coal. Other dark features on the surface were derived from regions where rigid macromolecular proton signal is suppressed by employing a short relaxation delay; the magnetization of the rigid phase is saturated due to the longer  $T_1$  of these protons.

An 80-micron thin section (slice) through the 3D radon reconstruction showed image contrast from the same sources affecting the 3D surface-rendering. Mobile proton phases resulting from relaxation of the secondary interactions in the coal by swelling with pyridine- $d_5$  appear bright. Void spaces or mineral deposits which lack protons appear dark. In addition to regions of low proton density, regions of the rigid macromolecular network with long  $T_1$ 's in the coal appear dark due to the  $T_1$  saturation effects.

The  $^1H$  single-pulse NMR spectrum of pyridine-swollen Lewiston-Stockton coal exhibited a single resonance from the pyridine protons exclusively, whose linewidth was 424 Hz. The  $^1H$  linewidth of pyridine in the Utah coal was 340 Hz. The  $T_1$  of pyridine protons in both samples was measured by progressive saturation, and a value of approximately 1.3 ms was obtained. The baseline-to-baseline projection width of the Lewiston-Stockton coal recorded with the GRE pulse sequence and the phase-encoding gradients off was 11.2 kHz, and that of the Utah coal was 13.5 kHz. The pyridine natural linewidths and baseline-to-baseline projection widths, along with the  $1\text{mm}^3$  specimen sizes, afforded an in-plane resolution of 50 and 40 microns, respectively, for the two coals.

The 3D surface-rendered GRE images of the Utah and Lewiston-Stockton pyridine swollen coals exhibited bright features resulting from regions in the coals which contain a high density of mobile pyridine; dark areas resulted from regions which are inaccessible to the solvent. Photographs of the Utah and Lewiston-Stockton coal showed a close correspondence between the shape of the coal specimens and the surface-rendered GRE image geometries. Also, features devoid of pyridine such as pits, cracks, and gouges appeared magnified in the images. The vertical feature on the front face of the 3D surface-rendering of the Lewiston-Stockton specimen showed a microscopic structure contiguous with the surface of the specimen which is inaccessible to pyridine. The photograph showed that this is a solid region in the coal rather than a void space.

Slices of the interior of the Lewiston-Stockton coal show the presence of contrasting horizontal bands in the  $xy$ -plane similar to the lamellar structures visible in the photograph of the coal. A dark vertical feature was seen which corresponds to the same region which appears as a void in the 3D surface-rendering, and indicated that this interior structure runs through the object to its surface. Since the photograph shows that this area of the specimen is solid, the dark structure in the images is clearly a region of low pyridine accessibility rather than a void space. When the coal was swollen with pyridine, the secondary interactions binding strata within the specimen were relaxed. Contrasting bands in the images showed that differential swelling in the bedding plane has produced microfractures and regions with greater or lesser pyridine accessibility.

This preliminary investigation has shown that 3D NMR imaging is a promising tool for studying solvent swelling of coals. This non-destructive technique revealed rich microscopic detail concerning the penetration and accessibility of a solvent into the interior of coal specimens. Further development of this technique also presents the possibility for visualization and analysis of the dynamics of the coal swelling process which can be used to elucidate coal physical structure. In addition, several preparatory pulse sequences prior to the imaging experiment may be employed for the quantitative characterization of NMR relaxation phenomena and solvent diffusion in coals. Image contrast produced by differences in the mobility of the macromolecular network in the coal will be compared with image contrast produced by differences in solvent accessibility in the same specimen. Coal

specimens with known petrography will be utilized and correlated with NMR images obtained using multiple-pulse proton decoupling methods prior to the solvent swelling measurements.

### Solvent Transport Studies

Significant insight into the character of solvent transport has been obtained through time-resolved, direct imaging of concentration gradients during solvent uptake. Early on, optical microscopic methods revealed that solvent transport in some macromolecular networks did not conform to Fickian kinetics.<sup>14</sup> Specifically, these systems exhibited steep-gradient solvent fronts which propagate into a sample at a constant velocity, much like a shock wave; such behavior has been called case II transport to distinguish it from Fickian transport.

Case II transport is not restricted to synthetic polymers. Biopolymers and geopolymers such as cellulose and bituminous coals, for example, also exhibit case II transport behavior under suitable conditions.<sup>10,14,15</sup> All that is required for case II transport is that the dry network exist initially in a glassy state and that the penetrating solvent is capable of suppressing  $T_g$ .

Given the interesting physical behavior of glassy networks near their glass transition, the search for a theoretical basis for non-Fickian behavior has been irresistible for both experimentalists and theorists. To date, numerous theories abound.<sup>16-24</sup> While the specific approaches to this problem vary from one model to another, universally they rely on the generality that case II behavior results from coupled solvent diffusion and network relaxation.<sup>25,26</sup> There are several rigorous approaches which quantify case II transport in terms of a relatively small set of physically based dynamic parameters.<sup>19-24</sup> These models tend to be valid only for very small displacements from equilibrium, because linear behavior of the governing equations is required in order to obtain an analytical solution. Large scale departures from equilibrium conditions requires that the concentration dependence on each of the dynamic parameters be considered explicitly. This has resulted in a complicated data analysis, stemming from a many-fold expansion of the parameter set and, consequently, an increase in the total number of degrees of freedom of the model.

Many, if not most, applications involving solvent-macromolecular systems are far from equilibrium. In the present paper, the essential characteristics of case II transport are exploited for the purpose of reducing the dynamic parameter set size, in order to simplify quantification under conditions far from equilibrium, e.g., the situation of solvent transport following immersion of a dry macromolecular network into a solvent reservoir. Case II transport of methanol in polyethylmethacrylate (PEMA) and pyridine in coal is explored and compared with Fickian transport of toluene in polybutadiene rubber (PBD) and hexafluorobenzene in polymethylsilicone (PMS) using magnetic resonance microscopy and optical microscopy.

The characteristic relaxation times for each solvent-network system were established at full dilution using a standard inversion-recovery pulse sequence to derive  $T_1$ , and a Hahn spin-echo pulse sequence to derive  $T_2$ . It is acknowledged that in protonated solvent systems, contributions to the signal intensity can arise from both the protons in the solvent and protons associated with the mobile network. Analysis of the NMR spectral and dynamic characteristics of these swollen networks in deuterated solvents reveals that, in general, only a minor contribution to the total signal intensity results from the mobile network protons. This contribution is significant, however, in the case of PBD in toluene. No signal is detectable from the rigidly bound protons in the glassy regions of PEMA or coal due to severe dipolar broadening (linewidth  $> 20$  kHz) in the rigid solid. Obviously, in the case of  $^{19}\text{F}$  imaging of solvent transport into polymethylsilicone, signal is derived from the solvent exclusively.

In the present experiments, two-dimensional (2D) images are sufficient to elucidate the fundamental aspects of the transport phenomena. In order to ensure that the transport process was also two dimensional, the upper and lower sample surfaces were protected from solvent infiltration by glass cover slips which restricted the flow of solvent to cross only the exposed faces of each sample. Each sample is rectangular with initial dimensions on the order of  $1.2 \times 1.2 \times 1$  mm. The experimental protocol involved immersing the sample in the solvent for a period of time, removing it from the solvent bath, acquiring an image, and re-immersing it. During the imaging stage the sample was placed in cell with "plugs" such that the free volume within the cell was minimized. It was anticipated that this would reduce the amount of desorption over the duration of the imaging.

In order to obtain sufficiently high quality images, given the dynamic behavior of the three protonated solvent/macromolecule systems, it was necessary to acquire 24 (128 point) transients with a recycle delay of 200 ms for each of 128 phase-encoded gradient positions using a standard imaging spin-echo pulse sequence.<sup>27</sup> This yielded reasonably high quality 2D images, with a resolution on the order of  $70 \mu\text{m}$ , which was obtained over intervals of approximately 10 min. Typically a 64-kHz spectral width was chosen, establishing an echo time on the order of 0.5 ms. In the case of  $^{19}\text{F}$  imaging, a longer  $T_1$  and an inherently lower sensitivity of the nucleus necessitated the acquisition of 32 scans per phase encoded position and a recycle delay of 500 ms; this resulted in a time interval on the order of 30 min to obtain a quality image. It is clear that during the time that the images are acquired some

spatial averaging does take place. However, in all cases, the entire uptake process takes between 3 to 4 hrs, and therefore, it is assumed that the averaging is relatively minor.

A 2D  $^{19}\text{F}$  image projection of a specimen of polymethylsilicone swelling in hexafluorobenzene, observed at some intermediate time, exhibited a shallow concentration gradient into the core of the specimen. The 2D image of polyethylmethacrylate in methanol was strikingly different; in this case a sharp front was observed with a nearly constant solvent concentration behind the front.

Magnetic resonance imaging data in the form of 1D slices, reconstructed from the center of the 2D image projections, revealed sequential cross-sections through PBD diluted in toluene; a sizable contribution to the image intensity arose from the protons associated with the rubbery PBD itself. Superimposed on this was the additional signal due to the solvent. Clearly evident, however, were the smooth, exponential, solvent gradients directed into the core of the sample, indicating a Fickian transport mechanism. Fickian transport was also revealed in the case of the fluorinated solvent in PMS. Smooth solvent gradients were clearly evident despite the lower signal-to-noise ratios obtained in the  $^{19}\text{F}$  images.

The character of transport was drastically different for PEMA swollen in methanol. The presence of a sharp solvent front and solvent absent core clearly indicated case II transport. This behavior is typical of many acrylate polymers swollen in a variety of solvents, and it has been detected previously by NMR imaging techniques.<sup>28-30</sup> The imaging results gave some indication of a sigmoidal solvent front similar to that derived numerically, and suggested that the NMR images might be used to help constrain values of the solvent activity. Pyridine transport in coal also exhibited case II behavior, whose signature was revealed by sharp solvent fronts moving into the sample. The situation was complicated by the formation of a crack on the left side of the lower most cross-section, which destroyed the symmetry of the solvent fronts. The formation of cracks accompanying case II transport is not unusual, nor unexpected, considering the magnitude of the strain gradients along the solvent front.

The measured front velocities were constant for both the PEMA and the bituminous coal, consistent with case II transport. There was some concern that a degree of spatial uncertainty or blurring may occur during evolution of the front within the imaging interval, leading to an apparent reduction in the gradient of the solvent front. Furthermore, distortions in image intensity due to  $T_2$  effects were expected to add some further degree of uncertainty. The accuracy of the magnitudes of the front velocities derived from magnetic resonance imaging, however, are not subject to these effects. Hence, the velocities provide a valuable and quantitative constraint for the parameterization of the uptake data.

Direct measurement of linear dilation accompanying swelling is a simple means to quantify the overall swelling behavior of rubbery networks.<sup>31,32</sup> Linear dilation behavior for PBD and PMS were consistent with Fickian transport in rubbery networks. Given the uptake data, it was trivial to derive a mass-fixed diffusion coefficient through linear fitting of the experimental data. The generation of a curve for Fickian transport, in the present case, requires solving the two-dimensional diffusion equation and integrating this solution with respect to time. Fitting of the dilation data results in values of  $D_R = 2.5 \times 10^{-6} \text{ cm}^2/\text{s}$  and  $1.1 \times 10^{-6} \text{ cm}^2/\text{s}$  for PBD-toluene and PMS-hexafluorobenzene, respectively. These relatively large values of  $D_R$  reflect the high degree of inter- and intra-molecular mobility of these networks, which explains the rapidity with which the rubbery systems respond to applied stresses that are osmotic in nature.

In the case of solvent transport in systems undergoing a glass transition, or case II transport, we have defined the uptake behavior using three parameters: a characteristic cooperative diffusion coefficient,  $D_c$ , governing dilation of the network; a molecular relaxation rate constant,  $\beta$ , which is given by the relationship  $\beta = K_{os}/\eta_1$ , where  $\eta_1$  is the bulk viscosity and  $K_{os}$  is the osmotic modulus; and a critical solvent concentration,  $C^*$ , above which there is a transformation of the network from a glass to a rubber. However, there are several degrees of freedom associated with the present model of case II transport. Without constraints on the magnitude of  $C^*$  or  $\beta$ , it is not possible to uniquely define the three transport parameters. In the present case the dilation data for both PEMA and bituminous coal were fitted to characteristic case II curves, using  $\beta$  as a floating variable while  $C^*$  was independently constrained. The final constraint used was the solvent front velocity,  $v$ , obtained from magnetic resonance imaging.

A relationship between  $C^*$  and solvent concentration was established by relating the change in free volume of the solvent-polymer system to contributions from the respective free volumes of polymer and solvent taken independently. Essentially linear  $T_g$  suppression with concentration is observed at low solvent concentrations,  $\Delta T = -kC_S$ , where  $\Delta T = T_{g,\text{supp}} - T_{g,\text{dry}}$ ,  $k$  is typically in the range of 200 - 500 °K for a variety of solvents, and  $C_S$  is the volume fraction of the solvent. Recalling that  $T_g$  of PEMA is only 308 °K, the value of  $C_S$ , accordingly, is anticipated to be very small. Using a lower value of  $k$ , we calculate  $C_S = 0.05$ , yielding  $C^* = 0.17$ . Bituminous coal is reported to have its  $T_g$  on the order of 650 to 700 °K, suggesting that  $C_S$  of pyridine must be very high. Indeed, calculations along these lines have indicated that  $C_S$  (calculated) actually exceeds the equilibrium  $C_S$  associated with coal diluted at room temperature at a solvent activity of 1.0.<sup>33</sup> On the basis of this analysis, it would appear that pyridine is not capable of suppressing coal's  $T_g$  to less than room temperature, which is inconsistent with the present results. Recent experimental results derived from incremental solvent sorption isotherm experiments on bituminous coal,

however, clearly indicate the presence of a glass transition at solvent activities less than 1.0, yielding a magnitude of  $C^*$  on the order of 0.65.<sup>34</sup>

The gross dilation behavior of both samples was clearly case II with an unambiguous sigmoidal uptake profile. The essential character of the present model for case II transport processes is revealed when comparing the swelling kinetics of these two glassy networks. Both samples are essentially the same size, with uptake occurring over essentially the same interval of time. The glassy diffusion coefficients for the two samples are also very similar in magnitude. The coal's network relaxation rate following the glass transition, however, is almost 15 times larger than that of PEMA. It is the relative magnitudes of the critical concentration parameter,  $C^*$ , which compensates for this disparity in the relaxation dynamics and results in comparable overall uptake times. For the case of PEMA swollen in methanol,  $C^*$  is relatively small. In the present model, network relaxation at the glass transition drives diffusion; all other things remaining equal, the sooner relaxation occurs the faster transport evolves.

Comparing all four samples, the nearly two order of magnitude difference in diffusion coefficients between the Fickian and case II systems is compensated by the lack of any phase-transition induced, network relaxation in the Fickian systems. Generally, these results confirm assertions made by authors of one of the earliest papers on the applications of magnetic resonance imaging to diffusion in glassy polymers;<sup>28</sup> i.e., it is the presence of the phase transition which drives the overall diffusion process.

#### Acknowledgement

This work was performed under the auspices of the Office of Basic Energy Sciences, Division of Chemical Sciences, U. S. Department of Energy, under contract number W-31-109-ENG-38.

#### References

1. Dieckman, S. L.; Gopalsami, N.; Botto, R. E. *Energy & Fuels* **1990**, *4*, 417.
2. Grangeat, P.; Hatchadourian, G.; Le Masson, P.; Sire, P. *Logiciel Radon, Notice Descriptive Des Algorithmes Et Des Programmes* 1990, Version 2.1 du 13-04-1990, LETI/DSYS/SETI/90-180 PS: Grenoble, 1990.
3. French, D. C.; Dieckman, S. L.; Botto, R. E. *Energy & Fuels* **1993**, *7*, 90.
4. Cody, G. D.; Botto, R. E. *Energy & Fuels*, **1993**, *7*, 561.
5. Sanada, Y.; Honda, H. *Fuel* **1966**, *45*, 295.
6. Green, T.; Kovac, J.; Brenner, D.; Larsen, J. W. *Coal Structure*; Meyers, R. A., Ed.; Academic Press: New York, 1982; Chapter 6.
7. Nelson, J. R.; Mahajan, O. P.; Walker, Jr., P. L. *Fuel* **1980**, *59*, 831.
8. Peppas, N. A.; Lucht, L. M. *Chem. Eng. Commun.* **1984**, *30*, 291.
9. Suuberg, E. M.; Lee, D.; Larsen, J. W. *Fuel* **1985**, *64*, 1668.
10. Brenner, D. *Fuel* **1985**, *64*, 167.
11. Quinga, E. M. A.; Larsen, J. W. In *New Trends in Coal Science*; Yurum, Y., Ed.; HRT NATO ASI Series 244; Kluwer Academic Publishers: Boston, 1988.
12. Quinga, E. M.; Larsen, J. W. *Energy Fuels* **1987**, *1*, 300.
13. Brenner, D. *Fuel* **1984**, *63*, 1324.
14. Alfrey, T. E.; Gurnee, E. F.; Lloyd, W. G., *J. Polym. Sci.*, **1966**, *12*, 249.
15. Maffei, P.; Kiéné, L.; Canet, D., *Macromolecules*, **1992**, *25*, 7114.
16. Ensore, D. J.; Hopfenberg, H. B.; Stannett, V. T. *Polymer*, **1977**, *18*, 793.
17. Jou, D.; Camacho, J.; Grmela, G. *Macromolecule*, **1991**, *24*, 3597.
18. Thomas, N. L.; Windle, A. H. *Polymer*, **1982**, *23*, 529.
19. Vrentas, J. S.; Duda, J. L. *J. Polym. Sci., Polym. Phys. Ed.*, **1977**, *15*, 403.
20. Jackle, J.; Frisch, H. L. *J. Poly. Sci. Polymer Phys. Ed.*, **1985**, *23*, 675.
21. Durning, C. J. *J. Poly. Sci. Polymer Phys. Ed.* **1985**, *23*, 1831.
22. Durning, C. J.; Tabor, M. *Macromolecules*, **1986**, *19*, 2220.
23. Neogi, P. *AIChE Journal*, **1983**, *29*, 829.
24. Neogi, P. *AIChE Journal*, **1983**, *29*, 833.
25. Hopfenberg, H. B.; Frisch, H. L., *J. Polym. Sci., Part B*, **1969**, *7*, 405.
26. Vrentas, J. S.; Duda, J. L. *AIChE J.*, **1975**, *21*, 894.
27. Callaghan, P. T. *Principles of Nuclear Magnetic Resonance Microscopy*, Oxford Science Publications, Clarendon Press, Oxford 1991.
28. Mareci T. H.; Dønstrup, M.; Rigamonti, A. J. *Mol. Liquids*, **1988**, *38*, 185.
29. Weisenberger, L. A.; Koenig, J. L. *Macromolecules*, **1990**, *23*, 2445.
30. Mansfield, P.; Bowtell, R.; Blackband, S. *J. Magn. Res.*, **1992**, *99*, 507.
31. Tanaka, T.; Fillmore, D. J. *J. Chem. Phys.*, **1979**, *70*, 1214.
32. Landau, L. D.; Lifshitz, E. M. *Theory of Elasticity*, Pergamon Press, New York, NY, 1959.
33. Lucht, L. M.; Larsen, J. M.; Peppas, N. A. *Energy & Fuels* **1987**, *1*, 56.
34. Green, T., *personal communication*.

David H. Buchanan  
Department of Chemistry  
Eastern Illinois University  
Charleston, IL 61920-3244

Keywords: Coal, Solvent Extraction, Swelling

### INTRODUCTION

The early history of solvent extraction in coal research has been reviewed by Van Krevelen. (1) From the beginning, solvent extraction has been used to isolate and characterize both soluble and insoluble coal fractions. The recent studies covered in this report fall into four broad areas: 1) Improvement in extraction yields or selectivity; 2) Correlation of solvent swelling and extraction behavior to structural models for the insoluble organic portion of coal; 3) Analyses of extracts to identify and perhaps quantify organic compounds in the raw coal and 4) Use of solvent extraction to predict or influence coal behavior in some other process such as liquefaction. To cover this active area in a brief Preprint, references were chosen to illustrate both the current status of the field and cite related studies.

The availability of the pristine Argonne Premium Coal Samples (2) has led to a significant improvement in the reproducibility of solvent extraction as an analytical tool. In 1984, Triolo and Child cautioned that solvent extraction may be an inherently unreproducible process. (3) Based on studies of how weathering affects solvent extraction, that was a fair statement at the time. (4) With the improvements and standardization of solvent extraction practices developed since then, it is now possible to obtain reproducible and reliable information from the solvent extraction of coal.

### EXPERIMENTAL

Protection of pristine coal samples and solvent extracts from air is necessary if colloid-free extract solutions are to be isolated. (4) Solvents must be of high purity if large volumes are to be concentrated by evaporation or distillation for product isolation. Soxhlet extraction, stirring -100 mesh coal with a large volume of solvent for several days or ultrasonic irradiation for 30-90 minutes at room temperature have all been reported to give the same extract yield for a given solvent/coal combination. (4) (5) (6) (7) Complete separation of extract from insoluble residue requires either membrane filtration (Nylon or Teflon of 0.45  $\mu$  pore size, pre-filter needed if colloids are present) or centrifugation at 24,000g or greater. Removal of hydrocarbon solvents such as toluene from extract and residue can be accomplished by drying to constant weight at elevated temperature and reduced pressure (100°, 0.1 Torr). Removal of nitrogen containing solvents requires washing with specific solvents such as 80% methanol/water for pyridine or DMF (4) or acetone/water for N-methyl-2-pyrrolidinone (NMP) (6) before vacuum drying.

### DISCUSSION

1) Improvement in yield or selectivity. "Solvent Extract" is an operational definition for material isolated from the complex and inhomogeneous mixture which is coal. Unless the separation process is specified, including filter pore size or centrifugation clearing factor, the material isolated is not well defined and may not be the same as that isolated by other workers. This is especially true for coals subject to weathering. We showed that insoluble colloids were present in polar solvent extracts of Argonne coals which were exposed to air during or after extraction. The colloids passed ordinary filter paper or fritted glass funnels but were removed by 0.45  $\mu$  membrane filtration or ultracentrifugation. (4) Weathered coals are less prone to colloid formation, presumably because the reactive material is no longer present. Additional insight into the effect of weathering and moisture removal on the accessibility of coals to solvents was given by Kispert using intercalation of epr spin probes. (8) Even brief air exposure caused measurable changes in the retention of polar probes by Ill. No. 6 coal. Most workers dry coal before extraction in order to determine extract yields and material balances; however this may collapse pore structure in low-rank coals and produce other changes in high-rank coals. Even drying at 100° can induce cross-linking reactions in low-rank coals which reduce pyridine swellability. (9)

Pyridine is a good solvent for many coals and has been extensively studied. Selected extraction data for the Argonne Premium Coals are given in Table 1. All material balances are 94-102% and the lab to lab variation in yield is typical of recent studies. Pyridine cannot be completely removed from coal or extracts by heating, either under reduced pressure or in a flow of nitrogen. In our experience, 80% methanol/water washing followed by vacuum drying is the most effective method to remove pyridine or DMF in terms of minimizing the time and volume of wash solvent used - which minimizes chances for air oxidation or loss of slightly soluble minerals. This wash solvent has a high heat of wetting for coal surfaces. (10) Trace amounts of either DMF or pyridine can be detected by FT-IR spectroscopy (4) and the human nose is quite sensitive to traces of pyridine on coal fractions.

Efforts to increase extraction yields include Liotta's addition of (n-Bu)<sub>4</sub>NOH in methanol for ultrasonic pyridine extraction of several coals. (11) For Argonne coal 301 the yield increased from 28 to 70% only when the good swelling agent, (n-Bu)<sub>4</sub>NOH in methanol, was present. Our results on the effect of acid demineralization on pyridine extraction yields of Argonne coals 201, 301, 401 and 801 are shown in Figure 1. The increase in yield for low-rank coals may be, in part, the effect of converting carboxylic acid salts into pyridine soluble acids. Our preliminary results on the effect of demineralization on toluene extraction yields for Ill. No. 6 coals show that, although the absolute yield is much smaller, the relative increase after demineralization is greater than with pyridine. This is consistent with the view that, given enough time for mass transport, a good swelling solvent such as pyridine can remove soluble material by diffusion through the organic matrix but a poorly swelling solvent such as toluene removes material only via the interconnected pore network, portions of which may be blocked by minerals.

Iino used CS<sub>2</sub>/NMP mixed solvent, with and without ultrasonic irradiation, to remove from 30-66% by weight of soluble material from 29 of the 59 coals they studied. (6) Results for the Argonne coals are also listed in Table 1. Based on analyses of coals, extracts and residues as well as extraction of separated macerals, they suggest a synergistic effect due to the good solvent and swelling character of the NMP and high diffusibility of the CS<sub>2</sub>. Morgan has recently reported that KOH or NaOH added to NMP or DMF extractions of South African and the Argonne coals gave extracts containing up to 80% of the carbon from the feed coals. (12) However, from the information given, the absence of colloids or material balances cannot be determined. Other strong base treatments of pyridine extract residues also lead to high total yields of extract at modest temperatures. (13)

Supercritical solvent extraction has been used by several groups to study coal porosity (14) or to remove organic (15) or elemental sulfur (16) from coal, either as a prototype desulfurization process or as an analytical method. For the isolation of analytical samples for GC or HPLC analyses the method is quick and equipment requirements modest. (17)

2) Correlation of solvent swelling and extraction with structure. Solvent extraction is often used to prepare the insoluble residue for solvent swelling studies which are used to infer structural information by reference to the literature on solvent swelling of cross-linked polymers. Access to this active field can be gained from recent papers by Green, (18) Iino, (19) Larsen, (20) Nishioka, (21) Painter (22) and Snape. (23) Current work shows that brief heating of coals with solvents in which they are not soluble, such as water or chlorobenzene, causes irreversible changes in swelling and extraction yields with good solvents (defined as those such as pyridine which swell and extract coal to the greatest extent.) The suggestion that new cross-links such as hydrogen bonds have been established (19) has been criticized by Painter who notes that hydrogen bonds are dynamic and cannot serve as true cross-links as do the covalent bonds in cross-linked polymers. (22) Physical association with strong concentration and temperature dependence is suggested as a better representation than a cross-linked network for the insoluble portion of most coals. (21) The implications for coal liquefaction if this model is substantiated are profound.

3) Analyses of Extracts. Modern size exclusion chromatography (SEC) is a powerful method for determining molecular weight

distributions of mixtures. Because coal fractions usually contain both polar and non-polar molecules, interpretation of SEC data is difficult. Advantages and problems with THF(24), NMP(25) and pyridine(26) as SEC mobile phases for coal fractions are discussed in the references cited. Solvents which prevent self-association of coal molecules (pyridine, DMF, NMP) give more realistic molecular weights but limit the choice of SEC detectors. The common refractive index detector over-estimates the contribution of oxygen rich species such as phenols and gives average molecular weights which are too high unless calibrated with appropriate compounds. Changes in SEC molecular size distributions find use in studies of the progress of coal liquefaction and other processes. A novel recent use is the screening of microorganisms which bio-degrade coal.(27)

Among the methods which have the possibility for identification of specific compounds in solvent extracts, GC/MS has been the most studied. For this purpose, solvents such as benzene/methanol(28) have the advantage of extracting only molecules which can be volatilized in a typical GC or MS inlet and thus need no fractionation before analysis. In contrast, during FIMS analysis of the toluene insoluble portion of a pyridine extract, only 34% of the sample was volatilized.(4) A disadvantage to non-polar solvents is that potentially soluble molecules may not be accessible to the solvent and their absence may bias the conclusions drawn. To avoid this problem, chromatographic fractionation of pyridine extracts is often used to isolate fractions which can be analyzed by mass spectroscopy. In the usual methods, elution from a silica gel(29) or alumina column(5)(30) produces increasingly polar coal extract fractions which may be further fractionated on other supports for specific analyses. A typical application is the study of terpenoid biomarkers in coal to better understand the progress of the coalification process.(31)(5)

Solvent extraction is often used to prepare samples for IR, NMR, X-ray and other analyses, the results of which are discussed by other speakers at this Symposium. Elemental sulfur in coal can be determined by perchloroethylene (PCE) extraction followed by HPLC analysis(32) or GC analysis of supercritical extracts.(15)

4) Solvent extraction as related to other processes. Pre-treatment of coals with solvents prior to liquefaction often leads to increased yields of desirable products, lower conversion temperatures or both. Studies utilizing both very polar(33) and non-polar solvents(34) illustrate the complexity of the effects in that both swelling and non-swelling solvents can improve liquefaction depending on the process and coal used. Recent work using chlorobenzene(35) appears to support the view that, since solvents which disrupt molecular aggregates without bond cleavage increase liquefaction conversions, physical association is an important structural feature in coal.(21)

Removal of noxious elements such as sulfur by simple solvent extraction of coal is an attractive idea. However the claim that PCE extraction removes organic sulfur in a coal desulfurization process is controversial. ASTM organic sulfur reductions of up to 40% following PCE extraction have been reported,(36) however the effect appears to be due to removal of elemental sulfur ("organic sulfur" by ASTM) produced by pyrite oxidation.(37)

#### **SUMMARY**

With careful attention to anerobic conditions and clarification of solutions, solvent extraction of coal is a useful, reproducible technique for coal science. Studies of the extraction process itself and the related solvent swelling provide important insights into coal matrix structure while analyses of the extracts provide increasingly detailed information about the chemical species present in both extract and raw coal.

#### **ACKNOWLEDGEMENTS**

In addition to those cited, experimental work at EIU was carried out by Cindy Ludwig, Stanislav Kalembasa and Yunsong Tong. Funding was provided, in part, by the Illinois Department of Energy and Natural Resources through the Illinois Clean Coal Institute (formerly CRSC) and by the US DOE (Grant Number DE-PC22-92PC 92521). The opinions and conclusion expressed herein are those of the author and do not necessarily reflect the views of IDENR, ICCI and the DOE.

## REFERENCES

- (1) Van Krevelen, D.W. "Coal: Typology-Chemistry-Physics-Constitution", Elsevier, Amsterdam; (1981); Chapter 10.
- (2) Vorres, K.S. *Energy Fuels* **1990**, 4, 420-426.
- (3) Triolo, R.; Child, H.R. *Fuel* **1984**, 63, 275.
- (4) a) Buchanan, D.H.; Warfel, L.C.; Mai, W.; Lucas, D. *Prepr. Pap.-Am. Chem. Soc., Div. Fuel Chem.* **1987**, 32(1), 146-153. b) Buchanan, D.H.; Osborne, K.R.; Warfel, L.C.; Mai, W.; Lucas, D. *Energy Fuels* **1988**, 2, 163-170.
- (5) Chang, H.K.; Bartle, K.D.; Markides, K.E.; Lee, M.L. in "Advances in Coal Spectroscopy", H.L.C. Meuzelaar, Ed.; Plenum Press, New York, (1992), Chap. 7.
- (6) a) Iino, M.; Takanohashi, T.; Ohsuga, H.; Toga, K. *Fuel* **1988**, 67, 1639-1647. b) Takanohashi, T.; Iino, M. *Energy Fuels* **1990**, 4, 452-455. c) Takanohashi, T.; Ohkawa, T.; Yanagida, T.; Iino, M. *Fuel* **1993**, 72, 51-55.
- (7) Pugmire, R.J.; Solum, M.S.; Bai, S.; Fletcher, T.H.; Woods, S.; Grant, D.M. *Prepr. Pap.-Am. Chem. Soc., Div. Fuel Chem.* **1993**, 38(2), 647-654.
- (8) a) Tucker, D.; Kispert, L.; Sady, W. *Prepr. Pap.-Am. Chem. Soc., Div. Fuel Chem.* **1993**, 38(4), 1330-34. b) Tucker, D.; Kispert, L. *Prepr. Pap.-Am. Chem. Soc., Div. Fuel Chem.* **1993**, 38(4), 1335-1340.
- (9) Suuberg, E. M.; Otake, Y.; Yun, Y.; Deevi, S.C. *Energy Fuels* **1993**, 7, 384-392.
- (10) Wightman, J.P.; Glanville, J.B.; Hollenhead, J.B.; Phillips, K.M.; Tisa, K.N. *Prepr. Pap.-Am. Chem. Soc., Div. Fuel Chem.* **1987**, 32(1), 205.
- (11) Matturro, M.G.; Liotta, R.; Reynolds, R.P. *Energy Fuels* **1990**, 4, 346-351.
- (12) Morgan, D.L. *Prepr. Pap.-Am. Chem. Soc., Div. Fuel Chem.* **1992**, 37(4), 1996-2001.
- (13) Winans, R.E.; McBeth, R.L.; Hunt, J.E. *Prepr. Pap.-Am. Chem. Soc., Div. Fuel Chem.* **1993**, 38(2), 561-564 and references therein.
- (14) Olson, E.S.; Diehl, J.W.; Horne, D.K.; Bale, H.D. *Prepr. Pap.-Am. Chem. Soc., Div. Fuel Chem.* **1988**, 33(4), 826-831.
- (15) a) Yurum, Y.; Ozyoruk, H.; Altuntas, N.; Gulce, H. *Energy Fuels* **1993**, 7, 620-624. b) Muchmore, C.B.; Chen, J.W.; Kent, A.C.; Tempelmeier, K.E. *Prepr. Pap.-Am. Chem. Soc., Div. Fuel Chem.* **1985**, 30(2), 24-34.
- (16) Louie, P.K.K.; Timpe, R.C.; Hawthorne, S.B.; Miller, D.J. *Fuel* **1993**, 72, 225-231.
- (17) Hawthorne, S.B. *Anal. Chem.* **1990**, 62, 633A-642A.
- (18) Green, T.K.; Selby, T.D. *Prepr. Pap.-Am. Chem. Soc., Div. Fuel Chem.* **1993**, 38(4), 1316-1322.
- (19) Fujiwara, M.; Ohsuga, H.; Takanohashi, T.; Iino, M. *Energy Fuels*, **1992**, 6, 859-862.
- (20) Larsen, J.W.; Mohammadi, M. *Energy Fuels* **1990**, 4, 107.
- (21) a) Nishioka, M. *Fuel* **1992**, 71, 941-948. b) Nishioka, M. *Fuel* **1993**, 72, 997, 1001, 1011.
- (22) Painter, P. *Energy Fuels* **1992**, 6, 863-864.
- (23) McArthur, C.A.; Hall, P.J.; MacKinnon, A.J.; Snape, C.E. *Prepr. Pap.-Am. Chem. Soc., Div. Fuel Chem.* **1993**, 38(4), 1290-1296.
- (24) Bartle, K.D.; Mills, D.G.; Mulligan, M.J.; Arnaechina, I.O.; Taylor, N. *Anal. Chem.* **1986**, 58, 2403-2408.
- (25) Lafleur, A.L.; Nakagawa, Y. *Fuel* **1989**, 68, 741-752.
- (26) Buchanan, D.H.; Warfel, L.C.; Bailey, S.; Lucas, D. *Energy Fuels* **1988**, 2, 32-36.
- (27) Polman, J.K.; Quigley, D.R. *Energy Fuels* **1991**, 5, 352-353.
- (28) Neill, P.H.; Xia, Y.; Winans, R.E. *Prepr. Pap.-Am. Chem. Soc., Div. Fuel Chem.* **1989**, 34(3), 745-751.
- (29) Farcasiu, M. *Fuel*, **1977**, 56, 9.
- (30) Later, D.W.; Lee, M.L.; Bartle, K.D.; Kong, R.C.; Vassilaros, D.L. *Anal. Chem.* **1982**, 53, 1612.
- (31) Hayatsu, R.; McBeht, R.L.; Neill, P.H.; Winans, R.E. *Energy Fuels* **1990**, 4, 456-463.
- (32) Buchanan, D.H.; Coombs, K.J.; Murphy, P.M.; Chaven, C. *Energy Fuels* **1993**, 7, 219-221.
- (33) Joseph, J.T. *Fuel* **1991**, 70, 179; 459.

- (34) Larsen, J.E.; Hall, P.J. *Energy Fuels* 1991, 5, 228.
- (35) McArthur, C.A.; Hall, P.J.; Snape, C.E. *Prepr. Pap.-Am. Chem. Soc., Div. Fuel Chem.* 1993, 38(2), 565-570.
- (36) a) Lee, S.; Kesavan, S.K.; Lee, B.G.; Ghosh, A.; Kulik, C.J. *Fuel Sci. Technol. Int.* 1989, 1, 443-468. b) Atwood, G.A.; Leeche, H.H. *Coal Prep.* 1991, 11, 77-86.
- (37) a) Hackley, K.C.; Buchanan, D.H.; Coombs, K.; Chaven, C.; Kruse, C.W. *Fuel Process. Technol.* 1990, 24 431-436. b) Chou, M.-I.M.; Lytle, J.M.; Ruch, R.R.; Kruse, C.W.; Chaven, C.; Buchanan, D.H. *Prepr. Pap.-Am. Chem. Soc., Div. Fuel Chem.* 1992, 37(4), 2002-2009.

TABLE 1. Solvent Extraction Yields of Argonne Premium Coals

APCS #	% C MAF <sup>a</sup>	Wt % Toluene <sup>b</sup>	Wt % Pyridine <sup>b</sup>	Wt % Pyridine <sup>c</sup>	Wt % Pyridine <sup>d</sup>	Wt % CS <sub>2</sub> /NMP <sup>e</sup>
801	73		2.9	3.1	3.1	2.3
201	75	2.3	7.1	7.4	6.2	9.9
301	78	7.0	25.8	27.5	27.9	33.1
601	81				32.1	33.6
401	83	5.8	29.7	29.8	26.5	39.0
701	83				14.7	27.1
101	86	0.6	20.9	6.9	14.9	59.4
501	91	0.4	1.2	0.8	0.5	2.8

<sup>a</sup> Ref. 2; <sup>b</sup> This work; <sup>c</sup> Ref. 5; <sup>d</sup> Ref. 7; <sup>e</sup> Ref. 6.

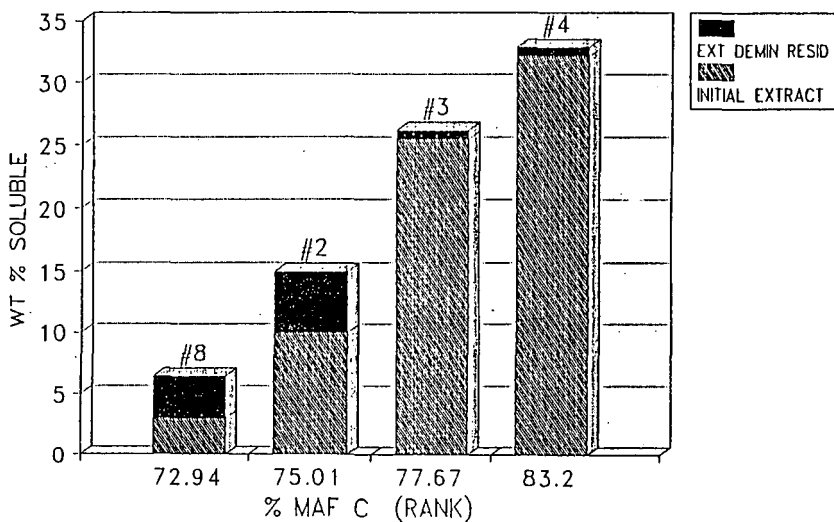


Figure 1. Yields of additional pyridine soluble material extracted from the demineralized, pyridine-insoluble residues of four Argonne Premium coals as a function of coal rank.

# PROGRESS IN COAL PYROLYSIS RESEARCH

Peter R. Solomon and Michael A. Serio  
Advanced Fuel Research, Inc.  
87 Church Street  
East Hartford, CT 06108

KEYWORDS: Pyrolysis, Coal, Crosslinking

## INTRODUCTION

This paper considers some of the recent progress in both the improved understanding and the identification of areas uncertainty with regard to coal pyrolysis, rates, and mechanisms. The paper addressed two questions:

- what are the controlling chemical factors in coal pyrolysis?
- what are the controlling physical factors in coal pyrolysis?

The factors considered are summarized in Table 1. The problem of answering the questions is that multiple chemical reactions occur whose results depend on how the reactants are bound in the coal macromolecular network. Species-selective transport of the reactants and products further complicate the interpretations. In what follows, we have tried to focus on topics where answers are needed or where significant new progress is being made.

TABLE 1

## FACTORS WHICH CONTROL COAL PYROLYSIS

<u>CHEMICAL</u>	<u>PHYSICAL</u>
Bond Breaking Reactions	Tar Vaporization
Retrogressive / Crosslinking Reactions	Viscosity
Effects of Cations	Network Effects
Effects of H <sub>2</sub> O	
Effects of O <sub>2</sub>	
Network Effects	

### Chemical Factors

**Bond Breaking** - The bond breaking reactions can be separated into two broad categories, those which release small molecular side groups attached to the macromolecular network and those which break bonds holding the network together to form a collection of fragments called *metaplast*. Study of the former category is easier because, in this case, reactions of a limited number of identifiable functional groups lead (without significant mass transfer limitations) to the production of a limited number of identifiable gas species. The chemistry has been organized into global reactions of functional groups to form specific products.

Study of the latter category of reactions is particularly complicated because: i) the reactants are large, heterogeneous and often insoluble; ii) multiple reactions are generally required to free a product, and iii) removal of products from the reacting *metaplast* is subject to mass transfer limitations. Global rates can be determined for the overall reactions.

In general, all reaction rates need to be represented by a distribution of reaction parameters about an average (e.g., a Gaussian distribution of activation energies) because of the heterogeneous chemical nature of coals. While much progress has been made in describing the classes of reactions and measuring global rates, a quantitative description of the detailed chemistry of pyrolysis is not yet possible. This objective remains as an important goal.

Of particular interest is the systematic rank dependence of the reaction rates (the rates for all reactions decrease with increasing rank) which has recently been reported (1-3). These experiments were performed at several low heating rates where the temperature of coal particles can be accurately determined and hence the rates accurately measured. Experiments at high heating rates, in which coal particle temperatures are measured (4-9), indicate that extrapolation of the rates measured at low heating rates to high heating rates is reasonable. In addition, some progress has been made in considering higher rank coals to be the results of nature's pyrolysis of lower rank coals in the coal bed over millions of years. These analyses employ pyrolysis rates extrapolated to the lower bed temperatures (6,10,11). For some pyrolysis products, nature's removal of the higher reaction rate part of the distribution can explain the systematic shift in the average rate with rank. This is illustrated in Figure 1 which compares the water evolution curves during pyrolysis of several Argonne coals with predictions for Zap lignite after a simulated maturation at various temperatures.

**Crosslinking** - Crosslinking reactions are particularly hard to identify because the products are insoluble. Crude measurements can be made of "crosslink density" without identification of the specific crosslinking bond. Such measurements are made by solvent swelling (12) or carbon NMR (9,13). In addition, measurements of the mobile phase by proton NMR (14,15) or by solvent extraction (16) provide data on the variation in the concentration of mobile molecules as they are formed or linked into the network.

The results from pyrolysis studies at heating rates between 0.5 and 1000 K/sec show that crosslinking is rank dependent, with lignites crosslinking at lower temperatures than bituminous coals (17,18). Crosslinking in lignites occurs prior to tar evolution and the rapid loss of weight and aliphatic hydrogen. Crosslinking in high volatile bituminous coals occurs at temperatures slightly higher than the temperature for maximum tar evolution, weight loss, and aliphatic hydrogen loss.

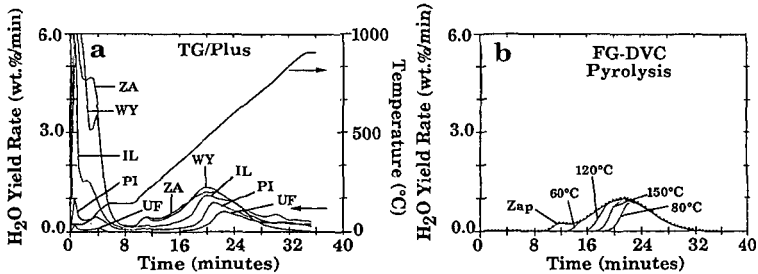


**Figure 1.** Evolution of H<sub>2</sub>O from Five Argonne Premium Coals: (a) Pyrolyzed at 30 K min<sup>-1</sup>; (b) Predicted for Slow Pyrolysis (geological ageing) at Different Temperatures followed by Pyrolysis at 30 K min<sup>-1</sup>. ZA, Beulah Zap Lignite; Wy, Wyodak Anderson Subbituminous; IL, Illinois No. 6 HVB; PI, Pittsburgh No. 8 HVB; UF, Upper Freeport MVB. (from Ref. 6).

Studies correlating the crosslink density with other pyrolysis reactions have identified a connection between low temperature crosslinking and CO<sub>2</sub> (and possibly H<sub>2</sub>O evolution). These low temperature crosslinking reactions are also related to a loss of carbonyl and hydroxyl functional groups in the coal (17), which is consistent with a loss of carboxyl groups. Similarly, a correlation exists between moderate temperature crosslinking and CH<sub>4</sub> evolution, and high temperature condensation of the macromolecular network and H<sub>2</sub> evolution (17,18).

As in the case of bond breaking reactions, global pathways and rates have been identified for crosslinking reactions but the detailed chemistry is still an important target for study.

**Effects of Cations** - Crosslinking has also been observed to be influenced by the presence of alkali metals, whose removal increases pyrolysis tar yields (19-22). These results would indicate that the role of carboxyl groups, as indicated above, is important, but it is the carboxylate (cation exchanged carboxyls) which are the key agents in retrogressive reactions for low rank coals. The role of calcium in reducing liquefaction yields from low rank coals has been suggested in previous work by Mochida et al. (23) and Joseph and Forrai (24). It is also consistent with work which shows an effect of calcium on reducing pyrolysis tar yields (19-22). The role of calcium may be to provide a nascent crosslink site in the coal by allowing coordination of groups like carboxyl and hydroxyl which are prone to such reactions. Otherwise, these sites would be more likely to coordinate with water (through hydrogen bonding) than with each other.

**Effects of H<sub>2</sub>O** - The presence of water appears to have a profound effect on the course of pyrolysis. Effects of water during pyrolysis have been studied by Lewen (25) and Monthieux and Landais (26). The impact of water is illustrated in Figure 2 modified from Ref. 26.

The figure presents the atomic H/C ratio as a function of O/C ratio for several pyrolysis experiments. For the line labeled path 1, the pyrolysis system is open and pyrolysis products escape the pyrolysis vessel as they are formed. For these experiments, both oxygen and hydrogen are lost in comparable amounts as pyrolysis proceeds. For path 2, the pyrolysis system is closed. Pyrolysis products fill the pyrolysis vessel and can re-react with the pyrolyzing char. The result is a reduction in the loss of hydrogen and an increase in the loss of oxygen. For path 3, the system is confined to minimize any space into which pyrolysis products can escape. Under these conditions, the loss of hydrogen is further retarded, while the loss of oxygen is accelerated. The path taken by the char is now similar to nature's maturation sequence shown by the shaded band in Fig. 2 for coals from the same bed. The interpretation of these results, as well as the other hydrous pyrolysis experiments suggests that the presence of water due to the confinement of the system results in significant changes in the pyrolysis chemistry. Since the loss of oxygen functional groups is desirable to improve liquid yields from

pyrolysis and liquefaction, and since it is one of the dominant mechanisms in the maturation of coal, understanding and controlling these reactions involving H<sub>2</sub>O is an important target.

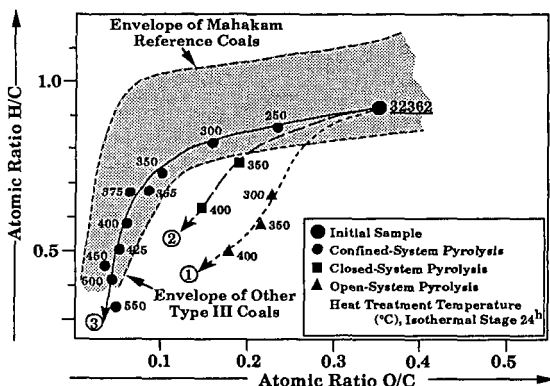


Figure 2. Influence of Confinement Conditions on Elemental Composition of Pyrolysis Chars (from Ref. 26).

**Oxygen** - The effect of oxygen on coal pyrolysis is most often exhibited through weathering. Low temperature oxidation of the coal results in reduced yields of tar and liquids as well as reduced fluidity. A feature of coal oxidation is that often a very small amount of oxygen added to the coal can cause significant effects in subsequent pyrolysis and liquefaction. Why oxidation has such a profound effect may be a result of changes in the network geometry as discussed in the next section.

**Network Effects** - Recognizing the macromolecular network nature of coal, a number of network models have been developed (27-30). These models assume the network to be made of thermally stable aromatic ring clusters connected by less stable bridges. When the network is heated, random cleavage of the less stable bridges leads to a collection of network fragments called the metaplast. The molecular weight distribution has been computed using chain statistics (31,32), percolation theory (6,29,30), and Monte Carlo methods (6,27,28). The lightest fraction of the metaplast can vaporize to form tar. Somewhat heavier molecules can be extracted. The heaviest molecules, which are mobile but are not easily extracted, and the extractable molecules provide the coal's fluidity. What is important about the network models is the effect of the network geometry (i.e., whether it is a chain-like or fish-net-like) on the products of pyrolysis. This effect is illustrated in Fig. 3 (from Ref. 6) which presents the molecular weight distribution of network fragments as a function of the average number of bridges per cluster,  $\alpha$ , for two geometries represented by the coordination number,  $1 + \sigma$ . The coordination number is the maximum number of bridge attachments per cluster. The figure presents results for  $\sigma + 1 = 2.2$  (Fig. 3a) which is chain-like (1 extra bridge or crosslink every

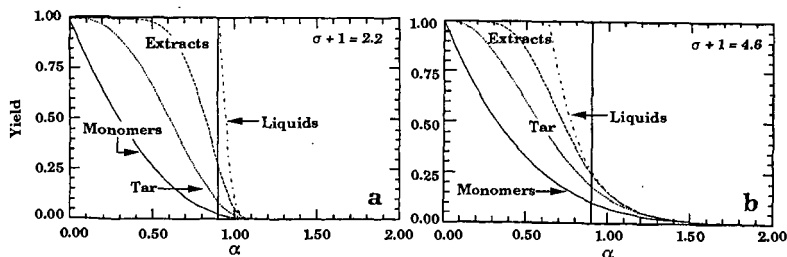


Figure 3. Percolation Theory Predictions for Macromolecular Network Fragment Molecular Weight Distribution as a Function of the Average Number of Attachments per Ring Cluster,  $\alpha$ . For a)  $\sigma + 1 = 2.2$ ; b)  $\sigma + 1 = 4.6$  (from Ref. 6). Monomers are all Single Clusters. Tar Consists of Monomers, Dimers, and Trimers. Extracts Consist of Molecules up to 10-nmers and Liquids Consist of Molecules up to 100-nmers.

5th cluster) and  $\sigma + 1 = 4.6$  (Fig. 3b) which is fish-net-like. As can be seen, the molecular weight distributions are quite different. In Fig. 3a there is nearly an even distribution of all molecular sizes, while in Fig. 3b the small molecules are favored. The former case would represent the highly fluid char of high volatile bituminous coal, while the latter would represent a non-softening (thermosetting) lignite or subbituminous coal. The importance of low temperature crosslinking events in low-rank coals or in oxidized high rank coals is that the network coordination number is increased. A few added crosslinks does not have a strong influence on the bond breaking chemistry, but rather changes the product distribution through its influence on the network geometry.

### **Physical Factors:**

**Tar Vaporization** - The tar fraction in pyrolysis consists of molecules heavy enough to condense at room temperature. The source for this material is the small unattached "molecular" fraction of the network plus small molecular fragments produced by pyrolysis. The removal of these molecules is controlled by mass transfer including: vaporization, diffusion, and convective transport. The removal process is in competition with the repolymerization process. Recent models suggest that the tars reach their equilibrium vapor pressure (or close to it) in the light gases produced in pyrolysis and are transported through the char primarily by convection through the pores or by bubble motion (6,28,33,34).

**Fluidity** - The fluidity of coal as it is heated is typically measured with a Geissler plastometer. High to medium volatile bituminous coals exhibit the highest fluidities. As temperature increases, measurable fluidity appears at a temperature of 350°C. The initial fluidity is reversible and is attributed to physical melting (35). As temperature increases, fluidity increases due to irreversible bridge breaking reactions and then decreases due to crosslinking (36). Low temperature crosslinking in low rank coals can prevent the onset of any observable fluidity.

Models relate fluidity to the amount of the liquid or mobile phase (16,36-38) which can be predicted from network models (6,27-30,35). Experiments which measure the liquid content or mobile phase (14-16) all show similar temperatures for the onset, peak and disappearance of the coal fluidity (6).

**Network Effects** - The physical effects (tar formation, solvent interactions, and fluidity) are related to the molecular weight distribution of small molecules in the coal, the network fragments forming the metaplast during pyrolysis, and the bonding forces holding these molecules together. Thus, the effect of the network is important because of the effect of network geometry on the molecular weight distribution (see Fig. 3). Low temperature crosslinking in low rank coals leads to a high effective coordination number and hence low amounts of tar and extracts and low fluidity. The lack of such crosslinking in bituminous coals leads to high yields of extracts and tars and high fluidity. Thus, the application of macromolecular network models appears to unify many observations of coal pyrolysis including tar formation, extract formation, metaplast formation, fluidity, and solvent swelling behavior.

### **CONCLUSION**

The progress during the past ten years of research in coal science has resulted in the maturation of many new experimental techniques to follow coal conversion chemistry including NMR, XPS, XANES, FT-IR, ESR, TG-FTIR, solvent swelling, solvent extraction, and MS. These techniques have been used on coals, chars, tars, extracts, model compounds, and model polymers containing natural and isotopically labeled compounds to follow the chemistry in a variety of coal conversion experiments. The results have led to a new understanding of bridge breaking and crosslinking and their variations induced by solvents, catalysts, water, and oxygen. The results have also led to new macromolecular network models of coal pyrolysis and liquefaction. Such models provide a vastly improved global understanding of coal conversion behavior, but detailed understanding of the controlling reactions has not yet been achieved. Such detailed understanding and the resulting strategies for controlling the conversion behavior is the central challenge of coal science in the future.

### **ACKNOWLEDGEMENTS**

Much of the work performed by the authors was supported by the Morgantown Energy Technology Center of the Department of Energy under Contract No. DE-AC21-86MC23075.

### **REFERENCES**

1. Burnham, A.K., Oh, M.S., Crawford, R.W., and Samoun, A.M., *Energy & Fuels*, **3**, 42, (1989).
2. Solomon, P.R., Serio, M.A., Carangelo, R.M., Bassilakis, R., Gravel, D., Baillargeon, M., Baudais, F., and Vail, G., *Energy & Fuels*, **4**, (3), 319, (1990).
3. Serio, M.A., Solomon, P.R., Charpenay, S., Yu, Z.Z., and Bassilakis, R., *ACS Div of Fuel Chem. Preprints*, **35**, (3), 808, (1990).

4. Solomon, P.R., Serio, M.A., and Markham, J.R., Kinetics of Coal Pyrolysis, Int. Conference on Coal Science Proceedings, IEA, Tokyo, Japan, p. 575, (October 23-27, 1989).
5. Serio, M.A., Hamblen, D.G., Markham, J.R., Solomon, P.R., *Energy and Fuel*, **1**, 138, (1987).
6. Solomon, P.R., Hamblen, D.G., Serio, M.A., Yu, Z.Z., and Charpenay, S., *Fuel*, **72**, 469, (1993).
7. Fletcher, T.H., *Combust. Sci. and Tech.*, **63**, 89, (1989).
8. Fletcher, T.H., "Time-Resolved Particle Temperature Measurements and Mass Loss Measurements of a Bituminous Coal during Devolatilization", *Combustion and Flame*, **78**, 223, (1989).
9. Fletcher, T.H., Solum, M.S., Grant, D.M., and Pugmire, R.J., *Energy and Fuels*, **6**, 643, (1992).
10. Braun, R.L., Burnham, A.K., and Reynolds, J.G., *Energy and Fuel*, **6**, 468, (1992).
11. Solomon, P.R., Serio, M.A., Carangelo, R.M., Bassilakis, R., Yu, Z.Z., Charpenay, S., and Whelan, J., *J. Anal. and Appl. Pyrol.*, **19**, 1-14, (1991).
12. Green, T.K., Kovac, J., and Larsen, J.W., *Fuel*, **63**, 935, (1984).
13. Solomon, P.R., Charpenay, S., Yu, Z.Z., Serio, M.A., Kroo, E., Solum, M.S., and Pugmire, R.J., "Changes During Coal Pyrolysis: Experiment and Theory", presented at the 1991 Int. Conf. on Coal Science, New Castle, England, (Sept. 1991).
14. Marzec, A., Jurkiewicz, A., and Pislewski, N., *Fuel*, **62**, 996, (1983).
15. Lynch, L.J., Webster, D.S., Sakurovs, R., Barton, W.A., and Mahér, T.P., *Fuel*, **67**, 579, (1988).
16. Fong, W.S., Peters, W.A., and Howard, J.B., *Fuel*, **65**, 251, (1986).
17. Solomon, P.R., Serio, M.A., Deshpande, G.V., and Kroo, E., *Energy and Fuels*, **4**, 42, (1990).
18. Suuberg, E.M., Lee, D., and Larsen, J.W., *Fuel*, **64**, 1668, (1985).
19. Tyler, R.J. and Schafer, H.N.S., *Fuel*, **59**, 487, (1980).
20. Morgan, M.E. and Jenkins, *Fuel*, **65**, 764, (1986).
21. Serio, M.A., Kroo, E., Teng, H., Solomon, P.R., *ACS Div. of Fuel Chem. Preprints*, **38** (2), 577 (1993).
22. Wornat, M.J. and Nelson, P.F., *Energy and Fuel*, **6** (2), (1992).
23. Mochida, I., et al., *Fuel* **62**, 659, (1983).
24. Joseph, J.T. and Forrai, T.R., *Fuel* **71**, 75 (1992).
25. Lewen, M.D., in Organic Geochemistry, (M.H. Engel and S.A. Macko, Eds. ), Plenum Press, NY, Chapter 24, to be published.
26. Monthioux, M. and Landais, P., *Energy and Fuels*, **2**, 794, (1988).
27. Gavalas, G.R., Coal Pyrolysis, Elsevier, NY, p. 51 (1982).
28. Solomon, P.R., Hamblen, D.G., Carangelo, R.M., Serio, M.A., and Deshpande, G.V., *Energy and Fuel*, **2**, 405, (1988).
29. Grant, D.M., Pugmire, R.J., Fletcher, T.H., and Kerstein, A.R., *Energy and Fuels*, **3** 175, (1989).
30. Niksa, S. and Kerstein, A.R., *Fuel*, **66**, 1389, (1987).
31. Solomon, P.R. and King, H.H., *Fuel*, **63**, 1302, (1984).
32. Niksa, S., and Kerstein, A.R., *Combustion and Flame*, **66**, 95, (1986); see also *Energy and Fuels*, **5**, 647, (1991).
33. Solomon, P.R., Hamblen, D.G., Carangelo, R.M., Serio, M.A. and Deshpande, G.V., *Combustion and Flame*, **71**, 137, (1988).
34. Niksa, S., *AIChE J.* **34**, (5), 790, (1988).
35. Waters, P.L., *Fuel* **41**, 3, (1962).
36. Solomon, P.R., Best, P.E., Yu, Z.Z., and Charpenay, S., *Energy & Fuel*, **6**, 143, (1992).
37. Fong, W.S., Khalil, Y.F., Peters, W.A., and Howard, J.B. *Fuel*, **65**, 195, (1986).
38. Oh, M.S., "Softening Coal Pyrolysis", Ph.D. Thesis, Massachusetts Institute of Technology, (1985).

## PROGRESS TOWARD THE DESULFURIZATION OF ORGANIC COAL MOLECULES

Leon M. Stock  
Chemistry Division, Building 200  
Argonne National Laboratory  
Argonne, IL 60439

Keywords: Organic Desulfurization

### Introduction

The broad occurrence of sulfur in coal greatly reduces its economic potential, and it is well recognized that the selective removal of the sulfur that is covalently bonded in organic coal molecules constitutes the key challenge for technology. This brief article concerns the character of the organic sulfur compounds, and strategies for the removal of these substances.

### The Organic Sulfur Compounds in Bituminous Coals

There is general agreement (1,2) that sulfur was introduced into coal through secondary reactions of the organic plant materials with inorganic sulfur compounds, and that these substances, which were produced by the microbiological reduction of sulfate ions, reacted with coal precursors in a variety of chemical processes including ionic and free radical substitution and addition reactions. Virtually every model compound experiment that has been performed between a plausible sulfur reagent and an organic substrate has successfully introduced sulfur into the organic matrix. Inasmuch as the natural processes occurred in a variety of different environments, the exact reaction pathways are difficult to define. However, it is evident that the amount of sulfur introduced into the coal precursors and retained in the coal varies significantly.

It has been recognized for a long time that heterocyclic sulfur compounds including thiophenes, benzothiophenes, dibenzothiophenes and other heterocycles and their alkylated derivatives, particularly the methylated compounds, are present in fossil fuels. In addition, many kerogens and the less mature coals have considerable amounts of aliphatic sulfur compounds. Although some workers in this field have been rather slow to accept this view, previous investigations by Attar (3), and Calkins (4) and the recent work of de Leeuw and his coworkers (5,6) on kerogens, and also of Gorbaty (7,8), and Huffman (9,10) and their coworkers on coals has demonstrated that these aliphatic materials are clearly present. Indeed, the aliphatic sulfidic sulfur content of the Argonne Premium Coal Samples increases systematically and the thiophenic sulfur content decreases systematically as the maturity of the coal decreases. The Argonne Premium Sample of lignite contains 30 to 40% aliphatic sulfidic sulfur, but the low volatile, much higher ranking bituminous coal sample contains only 3 to 15% aliphatic sulfidic sulfur (7,8,9,10). Presumably, natural thermal and hydrolytic processes convert the aliphatic sulfur compounds into thiophenic derivatives as the coals mature. The X-ray work and even more recent mass spectroscopic investigations are in good accord with the view that rather high levels of sulfidic sulfur can exist in low rank American coals (7-10,11).

Even more important Winans and White and their associates (11,12,13) have shown that many American coals and high sulfur, low rank coals from Europe such as the Rasa subbituminous coal examined by White and his research group (13) have many molecules with more than one heteroatom. This feature of the chemistry is especially relevant in desulfurization reactions when it is coupled with the concept that these lower ranking coals appear to be dominated by molecules with only one, two, and three rings (14).

In summary, the sulfur rich subbituminous and bituminous coals, of which the coals of the Illinois Basin are often described as representative, are heteroatom rich substances with a broad variety of sulfur compounds bonded to  $sp^3$  as well as to  $sp^2$  carbon atoms and many of the molecules that contain sulfur also contain oxygen atoms. Unfortunately, virtually all of the work on compound speciation has been qualitative, the few quantitative investigations (15) indicate that only a very small fraction of the organic sulfur compounds have actually been defined.

## Desulfurization Methods

New methods of the desulfurization of solid coals have been investigated in several laboratories. This work on coal contrasts with the generally well known strategies for the desulfurization of fossil petroleum materials. Molecules that are freely soluble in oils can generally be desulfurized through catalytic hydrogenation reactions involving catalysts that are based upon molybdenum sulfide (16). This chemistry is illustrated by the coprocessing of subbituminous and bituminous coals with petroleum resids. These catalytic reactions enable high coal and asphaltene conversions with the formation of pentane-soluble products in good yield (17). The pentane-soluble oils that are produced in these reactions are virtually free of oxygen, and have rather low concentrations of sulfur and nitrogen. Specifically, the coprocessing of Illinois No. 6 coal and Lloydminster resid provides a product spectrum in which 80% of the sulfur atoms and 40% of the nitrogen atoms have been removed; the oil that is produced contains 1.2% sulfur and 0.4% nitrogen compared to more than 4% sulfur in the resid and coal that were used as the starting fossil materials (17).

An array of other chemical strategies have been studied for the elimination of the organic sulfur from solid coal. Vigorous basic hydrolysis with molten hydroxides has been investigated in some detail (18). The approach requires very severe conditions for effective organic desulfurization, and as a consequence, many workers in the field have sought much lower severity reactions that might accomplish the goal of selective sulfur elimination without comprising the carbon content of the coal or the heat value of the product. One of the key problems that emerged in the early investigations was the fact that of pyritic, organic, and elemental sulfur simultaneously occur in coals that have been exposed to the atmosphere. The elemental sulfur arises from the air oxidation of pyrite and may be reported as organic sulfur as a consequence of the usual analytical scheme. Unfortunately, this complexity can lead to some confusion in the assessment of desulfurization strategies. One solution to this problem is the removal of pyrite and elemental sulfur from samples prior to research on organic desulfurization. Both oxidative and reductive procedures are available. We found that the reaction with lithium aluminum hydride, was convenient, quantitative, and, more important, was essentially free of byproduct formation (19). It is much easier to interpret the results of desulfurization experiments when these pyrite-free coals or other very low pyrite macerals or kerogens are used as the starting materials.

Our research for new approaches for selective organic desulfurization has been successful, and the primary goal has been realized in principal, but the chemistry cannot as yet be practically applied.

It seems pertinent to mention some of the strategies that have been considered. Acid-promoted hydrolysis reactions have received some attention. In one approach, we attempted to intercept and selectively to hydrolyze hemithioacetal intermediates, but the experiments with coals yielded discouraging results (20). We also examined thermal methods and thermal methods coupled with sulfur capture by metals as well as strategies based on organonickel compounds.

However, we placed most of our effort on single electron transfer reactions. Our ideas were based on the concept that the carbon-sulfur bond strengths in anion radicals would be greatly diminished when these substances were reduced to anion radicals, and on the fact, which has been known for many years, that single electron transfer reactions can eliminate sulfur from heterocyclic and aromatic molecules under quite mild reaction conditions. Investigations of these single electron transfer reactions for pure compounds and representative bituminous coal have been very encouraging and some coals can be almost completely desulfurized in such reactions (21,22). For example, the sulfur content of pyrite-free Illinois No. 6 coal could be reduced by SET chemistry to about 1.1% sulfur under quite mild conditions (21,22).

The study revealed that some sulfidic sulfur compounds in the Illinois coals resisted desulfurization by this SET strategy (22). We then considered the use of strong bases which might be more effective for aliphatic desulfurization (23), even though they are not usually effective for the removal of heterocyclic molecules. These basic reactions had to be carried out near 100°C, and the Illinois coals experienced extensive desulfurization. When the SET and base reactions were carried out sequentially, the organic sulfur content was reduced to about 0.7 wt%. Subsequent work has demonstrated that the remaining sulfur compounds have fragile carbon-sulfur bonds that are readily cleaved. Thus, we have demonstrated that chemical reagents can quite selectively remove or alter the properties of the organic sulfur compounds in coal under rather mild conditions and that these reactions can be performed without detrimental losses of material or heat content. The technological challenge remains to implement this chemistry by practical means.

## References

1. Smith, J. W.; Batts, B. D. *Geochimica et Cosmochimica Acta*, **1974**, *38*, 121.
2. Chou, C. L. In *Geochemistry of Sulfur in Fossil Fuels*, Orr, W. L.; White, C. M., Eds.; ACS Symposium Series, **429**, American Chemical Society: Washington, D.C., Chapter 2.
3. Attar, A., In *Analytical Methods for Coal and Coal Products*, Karr, C. Ed.; Academic Press, New York, **1979**.
4. Calkins, W. H. *Energy and Fuels*, **1987**, *1*, 59.
5. Sinninghe Damsté, J. S.; Eglinton, T. I.; DeLeeuw, J. W.; Schenck, P. A. *Geochim. Cosmochim. Acta* **1989**, *53*, 873.
6. Sinninghe Damsté, J. S. *Organically-Bound Sulphur in the Geosphere: A Molecular Approach*, Offsetdrukkerij Kanters B. V.: Alblasserdan, The Netherlands, **1988**.
7. George, B. N.; Gorbaty, M. L.; Kelemen, S. R.; Sansone, M. *Energy and Fuels*, **1991**, *5*, 93.
8. Calkins, W. H.; Torres-Ordonez, R. J.; Jung, B.; Gorbaty, M. L.; George, G. N.; Kelemen, S. R. *Energy and Fuels*, **1992**, *6*, 411.
9. Huffman, G. P.; Huggins, F. E.; Mitra, S.; Shah, N.; Pugmire, R. J.; Davis, B.; Lytle, F. W.; Greeger, R. B. *Energy and Fuels*, **1989**, *3*, 200.
10. Huffman, G. P.; Huggins, F. E.; Shah, N.; Lu, F.; Zhao, J. *Preprint Pap., Fuel Chem. Div., Am. Chem. Soc.*, **1993**, *38(2)*, 369.
11. Winans, R. E.; Neill, P. H. *Multiple-Heteroatom-Containing Sulfur Compounds in a High Sulfur Coal*, In *Geochemistry of Sulfur in Fossil Fuels*, Orr, W. L.; White, C. M., Eds., ACS Symposium Series, **429**, American Chemical Society: Washington, D.C., Chapter 15.
12. Winans, R. E.; Melnikov, P. E.; Dyrkacz, G. R.; Bloomquist, C. A. A. *Preprint Pap. Fuel Chem. Div., Am. Chem. Soc.*, **1993**, *38(2)*, 375.
13. White, C. M.; Douglas, L. J.; Anderson, R. R.; Schmidt, C. E.; Gray, R. J. In *Geochemistry of Sulfur in Fossil Fuels*; Orr, W. L.; White, C. M., Eds.; ACS Symposium Series **429**, American Chemical Society: Washington, D.C., Chapter 16.
14. Winans, R. E. *Mass Spectrometric Studies of Coals and Coal Macerals*, In *Advances in Coal Spectroscopy*, Plenum Press: New York and London, **1992**, Chapter 11.
15. Nishioka, M. *Energy and Fuel*, **1988**, *2*, 214.
16. Gates, B. C.; Katzer, J. R. Schuit, G. C. A. *Hydrodesulfurization*. In *Chemistry of Catalytic Processes*, McGraw-Hill Book Co.: New York, **1979**, Chapter 5.
17. Nafsis, D. A.; Humbach, M. J.; Gatsis, J. G. Coal Liquefaction Coprocessing, *Final Report*, DOE/PC/70002-T6, **1988**.
18. Meyers, R. A.; McClanahan, L. C.; Hart, W. D. Proc. Pittsburgh Coal Conf., **1985**, 112.
19. Westgate, L. M.; Anderson, T. F. *Anal. Chem.*, **1982**, *54*, 2136.
20. Wolny, R.; Stock, L. M. *The Protodesulfurization of Naphthalene Thiols and Sulfides*. In *New Trends in Coal Chemistry*, Y. Yurum, Ed., Kluwer Academic Publishers, **1988**, 287.
21. Chatterjee, K.; Wolny, R.; Stock, L. M. *Energy and Fuels*, **1990**, *4*, 402.
22. Stock, L. M.; Chatterjee, K. *Preprint Pap., Fuel Chem. Div., Am. Chem. Soc.*, **1993**, *38(2)*, 379.
23. Chatterjee, K.; Stock, L. M. *Energy and Fuels*, **1991**, *5*, 704.

## XAFS STUDIES OF COAL

G.P. Huffman, F.E. Huggins, N. Shah, F. Lu, and J. Zhao  
CFFLS, 233 Mining & Minerals Res. Bldg., University of Kentucky,  
Lexington, KY 40506-0107

**Keywords:** XAFS, sulfur, trace elements, calcium, chlorine, potassium

### INTRODUCTION

Over the past 10 years, x-ray absorption fine structure (XAFS) spectroscopy has been extensively applied to a variety of problems in coal science. The current paper will review those applications. Because of the fact that XAFS spectroscopy focuses on only one element at a time, it is ideally suited to examining the structure of individual elements in highly heterogeneous materials like coal and its derivatives. We will briefly review XAFS studies of S, Ca, K, Cl, and several trace elements (As, Cr, etc.) in coal. Applications of XAFS in studies of coal combustion, liquefaction, and gasification will be discussed, with emphasis on in situ studies.

### EXPERIMENTAL METHOD

The experimental procedure for obtaining high quality XAFS spectra from various elements in coal is discussed in detail in the references. Briefly, the x-ray beam emitted tangentially from a synchrotron is converted into a high-intensity, monochromatic x-ray beam using a double crystal monochromator. This x-ray beam is then collimated and directed onto the sample to be studied. The monochromator crystals are then turned through a range of Bragg angle in such a manner as to sweep the x-ray energy through the x-ray photoelectric absorption edge (usually the K-edge, occasionally the L-edge) of the element of interest. The x-ray absorption spectrum is measured either by detecting the x-rays that pass through a thin sample without being absorbed, or by detecting the fluorescent x-rays that are emitted by the element of interest after photoelectric absorption of the incident x-rays takes place. Variations on the experiment, such as in situ spectroscopy at elevated temperatures, the use of specialized detectors, etc., are discussed in the references.

The spectra are broken into two regions for detailed computer analysis: the x-ray absorption near edge structure (XANES) region and the extended x-ray absorption fine structure (EXAFS) region. The XANES consists of a series of peaks derived from inner-shell photoelectron transitions to vacant bound levels and scattering resonances. It can be deconvoluted to yield definitive information about the types of electronic bonding present. The EXAFS region can be subjected to a Fourier transform analysis procedure which yields radial distribution functions that are processed to derive information about the local atomic environment; i.e., the type, number, and interatomic distances of neighboring atoms.

### RESULTS

The principal results obtained for a number of different elements of interest in several areas of coal science are briefly summarized below. Topics of current and future interest are also discussed.

#### *Calcium*

One of the earliest coal-related XAFS studies conducted was an investigation of calcium in coal.<sup>(1,2)</sup> It was demonstrated that XAFS spectroscopy detected two major types of calcium: that contained in calcite in bituminous coals, and that bound to oxygen anions in carboxyl groups in lignites and subbituminous coals. The radial distribution functions derived from the XAFS spectra indicated that the carboxyl bound calcium is molecularly dispersed through the macerals.

In situ studies of the carboxyl-bound calcium in lignite were carried out during pyrolysis in He and gasification in CO<sub>2</sub> and He-O<sub>2</sub> at temperatures up to 500 °C.<sup>(3-6)</sup> Only small changes were observed in the calcium spectra, indicating that the calcium undergoes relatively little agglomeration and retains its nearest neighbor oxygen environment with relatively little change under these conditions. Pyrolysis at higher

temperatures (800-1000 °C) causes agglomeration of the calcium to form CaO, which exhibits a distinctive radial distribution function.

During combustion, calcium is rapidly transformed to CaO, which can either react with aluminosilicates to form a Ca-containing aluminosilicate slag, or with SO<sub>2</sub> to form CaSO<sub>4</sub>. XAFS studies combined with other characterization research have demonstrated that these reactions play an important role in slagging and fouling during coal combustion.<sup>(6,7)</sup>

### **Potassium**

Potassium occurs almost exclusively in bituminous coals in the form of illite, which exhibits a very distinctive XANES spectrum.<sup>(8)</sup> Under combustion conditions, the illite melts and contributes significantly to ash deposition problems during combustion.<sup>(7,9)</sup>

In situ XAFS studies of the pyrolysis and gasification reactions of potassium ion-exchanged into lignite have been carried out.<sup>(6)</sup> The ion-exchanged, carboxyl-bound potassium exhibits little change up to 500 °C in He, but converts rapidly to K<sub>2</sub>CO<sub>3</sub> when O<sub>2</sub> is admitted into the hot cell.

### **Chlorine**

The authors have recently completed an XAFS investigation of chlorine in a wide variety of coals.<sup>(10,11)</sup> Chlorine XANES spectra for coals of rank higher than subbituminous are closely similar regardless of chlorine content, rank, and geographic origin, indicating one major mode of occurrence. The evidence indicates that this mode of occurrence is chloride anions in moisture anchored to the surfaces of micropores in coal by organic ionic complexes, such as quaternary amine groups and alkali carboxyl groups. It would appear that the observation of NaCl and other inorganic chlorides is an artifact resulting from precipitation of solid chlorides upon release of moisture from the coal during size reduction and storage.

### **Sulfur**

Extensive XAFS research has been conducted on sulfur in coal in recent years.<sup>(12-18)</sup> It is no exaggeration to say that, as a result of this work, analysis of sulfur XANES spectra has become widely recognized as the best method yet developed for the non-destructive, in situ characterization of the organic sulfur functional forms in coal. Sulfur K-edge XANES can distinguish and quantify with an accuracy of ~±5-10% the amounts of the following major forms of sulfur: thiophene, sulfide, disulfide, elemental sulfur, sulfoxide, sulfone, sulfate, pyrite, and pyrrhotite. S K-edge XANES has been used to study the reactions of sulfur during pyrolysis<sup>(16)</sup> and desulfurization<sup>(17,18)</sup>.

Recently, it has been demonstrated that sulfur L-edge XANES spectroscopy also has great potential for quantification of sulfur functional forms.<sup>(19,20)</sup> The L-edge XANES spectra appear to have better resolution for different sulfur groups than the K-edge spectra. However, the technique is considerably more difficult experimentally, and much model compound calibration work remains to be done. Nevertheless, a preliminary comparison of sulfur K-edge and L-edge results for the analysis of sulfur forms in Mequinenza lignite gave reasonable results.<sup>(21)</sup>

An excellent review of the XANES methods and other methods of characterizing sulfur in coal has recently been written by Davidson.<sup>(22)</sup>

### **Trace Elements**

Recently, by using an array detector with 13 germanium detection elements, it has been possible to obtain quality XAFS spectra of several critical trace elements in coal.<sup>(23,24)</sup> The primary work to date has been on arsenic and chromium. High quality spectra were obtained at concentration levels as low as 10 ppm. The principal observation of interest for chromium is that there appears to little if any (<5% of the total) Cr<sup>+6</sup> present in either the coals or the combustion ashes investigated to date. Only Cr<sup>+3</sup> is observed. In coal, the form of chromium has been tentatively identified as chromium hydroxide. For arsenic, it is found that most of the arsenic in fresh coals is contained as As in pyrite. In only one coal (Pittsburgh #8, DECS-12) was arsenopyrite observed. Arsenic was also present, however, in all of the coals studied

as arsenate(As(V)). The amount of arsenate was observed to increase fairly rapidly as a result of oxidation under ambient conditions, becoming the dominant form of arsenic present after ~6 months.

### **Current and Future Research**

XAFS spectroscopy has proven to be an excellent method for investigating the structures of the many important elements in coal. Research currently underway or planned for the future that is expected to yield significant results is summarized briefly below.

1. Nitrogen XANES spectroscopy may prove to be as informative as sulfur XANES spectroscopy. Initial studies by Mitra-Kirtley et al.<sup>(25)</sup> look quite promising.

2. XAFS studies of trace elements will undoubtedly increase. Investigation of the reactions of As and Cr during combustion, cleaning or other processes are in progress, and several additional trace elements will be studied.

3. In situ studies under more severe conditions will be emphasized in future research. These include in situ studies of the reactions of such elements as Fe, Ca, K, and S during coal combustion, and studies of liquefaction catalysts at high temperatures and hydrogen pressures.

4. Carbon XANES has recently been shown to have promise in the area of imaging. Using a highly collimated beam, Botto and his co-workers<sup>(26)</sup> have succeeded in imaging macerals in coal by bracketing the characteristic XANES peaks from aromatic and aliphatic carbon and scanning a thin sample.

It appears that this highly versatile technique will continue to have many applications in coal science for years to come.

### **ACKNOWLEDGEMENT**

This work has been supported by the office of Exploratory Research at the Electric Power Research Institute under contract RP-8001, by the U.S. Department of Energy under several contracts, and by the Gas Research Institute.

### **REFERENCES**

1. F. E. Huggins, G. P. Huffman, F. W. Lytle, and R. B. Gregor, Proceedings of the 1983 International Conference on Coal Science, Pittsburgh, PA; pp. 679-682 (International Energy Agency, 1983).
2. G. P. Huffman and F. E. Huggins, ACS Symposium Series No. 264, pp. 159-174, Chemistry of Low-Rank Coals, Ed., H. H. Schobert, Amer. Chem. Soc., 1984.
3. G. P. Huffman, F. E. Huggins, R. G. Jenkins, F. W. Lytle, and R. B. Gregor, Fuel **65**, 1339-1344 (1986).
4. F. E. Huggins, N. Shah, G. P. Huffman, R. G. Jenkins, F. W. Lytle, and R. B. Gregor, Fuel, **67**, 938-941 (1988).
5. F. E. Huggins, N. Shah, G. P. Huffman, R. G. Jenkins, F. W. Lytle, and R. B. Gregor, Fuel, **67**, 1662-7 (1988).
6. G. P. Huffman, F. E. Huggins, A. A. Levasseur, J. Durant, F. W. Lytle, R. B. Gregor, and Arun Mehta, Fuel, **68**, 238-242 (1989).
7. G. P. Huffman, F. E. Huggins, and N. Shah, Progress in Energy and Combustion Science, **16**, #4, 293-302 (1990).
8. G. P. Huffman, F. E. Huggins, R. A. Shoenberger, J. S. Walker, R. B. Gregor, and F. W. Lytle, Fuel **65**, 621-632 (1986).
9. S. Srinivasachar, J. J. Helble, A. A. Boni, G. P. Huffman, F. E. Huggins, and N. Shah, Progress in Energy and Combustion Science, **16**, #4, 243-252 (1990).
10. F. E. Huggins and G. P. Huffman, "An XAFS Investigation of the Form-of-Occurrence of Chlorine in U.S. Coal," Chlorine in Coal, First International Conference, Ed., J. Stringer, Vol.17, Coal Science and Technology, Elsevier, 1991, pp.45-58.
11. F. E. Huggins and G. P. Huffman, "Chlorine in Coal: An XAFS Spectroscopic Investigation," 1993, Fuel, submitted.
12. G.N. George and M.L. Gorbaty, 1989, J. Am. Chem. Soc., **111**, 3182.

13. S.R. Kelemen, M.L. Gorbaty, G.N. George, **1990**, *Fuel*, **69**, 939.
14. G.N. George, M.L. Gorbaty, and S.R. Kelemen, **1991**, *Energy & Fuels*, **5**, 93.
15. G.P. Huffman, S. Mitra, F.E. Huggins, N. Shah, S. Vaidya, and F. Lu, **1991**, *Energy & Fuels*, **5**, 574-581.
16. M. Mehdi Taghiei, F.E. Huggins, N. Shah, and G.P. Huffman, *Energy & Fuels*, **1992**, **6**, 293-300.
17. F.E. Huggins, S.V. Vaidya, N. Shah, and G.P. Huffman, *Fuel Processing Technology*, in press.
18. G. Huffman, N. Shah, F. Huggins, L. Stock, K. Chatterjee, J. Kilbane, M. Chou, and D. Buchanan, "Sulfur Speciation of Desulfurized Coals by XANES Spectroscopy", submitted to *Fuel*; preprint version published in *Amer. Chem. Soc. Div. of Fuel Chem. Preprints*, **1992**, **37(3)**, 1094-1102.
19. M. Kasrai, J.R. Brown, G.M. Bancroft, K.H. Tan, and J.M. Chen, **1990**, *Fuel*, **69**, 411-414.
20. J.R. Brown, M. Kasrai, G.M. Bancroft, K.H. Tan, and J.M. Chen, **1992**, *Fuel*, **71**, 649-653.
21. C.M. White et al., "A Study of Mequinenza Lignite," **1993**, *Fuel*, in press.
22. R.M. Davidson, *Organic Sulphur in Coal*, **1993**, IEA Coal Research, London.
23. F.E. Huggins, N. Shah, J. Zhao, F. Lu, and G.P. Huffman, *Energy & Fuels*, **7**, 482-489.
24. G.P. Huffman, F.E. Huggins, N. Shah, and J. Zhao, "Speciation of Critical Trace Elements in Coal and Combustion Ash by XAFS Spectroscopy," *International Trace Elements Workshop*, Scottsdale, AR, April, 1993; to be published in *Fuel Processing Technology*.
25. S. Mitra-Kirtley, O.C. Mullins, J. Branthaver, J. Van Elp and S.P. Cramer, **1993**, *Amer. Chem. Soc., Div. Fuel Chem. Preprints*, **38(3)**, 762-768.
26. R.E. Botto, reported during a presentation at the 7th ICCS Conference, Banff, Canada, 1993.

## STATUS OF COAL ASH BEHAVIOR RESEARCH

Steven A. Benson, Everett A. Sondreal, and John P. Hurley  
Energy & Environmental Research Center  
PO Box 9018  
Grand Forks, ND 58202-9018

Keywords: Coal, Combustion, Gasification, Inorganic Species, Ash Deposition

### INTRODUCTION

The inorganic impurities in coal are converted to ash during combustion and gasification. The problems associated with ash in combustion and gasification systems include deposition on refractory and heat-transfer surfaces, corrosion and erosion of system parts, fine particulate that is difficult to collect, and maintaining slag flow in slagging systems. An overview of ash formation and deposition in utility boilers was performed by Benson and others (1993).

In recent years, significant advances have been made in understanding and predicting the behavior of ash in combustion and gasification systems. These predictions are based on a detailed knowledge of ash formation and deposition mechanisms that have been obtained through bench-, pilot-, and full-scale testing. The mechanisms have been elucidated through the use of advanced methods of coal and coal ash analysis. These techniques are based on scanning electron microscopy and microprobe analysis to determine both the chemical and physical characteristics of coal minerals, fly ash, agglomerates, and deposits. Several methods to predict ash behavior are being developed, including advanced indices and phenomenological models. The analytical methods and predictive methodologies have been described in detail by Benson and others (1993).

This paper summarizes Energy & Environmental Research Center (EERC) work that has been accomplished on ash-related research pertaining to coal-fired utility boiler and provides a brief overview of ash issues related to emerging and advanced technologies that utilize coal. Much of the discussion focuses on the behavior of ash produced from lower-ranked coals, such as lignites and subbituminous from the U.S.

### ASH FORMATION

Depending upon the severity of the process, the inorganic impurities can go through significant physical and chemical transformations. Physical transformations involved in high-temperature suspension- or entrainment-type combustion and gasification systems include 1) selective elemental vaporization and subsequent reaction/condensation to form surface coatings or homogeneous fine particulates, 2) coalescence of mineral grains within hot reactive char particles, 3) char fragmentation and partial coalescence of included minerals, 4) shedding of particles from the char surface, 5) fragmentation or fusion of liberated mineral grains, 6) convective transport of volatile species within and between char/mineral particles, and 7) formation of thin-walled ash spheres known as cenospheres. The typical result of these interactions is an ash having a multimodal size distribution, including larger particles that resemble the inorganic constituents in the parent coal and a very fine submicron fractionate resulting from condensation and fragmentation. Some liberated minerals with high melting temperatures, such as quartz ( $\text{SiO}_2$ ), are carried through a reactor in their original angular form. However, at high temperatures, the bulk of the total inorganic content, made up of silicate and aluminosilicate particles, in dynamic association with other condensed or fused phases, will tend to form molten glassy spheres.

The extent to which different elements initially vaporize and subsequently remain in the vapor state depends on their original association in the coal, the process temperature, and the gas composition (e.g., oxidizing or reducing, water vapor concentration, HCl concentration). In general, alkaline earth elements (Ca, Mg) will tend to remain primarily in a condensed form. Silica and alumina can only be volatilized as suboxides in a reducing atmosphere, causing their vapor or submicron fume to play a very minor role in combustion systems, but possibly a significant role in gasification. The fraction of potassium originally present in illite-type clays tends to be retained in the bulk aluminosilicate ash, as evidenced by the high temperatures (up to 1350°C) required to revolatilize potassium from combustion fly ash (Sondreal, Gronhovd, and Severson, 1985). All available evidence indicates that the sodium in low-rank coal (along with the organically associated potassium) is substantially vaporized and subsequently distributed throughout a reactor system, primarily as a surface coating on ash particles or as discrete particles (with enrichment in finer particle-size fractions), but also as a persistent vapor under certain conditions of concern in advanced power systems.

Reactions of organically associated alkali and alkaline earth elements are initiated by the decomposition of carboxylates to form carbonates between 400° and 600°C (Stewart, Stinespring, and Davidovits, 1982). At higher temperatures, the carbonates are believed to decompose to metal oxides that are subsequently reduced to metal vapor by carbon monoxide or char. In a quadrupole mass spectrometry profile of a laboratory-pulverized lignite-air flame, vapor-phase sodium atoms appeared first, followed by vapor-phase sodium hydroxide

(Greene and O'Donnell, 1987). Quenched sampling of an entrained flow combustion reactor operated on Montana lignite indicated that up to 80% of the coal sodium was vaporized and converted to a submicron fume at 1900 K (1627°C, 2961°F) (Neville and Sarofim, 1985). Up to 20% of the magnesium and a small percentage of the calcium were vaporized (Quann and Sarofim, 1986).

Thermal reaction products from discrete mineral grains in low-rank coals produced by laboratory ashing (oxidation in air) at temperatures between 250° and 1300°C include the major x-ray diffraction (XRD) groupings (Falcone and Schobert, 1986; Falcone, Schobert, Rindt, and Braun, 1984). Laboratory thermogravimetric analysis (TGA) and differential thermal analysis (DTA) have also been used to study phase transformations as a function of temperature (O'Gorman and Walker, 1973). With heating in air, clays first lose their absorbed interlayer water between 50° and 150°C. Gypsum ( $\text{CaSO}_4 \cdot 2\text{H}_2\text{O}$ ) dehydrates in this same temperature range, first to bassanite ( $\text{CaSO}_4 \cdot \frac{1}{2}\text{H}_2\text{O}$ ) and then to anhydrite ( $\text{CaSO}_4$ ) at 180°C. Clay structures are further dehydrated and collapsed by loss of hydroxyl water between about 350° and 600°C, with attending substitution of cations derived from carboxylates, carbonates, oxides, and sulfates into the structure. The oxidation of pyrite ( $\text{FeS}$ ) to produce iron oxides occurs between 325° and 620°C, and calcite ( $\text{CaCO}_3$ ) decomposes to calcium oxide between 700° and 830°C. Quartz is stable up to 1000°C. Various glassy and amorphous phases are observed at 1300°C. The amorphous glass and liquid phases have special importance as bonding agents in high-temperature sintered deposits. In crystalline materials the structural units observed for some of the common silicate systems typical of many lower-rank coal deposits are summarized in Table 1.

The crystallization behavior of ashes and slags can provide insight into the temperature at which the deposit or fly ash formed. In addition, crystallization from a liquid phase changes the composition of the residual liquid and that influences its physical properties. This is extremely important in determining slag viscosity. The temperature of critical viscosity,  $T_{cv}$ , is the temperature when crystallization from the liquid phase occurs. This crystallization causes the flow characteristics to go from a Newtonian liquid to a non-Newtonian liquid.

Sulfates also contribute to the formation of deposits in combustion systems. The sulfate phases form as a result of the reaction of  $\text{SO}_2$  with alkali and alkaline earth elements such as sodium and calcium, respectively. Sulfates are formed primarily by vaporization and condensation processes. During combustion, sulfur oxides form primarily from the oxidation of sulfides and organic sulfur in the flame. At the high temperatures in a flame, sulfur dioxide forms first followed by the formation of sulfur trioxide. At lower temperatures, equilibrium favors the formation of  $\text{SO}_2$ . Sulfur oxides can interact with the surface of fly ash particles. It has been shown that the maximum amount of reaction occurs between sulfur oxides and ash at approximately 560°C and is dependent upon the quantity of alkali and alkaline earth oxides in the ash. The exact way alkali and alkaline earth sulfates form in combustors appears to be poorly understood. It is assumed that the alkali elements volatilize in the flame and are converted to oxides. The alkali oxide then reacts with  $\text{SO}_2$  and  $\text{O}_2$  or  $\text{SO}_3$  to form sulfates. It has been postulated that sulfates form in the gas stream and condense on the surfaces of materials such as fly ash particles or boiler steel surfaces. Another possible path for the reaction is on the surface of entrained fly ash particles where an alkali layer ( $\text{NaOH}$ ) is first deposited and the subsequent sulfur oxide interaction.

## ASH DEPOSITION AND AGGLOMERATION

### Pulverized Coal Combustion

Ash deposition mechanisms in pulverized coal combustion systems have been extensively investigated by the EERC under sponsorship of industry consortia (Benson and others, 1988, 1992; Hurley and others, 1992). At the microscopic level observable by scanning electron microscope point count (SEMP) techniques developed at the EERC, ash deposits in combustion systems are shown to be caused by sodium-rich glass/liquid cementing phases and recrystallized alkaline earth aluminosilicates at temperatures above about 1900°F (1038°C) and by low melting sulfate-rich phases that bond deposits at lower temperatures. Sodium enrichment of the aluminosilicate-based amorphous phase is the foremost cause of the low liquid-phase viscosity and sintering that characterize severe fouling at higher temperatures. This type of ash deposition has been successfully modeled by a viscous flow sintering mechanism, where the growth and strength of the deposit are directly related to the amount of the liquid phase and inversely proportional to its viscosity.

At temperatures below 1900°F (1038°C), the thermodynamic equilibrium shifts to allow sulfation of alkali and alkaline earths, leading to several modes of ash deposition when high-calcium coals are burned in pc-fired boilers. Laboratory strength tests and SEM observations indicate that calcium sulfate crystals form an interlinked lattice that imparts strength over periods of 1 to 10 days, with more rapid strength development occurring at higher temperatures up to 1850°F (1010°C), at higher ratios of total alkali to silica ( $\text{Na}_2\text{O} + \text{K}_2\text{O} + \text{MgO} + \text{CaO/SiO}_2$ ), and with more uniform diffusion of  $\text{SO}_2$  through the deposit. Deposits formed on leading edge tube banks just below 1900°F rapidly become sulfated and hard. Tubes downstream of this screening action are coated with calcium-rich enamel-like deposits that are hard upon deposition and formed from particles smaller than about 3  $\mu\text{m}$ . Loose powdery deposits formed on the downstream side of tubes, by ash particles smaller than

10  $\mu\text{m}$  being trapped in gas eddies behind the tubes, are somewhat stronger at higher gas velocities and correspondingly smaller, affected particle sizes. A low-temperature engineering algorithm of deposition risk (LEADER) has been developed at the EERC to predict low-temperature deposition.

#### Fluidized-Bed Combustion

The FBC process consists of two subprocesses: a) the fluidization of solids, by which solid particles/granules are suspended in an upward flowing stream of gas and b) the combustion process, in which fuel particles are burned to sustain temperature. The solids in FBCs are typically fuel ash, bed material, sorbent used to control pollutants, and reaction products formed by sulfur capture and other sorbent-coal interactions. FBC systems operated at atmospheric pressure are classified as atmospheric fluidized-bed combustors (AFBCs), which usually also denotes low fluidization velocities resulting in a bubbling bed. Circulating fluidized-bed combustors (CFBCs) operate at fluidization velocities approximately 7 to 8 times higher. At these velocities, the rising gas entrains the bed materials; the resulting bed consists of a turbulent cloud of solids that fills the combustion chamber. A portion of the bed material is continuously carried out with the offgas and recirculated back to the combustion chamber. Pressurized fluidized-bed combustion (PFBC) systems are similar to AFBCs, but operate under pressure. The compressed air used contains more oxygen per unit volume and, therefore, sustains a higher intensity of combustion, allowing for the design of smaller combustors. The other principal advantage of the PFBC is the increased conversion efficiency (coal-to-electricity) that can be achieved by passing the hot, pressurized combustion gases through both a gas turbine and a waste-heat boiler serving a steam turbine to extract more usable energy in a combined cycle system.

Although FBCs typically operate at low temperatures (1450° to 1700°F), evidence from pilot, industrial, and utility boilers indicates that certain ash components have the potential to cause ash-related problems. These problems can manifest themselves as agglomeration and sintering of the bed material or as deposition on the heat exchanger tube surfaces.

Agglomeration, sintering, and deposition have all been observed in a number of operational FBCs (Steen and Imsdahl, 1989; Makansi, 1988; Miller, 1988; Mann and others, 1992). Analytical results of samples from these various units indicate that the material that forms the initial layers on the bed material, in the case of agglomeration, and on tube surfaces, in the case of deposition, is the result of the presence and behavior of sodium- and potassium-rich calcium sulfates. The sodium, potassium, and sulfur are readily volatilized during combustion and condense on the cooler surfaces. Calcium released from the coal during combustion also reacts with the sulfate matrix. This sulfate matrix may be molten at the operating temperatures of the fluid bed and serve to glue particles together in the form of agglomerates or form thicker deposits. The sulfate matrix sinters over time to form a strongly bonded deposit.

Certain requirements are necessary for these phenomena to occur. The fuel must contain alkali or alkaline earth elements that can be liberated during combustion. Organically bound elements are typically liberated during combustion and have been shown to be the major precursors to in-bed tube deposition and agglomeration. In addition, competing reactions with other coal mineral components can reduce the alkali availability. The fate of these potential deposit- and agglomerate-forming minerals will ultimately influence the extent of deposition and agglomeration. Therefore, it is important to understand the nature of the mineral matter in the original coal so that improvements can be made in the prediction of FBC performance.

Bed material agglomeration is the process which causes relatively small bed particles to stick together, forming larger masses of material. Coal ash reacting with bed material forms the substance which acts as the "glue" in agglomeration. These ash-related interactions occur under normal FBC-operating conditions and include the formation of low melting eutectics between sodium-, potassium-, calcium-, and sulfate-rich components and, possibly, some solid-solid reactions. Agglomeration can also occur as a result of localized hot spots of bed material, where temperatures in the FBC system can exceed the typical 1700°F limit. Temperatures capable of melting various ash species can be attained even during relatively stable operation of the FBC.

A very fine-grained coal ash matrix deposited on in-bed superheat surfaces has been noted in both pilot facilities and utility-scale systems. This deposition is related to the coal ash chemistry and has been observed in stations operating with a bed temperature as low as 1450°F, despite the high erosive forces of bed material in a bubbling fluid bed. The mechanism of adherence and growth appears to be via a molten sulfate matrix, due to the fluxing action of alkali.

#### Coal Gasification

In coal gasification systems, the coal is converted to a combustible gas, volatiles, char, and ash/slag. Coal gasification has been technically and economically feasible for many years. Commercial gasifiers differ widely in the way in which they produce ash, and either a dry ash, an agglomerated ash, or slag may result. The Lurgi and other fixed-bed gasifiers

operate by passing air or oxygen and steam under pressure up through a bed of coal, which is fed to the top of the bed through a lock hopper. Coal and char move to the bottom as they are gasified, and the dry ash is removed through a bottom grate. Alternatively, a fixed-bed gasifier can be designed to operate at high temperatures, producing a bottom slag that is tapped through a hearth, i.e., the British Gas Lurgi (BGL) process. Fluidized-bed gasifiers, including the U.S. Kellogg Rust Westinghouse (KRW) and Institute of Gas Technology (IGT) processes and the German Winkler process, operate in a gasification mode using steam and air or oxygen in a fashion resembling PFBC. Either dry ash or a fused agglomerated ash may be produced depending on the design, operating temperatures, and the fusion temperature of the ash. Entrained flow gasifiers, including Dow, Texaco, and Shell designs, all operate at very high temperatures and produce a vitreous slag. Integrated gasification combined cycle (IGCC) systems directly link these various types of gasifiers with a gas turbine/steam turbine cycle to achieve high conversion efficiency.

In a dry ash fixed-bed gasifier or grate-type combustor, bed temperatures are maintained below the fusion temperature of the ash, and the bulk of the ash along with a substantial part of the coalesced vapor and liquid species are consolidated in the grate discharge. In very high-temperature slagging gasifiers and combustors, all of the physical transformations described are operative, but the consolidation of ash and slag depends on reactor configuration. In a fixed-bed slagging reactor (e.g., the BGL gasifier), virtually all of the inorganic reaction products are recaptured in the relatively cool descending fuel bed and consolidated into the slag discharge. In an entrained flow reactor (e.g., Texaco, Dow, and Shell gasifiers or cyclone-type combustors), slag is partially separated by impingement or cyclonic action while a (potentially small) fraction is carried forward with the hot gas.

The chemical, mineralogical, and physical characteristics of gasifier ash have been investigated (Eklund, 1986; McCarthy and others, 1985; Stevenson and Larson, 1985; Hassetting and others, 1985), and the characteristics of ash produced from the Shell pilot-scale testing (Mahagaokar and others, 1990) and Texaco testing (EPRI, 1990) have been reported. Slag/ash samples have been characterized from eight gasifiers (Eklund, 1986). The types of materials examined included coarse ash or slag and cyclone dust. The materials were found to be nonhazardous, but the physical characteristics and chemical compositions varied significantly as a function of process configuration, operation, coal feed composition, and coal handling. The elemental compositions of the slags produced in gasification systems were similar to the bottom ash from conventional coal combustion systems (Turner and Lowry, 1983). The bulk compositions of cyclone dust samples were found to be similar to conventional coal combustion fly ash (Wetzel and others, 1982). The mineralogical examination of slags (McCarthy and others, 1985) indicated that many of the same high-temperature silicate minerals are present in the slag samples along with reduced iron-bearing compounds. The key difference in coal gasification ash and slag compared to combustion ash is the lack of sulfur. Sulfur is present in small quantities in the ash, usually in the form of a sulfide. In addition, the other ash species in the system may also be in reduced form. The entrained-flow slagging gasifiers recycle all fly ash back to the vitreous slag. Slag samples produced in the Shell process (Mahagaokar and others, 1990) were shown to be depleted in several trace elements. The fine fly slag contained carbon and a higher level of trace metals.

#### Slagging Combustors and Direct-Fired Gas Turbines

A pressurized slagging combustor coupled with hot-gas cleaning is a potentially simple system for producing hot gas for a gas turbine combined cycle. The major problems encountered in using coal directly as a gas turbine fuel are due to the inorganic components in the fuel. Direct-fired slagging combustors offer potential capital cost savings for coal-fired combined cycle systems, but only if the hot gases generated can either be used directly or economically cleaned to remove particulates, sulfur, and alkalis. A slagging combustor direct-fired gas turbine system is being tested and so is a three-stage slagging combustor (Lecren and others, 1992). The ash by-products produced from these systems are a vitreous slag and the particulate collected in collection devices. Slagging combustors retrofit to a package boiler (Zauderer and Fleming, 1991) were able to produce a vitreous slag with relatively high ash retention. The fly ash produced was chemically and physically similar to typical pulverized coal fly ash. The fine particulates generated from volatilized inorganic components or organically associated inorganics in low-rank coals would be expected to reduce the percentage of total ash that could be removed in the slag cyclone or impactor alone, thereby adding to the need for a barrier filter. High-alkali coals would likely require alkali gettering. In reference to controlling sulfur along with slag, the reported high levels (up to 90%) of nonequilibrium sulfur captured on limestone in the reducing section of a slag combustor have, in fact, provided no more than about 50% sulfur control overall, even with rapid slag removal, owing to reemission of sulfur at high temperature under more fuel-lean conditions (Diehl and others, 1992). Sulfides that may occur in reduced slag would pose problems in either use or disposal, possibly requiring subsequent oxidative treatment. Calcium sulfide produces poisonous and odoriferous hydrogen sulfide on contact with water.

#### Externally Fired Combined Cycle Systems

Externally fired combined cycle systems, based on currently available gas turbine technology supporting a turbine inlet temperature of 2500°C when using air as the working fluid, offer potential efficiencies of 47% to 50%, fired either on coal alone or on a combination of coal and

natural gas. Accordingly, DOE is vigorously pursuing a system development program, Combustion 2000, based on high-temperature coal-fired air heaters using advanced ceramic materials such as high-density silicon carbides (SiC) and SiC-alumina blends. Lead contractors for Combustion 2000 are United Technologies (Seery, 1993) and Foster Wheeler (FW) (Shenker and McKinsey, 1992), with a separate program being pursued by Hague International (Vandervort and Orozco, 1992). The generic system configuration includes a high-temperature advanced furnace consisting of the combustor, slag screen, radiant and convective air heaters, and a heat recovery steam generator, together with the gas turbine/steam turbine combined cycle power system and conventional SO<sub>2</sub> and particulate control modules. The FW system uses a series of three air heaters fired on coal char, pyrolysis gas, and natural gas. Low NO<sub>x</sub> emissions in these various systems would be achieved by combustion controls, using staging (rich-lean) or aerodynamically controlled mixing. Combustion 2000 aims at commercial demonstration by 1999 of an ultraclean system for achieving a minimum efficiency of 47% operating on a wide range of coals. The characteristics of the ash and slag from these systems will likely be similar to those found in conventional combustion systems. Higher carbon contents may be found in the ash owing to the low-NO<sub>x</sub> combustion technologies under consideration.

#### SLAG AND ALKALI ATTACK ON CERAMIC MATERIALS

Candidate ceramic materials used in hot particulate filters and heat exchangers are subject to corrosive attack by molten slag and alkali vapor, augmented by other agents including sulfur oxides, sulfides, chlorides, hydrogen, steam, carbon monoxide, char, and ceramics impurities. Failures of ceramic filters in short-term tests conducted to date, up to about 1000 hours, are attributed primarily to mechanical flaws in design or manufacturing; long-term reliability over a desired service life of 10,000 hours will be largely determined by stability to chemical attack. Candidate materials include both oxides, such as mullite, alumina, and cordierite, and non-oxides, such as silicon carbide and silicon nitride, in various bonded matrices. Extensive research is continuing to understand the synergistic interaction of chemical, thermal, and mechanical failure mechanisms (Alvin and others, 1991; Vass and others, 1990). The corrosive mechanisms which have special relevance to low-rank coals are those involving alkali vapors and low-viscosity basic slags.

Alkali attack on aluminosilicates such as mullite occurs by formation of low melting alkali-silica glassy phases on surfaces and in grain boundaries, involving the same types of chemical reactions as occur in ash deposition; resistance to alkali attack is increased by increasing alumina content up to about 60%. Silicon carbide and silicon nitride materials suffer alkali attack when the protective surface layer of silica resulting from passive oxidation during manufacture and later use is converted to an alkali-silica glassy phase, exposing the unprotected SiC and Si<sub>3</sub>N<sub>4</sub> surface to further oxidation and alkali attack. In other contributing mechanisms, hydrogen and steam can cause silica volatilization in reduced (SiO) or oxidized (H<sub>2</sub>SiO<sub>3</sub>) states, and the decomposition of carbon monoxide to carbon at 400° to 700°C can lead to the chemical reduction of iron oxide impurities in ceramics, triggering iron-based catalytic disintegration reactions. These various mechanisms are strongly temperature-dependent, but all are significant at or above the 1600°F (871°C) maximum operating temperature of first-generation ceramic filters and at the 2000°-2500°F (about 1100°-1400°C) temperatures of structural or insulating refractories used in direct coal-fired turbine combustors and heat exchangers for externally fired combined cycle systems. The phase changes resulting from chemical attack together with thermal cycling lead to volume expansion, cracking, spalling, viscous creep, loss of mechanical strength, and eventual structural disintegration. Susceptibility to progressive corrosive attack can be critically influenced by the viscosity of the melts and coal-ash slags on refractory surfaces. Chemically basic slags from some low-rank coals exhibit a rapid reduction in viscosity over a relatively narrow range of temperature increase. Tests at Oak Ridge National Laboratory on heat exchanger ceramics at temperatures up to 2260°F (1238°C) (Ferber and Tenney, 1981) indicated that the most corrosion-resistant (silicon carbide) material survived 500 hours of exposure without degradation under a dry acidic slag, but was severely attacked by a runny basic slag. However, differences in the reported corrosion resistance of various ceramics suggest that subtle differences in the slag composition may play an important role that is unexplained by the currently available data or theory.

#### SUMMARY AND CONCLUSIONS

The advances made over the past several years in understanding ash behavior in coal utilization systems have been made possible as a result of more detailed and better analysis of coal and ash materials. These advanced techniques are able to quantitatively determine the chemical and physical characteristics of the inorganic components in coal and ash (fly ash and deposits) on a microscopic scale. Many of the mechanisms of ash formation, ash deposition, and ash collection in pulverized coal combustion systems are more clearly understood as a result of these new data. This understanding is leading to the development of better methods of predicting ash behavior in pulverized coal combustion systems. Currently, these same methods are being applied to emerging and advanced coal utilization technologies.

## REFERENCES

- Alvin, M.A.; Lippert, T.E.; Lane, J.E. "Assessment of Porous Ceramic Materials for Hot Gas Filtration Applications," *Ceramic Bulletin* 1991, 70 (9), 1491.
- Benson, S.A.; Jones, M.L.; Harb, J.N. "Ash Formation and Deposition," In *Fundamentals of Coal Combustion for Clean and Efficient Use*, Smoot, L.D. Ed.; Elsevier: Amsterdam, 1993; pp 299-373.
- Benson, S.A. et al. "Project Sodium Final Technical Report: Follow-On Work to the Original Evaluation of Sodium Effects in Low-Rank Coal Combustion Systems," EERC publication, 1992.
- Benson, S.A. et al. "Project Sodium," final technical report; Energy and Mineral Research Center, University of North Dakota, 1988.
- Diehl, R.C. et al. "Development of a Slagging Combustor for a Direct-Coal-Fired Combined Cycle," In Proceedings of the 9th Annual International Pittsburgh Coal Conference; Oct. 12-16, 1992, pp 322-327.
- Eklund, A.G. "Coal Gasification Environmental Data Summary: Solid Wastes and Tar By-Products," EPA/600/7-86/015c, April 1986.
- Electric Power Research Institute. "Cool Water Coal Gasification Program," final report; EPRI GS-6806, Project 1459, 1990.
- Falcone, S.K.; Schobert, H.H. "Mineral Transformations During Ashing of Selected Low-Rank Coals," In *Mineral Matter and Ash in Coal*; Vorres, K.S. Ed.; ACS Symposium Series No. 301, 1986; pp 114-127.
- Falcone, S.K.; Schobert, H.H.; Rindt, D.K.; Braun, S. "Mineral Transformations During Ashing and Slagging of Selected Low-Rank Coals," *Prepr. Pap.-Am. Chem. Soc., Div. Fuel Chem.* 1984, 29 (4), 76-83.
- Ferber, M.K.; Tennery, V.J. "Evaluation of Tabular Ceramic Heat Exchanger Materials in Basic Coal Ash from Coal-Oil Mixture Combustion," ORNL/TM-8385, 1981.
- Greene, F.T.; O'Donnell, J.E. "Investigation of the Mechanisms of Ash Deposit Formation from Low-Rank Coal Combustion," DOE/FC/10287-2416, 1987.
- Hassett, D.J.; McCarthy, G.J.; Henke, K.R.; Korynta, E.D. "Characterization of a Lignite Ash from the METC Gasifier III: Correlations with Leaching Behavior and Mineralogy," In *Fly Ash and Coal Conversion By-Products: Characterization, Utilization, and Disposal I*; McCarthy, G.J.; Lauf, R.J., Eds.; Materials Research Society, Pittsburgh, PA, 1985.
- Hurley, J.P.; Benson, S.A.; Erickson, T.A.; Allan, S.E.; Bieber, J.A. "Project Calcium, Final Report," EERC publication, 1992.
- Lecren, R.T.; Stephenson, M.D.; Cowell, L.H.; Wen, C.S.; Galica, M.A. "Mineral Matter Management in Solar's Coal-Fueled Gas Turbine," In *Inorganic Transformations and Deposition During Combustion*; Benson, S.A., Ed.; ASME: New York, 1992.
- Mahagaokar, U.; Krewinghouse, A.B.; Kiszka, M.B. "Shell Coal Gasification Project: Gasification of Six Diverse Coals," EPRI report; GS-7051s, 1990.
- Makansi, J. "Users Pause, Designers Wrestle with Fluid-Bed-Boiler Scaleup," *Power* 1988, July.
- Mann, M.D.; Galbreath, K.C.; Kalmanovitch, D.P. "The Role of Ash Chemistry and Operating Parameters on Ash Agglomeration and Deposition in FBC Systems," In *Inorganic Transformations and Deposition During Combustion*; Benson, S.A., Ed.; ASME: New York, 1992.
- McCarthy, G.J.; Keller, L.P.; Stevenson, R.J.; Galbreath, K.C.; Steinwand, A.L. "Characterization of a Lignite Ash from the METC Gasifier I. Mineralogy," In Proceedings of the Fly Ash and Coal Conversion By-Products: Characterization, Utilization, and Disposal I Symposium; McCarthy, G.J.; Lauf, R.J., Eds.; Materials Research Society, Pittsburgh, PA, 1985.
- Miller, J.R. "Operating Experience on a 19-MW CFBC," 1988 Seminar on Fluidized-Bed Combustion Technology for Utility Applications, Volume 1: Atmospheric Fluidized-Bed Combustion, Palo Alto, CA, May 1988.

- Neville, M.; Sarofim, A.F. "The Fate of Sodium During Pulverized Coal Combustion," *Fuel* 1985, 64, 38-390.
- O'Gorman, J.V.; Walker, P.L. "Thermal Behaviour of Mineral Fractions Separated from Selected American Coals," *Fuel* 1973, 52, 71-79.
- Quann, R.J.; Sarofim, A.F. "A Scanning Electron Microscopy Study of the Transformations of Organically Bound Metals During Lignite Combustion," *Fuel* 1986, 65, 40-46.
- Seery, D.J. "Combustion 2000: Burning Coal in the Twenty-First Century," Prepared for the 1993 Low-Rank Symposium, May 1993, 8 p.
- Shenker, J.; McKinsey, R. "Development of a Coal-Fired, Combined-Cycle Power Generation System with a Pyrolysis Gas and Char-Fired High-Temperature Furnace," In Proceedings of the Pittsburgh Coal Conference; 1992, p 670.
- Sondreal, E.A.; Gronhoyd, G.H.; Severson, D.E. "Alkali Metals in Low-Rank Coals," Coal Energy Technology Consultants, Grand Forks, ND, 1985.
- Steen, D.; Imsdahl, B. "Montana-Dakota Utilities Company Bubbling Fluid-Bed Retrofit O Original Performance," In Proceedings of the 1989 International Conference on Fluidized Bed Combustion; Manaker, Arnold, Ed., San Francisco, CA, pp 793-800, May 1989.
- Stevenson, R.J.; Larson, R.A. "Characterization of a Lignite Ash from the METC Gasifier II. Scanning Electron Microscopy," In Proceedings of the Fly Ash and Coal Conversion By-Products: Characterization, Utilization, and Disposal I. Symposium; McCarthy, G.J.; Lauf, R.J., Eds.; Materials Research Society, Pittsburgh, PA, 1985.
- Stewart, G.W.; Stinespring, G.W.; Davidovits, P. "The Fate of Alkalies in Coal Combustion," *Prepr. Pap.—Am. Chem. Soc., Div. Fuel Chem.* 1982, 27 (1), 138-144.
- Turner, R.R.; Lowry, P.D. "Comparison of Solid Wastes from Coal Combustion and Pilot Coal Gasification Plants," Performed by Oak Ridge National Laboratory for EPRI under EA-2867, Feb. 1983.
- Vandervort, C.L.; Orozco, N.J. "Development Status of a Utility-Scale Externally Fired Combined Cycle," In Proceedings of the 9th Annual International Pittsburgh Coal Conference; Oct. 12-16, 1992, pp 316-321.
- Vass, R.J.; Brown, N.R.; Brown, J.J., Jr. "Corrosion and Degradation of Ceramic Particulate Filters in Coal Combustion Environments," In *Ceramic Transactions: Corrosion and Corrosive Degradation of Ceramics*; 1990; Vol. 10, pp 411-423.
- Wetzel, R.E.; Crawford, R.W.; Yee, W.C. "Environmental Aspects of the GKT Coal Gasification Process," In Proceedings of the Environmental Aspects of Fuel Conversion Technology-VI Symposium; EPA-600/9-82-017, PB83-128181, Aug. 1982.
- Zauderer, B.; Fleming, E.S. "The Demonstration of an Advanced Cyclone Coal Combustor," final report; DOE/PC/79799-t7, Aug. 30, 1991.

**TABLE 1**  
**Crystalline Forms and Examples of Specific Crystal Species (Benson and others, 1993).**

<u>Crystalline Forms</u>	<u>Structural Units</u>	<u>Examples</u>
Orthosilicates	(SiO <sub>4</sub> ) <sup>4-</sup>	Fayalite - Fe <sub>2</sub> SiO <sub>4</sub>
Pyrosilicate	(Si <sub>2</sub> O <sub>7</sub> ) <sup>6-</sup>	Melilite (Gehlenite-Alkermanite) Ca <sub>2</sub> Al <sub>2</sub> SiO <sub>7</sub> - Ca <sub>2</sub> MgSi <sub>2</sub> O <sub>7</sub>
Metasilicate	(SiO <sub>3</sub> ) <sub>n</sub>	Pyroxenes (Diopside - Augite) CaMgSi <sub>2</sub> O <sub>6</sub> - Ca(Fe, Mg)Si <sub>2</sub> O <sub>6</sub>
Framework Silicates	Al <sup>3+</sup> replaces Si <sup>4+</sup> in tetrahedra	Plagioclase (Albite - Anorthite) NaAlSi <sub>3</sub> O <sub>8</sub> - CaAl <sub>2</sub> Si <sub>2</sub> O <sub>8</sub>

A METHOD FOR COUNTING THE HYDROGEN BOND CROSS  
LINKS IN COAL

John W. Larsen and Ilona Gurevich  
Department of Chemistry  
Lehigh University  
Bethlehem, Pennsylvania 18015

Keywords: Coal, Macromolecular  
Structure, Hydrogen  
Bonding, Solvent Swelling

ABSTRACT

A method has been developed which is able to count the number of hydrogen bond crosslinks in coals. The method consists of swelling the coal in non-polar solvents to which small amounts of a good hydrogen bond acceptor have been added. In an entropy controlled process, the hydrogen bond acceptor selectively interacts with those hydroxyl groups which are participating in hydrogen bond crosslinks. This results in a rapid decrease in the effective cross link density of the coals, rapid uptake of the non-polar solvent, and a rapid increase in the swelling. The resulting "titration curve" readily yields an estimate of the number of hydrogen bond crosslinks in the coal.

INTRODUCTION

We begin by discussing the interactions of a good hydrogen bond acceptor, for example pyridine, with hydroxyl groups in coals. For the sake of simplicity, we shall assume in our idealized experiment that all of the hydroxyl groups are phenolic. This is not necessary in the real system, it just makes the explanation easier to follow. We divide the hydroxyl groups in coals into three types. Free hydroxyls which are not participating in any hydrogen bond, hydroxyls which are hydrogen bonded but within the cluster or to a nearby molecule such that the hydrogen bond is not a crosslink, and hydrogen bonds between different macromolecular units such that the hydrogen bond is a non-covalent crosslink in the system.

We now inquire into the selectivity of a hydrogen bond acceptor for the three different types of hydroxyl groups. In thermodynamic terms; for which hydroxyl group is the free energy ( $\Delta G$ ) of interaction with pyridine most favorable. To do this, in a gedanken experiment we envision two extreme situations. Consider first the one in which the enthalpy dominates. That is,  $\Delta H$  for hydrogen bonding will be much larger than  $T\Delta S$  and control the situation. In this case, the pyridine will selectively hydrogen bond to the free hydroxyls. The reasons for this are straightforward. The heat of hydrogen bond formation between pyridine and phenol is  $-7.5$  kcal/mole (exothermic).<sup>1</sup> If the pyridine interacts with a hydroxyl group which is already hydrogen bonded, then the heat of its interaction will be reduced by the enthalpy of the existing hydrogen bond. A  $2.8$  kcal/mole hydrogen bond existing in the coal would lead

to a 100 to 1 preference of the pyridine for the free hydroxyls, given constant entropy. A plot of solvent swelling as a function of the pyridine concentration in the non-polar solvent would start almost flat as the free hydroxyls are saturated with pyridine while the cross-link density of the coal remains constant. Once all of the free hydroxyls have been bonded, the hydrogen bond cross links in the coal would be broken by pyridine thus reducing the cross-link density of the coal and leading to a very rapid increase in solvent swelling. The result is a curve which is initially nearly independent of pyridine concentration but which then rises sharply at some higher pyridine concentration.

The next situation to consider is that of entropy control, where the TAS term is much larger than the  $\Delta H$  term. If pyridine hydrogen bonds to a free hydroxyl or to a hydroxyl which is hydrogen bonded but not a crosslink, there will be a net loss of transnational entropy of the pyridine. The overall entropy change will be modestly unfavorable. If the pyridine breaks a hydrogen bond crosslink, the two macromolecular chain segments which were pinned together by the hydrogen bond are now free from each other and can adopt many more configurations. This provides a potentially large and favorable entropy term. It is this configurational entropy which is responsible for the elastic restoring force in rubbers.<sup>2</sup> It can be quite large. In this case, the pyridine driven by the favorable and dominant entropy change would first interact with the cross-linking hydroxyls in the coal to destroy the crosslinks, and only when these had been saturated would it interact with the other two classes of hydroxyls. The prediction here is that a plot of swelling versus pyridine concentration would show an initial very steep rise eventually almost leveling off as all of the crosslinks are broken. A further and striking prediction is that this swelling behavior will be independent of the hydrogen bond acceptor used. The driving force for the selectivity is the increase in configurational entropy of the coal which occurs when the hydrogen bond cross link is broken. This is independent of the solvent used to break the hydrogen bond. Thus, over an as yet undetermined range of hydrogen bond acceptor strengths, the selectivity for the cross-linking hydroxyls will be independent of the hydrogen bond acceptor. This would not be the case in an enthalpy controlled process.

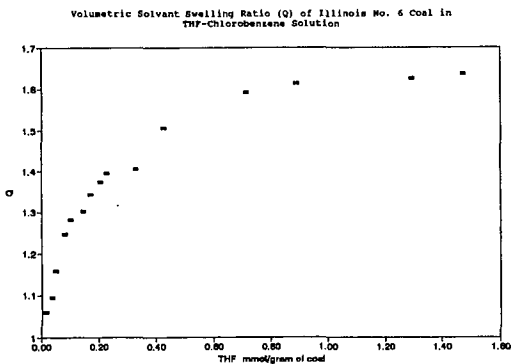
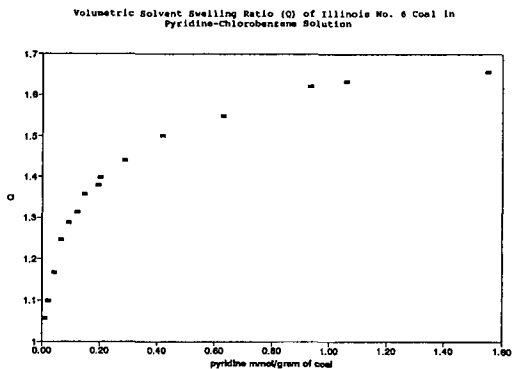
Our data for Illinois No. 6 coal swollen with pyridine in toluene and THF in toluene are shown in Figures 1 and 2. It is clear from these figures that the predictions of an entropy controlled selective "titration" of the hydroxyl crosslinks in coal are followed. Superposition of the two plots reveals essentially identical behavior by both hydrogen bond acceptors in spite of a 1.7 kcal/mole difference in their heats of hydrogen bonding with phenol.<sup>1</sup> Extension of this technique to other materials and other interactions is underway.

## ACKNOWLEDGEMENTS

We are grateful to the U. S. Department of Energy for support of this work.

## REFERENCES

1. Arnett, E. M.; Joris, L.; Mitchell, E.; Murty, T.S. S. R.; Gorric, T.M.; Schleyer, P v.R. J. Am. Chem. Soc. 1970, 92, 2365-2377.
2. Treloar, L.R.G. The Physics of Rubber Elasticity, 3rd Ed; Oxford University Press: New York, 1975.



## ANALYSIS OF WILSONVILLE LOW RANK COAL LIQUEFACTION DATA

Glenn Munkvold, Anthony M. Valente, Donald C. Cronauer  
Amoco Oil Company  
P. O. Box 3011  
Naperville, IL 60566

Keywords: Coal liquefaction, Low rank coal, Wilsonville

### ABSTRACT

The use of both dispersed and supported catalysts for the liquefaction of low rank coals in the Wilsonville, AL facility has been evaluated using a statistical approach. This analysis was undertaken to identify the most important operating variables and their effects upon coal conversion and product distributions. The preferred two-stage configuration for the liquefaction of low rank coal consists of a slurry first-stage reactor followed by an ebullated-bed second stage reactor. The presence of a dispersed catalyst promotes the initial liquefaction steps. An ebullated-bed second stage reactor is effective for hydrocracking the coal-derived products and hydrogenating a stream to be recycled as liquefaction solvent. The effect of process configuration upon coal conversion and product distributions is significant.

### INTRODUCTION AND BACKGROUND

The principal goal of this study of Wilsonville low rank coal conversion data was to identify the primary operating variables and their effects upon conversion and product distributions. The goals of Wilsonville operation with low rank coal were to demonstrate operation with increasing yields, to provide an overall design concept, and to evaluate different coals. A total of 41 run periods was made with several low rank coals over a wide range of conditions. Only those periods that were lined-out were included in this study. In addition, the runs were not carried out using a statistical approach, so there may be some confounding of results.

The Department of Energy Advanced Two-Stage Coal Liquefaction Facility was located in Wilsonville, Alabama. The Wilsonville pilot plant was run by Southern Company Services (SCS) with funding by the United States Department of Energy (DOE), the Electric Power Research Institute (EPRI), and Amoco Corporation. The unit capacity was about 6 tons of coal per day. Only the recent runs with low rank coals using the close-coupled, integrated two-stage liquefaction (CC-ITSL) mode with and without interstage separation with "ashy recycle" are discussed herein. "Ashy recycle" refers to the recycle of a portion of the mineral matter and unconverted coal with the recycle solvent to the feed tank and first reactor. Solids separation was achieved using a Kerr-McGee ROSE-SR<sup>SM</sup> unit. A description of the process has been reported.<sup>(1)</sup>

Four low rank coals were considered in this data analysis (three Wyoming subbituminous coals and a Texas lignite).

Consideration was made for differences in catalyst bed configurations. The pilot plant had two reactors. The reactor volumes were varied (50, 75, or 100%), and an ebullated supported-catalyst bed was used in none, one, or both reactors. In this paper, a "thermal" stage (T) indicates that no supported catalyst was used; however, the feed to the stage included red mud (an iron ore with limited catalyst activity). A "catalytic" stage (C) refers to the use of an ebullated-bed reactor. A "soluble catalyst" stage (S) refers to the use of a oil-soluble catalyst precursor. Combinations were used; for example, a T/C mode indicates that the first reactor was thermal and the second was catalytic. In addition, when a soluble catalyst precursor was added to the feed, it would be carried into the second stage. When the second stage was catalytic, the designation was S/C. Each of these modes called for different reactor temperatures, and because of the lack of experimental design, reactor temperatures were confounded with reactor configuration.

The data analysis was based on t-tests of the primary dependent variables grouped by reactor mode (T/C, C/C, C/T, S/T, and S/C). The primary assumptions were that differences between the coals were minimal and any effects of temperature, hydrogen partial pressure, and reactor volumes were lumped into the mode distinction.

## SUMMARY OF WILSONVILLE LOW RANK LIQUEFACTION RUNS

Overall coal conversion ranged between 87 and 95% (all yields and conversions were calculated on a moisture-ash-free basis: MAF). The average of the statistical group was 92.2%. This conversion was calculated as the MAF portion of the feed coal that was converted to creosote soluble materials. The conversion of the organic portion of the feed coal to total products other than solids recovered from the ROSE-SR unit was reported as 100%-energy rejection. This energy rejection included unconverted coal plus any heavy materials carried along with the solids in the reject stream from the ROSE-SR unit. Energy rejections ranged from about 9 to 24% with an average of 19%. This rejected energy isn't really lost in that the stream could be gasified along with additional coal to generate needed hydrogen and heat for the process.

The yield of distillable liquids (C<sub>4</sub>+distillate) averaged 54.7% with a range of about 47 to 57%. That of resid (material boiling above 1000°F) was about 5.5% with a range of 0 to 13%. It was regarded that the resid could have been further converted to distillate by being recycled to extinction in a commercial facility; therefore, the overall yield of liquids was projected to be about 60% with a maximum approaching 65%. The yields of light hydrocarbons (C<sub>1</sub>-C<sub>3</sub>) was sizeable with a range of 4.2 to 14.2% MAF. The average was 8.3% based on total MAF coal feed; this average calculated on a basis of coal converted to C<sub>4</sub>+distillate was 15.2%.

Hydrogen consumption is a significant factor in determining the cost of coal conversion to liquids. In the ideal case, all hydrogen should be consumed in generating distillate liquids. However, light hydrocarbon gases are generated and hetero-atom reduction (deoxygenation, desulfurization, and denitrogenation) add to hydrogen consumption. The level of hydrogen consumption in these low rank coal runs averaged 5.4% on an MAF coal feed basis (9.9% on a basis of coal conversion to C<sub>4</sub>+distillate). The range of hydrogen consumption was 4.3 to 7.7% MAF.

## STATISTICAL ANALYSIS OF WILSONVILLE RESULTS

### Designations and Definitions of Variables:

The following measures of yield/quality (with units in square brackets) were considered in this statistical evaluation:

1. Overall coal conversion [wt% MAF coal],
2. Energy rejection [ratio of combustibles in the ROSE-SR reject stream, "ash concentrate," to that of the feed coal, given as %],
3. Residuunconverted coal conversion [wt% MAF feed],
4. Individual distillate fraction yields [wt% MAF coal],
5. Overall resid (1000°F+) yield [wt% MAF coal],
6. Hydrogen yield/consumption [wt% MAF coal], and
7. Hydrogen efficiency [C<sub>4</sub>+ distillate/hydrogen consumed].

Table 1 summarizes the averages of the nominally independent variables for each of the modes considered. Note that temperatures for the soluble catalyst runs were higher in both stages than for the other run periods.

### Overall Coal Conversion (wt% MAF):

Figure 1 shows coal conversion as a function of operating mode. The highest level of coal conversion was achieved in the C/C mode. The C/T mode has very poor conversion compared to the other modes. Significant differences exist between C/C and C/T, C/C and S/C, and C/T and S/T modes. Conversion is improved by either switching to the soluble catalyst in the first stage or adding supported catalyst in the second stage.

### Energy Rejection:

Reactor operating mode has little effect on energy rejection as shown in Figure 2. The best (lowest) level of energy rejection was achieved in the C/C mode; this is consistent with this mode having the highest level of coal conversion. Only the difference between soluble catalyst and supported catalyst when using supported catalyst in the second stage is significant at 90% confidence.

(Resid+Unconverted Coal) Conversion (Wt% MAF feed):

Figure 3 summarizes the resid + UC conversion data. Significant differences exist between C/C and C/T, C/C and S/C, S/C and S/T, and C/T and S/T modes. Highest conversions again occur in C/C mode. This would be anticipated considering that an active, supported catalyst was used in both stages.

Overall Cl-C3 Yield (wt% MAF coal):

Figure 4 shows Cl-C3 yield as a function of operating mode. The lowest gas yield was that of the C/T mode periods. The highest yield of light hydrocarbon gases occurred in the C/C mode. This mode generated more light gases than the S/C mode in spite of having much lower temperatures (826/681° vs. 841/810°F).

Overall C4+ Total Yield (wt% MAF coal):

Figure 5 shows C4+ total yield as a function of operating mode. None of the differences are significant at 90% confidence (note the scale is expanded). While the operating mode has no significant effect on C4+ total yield, it is interesting that the pattern of C4+ yields is similar to that of the Cl-C3 yields as first stage and second stage modes are changed.

Overall Resid (1000°F+) Yield (wt% MAF coal):

Figure 6 shows resid (1000°F+) yield as a function of operating mode. None of the primary comparisons is statistically significant. The lowest yields occurred when operating in the S/C and C/C modes (averaging about 4%) while the averages of those of the other modes were in the range of 5% to 6%.

Overall Hydrogen Consumption (Wt% MAF coal):

Figure 7 shows hydrogen consumption as a function of operating mode. Significant differences exist between T/C and C/C, C/C and S/C, C/T and S/T, C/C and C/T, and S/C and S/T modes. Using supported catalyst in both stages consumes the most hydrogen, and the substitution of soluble catalyst for supported catalyst in the first stage resulted in reduced hydrogen consumption. It is interesting to note, however, that while the C/C mode consumes the most hydrogen, it is least efficient in putting that hydrogen into the distillate product.

#### CONCLUSIONS AND OBSERVATIONS

It is concluded that when liquefying low rank coals in a close-coupled, two-stage system similar to that at Wilsonville, the second stage should use supported catalyst in an ebullated bed configuration. The first stage should be catalytic, but the differences between soluble and supported catalysts are not particularly pronounced. (The use of a soluble catalyst was effective in limiting operating problems not discussed herein.) Operation with a supported catalyst in both stages generates more light oil fractions, but wastes hydrogen by making more light gases. Operation using a soluble precursor in the first stage makes more efficient use of hydrogen, but a slightly heavier product is generated.

#### ACKNOWLEDGMENTS

The authors are indebted to Drs. R. E. Lumpkin, A. Basu, and N. C. Stewart for their aid in the field of coal liquefaction and numerous individuals at DOE and Southern Company Services who participated in the operation of the Wilsonville facility.

#### REFERENCES

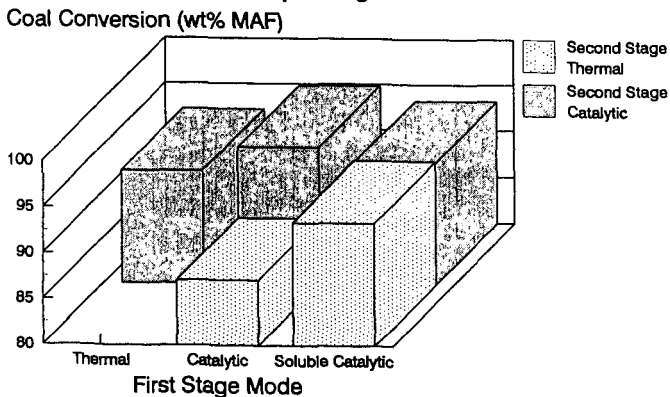
1. Lamb, C. W., Nalithan, R. V., Johnson, T. W., PREPRINTS: Am. Chem. Soc., Div. Fuel. Chem., 1986, 24, 1091.

Table I. Variable Averages by Operating Mode

Variable	Operating Mode					
	All runs	C/T	C/C	T/C	S/T	S/C
CoalConc	29.2	30.1	32.7	30.4	24.7	29.8
Vol1	62.5	75	100	63.889	50	50
Temp1	832	784	826	837	836	841
SpRate1	33.8	28.6	23.9	31.4	37.6	46.9
Vol2	63.971	100	100	62.5	50	50
Temp2	774	792	681	760	809	810
SpRate2	33.3	21.4	23.9	31.7	37.6	46.9

1. Coal Concentration in Feed Slurry [wt% MF], CoalConc - Coal concentration in the feed is defined as the concentration of coal on a MF basis in the slurry that is fed to the first reactor.
2. Relative Reactor Volume [%], Vol 1 or Vol 2. - Total liquid volume as a percent of full reactor volume.
3. Reactor Temperature [°F], Temp1, Temp2 - Individual reactor temperatures are designated as the average temperature over the length of the reactor.
4. Space Rate [%], SpRate1, SpRate2 - Space rate is calculated as the lb/hr feed rate of MF coal per ft<sup>3</sup> of single reactor volume and reported as a ratio to a standard value.

**Figure 1**  
Coal Conversion as a Function  
of Operating Mode



**Figure 2**  
**Energy Rejection as a Function**  
**of Operating Mode**

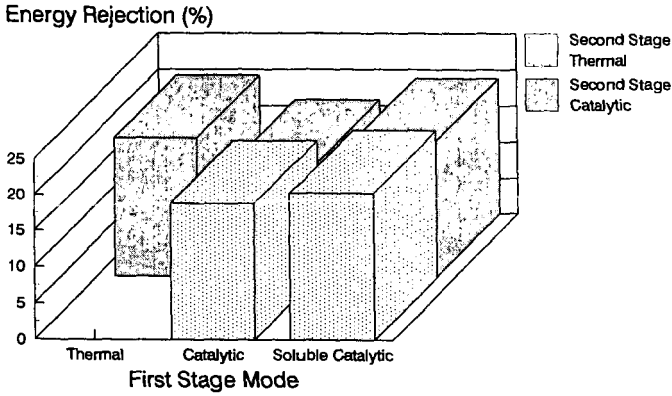


**Figure 3**  
**Resid+UC Conversion as a Function**  
**of Operating Mode**

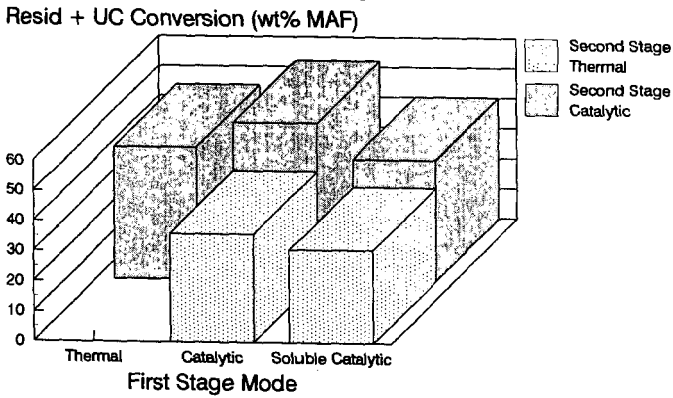


**Figure 4**  
**Overall C1-C3 Yield as a Function**  
**of Operating Mode**

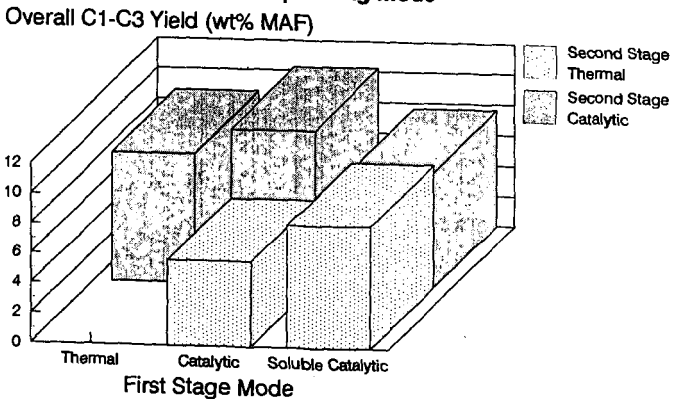


### Figure 5

Overall C4+ Total Yield as a Function of Operating Mode

Overall C4+ Total Yield (wt% MAF)

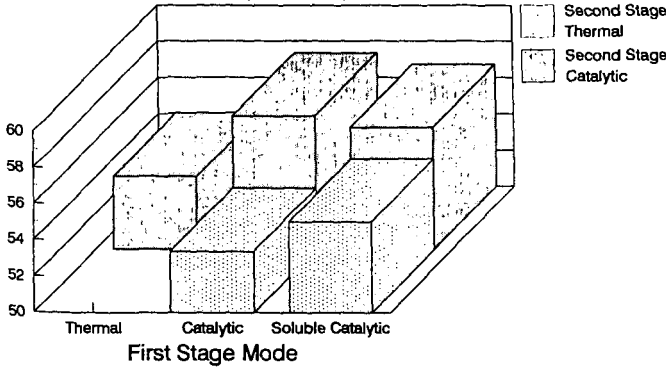


### Figure 6

Overall Resid Yield as a Function of Operating Mode

Overall Resid Yield (wt% MAF)

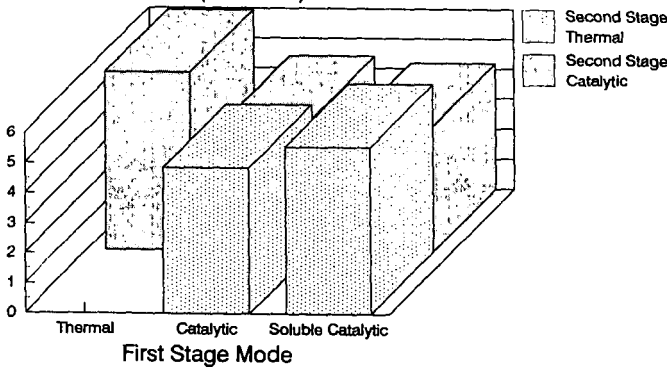
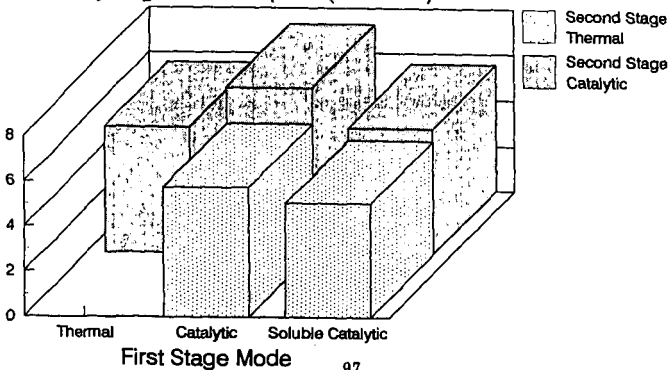


### Figure 7

Overall Hydrogen Consumption as a Function of Operating Mode

Overall Hydrogen Consumption (wt% MAF)



## Progress in Donor Assisted Coal Liquefaction : Hydroaromatic Compound Formation

R.J. Kottenstette and H.P. Stephens

Process Research Department Sandia National Laboratories

P.O. Box 5800

Albuquerque, New Mexico 87185-0709

**Keywords:** Hydrogen Donor, Coal liquefaction, Fluoranthene

### Introduction

The role of hydrogen donor compounds in coal liquefaction has been extensively investigated since the mid 1960's using model compounds and process derived hydrogen donor solvents [1-4]. Our recent research [5] and that of other investigators [4] have shown that two model compounds in particular have great efficacy in solvating low rank coals. 1,2,3,10b tetrahydrofluoranthene ( $H_4F$ ) and 1,2,3,6,7,8 hexahdropyrene ( $H_6Py$ ) have been used to dissolve Wyodak coal to > 95% soluble material as measured by tetrahydrofuran (THF). Although these hydrogen donors are very effective, they may not be found in any significant concentrations in actual liquefaction process recycle solvents. Therefore, studies with process derived recycle materials are necessary to understand donor solvent chemistry. The objective of this paper is to present results of solvent hydrogenation experiments using heavy distillate solvents produced during testing at the Wilsonville Advanced Coal Liquefaction Test Facility. We evaluated the impact of hydrogenation conditions upon hydrogen donor formation in process derived distillates and compared these process derived solvents with the highly effective  $H_4F$  and  $H_6Py$  donors in coal liquefaction tests. This paper presents data on reaction conditions used for distillate hydrotreating and subsequent coal liquefaction, with an aim toward understanding the relationship between reaction conditions and donor solvent quality in recycle distillates.

### Experimental

To evaluate distillate hydrotreating conditions, tests were performed with a laboratory-scale trickle-bed reactor. Coal liquefaction tests were performed with the hydrogenated distillates and model compounds to evaluate solvent quality. Proton NMR spectroscopy was used to evaluate distillate solvent quality by measuring hydroaromatic content.

**Materials-** Wyodak subbituminous coal was used as -100 mesh from the Argonne Premium Coal Sample Bank. Fluoranthene,  $H_6Py$ , and n-hexadecane with a 99% purity were purchased from the Aldrich Chemical Company.  $H_4F$  was produced by hydrogenating fluoranthene with the trickle-bed reactor at 260°C followed by separation from the hydrogenated mixture with a spinning band distillation column (Perkin Elmer 19" adiabatic); the final  $H_4F$  purity was ~96%. Dewaxed heavy distillate was prepared and supplied by Consol from the V1074 process stream (B.P. 650-1050°F) at the Wilsonville Advanced Coal Liquefaction Test Facility (Run 262/Wyodak coal feed).

**Apparatus-** Heavy distillate solvent was hydrogenated in a microflow reactor consisting of 0.5" O.D., 0.37" I.D. type 316 stainless steel tube that was enclosed in a convectively heated oven. The reactor tube was packed with the NiMo/Alumina catalyst, which was activated with  $H_2S$  in hydrogen. Heavy distillate feed was pumped into the reactor with an Eldex A-30 liquid chromatography pump and hydrogen was metered into the microflow reactor with a Brooks 5850 flowmeter. Gases and liquids were separated at high pressure, and liquids were periodically sampled from the product receiver vessel. Constant pressure was maintained with a Circle Seal BPR-7A back pressure regulator. Hydrotreating temperature was 320°C or 360°C, hydrogen pressure was 7 MPa (1000 psig), hydrogen flow was 330 sccm  $H_2$ /ccm distillate, and typical volume liquid hourly space velocities were  $\sim 1hr^{-1}$ . Proton NMR spectroscopy was performed on the hydrogenated heavy distillate with a 200.13 megahertz Bruker instrument after dissolution in chloroform according to the method of Winschel et al [6].

Coal liquefaction tests using microautoclave batch reactors [7] were performed to evaluate donor solvent quality. Hydrogenated solvent was tested in either of two microautoclaves (40 cc or 22 cc total gas volume) consisting of a Swagelok tubing tee which was heated in a fluidized sand bath while being shaken horizontally at 200 cycles per minute. The larger microautoclave has a slurry capacity of approximately 8cc while the smaller microautoclave has a slurry capacity of 2cc.

**Procedure -** After the heavy distillate was hydrogenated with the microflow reactor, proton NMR analyses were used to evaluate hydroaromatic content and coal liquefaction tests were performed to measure coal conversion with the distillates. Heavy distillate solvents representing various

hydrotreating conditions or H<sub>6</sub>Py or H<sub>4</sub>Fl were weighed into the microautoclave reactor with as-received coal. The microautoclaves were sealed and pressurized with 2.1 MPa (300 psig) nitrogen before reaction, fastened to the shaker and immersed in the fluidized sand bath. The microautoclaves were heated to reaction temperature until the desired time at temperature elapsed, and then cooled and depressurized. Gases were collected and the microautoclave was dismantled to recover the reaction products. The gas samples were analyzed for hydrogen, carbon monoxide, carbon dioxide and C<sub>1</sub>-C<sub>2</sub> hydrocarbons using a Carle series 400 Gas Chromatograph. Liquid and solids were recovered from the reactor with THF; THF insolubles were determined by pressure filtration. After the THF filtrate was roto-evaporated to remove most of the THF, pentane was added to these samples to precipitate the preasphaltene/asphaltene material. The product was pressure filtered to remove pentane insolubles which were dried and weighed. Coal conversion was calculated on a dry mineral matter free (dmmf) basis.

## Results and Discussion

**Solvent hydrogenation** - Hydrogen donor compounds are produced in recycle solvents by hydrogenating aromatic compounds in the catalytic stage of a two-stage liquefaction process or in a separate hydrotreating reactor. One measure of the effectiveness of this hydrogenation is the concentration of hydroaromatic compounds in the product oil. To illustrate this point fluoranthene was hydrogenated in a trickle-bed reactor at different temperatures. As can be seen in Figure 1, fluoranthene is readily hydrogenated to >80% of the desirable H<sub>4</sub>Fl at 250°C, but is hydrogenated to H<sub>10</sub>Fl and more extensively hydrogenated fluoranthene compounds at 300°C. These results illustrate that polynuclear aromatic hydrocarbons can be "overhydrogenated" to form alicyclic compounds which are poor hydrogen donors. Process solvents can be overhydrogenated in the same way and often become enriched in saturated material. Figure 2 presents the results of proton NMR analyses of heavy distillate samples hydrotreated at 360°C and shows that alkyl hydrogens, which make poor hydrogen donors, are more abundant, at the lower space velocities (0.7-0.9 hr<sup>-1</sup>) than at the higher space velocity (1.1 hr<sup>-1</sup>). However, hydroaromatic hydrogen (cyclic α+β) concentrations remain constant or are only slightly increased. Thus the content of hydroaromatic compounds can be controlled by the solvent residence time in the hydrogenation reactor. The accumulation of paraffinic material is somewhat process dependent in that different processes and feedstocks accumulate different amounts of these non-donor compounds [8]. Results from proton NMR analyses of several process derived distillate solvents are shown in Figure 3. Solvent A is a sample of V1074 heavy distillate that had been dewaxed by Consol. The dewaxed heavy distillate has been enriched in aromatic (from 15% to 22%) and hydroaromatic hydrogen (from 30% to 36%) compared to the original heavy distillate[9]. Sample B is a sample of Distillate A that was hydrogenated at 320°C with the trickle-bed reactor. This hydrogenation increased the hydroaromatic hydrogen concentration from 35.8% to 39.2%. Sample C is a sample of a pasting solvent from the Lummus process using Illinois #6 coal [8,10], and exhibits a higher aromatic character than the Wilsonville distillate. For comparison purposes a sample of H<sub>6</sub>Py was analyzed by the proton NMR method and included in the figure. The hydroaromatic cyclic α protons account for 50% of the H<sub>6</sub>Py hydrogen and because of proton assignments, some cyclic β protons in H<sub>6</sub>Py report to the alkyl designation. In any event, results in Figure 3 give a realistic picture of what can be expected from a recycle distillate in terms of hydrogen donor content, with H<sub>6</sub>Py being an upper bound with nearly 2.9% donatable hydrogen. Most recycle distillates have significantly more alkyl hydrogen, however, than pure donors such as H<sub>6</sub>Py and H<sub>4</sub>Fl as liquefaction experiments attest.

**Coal liquefaction tests** - Coal conversion experiments were performed to test the ability of the hydrogenated distillate or model compounds to liquefy coal. The tests were performed non-catalytically to evaluate the effectiveness of the solvents for coal conversion. Coal conversions for the model compound liquefaction tests are presented in Tables 1 and 2 along with the results from high resolution gas chromatography (HRGC) analyses for solvent recovery and amount of donor remaining. "Solvent recovery" is the sum of hydrogenated and dehydrogenated solvent compounds, while "donor remaining" is the amount of the original donor compound remaining in the product. Table 1 shows that coal conversion was >94% for all tests with H<sub>4</sub>Fl. HRGC analyses indicate that solvent recovery (% of initial solvent) decreases from 98% at 10 minutes to 73% at 60 minutes of reaction. The HRGC analyses show that the balance of the solvent is present as lower molecular weight cracked products. This observation is consistent with previous reports of disappearance of fluoranthene compounds from coal liquefaction recycle streams[2]. Table 2 presents the results of coal liquefaction tests using H<sub>6</sub>Py as the donor solvent. Coal conversion was greater than 92% for all of the 450°C runs. Solvent recoveries were also lower at the more severe conditions due to solvent cracking but the effect was not nearly as notable as for H<sub>4</sub>Fl. In general, H<sub>4</sub>Fl and H<sub>6</sub>Py are excellent hydrogen donors, which carry approximately 2-3% donatable hydrogen by weight and readily liquefy Wyodak coal. However, severe processing (long residence times at high temperatures) incurs solvent losses due to cracking.

Table 3 presents the results of coal liquefaction with the process solvents shown in Figure 3. Coal conversions were about 10% lower than similar experiments with H<sub>4</sub>Fl. The increased alkyl nature of the heavy distillates as compared with the pure hydrogen donor compound (Figure 3) would explain the lower conversions. More notable however, are the pentane solubility analyses of products using Sample A (unhydrogenated) and Sample B (hydrogenated) V1074 samples. Experiments with Sample A gave a negative seven percent pentane soluble yield indicating solvent adduction using Wyodak coal. Reaction at 425°C showed still further decreases in pentane soluble material (-31%) with the unhydrogenated distillate A, indicating that the solvent hydrogen was insufficient for preventing solvent adduction.

### Conclusions

Because they contain an overburden of saturated compounds, and therefore are unable to accept hydrogen to form higher concentrations of hydroaromatic compounds, hydrogenated process derived heavy distillate samples, in general, have less donatable hydrogen than pure hydrogen donor model compounds. However, processing steps such as dewaxing and carefully controlling hydrotreating conditions can significantly improve donor solvent content of the distillates. Model compounds such as H<sub>4</sub>Fl and H<sub>6</sub>Py are known to be excellent hydrogen donors, having two and three percent donor hydrogen by weight. Liquefaction tests with these compounds have shown high (>95%) conversion, yet illustrated that severe processing can reduce desirable solvent qualities by solvent cracking. Our experiments with model donor and heavy distillate solvents confirm that solvent hydrogen is very effective for coal liquefaction and appears to minimize solvent adduction reactions during coal thermolysis. Progress in coal liquefaction using donor hydrogen will occur by optimizing processing conditions to generate and maintain hydroaromatic species in the recycle distillate. Such processing conditions would consist of, but not be limited to, selective paraffin cracking, proper temperature, pressure and residence time for solvent hydrogenation and ensuring aromaticity of the solvent fed to a recycle hydrotreater.

### Acknowledgments

We gratefully acknowledge Consol Inc. for providing the dewaxed heavy distillate. This work was supported by the U.S. Department of Energy at Sandia National Laboratories under contract DE-AC04-94AL8500.

### References

- 1) Ruberto, R. G. , Cronauer, D. C. , Jewell D. M. , Seshadri, K. S. *Fuel* 1977, **56**, 17.
- 2) Kuhlman, E. J. , Jung, D. Y. , Guptill, R. P. , Dyke, C. A. , Zang, H. K. *Fuel* 1985, **64**, 1552.
- 3) Bien, C. N. , Luttin, K. P. , Smith, B. E. , White, N. , *Energy and Fuels* 1988, **2**, 807.
- 4) Mochida, I. , Takayama, A. , Sakata, R. , Sakanishi, K. *Energy and Fuels* 1990, **4**, 398.
- 5) Kottenstette, R. J. , Stephens, H. P. , Preprints of Papers, Amer. Chem. Soc. Div. Fuel Chem. 1993, **38(2)**, 534.
- 6) Winschel, R. A. , Robbins, G. A. , Burke, F. P. , *Fuel* 1986, **65**, 526.
- 7) Kottenstette, R. J. , Sandia National Laboratories Report SAND82-2495, 6 (1983).
- 8) Burke, F. P. , Winschel, R. A. , Robbins, G. A. , Coal Liquefaction Process Solvent Characterization and Evaluation. DOE/PC 70018-70, September 1989.
- 9) Winschel, R. A. , Lancet, M. S. , Robbins, G. A. , Burke, F. P. , Kottenstette, R. J. , Stephens, H. P. , Proceedings of the 1993 International Conference on Coal Science, Vol. 2, 279.
- 10) Gupta, A. , Peluso, M. , Schiffer, A. , Greene, M. , "The Development of Lummus Crest Inc. Integrated Two-Stage Coal Liquefaction Process: Enhanced ITSL Configuration", Proceedings of the DOE Direct Liquefaction Contractors' Review Meeting, 1985, Pittsburgh, PA.

**Figure 1. Concentration of Hydrogenated Fluoranthene Component in Hydrotreated Model Compound Mixture**

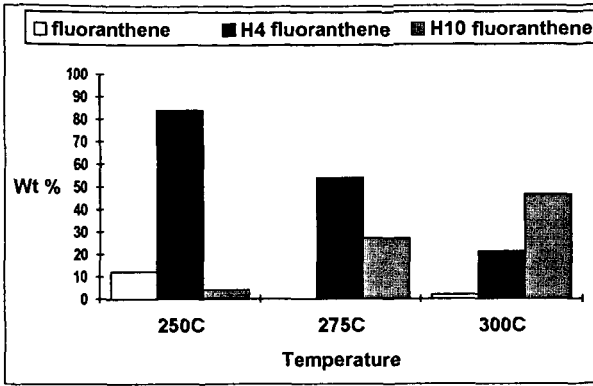


**Figure 2. Effect of Increased Hydrotreater Feed Rate upon Proton Distribution in Heavy Distillate.**

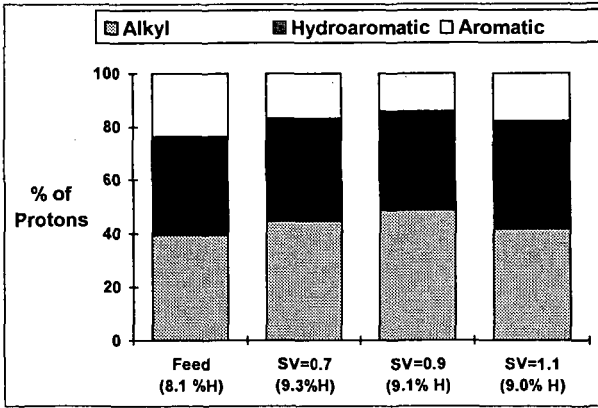
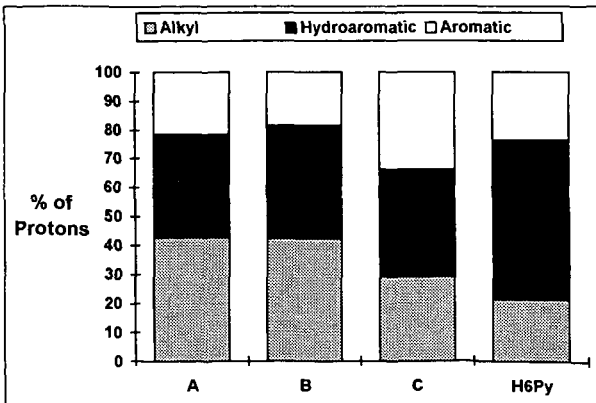


**Figure 3. Proton Distributions for Heavy Distillate Solvents and Hexahydropyrene**



A=Dewaxed V1074; B=Hydrotreated A; C=Lummus Pasting Solvent;

**Table 1. Wyodak Coal Liquefaction Results for 1,2,3,10b Tetrahydrofluoranthene. Solvent to Coal Ratio 2:1**

Time (min)	Temperature °C	THF conversion (%dmmf)	Donor remaining (wt%)	Solvent recovery (wt%)
10	450	94	48	98
20	450	96	26	91
40	450	97	14	80
60	450	98	8	73

**Table 2. Wyodak Coal Liquefaction Results for 1,2,3,6,7,8 Hexahydroperylene. Solvent to Coal Ratio 1.3:1**

Time (min)	Temperature °C	THF conversion (%dmmf)	Donor remaining (wt%)	Solvent recovery (wt%)
10	450	93	58	100
20	450	97	49	98
40	450	96	35	92
60	450	95	26	87

**Table 3. Wyodak Coal Liquefaction Results for Heavy Distillate Solvents. Solvent to Coal Ratio 2:1**

Time (min)	Solvent	Temperature °C	THF conversion (%dmmf)	% Pentane soluble yield
20	H4FI	400	73	ND
40	H4FI	400	79	ND
30	B	400	68	19
30	A	400	68	-7
30	B	425	81	10
30	A	425	75	-31

Coal Conversion = (dmmf coal in - iom out)/(dmmf coal in); Pentane (c5) soluble yield was calculated as (dmmf coal in - iom - c5 insol - gas make)/(dmmf coal in).

# EFFECT OF TEMPERATURE ON FUNCTIONALITY CHANGES DURING COAL LIQUEFACTION

J. T. Joseph, D. C. Cronauer, N. H. Rosenbaum  
Amoco Oil Company, Research and Development Department  
P. O. Box 3011, Naperville, IL 60566

A. Davis  
Department of Materials Science and Engineering  
The Pennsylvania State University  
University Park, PA 16802

*Keywords: Liquefaction, functional groups, FTIR analysis*

## INTRODUCTION

This paper discusses characterization of solids from the liquefaction of Black Thunder subbituminous coal using Wilsonville coal-derived solvents with and without dispersed molybdenum-containing catalyst precursors. The overall goals of the present investigation are to investigate low cost subbituminous coal liquefaction concepts using dispersed catalysts and to evaluate low temperature, short contact coal pretreatment to decompose carboxylic acids.

## EXPERIMENTAL

A sample of Black Thunder subbituminous coal was used for the present investigation. The coal was pulverized under  $N_2$  and screened to pass 100 mesh. The liquefaction solvents were coal-derived liquids obtained from the Wilsonville Advanced Coal Liquefaction Facility from runs made with Black Thunder subbituminous coal. Elemental analyses of the coal and solvent samples on a dry basis are given in Table I.

The liquefaction runs were made in a 300 cc, stirred tank single-stage continuous feed unit at temperatures of 316-449°C and space times of 14-30 minutes. The space time was calculated by dividing the reactor volume by the volumetric feed rate. The lower temperature runs (316 to 371°C) were carried out with Solvent A, a solvent blend consisting of 40 wt% ROSE®-SR resid and 60 wt% V-1074 vacuum bottoms (343-538°C). The higher temperature (399-449°C) runs were made Solvent B, which consisted of only V-1074 vacuum bottoms. Neither solvent had any THF insoluble materials to start with. After a line-out operating period, product slurry samples were extracted with tetrahydrofuran (THF). The residue was dried in a  $N_2$  swept vacuum oven at -60°C. Coal conversion was calculated on a moisture-ash-free (MAF) basis as the difference between weights of the feed coal and THF insoluble residue.

Infrared Spectroscopic Analysis of Liquefaction Residues: The THF insoluble residues in KBr pellets were analyzed by quantitative FTIR spectra on a Mattson Cygnus 100 FTIR spectrometer with a MCT detector. Sample preparation and spectral acquisition were performed in an inert atmosphere to prevent moisture absorption and air oxidation of the sample. Transmission FTIR spectra were obtained at 4  $cm^{-1}$  resolution using 1000 averaged scans. The following data manipulations were performed on the FTIR spectra: 1) mild smoothing to eliminate spectral fringing, 2) spectral subtraction of the H-bonded water spectrum to eliminate the absorbance band near 1630  $cm^{-1}$  due to the bending vibration of water absorbed or chemically bound to the sample or KBr, 3) a baseline correction in the 1500-1750  $cm^{-1}$  region that consisted of overlapped bands of carbonyl and aromatic functional groups, and 4) curve fitting (Curvefit in Spectra Calc Software of Galactic Industries) to fit spectra to individual line shapes (Gaussian/Lorentzian profile.)

All FTIR intensities were normalized to the weight of the starting coal sample, to reflect the concentration of each functional group present in the residue on a starting material basis. This method of weighting is only qualitative, because the soluble portion and the residue do not have the same distribution of functional groups.

## RESULTS AND DISCUSSION

Coal Conversion. Coal conversion to THF solubles in the thermal and catalytic liquefaction runs is summarized in Figure 1. At 399 and 427°C catalyst addition caused 2 - 5% increase in the THF solubles. At 441 and 449°C this difference increased to ~8%. The THF insoluble fraction is considered to be "unconverted coal"; however, previously dissolved coal-derived components that have undergone retrogressive coking reactions also may become insoluble in THF.

Elemental Composition of THF Insolubles. The H/C and O/C ratios of the THF insolubles from both non-catalytic and catalytic runs are summarized in Table II. These results follow expected trends with increasing liquefaction temperature. The H/C ratios of the 316 and 329°C THF insolubles were marginally higher than that of the feed coal. This is presumably due to some incorporation of the solvent into the coal solids. With the start of liquefaction, the H/C ratio decreased with increasing temperature and coal conversion. The O/C ratio also decreased as temperature increased.

**Petrographic Examination of Unconverted Coal.** A visual separation of the unconverted coal from coke can be achieved by petrographic analysis. Selected results of the microscopic examination of samples of raw coal and THF insolubles are presented in III. In summary, the resinous liptinite was completely converted as reaction temperature increased, the vitrinite and semi-inertinite macerals were progressively converted, and the inertinite underwent little conversion and was concentrated in the THF insolubles. Vitroplast (coke) formation was high at 449°C.

**FTIR Characterization of THF Insoluble Fractions.** The functional groups that were studied included aliphatic C-H, carboxyls, and ethers. The weighted FTIR intensities of these functional groups were plotted on an arbitrary scale against liquefaction temperature in Figures 2-7. Hydroxyl groups were not analyzed because of the difficulty in quantifying the O-H stretching bands due to the interference from moisture.

**Aliphatic C-H:** For most organic compounds, the aliphatic C-H bond stretching bands can be found in the 2890-2970  $\text{cm}^{-1}$  region<sup>(1,2)</sup>. Although the liquefaction residue is highly aromatic, the aromatic C-H bonds are less abundant than the aliphatic C-H bonds because of the preponderance of multinuclear aromatic structures present in the residue<sup>(2)</sup>. The weighted intensities of the absorption bands in the range of 2800-3000  $\text{cm}^{-1}$  for non-catalytic and catalytic residues are plotted against reaction temperature in Figures 2 and 3, respectively. The data indicate that for the non-catalytic residue, the C-H intensity stays the same up to 371°C and then slowly decreases. For the catalytic residue, the C-H intensity of the residue increases after the liquefaction at 343°C and then decreases at a faster rate than the non-catalytic residue. Both catalytic and non-catalytic liquefaction at 449°C produces similar residues, indicating a maximum coal conversion at that temperature. It appears that the soluble catalyst assists hydrogenation at lower temperatures and dehydrogenation at higher temperatures. Therefore, attention should be given to the appropriate temperature range when selecting the most beneficial coal liquefaction catalysts.

**Carboxylate Groups:** The weighted intensities of aliphatic acids (1675-1725  $\text{cm}^{-1}$ ), aromatic acids (1645-1665  $\text{cm}^{-1}$ ), and carboxylate anions (1534-1560  $\text{cm}^{-1}$ ) in non-catalytic and catalytic residues are plotted against reaction temperature in Figures 4 and 5, respectively. These data indicate that the aliphatic acids decompose much more rapidly than the other two types, and the levels of decomposition in both the non-catalytic and catalytic runs are essentially the same. This observation is consistent with published data<sup>(2)</sup>. It is also known that the shorter the aliphatic chain, the faster the carboxyl group decarboxylates<sup>(3)</sup>. Therefore, it appears that Black Thunder coal may not contain significant quantities of long chain fatty acids.

While aliphatic acids begin to decarboxylate at lower temperatures, in the absence of a catalyst, aromatic acid content decreases significantly only above 399°C. It has been reported that thermally, aromatic acids decarboxylate easily if there are activating groups present on the aromatic ring.<sup>(4,5)</sup> For example, a hydroxyl group in the *ortho* position can stabilize the carboxylate activated complex by hydrogen bonding and thus enhance the rate of decarboxylation. The results of the non-catalytic liquefaction runs indicate that the Black Thunder aromatic acids do not contain suitable activating groups for facile decarboxylation. However, the dispersed catalyst assists decarboxylation of the aromatic acids even at 343°C.

It appears that the carboxylate ions are virtually unaffected in the non-catalytic runs. However, in the presence of the catalyst, the carboxylate concentration decreases slowly with temperature and substantial decarboxylation occurs at 449°C.

In short, during non-catalytic liquefaction only the aliphatic acids decarboxylate significantly. In contrast, decarboxylation of all three carboxylate types are enhanced by the dispersed molybdenum catalyst.

**Ether and Hydroxyl Groups:** Identification of ether groups from the infrared spectra of complex organic molecules is notoriously difficult because the characteristic bands (1100-1300  $\text{cm}^{-1}$ ) of these groups appear in the midst of absorbance bands of many other groups, especially those of water and hydroxyl groups. (Because the samples were dried under nitrogen and the KBr pellets were handled in a dry atmosphere, the amount of moisture present in the test samples is assumed to be negligible compared to that of the hydroxyl groups.)

For this discussion, the absorption band centered at the 1100  $\text{cm}^{-1}$  (1140-1065  $\text{cm}^{-1}$ ) is considered to be due to the ether groups, the bands in the range of 1065-1020  $\text{cm}^{-1}$  (peaking at 1040  $\text{cm}^{-1}$ ) are assigned to both ethers and hydroxyls, and the bands in the range of 1020-990  $\text{cm}^{-1}$  (peaking at 1010  $\text{cm}^{-1}$ ) are assigned to substituted furans - possibly dibenzofurans<sup>(6,7)</sup> and to alcohols  $\beta$  to an aromatic ring<sup>(7,8)</sup>. Several layered silicates also have strong bands in this region<sup>(9,10)</sup>. However, because of the small amount of mineral matter present in the starting coal, the contribution from the silicates is not considered predominant.

The ether group intensities in the non-catalytic and catalytic residues are plotted against liquefaction temperature in Figures 6 and 7, respectively. For the non-catalytic runs, the ether band intensity at 1100  $\text{cm}^{-1}$  increases with temperature above 343°C. This is a clear indication of the formation of ether bonds as the liquefaction severity is increased. Most likely the ether bonds are of diaryl type

and could be formed by condensation of phenolic groups with other phenolic groups or with aromatic structures. The diaryl ether bonds are thermally very stable, and their formation indicates significant retrogressive reactions during uncatalyzed coal liquefaction above 399°C.

The 1040  $\text{cm}^{-1}$  band shows a slight increase in intensity in the residue from the 399°C reaction, but decreases with further increases in temperature. The high intensity of this band at lower temperatures is probably due to the formation of hydroxyl groups (alcohols or phenols) by the hydrolysis of ethers. These hydroxyl groups disappear by hydrogenation at higher temperatures and therefore, their intensities are reduced.

The ether and hydroxyl group intensities of the residues from the catalytic runs show a significantly different pattern from that of the residues from the non-catalytic runs. The changes in the 1100  $\text{cm}^{-1}$  band intensity with temperature for the catalytic runs are much less marked than those for the non-catalytic runs. In contrast, the intensity of the ether band at 1040  $\text{cm}^{-1}$  approximately doubled with a temperature increase from 316 to 343°C, and it subsequently decreased with increase in temperature, indicating substantially different reactions in the catalytic and non-catalytic runs. The overall effect of the catalyst is to reduce in the ether/hydroxyl group concentration in the residue.

The behavior of the 1010  $\text{cm}^{-1}$  band also differs in the presence of the catalyst. The intensity of this band, which may be due mainly to dibenzofurans and hydroxyls  $\beta$  to an aromatic ring, increases significantly above 399°C. Above 399°C, the contribution to this band could be primarily from dibenzofurans. Since the curves for the 1040  $\text{cm}^{-1}$  and the 1010  $\text{cm}^{-1}$  band intersect slightly above 399°C, it is tempting to conclude that at this temperature, the hydroxyl groups may be effectively converted to the dibenzofurans in the presence of the catalyst. Quantitative measurement of hydroxyl and dibenzofuran groups is necessary to confirm this hypothesis.

## CONCLUSIONS

The following conclusions are drawn from the characterization of THF insolubles generated from the liquefaction of Black Thunder subbituminous coal using a short contact time, single-stage, continuous flow reactor: Dispersed molybdenum catalyst precursor enhances the dissolution of coal to THF solubles by 3 to 8% depending upon reaction temperature. It assists hydrogenation at lower temperatures and dehydrogenation at higher temperatures. The addition of the catalyst also serves to decrease the level of ether/hydroxyl groups left in the residue.

Aliphatic acids decompose much more rapidly than the other types of acids, and the level of their decomposition is not influenced by the presence or absence of the catalyst. The aromatic acids and carboxylate ions do not undergo facile thermal decarboxylation. The dispersed molybdenum catalyst facilitates decarboxylation of all carboxylate groups.

A number of retrogressive reactions occur during coal liquefaction above 427°C. This is confirmed by the presence of a high concentrations level of vitroplast and dibenzofuran type structures in the THF insoluble residues.

## REFERENCES

1. Bellamy, L. J. *The Infra-red Spectra of Complex Molecules, Volume 1*, Chapman and Hall, London, 1975.
2. Solomon, P. R., Miknis, F. P. *Fuel*, **1980**, *59*, 893.
3. Seshadri, K. S., Young, D. C., Cronauer, D. C. *Fuel*, **1985**, *64*, 22.
4. Bredig, G., Balcom, R. W. *Chem. Ber.*, **1908**, *41*, 740.
5. Clark, L. W. in *The Chemistry of Carboxylic Acids and Esters*, Patai, S. Ed; Interscience-Publishers, London, 1969, *Chapter 12*.
6. Clark, L. W. *J. Phys. Chem.*, **1963**, *67*, 2831.
7. Pouchert, C. J. *The Aldrich Library of FT-IR Spectra, Volume I*, Aldrich Chemical Company, Milwaukee, 1985.
8. Clark, L. W. *J. Phys. Chem.*, **1965**, *69*, 3565.
9. Socrates, G. *Infrared Characteristic Group Frequencies*, John Wiley & Sons, New York, 1980.
10. Farmer, V. C. in *The Infra-red Spectra of Minerals*, Mineralogical Society, London, 1974, *Chapter 15*.

TABLE I  
ELEMENTAL ANALYSES OF COAL AND SOLVENTS

	Coal	Solvent A	Solvent B
Elemental Analyses, Wt% (Dry basis)			
Carbon	69.60	89.56	87.23
Hydrogen	5.01	8.26	9.68
Nitrogen	1.07	0.80	0.53
Oxygen (diff)	17.14	1.33	2.52
Sulfur	0.46	0.05	0.04
Ash	6.72	0.0	0.0

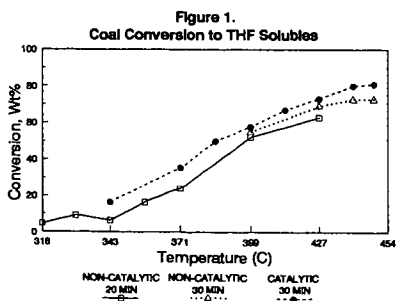
TABLE II  
CHANGES IN THE ATOMIC RATIOS OF LIQUEFACTION RESIDUE FROM  
BLACK THUNDER COAL WITH TEMPERATURE

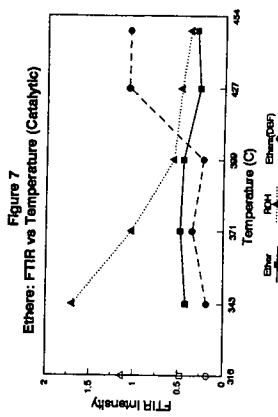
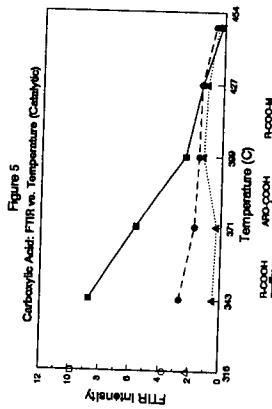
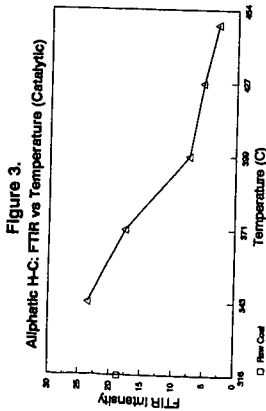
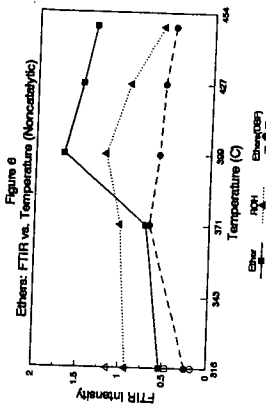
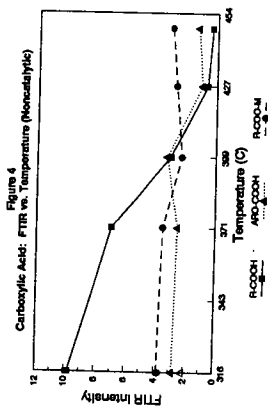
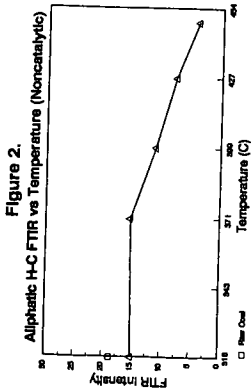
Temperature(C)	Conversion,wt%		H/C		O/C	
	n-c	c	n-c	c	n-c	c
316	4.8	-	0.85	-	0.17	-
329	9.3	-	0.84	-	0.17	-
343	6.5	16.5	0.81	0.91	0.14	0.21
357	16.5	-	0.80	-	0.15	-
371	24.2	35.8	0.79	0.89	0.14	0.19
399	52.5	57.9	0.79	0.87	0.17	0.18
427	63.1	73.3	0.77	0.87	0.15	0.18
441	72.9	-	0.74	-	0.11	-
449	72.9	81.2	0.68	0.77	0.09	0.14

n-c = non-catalytic; c = catalytic

TABLE III  
PETROGRAPHIC ANALYSIS OF BLACK THUNDER COAL AND  
LIQUEFACTION RESIDUES

	Coal	399°C Residue	449°C Residue
THF Insolubles, wt%	99	42	19
Maceral Distribution, wt%			
Huminite(vitrinite)	82	78	39
Liptinite	3	1	0
Semi-inertinite	7	6	8
Inertinite	5	10	26
Vitroplast	3	5	27





# CHEMICAL STRUCTURE CHANGES OF COAL, CHAR, AND TAR DURING DEVOLATILIZATION

Thomas H. Fletcher<sup>†</sup> and Ronald J. Pugmire<sup>‡</sup>

<sup>†</sup>Chemical Engineering Dept., Brigham Young University, Provo, UT 84602

<sup>‡</sup>Dept. of Chemical and Fuels Engineering, The University of Utah, Salt Lake City, UT 84112

Keywords: coal, pyrolysis, <sup>13</sup>C NMR

## Introduction

Enormous progress has been made in coal pyrolysis research during the last decade. Models of coal devolatilization have progressed from simple rate expressions based on total mass release<sup>1, 2</sup> to empirical relationships based on the elemental composition of the parent coal<sup>3</sup> to models that attempt to describe the macromolecular network of the coal.<sup>4-6</sup> Measurements of particle temperature during devolatilization have eliminated much of the controversy regarding overall rates of devolatilization.<sup>7-10</sup> In the last several years, advancements in chemical analysis techniques have allowed quantitative investigations of the chemical structure of both coal and its pyrolysis products, including the nature of the resulting char. A prominent research goal is to accurately predict the rates, yields, and products of devolatilization from measurements of the parent coal structure. This goal necessitates modeling the reaction processes on the molecular scale, with activation energies that relate to chemical bond breaking rather than release of products from the coal. <sup>13</sup>C and <sup>1</sup>H NMR spectroscopy have proven particularly useful in obtaining average values of chemical structure features of coal, char, and tar.<sup>11-14</sup> This paper reviews experimental data regarding chemical structure features of coal, char, and tar during rapid devolatilization, and how these data have impacted the development and input parameters for devolatilization models. In particular, the relationship between pyridine extract yields and extract yields predicted purely from NMR chemical structure data is discussed.

## Parent Coal Structure

Coal consists of a macromolecular structure of fused aromatic rings connected by non-aromatic bridges and loops. Although measurement of carbon aromaticity in coals has been possible for a number of years, more detailed quantification of chemical features of coal structure has become possible in the last five years. Advanced solid state <sup>13</sup>C NMR techniques (CP/MAS and dipolar dephasing), combined with carbon counting, have been used to determine the chemical structure features of the Argonne Premium Coals.<sup>11, 15</sup> In addition to carbon aromaticity ( $f_a$ ), the distinction between aromatic carbons with and without attachments (such as hydrogen, carbon, or oxygen) is measured. A correlation was made to determine the average number of aromatic carbons per fused aromatic cluster assuming circular rather than linear catenation.<sup>11</sup> The specification of the number of aromatic carbons per cluster ( $C_c$ ) provides the basis for the determination of many interesting chemical structure features. Probably one of the most useful quantities is the number of attachments per aromatic cluster, referred to as the coordination number ( $\sigma+1$ ), which is determined from the number of alkylated ( $f_a^P$ ) and phenolic ( $f_a^S$ ) attachments to aromatic carbons, as follows:

$$\sigma + 1 = \frac{(f_a^P + f_a^S) C_c}{f_a} \quad (1)$$

In addition to the total number of attachments per cluster, it is possible to determine the fraction of total carbons in methyl and methoxy groups. This quantity identifies methyl groups, which, to a first approximation, are considered to be the only chain terminators. This allows quantification of the total attachments per cluster into chains that terminate (i.e., attachments with methyl groups, referred to as side chains) and chains that connect to other aromatic clusters (referred to as bridges and loops). Since this is a carbon counting method, there may be some discrepancy in that oxygen bridges are not counted. The fraction of attachments that are bridges between clusters ( $p$ ) is determined as follows:

$$p = \frac{f_a^P + f_a^S - f_{al}^*}{f_a^P + f_a^S} \quad (2)$$

and (1-p) is the fraction of attachments that are side chains. Orendt, et al.<sup>15</sup> showed that the coordination number varies from 3.9 to 5.6 for the Argonne premium coals, while the fraction of attachments existing as bridges and loops ( $p_0$ ) ranged from 0.49 to 0.74. This means that on average, each aromatic cluster is connected to other aromatic clusters at  $p(\sigma+1)$  or 2.5 to 3.6 points. In contrast, a long chain-like polymer with no crosslinks contains 2.0 connecting bridges

per aromatic cluster. In general, the more crosslinks per aromatic cluster (i.e., as the coordination number increases beyond 2.0), the harder it is for a material to thermally decompose.

Once the number of aromatic carbons per cluster and the number of total attachments per cluster are determined, the average cluster molecular weight ( $M_{cl}$ , including side chains and one-half the bridges and loops) can be determined using the elemental carbon composition ( $x_C$ ) and the molecular weight of carbon ( $M_C$ ).<sup>4, 11</sup>

$$M_{cl} = \frac{C_{cl} M_C}{f_a' x_C} \quad (3)$$

This corresponds to the size of the average monomer unit in the coal macromolecule. The average molecular weight of a side chain ( $M_\delta$ ) can also be determined:

$$M_\delta = \frac{M_{cl} - C_{cl} M_C}{\sigma + 1} \quad (4)$$

Values of cluster molecular weights ( $M_{cl}$ ) in parent coals determined using this method range from 270 to 410 amu, with no clear trend with coal rank. Side chain molecular weight ( $M_\delta$ ) show a clear trend with coal rank, ranging from 12 amu for the high rank coals to 52 for the low rank coals (see Fig. 1). These average values of  $M_\delta$  roughly correspond to methyl groups (15 amu) and carboxylic acid groups (45 amu), respectively. It must be remembered, however, that these values represent weighted average of many types of attachments.

### Structure of Pyrolysis Products (Chars and Tars)

Char and tar samples were obtained as a function of residence time in a devolatilization experiment (1250 K,  $2 \times 10^4$  K/s in nitrogen) and just subsequent to devolatilization in a laminar flame-fired experiment (1500 K,  $5 \times 10^4$  K/s).<sup>14</sup> Quantitative measurements of chemical structure were performed on the coals and chars using the <sup>13</sup>C NMR techniques described above. Results show that the chemical structures of fully-devolatilized chars are very similar, even though a wide diversity is seen in the parent coal structures. For example, the average cluster molecular weights of the fully-pyrolyzed chars span a range of only 50 amu, in contrast to the span of 150 amu observed in the parent coals. Side chain molecular weights of the fully-pyrolyzed chars span a narrow range from 11 to 18 amu, which contrasts even more with the parent coal data (see Fig. 1). The change in side chain molecular weight is most dramatic for the low rank coals, corresponding to the release of large amounts of aliphatic material as light gases. The similarity in chemical structure of fully-devolatilized coal chars suggests that differences in measured heterogeneous char reactivities may be influenced primarily by physical structure.<sup>14</sup>

### Use of Chemical Structure Features in Devolatilization Models

The use of statistics applied to polymer chains was applied to coal devolatilization by Niksa and Kerstein.<sup>16</sup> Devolatilization models have evolved to use network structures that represent coal as aromatic clusters connected by labile bridge material.<sup>4-6</sup> A summary of these three models was recently published.<sup>17</sup> A non-linear relationship exists between the number of intact labile bridges and the amount of clusters disconnected from the "infinite" lattice structure.<sup>18</sup> Closed-form solutions have been formulated to relate the breakup of the lattice structure to the bridge population and the initial characteristics of the lattice. Both straight chain lattices<sup>5</sup> and Bethe lattices<sup>6, 18</sup> have been used to represent the coal macromolecular structure.

The three coal devolatilization models utilize the chemical structure features available from solid-state NMR analyses in different ways. All of the models use or reference the number of aromatic carbons per cluster (i.e.,  $MW_{cluster}$ ). The number of attachments per cluster ( $\sigma+1$ ) are used directly in the CPD and FG-DVC models, but straight chains are used in FLASHCHAIN. The molecular weight per side chain ( $MW_\delta$ ) is used directly in the CPD model, and directly impacts the light gas yield. In the FG-DVC model, the light gas species evolution is specified based on empirical fits of light gas yields in TG-FTIR experiments, and therefore does not link the light gas evolution directly to the lattice structure of the parent coal. In FLASHCHAIN, the molecular weights of the bridge material are much larger than the NMR data, and a correction factor is used to specify the final molecular weight of the light gas.

The direct use of NMR data to specify the coal-dependent parameters is illustrated in Fig. 2, which compares predicted tar and total volatiles yields for sixteen coals during devolatilization at heating rates from 1 to 10,000 K/s agree with measured values.<sup>14</sup> For most coals, no adjustable parameters were used to tune the predictions to match the yields. However, one adjustable parameter was used for lignite to represent early crosslinking, while this same parameter was adjusted to represent stable bi-aryl bridges in high rank coals (i.e., Iv bituminous). In these predictions, the total gas yield was calculated without the use of yield factors from previous pyrolysis experiments.

The initial fraction of the labile bridges that are intact specifies the connectivity of the lattice. The initial lattice is generally not fully connected, and a certain amount of free or

disconnected material is predicted by the lattice statistics. This material is generally thought to correspond to the solvent extracts from unreacted coals. However, there seems to be a discrepancy between the amount of "extracts" predicted by using the solid state NMR data and measured pyridine extract yields. Figure 3 shows pyridine extract yields from the Argonne Premium coals measured by Fletcher, et al.<sup>19</sup> Also shown are the predicted amounts of unattached material (i.e., extract) based on a Bethe lattice with coordination number and fraction of intact bridges taken directly from NMR measurements using the CPD model. The measured pyridine extract yields are as high as 26% for the Pittsburgh #8 coal, while the predicted yields for this coal are significantly lower.

Possible reasons for the lack of agreement between measured pyridine extracts and predictions based on NMR structural data are:

- (i) errors in the NMR measurements and their interpretation
- (ii) the use of average NMR structural data rather than distributions
- (iii) the use of Bethe lattices as approximations of coal molecular structure
- (iv) the representation of the extract and the residue by the same lattice structure, even though they are chemically different

Of these hypotheses, (iv) seems to be the most rationale explanation for the disagreement shown in Fig. 3. For example, the total number of attachments per cluster ( $\sigma+1$ ) determined by <sup>13</sup>C NMR in the pyridine extracts is an average of 15% lower than in the corresponding residue, as shown in Fig. 4 for the Argonne Premium coals.<sup>19</sup> The number of aromatic carbons per cluster in the pyridine extracts is also consistently lower than in the corresponding residues, and the result is lower molecular weights per cluster in the extracts (Fig. 5). The number of bridges and loops per cluster is also lower in the extracts than in the residues, although the molecular weight per side chain in the extracts is similar to that in the corresponding residues. The differences in average chemical structure features between the extracts and residues seems to confirm hypothesis (iv) above; the extract is chemically different from the residue and should not be treated with the same lattice structure. These results obviously have the most impact for those coals with high pyridine extract yields.

### Conclusion

Coal pyrolysis research has progressed to the point that measurements of the chemical structure features of parent coals is useful in current devolatilization models. Chemical structure features of particular importance to modeling efforts seem to be the number of aromatic carbons per cluster, the number of attachments per cluster, and the total molecular weight per cluster (including attachments). Most current models are able to describe tar and gas yields as a function of time, temperature, heating rate, coal type, and pressure, although the network models of devolatilization appear to have the closest ties with coal structure. However, the models selectively use chemical structure information in order to attain agreement with measured tar and gas yields, while other pertinent data are ignored. One such example is that the models use as input parameters either measured pyridine extract yields *or* the fraction of intact connecting bridges. Chemical structure features of pyridine extracts do not match those of the corresponding residue, suggesting that models should treat extracts as a different chemical than the coal. The challenge for the models is to reduce the number of empirical parameters by using chemical structure information.

### Acknowledgments

This work was sponsored by the Advanced Combustion Engineering Research Center at Brigham Young University and the University of Utah. Funds for this center are received from the National Science Foundation, the State of Utah, 31 industrial participants, and the U. S. Department of Energy. The authors also acknowledge the contributions of Dave Grant and Mark Solum at the University of Utah who were key participants in much of the work reviewed here.

### References

1. Anthony, D. B., J. B. Howard, H. C. Hottel and H. P. Meissner *15th Symposium (International) on Combustion*; The Combustion Institute, Pittsburgh, PA: 1974; pp 1303-1317.
2. Kobayashi, H., J. B. Howard and A. F. Sarofim *16th Symposium (International) on Combustion*; The Combustion Institute, Pittsburgh, PA: 1976; pp 411-425.
3. Ko, G. H., D. M. Sanchez, W. A. Peters and J. B. Howard *22nd Symposium (International) on Combustion*; The Combustion Institute, Pittsburgh, PA: 1988; pp 115-124.
4. Fletcher, T. H., A. R. Kerstein, R. J. Pugmire and D. M. Grant *Energy and Fuels* 1992, 6, 414.
5. Niksa, S. *Energy and Fuels* 1991, 5, 673-683.

6. Solomon, P. R., D. G. Hamblen, R. M. Carangelo, M. A. Serio and G. V. Deshpande *Energy and Fuels* **1988**, 2, 405-422.
7. Solomon, P. R., M. R. Serio, R. M. Carangelo and J. R. Markham *Fuel* **1986**, 65, 182-193.
8. Fletcher, T. H. *Combustion Science and Technology* **1989**, 63, 89.
9. Fletcher, T. H. *Combustion and Flame* **1989**, 78, 223.
10. Solomon, P. R., T. H. Fletcher and R. J. Pugmire *Fuel* **1993**, 72, 587-597.
11. Solum, M. S., R. J. Pugmire and D. M. Grant *Energy and Fuels* **1989**, 3, 187.
12. Fletcher, T. H., M. S. Solum, D. M. Grant, S. Critchfield and R. J. Pugmire *23rd Symposium (International) on Combustion*; The Combustion Institute, Pittsburgh, PA: **1990**; pp 1231.
13. Pugmire, R. J., M. S. Solum, D. M. Grant, S. Critchfield and T. H. Fletcher *Fuel* **1991**, 70, 414.
14. Fletcher, T. H., M. S. Solum, D. M. Grant and R. J. Pugmire *Energy and Fuels* **1992**, 6, 643-650.
15. Orendt, A. M., M. S. Solum, N. K. Sethi, R. J. Pugmire and D. M. Grant In *Advances in Coal Spectroscopy*; H. L. C. Meuzelaar, Ed.; Plenum Press: New York, **1992**; pp 215-254.
16. Niksa, S. and A. R. Kerstein *Combustion and Flame* **1986**, 66, 95-109.
17. Smith, K. L., L. D. Smoot and T. H. Fletcher In *Fundamentals of Coal Combustion for Clean and Efficient Use*; L. D. Smoot, Ed.; Elsevier: New York, **1993**; pp 131-298.
18. Grant, D. M., R. J. Pugmire, T. H. Fletcher and A. R. Kerstein *Energy and Fuels* **1989**, 3, 175-186.
19. Fletcher, T. H., S. Bai, R. J. Pugmire, M. S. Solum, S. Wood and D. M. Grant *Energy and Fuels* **1993**, 7, 734-742.

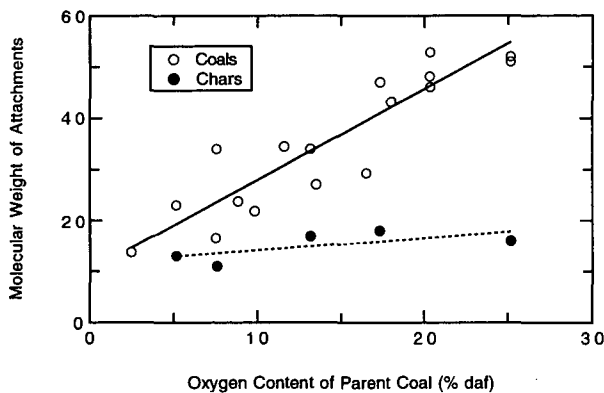


Figure 1. Average molecular weight of side chains attached to aromatic clusters in unreacted coals and fully-devolatilized chars. Oxygen content of the parent coal is used as a rank indicator. Lines represent linear correlations of the data (see Fletcher et al.<sup>14</sup>)

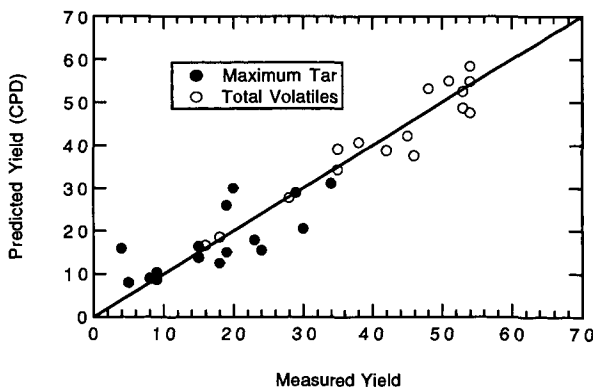


Figure 2. Comparison of predicted tar and total volatiles yields from NMR structural data versus measurements. Data are from sixteen coals during pyrolysis over a range of heating rates (see Fletcher et al.<sup>4</sup>)

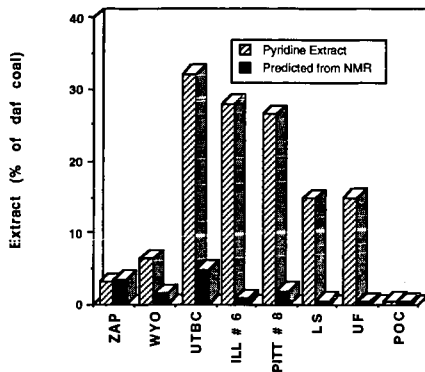


Figure 3. Measured pyridine extract yields compared with predictions of unconnected fragments in a Bethe lattice using  $^{13}\text{C}$  NMR characterizations of average chemical structure (see Fletcher, et al.<sup>19</sup>).

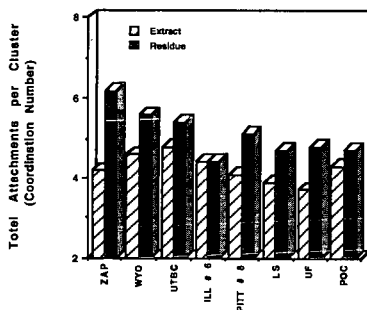


Figure 4. Coordination numbers ( $\sigma+1$ ) determined from  $^{13}\text{C}$  NMR analyses of pyridine extractions of the Argonne premium coals (see Fletcher, et al.<sup>19</sup>).

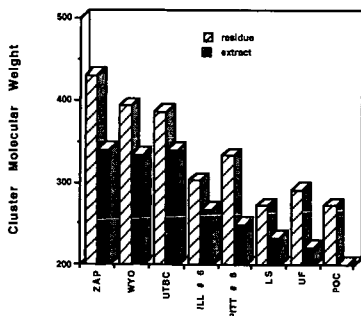


Figure 5. Average molecular weight per cluster determined from  $^{13}\text{C}$  NMR analyses of pyridine extractions of the Argonne premium coals (data from Fletcher, et al.<sup>19</sup>).

## THE PRODUCTION OF MATERIALS AND CHEMICALS FROM COAL

Frank Derbyshire, Marit Jagtoyen, You Qing Fei, and Geoff Kimber

University of Kentucky Center for Applied Energy Research,  
3572 Iron Works Pike, Lexington KY 40511-8433

**Keywords:** Coal, Chemicals, Carbon Materials

### Introduction

When coal came to prominence as a fuel during the Industrial Revolution, there developed, in parallel, its use for the production of materials and chemicals. By-product liquids and gases from coal carbonization processes became the basic raw materials for the organic chemical industry, and the production of metallurgical coke from coal was essential to the development of steel manufacture. Coal tar constituents were used for the industrial syntheses of dyes, perfumes, explosives, flavorings, and medicines. Processes were also developed for the conversion of coal to gas and liquid fuels. Gases from coal carbonization and coke production were used for illumination as long ago as the late eighteenth century. By the 1930s direct and indirect liquefaction technologies became available for the substantial conversion of coals to liquid fuels and chemicals. Subsequently, the advent of readily available petroleum and natural gas, and the decline of the steel industry, reduced dependence on coal as a resource for the production of chemicals and materials.

For the last several decades, the availability of coal tar chemicals has depended on the production of metallurgical coke, which in turn is tied to the fortunes of the steel industry. In recent times, coke manufacture has been severely cut back, due to reduced demand for steel, which is facing competition from alternative materials, principally engineering polymers, and to improvements in steel-making technology that have reduced the amount of coke required to produce pig iron. In the US, the coke rate, or tons of coke needed to produce a ton of pig iron, has decreased from 0.75 in 1960, to 0.58 in 1978, while elsewhere rates are as low as 0.4, and new technologies completely obviate the use of coke (Song and Schobert, 1993a). In the 1970s, coal liquefaction processes seemed on the point of commercialization, and would have provided new sources of coal liquids for chemical use, as well as fulfilling the principal intended function of producing alternate fuels. Because of the low price of petroleum crude, this prospect is unlikely to come to fruition in the immediate future, due to the question of economic viability, albeit not technical feasibility. The combination of these and other factors has contributed to sharpening the focus on the use of coal for the production of heat and power, and lessening or eclipsing its possible use as a starting point for other processes. To illustrate this, in the US in 1991, approximately 80 percent of the coal produced was consumed by utilities.

However, coal tars still continue to make an important contribution to the demand for aromatic chemicals. According to Song and Schobert (1993a), metallurgical coke production in 1987 generated 15-17 million tons of coal tar and 5 million tons of benzol as by-products. The worldwide consumption of BTX is about 25 million tons and 5 million tons for two- to four-ring aromatics. Coal liquids accounted for 15-25% of the demand for BTX and about 95% of the demand for polycondensed aromatics and heterocyclics. Other important products of coal tar distillation are phenolics (creosote), feedstocks for carbon black manufacture (Donnet and others, 1993), and pitch that is used as a binder and source for materials such as carbon fibers and needle cokes.

In the US, coal is by far the largest indigenous fossil fuel resource. At the same time, petroleum imports now account for over 50 percent of total consumption, and domestic petroleum and natural gas reserves are limited. Similar situations prevail in other industrialized nations. Consequently, there is a considerable incentive to explore the expanded uses of coal, both as a fuel and as a materials source. In either case, there are also contingent needs and challenges to develop environmentally acceptable manufacturing processes.

Over the last few years, there has been a growing or revived interest in the non-fuel uses of coal, as evidenced by symposia at national meetings, and publications in scientific journals (ACS, 1992; ACS, 1993; Pitts Coal Conf., 1993; EOSS, 1993; Fuel Proc Technology Special Issue, 1993). Optimistically, one would hope that this is driven by a sense of scientific and technical relevance, rather than a new gimmick in the endless quest for research funds. There certainly appear to be some compelling reasons to re-evaluate the utility of coal as a source of non-fuel products. Research and development in Japan has provided a leading example of how this can be accomplished. The development of alternative uses for coal could lead to the diversification of resource use, and new industries. Further, the ability to utilize by-products or process streams for non-fuel applications could also assist the economics of coal utilization processes, and may lead to new materials. [In this context, it must be stressed that the higher the product selling price, the smaller the market, and the quantities of by-product streams that can be realistically utilized may be very limited.] For example, low-rank coals have long provided sources of wax and resin, obtained by solvent extraction (Kirk-Othmer, 1984). It has also been shown that paraffinic waxes, and

some naphthenic compounds, are produced during the liquefaction of subbituminous coals, and that they concentrate in the recycle distillate stream, reaching levels of 15-20 wt% or more. Their presence can adversely affect process solvent quality, while their removal by solvent dewaxing offers a method to improve process performance and recover potentially valuable by-product waxes (Derbyshire and others, 1993).

In addition to taking a new look at more traditional uses of coal products, there are a number of emerging technologies for which coal may be the most appropriate resource. Song and Schobert (1993a, 1993b) have discussed, at some length, the growth potential for high performance engineering polymers based on one- to four-ring aromatics, and that many of the aromatic monomers are not readily available from petroleum and could be derived, perhaps more easily, from coal. There is also a host of carbon-based products that can be obtained starting from coal. As can be seen in Table I, these include a high proportion of advanced materials. The connection between coal and high technology materials may serve another useful purpose in dispelling the air of antiquity that is presently associated with coal science, and elevate it to a more respected status.

This paper will address the role of coal as a resource for non-fuel products. Rather than attempt a comprehensive coverage, a few selected materials, electrode coke, activated carbons, and carbon fibers, are reviewed in terms of their production, applications, and existing and future markets.

### Electrode Coke

Graphite electrodes for arc-steel furnaces are generally manufactured from needle coke that is produced from selected petroleum feedstocks: one example is decant oils from fluid catalytic cracking. Feedstock properties such as high aromatic carbon content are important. During the process of delayed coking, it is critical to produce a mesophase coke with extended domain structures that will readily graphitize upon subsequent processing. The presence of heteroatoms, for example, can impede mesophase development through crosslinking reactions, resulting in an isotropic coke. The name needle coke arises from the acicular shape of the coke particles that reflects the anisotropic nature of the coke structure. The aromatic character of coals implies that they could present an attractive alternative source for the production of needle coke. In fact, highly aromatic coal tar pitch gives excellent needle cokes with developed anisotropy and low thermal expansion. The high coke yield from coal ~60 wt.% versus ~30% for petroleum makes the coke the principal product of the delayed coking process, although the properties of coal tar, and hence of the coke, are dependent on the coal coking conditions (Mochida and others, Carbon 1989).

### Production

During the 1970s, the British Coal Corporation (formerly the National Coal Board) developed a process to produce a suitable substitute needle coke from coal via solvent extraction (Kimber, 1981). In this process, bituminous coal is slurried with about three times its mass of anthracene oil (itself a product of coal tar distillation), and heated to 415°C for 60 min at 0.8 MPa (autogenous pressure), when approximately 70-80% of the coal (dmf) is solubilized. The mineral matter and undissolved coal are then separated by hot pressure filtration to afford a coal extract solution (filtrate) containing around 0.1% ash. The extract is then preheated to ~ 520°C and fed to a delayed coker. The coker overhead is recycled as solvent, and the coke is removed after water quenching the contents of the coker drum.

Laboratory tests showed that cokes with a wide range of properties could be produced, ranging from isotropic to anisotropic, depending on the coal precursor and extraction conditions. Consistent with the above-mentioned influence of heteroatoms on mesophase development, increasing coal rank and/or the severity of extraction were more conducive to the formation of anisotropic cokes (Kimber, 1977). The ability to control the properties of extracts through the selection of the coal and reaction parameters allows considerable latitude in the preparation of precursors for different end-products: as discussed later, the requirements for isotropic and mesophase pitch fibers are quite different.

The coal extraction process was scaled up to construct and operate a pilot plant, which was later used in a project to demonstrate the feasibility of producing quality graphite electrodes from coal. Thirty tonnes of coke were produced from a medium volatile bituminous coal, and used by Anglo Great Lakes Corporation to fabricate graphite electrodes (coal tar pitch binder) that were then tested in a 25 ton steel production furnace by British Steel Corporation (Kimber, 1981).

A comparison of the properties of these electrodes with their petroleum-based equivalents predicted poor furnace performance, based upon the criteria normally considered to be important. However, the results of working trials showed that the coal-based electrodes behaved comparably: this was mainly due to their toughness - although cracks developed relatively quickly, crack propagation was inhibited. While the demonstration project confirmed the potential of coal as a materials source for electrode manufacture, the work was not continued beyond 1979. Because of limited quantities of coke, it was not possible to optimize the steps of electrode fabrication and furnace testing, and potential clearly exists for further improvement.

Kimber and Gray (1976) also showed that there are other advantages in using coal-derived electrode coke. The evolution of heteroatoms, when carbonized coal extracts are subjected to graphitizing conditions, is quite different to that for petroleum cokes. In particular, sulfur evolution from petroleum cokes continues to elevated temperatures, when it causes expansion and cracking of the artefact (puffing). This does not occur with coal extract cokes, presumably as the organic sulfur is in a different form, leading to a stronger, denser carbon product, and eliminating the need to add iron oxide as a puffing inhibitor.

Recent work by Zondlo and others (1993) has confirmed these earlier results, showing that different graphitic products can be obtained from the same coal, depending on the conditions of extraction. Extracts obtained under hydrogenation conditions were more anisotropic than those obtained by non-hydrogenative solvent extraction. It is supposed that the former have a lower content of heteroatoms, which would reduce the propensity for crosslinking reactions upon carbonization, and allow more extensive mesophase development.

### **Markets**

The global capacity for coke production of all types in 1992 was about 21 million tons. Needle coke production in 1992 was 1.3 million tons per annum of which approximately 10% was produced from pretreated coal tar after the removal of free carbons (quinoline insoluble substances) by anti-solvent techniques. The production of anode coke for aluminum manufacture was around 10 million tons, and the remaining coke was used as fuel, where the sulfur content allowed.

The consumption of carbon in arc-steel making is about 3.5 kg per ton of steel, and the principal criteria for needle coke quality are the carbon structure, impurity content (nitrogen and sulfur), and CTE (Coefficient of Thermal Expansion). The selling price of needle coke is about \$500 per ton.

For anode coke, carbon consumption is 0.5 tons per ton of aluminum, the higher consumption because the carbon serves as a reductant. In this case, a low content of metal impurities is desired, especially of metals such as Fe, Na. The cost of anode coke corresponds to its fuel value and is around \$100 per ton.

### **Activated Carbons**

Activated carbons are materials with highly developed internal surface area and pore volume, and hence have a large capacity for adsorbing chemicals from gases or liquids. The extensive industrial use of activated carbons is related to their unique properties and low cost compared to that of possible competitive adsorbents (Baker, 1992; Derbyshire and others, 1993; Bansal and others, 1988)

Activated carbons can be synthesized from almost any carbonaceous precursor, naturally occurring or synthetic. An essential criterion is that the starting material is thermosetting, or can be so rendered during processing. Common commercial feedstocks are biomass materials such as wood, coconutshell, and nut kernels, and degraded or coalified plant matter - peat, lignite, and all ranks of coal. The properties of activated carbons can be very diverse. While they are influenced to some extent by the process route and conditions, they are predominantly determined by the precursor structure. Generally, microporous carbons (pore diameter <2 nm) are synthesised from high rank coals, or coconutshell precursors. Carbons with larger pore sizes (mesopores with 2nm <d <50nm) are synthesised from wood, peat, lignite and lower rank coals. In 1988, coals accounted for almost 30% of the raw materials for activated carbon manufacture, lignite 14%, peat, 10%, with wood at 35% and coconut shell, 10% (Bansal and others, 1988).

### **Production**

Activated carbons are produced in the form of powders, granules, and shaped products (pellets and extrudates). Activated carbons have also been produced in fibrous form from cellulose (Audley, 1989) and pitch (see later section). There are two main routes for the synthesis of activated carbons, thermal activation or chemical activation. Thermal activation is a two-step process where the precursor is first carbonized in an inert atmosphere at temperatures from 500-700°C to produce a low surface area char. Subsequent controlled gasification or activation at 800-1000°C in steam or CO<sub>2</sub> greatly increases the pore volume and surface area, through volatile loss and carbon burn-off. Coconut shell, anthracite, and certain woods can be carbonized in granular form to produce hard carbons. Precursors that tend to form soft carbons must be reconstituted at some stage using a binder if strong shaped carbons are required. Bituminous coals are first pulverized and then reconstituted by briquetting under pressure, optionally with added binder. Thermoplasticity is eliminated by the promotion of crosslinking reactions, either by air oxidation, or the use of additives.

Chemical activation is normally used for lignocellulosic precursors, and consists of mixing the precursor with a chemical reagent such as H<sub>3</sub>PO<sub>4</sub> or ZnCl<sub>2</sub> and heat treating in a single stage at

temperatures between 400-700°C. The reagent is then recovered in a leaching step to recover the reagent for recycle. Porosity is developed as a consequence of dehydration reactions occurring at low temperatures. Recent studies of the phosphoric acid activation of hardwood have revealed that reaction with the acid first causes shrinkage at temperatures around 150°C, which is attributed to the promotion of dehydration reactions, and there then follows a dilation of the structure, corresponding to the development of porosity (Jagtoyen and Derbyshire, 1993).

A different chemical activation process has been developed that uses KOH to produce exceptionally high surface area carbons from precursors such as bituminous coals and petroleum coke (Wennerberg and Grady, 1978; Jagtoyen and others, 1993). Activation with KOH can also be used to produce high surface area, hard extruded carbons from low-rank coals (Guy and others, 1989) or preoxidized bituminous coals (Verheyen and others, 1993). The chemical activation of viscose with Lewis acids (e.g. aluminum chloride, ferric chloride or zinc chloride) has been used to produce activates in the form of fibers or cloth (Baker, 1992).

### **Applications**

Activated carbons are used in both liquid and gas phase applications for purification, environmental applications, chemical recovery, and catalysis. Liquid phase applications require carbons with a higher proportion of wide pores (macro- and mesoporosity) than gas phase applications, in order to reduce diffusional restrictions on the adsorption of impurities. The presence of wide pores (mesopores) also allows adsorption of large molecules such as color bodies and humic acids. Liquid phase carbons are used in both powder (typically 15 - 25 µm) and granular or shaped (0.3 - 3.0 mm) forms. Powdered carbons are normally used on a once-through basis. Their advantage over larger particles is their lower diffusional resistance to adsorption. Granular or shaped carbons are more desirable for continuous or cyclic processes, and can be removed for regeneration.

In 1987, liquid phase applications accounted for about 80% of the total activated carbon use in the USA (Goin and others, 1989). The principal uses are in potable water treatment (24%), industrial waste water treatment (17%), and the removal of color from sugars and foods (21%). Other applications include the refining of foods, beverages and cooking oils, gold recovery from low-grade ores, medical applications such as the recovery of antibiotics, vitamins and steroids from fermentation broths, the removal of blood toxins, and as catalyst supports (Goin and others, 1989, The Economics of Activated Carbon, 1990, Hassler, 1974).

Activated carbons for gas phase applications are mostly microporous and usually in a shaped or granular form. They are used for solvent recovery (26%), gasoline emission control in Evaporative Loss Control Devices (24%), air purification to remove toxic constituents and odors (18%), gas separation by pressure swing adsorption (6%), and catalysis (16%). [Percentages are figures for the USA in 1990, Chemical Economics Handbook, 1993]

### **Market**

The world annual production of activated carbons was estimated to be in the region of 375,000 tonnes in 1990 (Baker, 1992), excluding Eastern Europe and China. About 55% of production is in powder form, 35% as granules, and the remainder as shaped carbons. The highest production capacity is in the US (40%), followed by Western Europe (30%), and Japan (20%).

The approximate selling price for granular or shaped carbons is in the region of \$4.50 - 5.50/kg, while for powdered carbons it is closer to \$2.00/kg. The actual price depends upon the adsorption capacity (typical surface areas fall in the range 800 to 1500 m<sup>2</sup>g<sup>-1</sup>), hardness, and whether impregnants have been added to enhance performance. Speciality carbons can be much more expensive.

Consumption is increasing by about 5 - 7% per year (Baker, 1992, Irving-Monshaw, 1990). Growth will be primarily in areas affected by environmental regulations for the improvement of air and water quality.

### **Isotropic and Mesophase Pitch-Based Carbon Fibers**

Carbon fibers can be divided into four main types based upon polymers, rayon and polyacrylonitrile (PAN), upon pitch, or are vapor-grown, Singer (1992). The focus here is on fibers that can be produced from pitch: petroleum and coal tar pitches are used industrially (Okuda, 1982; Matsumura, 1987; Thwaites, 1992). Fibers have also been produced from coal extracts (Jorro and Ladner, 1974), and recent work has shown that continuous filaments of isotropic carbon fibers and activated carbon fibers can be produced from coal liquefaction products (Fei and others, 1993). Appropriate precursor materials could be produced from coal by several methods: solvent extraction; carbonization; hydrolysis; and coal liquefaction. Pitch-derived fibers can be divided into those produced from isotropic precursors, and those derived from pitch that has been pretreated to introduce a high concentration of carbonaceous mesophase. The former are low-

performance, general purpose fibers while the latter are high performance products that can be produced with high tensile strength and very high modulus. An extensive discussion of the synthesis and applications of isotropic pitch-based and mesophase pitch-based carbon fibers has been given by Edie (1990).

### **Production**

The steps involved in the synthesis of both types of fibers are illustrated in Figure 1. In each case, care must be taken in the selection and preparation of the starting material, although the requirements are quite different, and the pretreatment required to produce mesophase fibers is much more extensive. Accurate control of process conditions is also critical to the production of isotropic and mesophase fibers. However, the end-uses of isotropic fibers also allow them to be produced by melt-blowing, which produces short blown fibers and is relatively inexpensive, while the applications of high performance fibers necessitate the production of continuous filaments.

Whether produced from mesophase or isotropic pitch, the as-formed, "green" fibers require to be stabilized to render them thermosetting before carbonization. Stabilization is normally accomplished by air oxidation, although other methods may be used (Otani, 1971). Oxidation must be initiated at temperatures below the softening point of the fibers. As this temperature is lower for isotropic fibers than mesophase fibers, the process of oxidative stabilization is much slower in the former case.

For the development of tensile strength, the fibers are carbonized at temperatures up to 1700°C, or graphitized by heat treatment at temperatures approaching 3000°C. The final fiber properties are determined by the degree of orientation of layer planes along the fiber axis, and the size and perfection of individual crystallites. The lack of orientation in the structure of isotropic fibers causes their modulus to be about 1/20 of that of mesophase fibers, while their tensile strength is around 1/3. While there is little improvement in the properties of isotropic fibers on graphitization, graphitized mesophase fibers develop very high modulus. Compared to carbonized or graphitized PAN fibers, they have higher modulus and lower tensile strength, giving advantages in applications requiring high stiffness, high electrical and thermal conductivity, low thermal expansion, and high temperature oxidation resistance, while the former are employed where high strength is required.

### **Applications**

The costs of PAN, isotropic pitch and mesophase pitch fibers are in the region of \$60, \$22, and \$90 per kg. The low precursor cost, lower processing costs and higher carbon yields contribute to isotropic pitch fibers being much cheaper than PAN fibers. For mesophase fibers, the additional step of mesophase formation, and higher complexity of other processing steps result in a much higher fiber price.

Low cost makes isotropic pitch fibers attractive for applications where high tensile strength or stiffness are not required. Examples include: enhancing the properties of composite friction materials for brake pads and clutches; the reinforcement of engineering plastics; ablation and thermal insulating materials; electrically conductive fillers for polymers; filter media; paper and panels; the production of hybrid yarns with other fibers; reinforcing concrete to improve flexural strength and other properties (Okuda, 1992; Soroushian and others, 1991); and as potential replacements for asbestos.

Because of their high modulus, mesophase fibers are used in aerospace structures, and the very high thermal conductivity of more recently developed fibers has opened applications for heat dissipation in areas such as high speed machinery, aircraft structures, and electronics. The cost of some of these specialized, ultra high performance fibers can be many hundreds of dollars per kg. Even for the lower cost products, their use is only readily justified in military and commercial aircraft applications and aerospace, where they can be used in materials that have performance characteristics unobtainable elsewhere. Reductions in the cost of mesophase fibers would substantially expand their applications into areas such as automotive structures.

### **Market**

The worldwide production of all types of carbon fiber is in the region of 9000 tonnes (1993). The largest growth is in general purpose fibers which accounted for about 2500 tonnes in 1992, representing a threefold increase since 1989: projections for 1994 are over 5000 tonnes, and by the year 2000, one estimate predicts 40,000 tonnes.

In 1989-90, approximately 25% of pitch-based fibers were produced from coal tar pitch, and the remainder from petroleum pitch. At that time, the production capacity for mesophase pitch fibers was 800 tonnes, about 65% from coal tar pitch and 35% from petroleum pitch.

## Activated Carbon Fibers from Pitch

In recent years, interest has developed in the activated forms of isotropic carbon fibers, where high surface areas can be produced by partial gasification in steam or other oxidizing gas (Thwaites and others, 1993, Suzuki, 1993). Carbon fibers have only been commercially available since the 1960s, and the development of activated carbon fibers has been a direct consequence of this technology.

Activated carbon fibers have novel properties that make them more attractive than other, more conventional forms (powder or large-size carbons) for certain applications (Suzuki, 1993). While porosity could be generated in most types of carbon fiber, low-modulus, isotropic pitch fibers are particularly well-suited for activation due to their unique structure in which the random packing of small crystallites allows the development of an extensive pore structure. A growing and completely different array of applications exists for the activated forms of isotropic carbon fibers (Suzuki, 1993; Mochida and others, 1991 and 1992; Foster and others, 1992; Economy and others, 1992).

High surface areas can be produced and most commercially produced fibers are microporous (< 2nm diameter pores). The narrow fiber diameter essentially eliminates mass transfer limitations, and adsorption and desorption rates are very rapid, roughly two orders of magnitude higher than for granular carbons. The fibrous form facilitates incorporation into woven and non-woven fabrics, felt, paper, and specific formed shapes. Among the possible applications, activated carbon fibers are of interest for the adsorption and recovery of organic vapors (Suzuki, 1993, Foster and others, 1992), removal of SO<sub>x</sub> and NO<sub>x</sub> from flue gas (Mochida and others, 1991, 1992), and for water treatment (Suzuki, 1991).

Despite the singular attributes of carbon fibers and activated carbon fibers from isotropic pitches, the potential of these materials has not yet been realized: in 1992, only 200 tons were produced in Japan (Suzuki, 1993). One reason is that production costs are still too high to attract widespread use and hence economies of scale. Lowering production costs through technological advances would help to reverse this situation, increasing the volume of sales and providing the incentive for larger scale production which would, in turn, effect further economies - a pattern that has already been realized for high performance carbon fibers. The high material costs and low yield for polymer derived fibers makes pitch a viable alternative with greater potential for reducing processing costs.

## Literature

American Chemical Society (1992), Preprints Fuel Science Division, "Symposium on High Value Materials from Fossil Fuels", San Francisco, CA, April 5-10, 37, No. 2, p. 497-619.

American Chemical Society (1993), Preprints Fuel Science Division, "Symposium on Alternate Uses for Fossil Fuels", Denver, CO, March 28-April 4, 38, No. 2, p.400-468.

Audley, G. J.(1989), European Patent 0312 395 A2.

Baker, F. S. (1992), Kirk-Othmer Encyclopedia of Chemical Technology, John Wiley & Sons, Inc., 4th. Ed., 4.

Bansal, R. C., Donnet, J. B. and Stoekli, F. (1988), Active Carbon, Marcel Dekker, New York.

Chemical Economics Handbook (1993)-SRI International, Menlo Park, Calif.

Derbyshire, F., Jagtoyen, M. and Thwaites, M. (1993), Active Carbons-Production and Applications, in book to be published by Butterworths.

Donnet, J. B., Bansal, R. C. and Wang, M. J. (1993), Carbon Black, Second Edition, Marcel Dekker, Inc.

Economy, J., Foster, K., Andreopoulos, A., and Jung, H. (1992), Chemtech, October, 597-603.

Edie, D. D.(1990), Carbon Fibers Filaments and Composites, Kluwer Academic Publishers, Netherlands, p. 43-72.

Eastern Oil Shale Symposium (1993), Papers presented in "Symposium on New Products and Uses of Oil Shales and Oil Sands", Lexington, KY, Nov. 17-19, 1993.

Fei, Y. Q., Derbyshire, F., Jagtoyen, M. and Mochida, I.(1993), Paper presented at 1993 Eastern Oil Shale Symposium, Lexington, KY, Nov. 17-19.

Foster, K. L., Fuerman, R. G., Economy, J., Larson, S. M., and Rood, M. J.(1992.),

Chem. Mater., 4, p.1068-1073.

Fuel Processing Technology (1993), Special Issue: High Value Materials from Coal, 34 (2).

Goin, J., von Schuller-Goetzburg, V. and Sakuma, Y.(1989), Chemical Economics Handbook-SRI International, Menlo Park, Calif.

Guy, P.J. , Verheyen, T. V. , Heng, S., Felber, M. D. and Perry, G. J.(1989), Proc. Int. Conf. Coal. Sci., p. 23.

Hassler, J. W.(1974), in Purification with Activated Carbon, 3rd. ed., Chemical Publishing Company, Inc., New York, p. 353.

Irving-Monshaw, S.(1990), Chemical Engineering, Feb., p. 43.

Jagtoyen, M. and Derbyshire, F. J. (1993),Carbon, 31(7), p.1185.

Jagtoyen, M., Toles, C. and Derbyshire, F.( 1993), Preprints Fuel Science Division, ACS meetingDenver, CO, March 28 - April 4, 38, No.2, p. 400.

Jorro, M. A. A. and Ladner, W.R.(1974), Proc., 4th Int. Carbon-Graphite Conference, London, Sept, p. 287-303.

Kimber, G. M. , Brown, A. and Kirk, J. N.(1981), High Temperatures-High Pressures, 13, p. 133-137.

Kimber, G. M., Proceedings 13th Carbon Conference, Irvine, CA, 1977.

Kimber, G. M. and Gray, M. D. (1976), in Petroleum Derived Carbons, 31, p. 444-450.

Kirk-Othmer (1984), Encyclopedia of Chemical Technology, John Wiley & Sons.,3rd. ed, 24, p. 472.

Matsumura, Y.(1987), Seikiyu Gakaishi, 30(5), p. 291.

Mochida, I., Hirayama, T., Kisamori, S., Kawano, S., and Fijitsu, H.( 1992), Langmuir, 8 (9), p. 2290-94.

Mochida, I., Sun, Y-N., Fijitsu, H., Kisamori, S., and Kawano, S. (1991), Nippon Kagaku Kaishi (J.Chemical Society of Japan), 6, p. 885-890.

Mochida, I., Fei, Y.Q., Korai, Y. and Fujimoto, K.(1989), Carbon, 27 (3), p. 375.

Otani, S. (1971), U.S. Patent # 3,629,379.

Okuda, K.(1992), TANSO, 155, p. 426.

Okuda, K.( 1982), Petrotech, 5(1), p. 37.

Pittsburgh Coal Conference (1993), Session on "Non-Fuel Use of Coal", Proceedings, September 20-24, p. 379-416.

Singer, L. S.(1992), Proc. Eighth Annual Conference on Materials Technology: Structural Carbons, Sept. 1-2, 1992, Southern Illinois University at Carbondale, Carbondale, IL 2901, USA, p. 3-32.

Song, C. and Schobert, H.H (1993a), Fuel Processing Technology, 34, p. 157-196.

Song, C. and Schobert, H.H (1993b), Proceedings, 10th Internatl. Pittsburgh Coal Conference, September 20-24, p. 384.

Soroshian, P., Aouadi, F. and Nagi, M.(1991), ACI Materials Journal, 88, No. 1, p. 11-18.

Suzuki, M.(1993.), Proc. 21st Biennial Carbon Conference, Buffalo, June 13 to 18.

Suzuki, M.(1991), Water Science technology, 23, p. 1649.

The Economics of Activated Carbon (1990), 3rd. Ed., Roskill Information Services Ltd., London, p.8,9.

Thwaites, M.W., Stewart, M. L., McNeese, B. E., and Sumner, M. B.( 1993), Fuel Proc. Tech., 34, p. 137-145.

Verheyen, V., Rathbone, R., Jagtoyen, M. and Derbyshire, F. (1993), paper submitted to Carbon.

Wennerberg, A. N, Grady, T. M.(1978), United States Patent 4 082 694 .

Zondlo, J., Stansberry, P. and Stiller, A.(1993), Proceedings, 10th Pittsburgh Coal Conference, September 20-24, p. 379.

**Table 1: Carbon materials based on coal-derived feedstocks (adapted from Song and Schobert, 1993a)**

- |  |  |
|--|--|
| <ul style="list-style-type: none"><li>* Pitch-based carbon fibers</li><li>* Mesophase-based carbon fibers</li><li>* Carbon fiber reinforced plastic</li><li>* Carbon whiskers or filament</li><li>* Graphite and graphite-based materials</li><li>* Electrodes</li><li>* Composite materials</li><li>* Molecular sieving carbons</li><li>* Mesocarbon microbeads</li></ul> | <ul style="list-style-type: none"><li>* Activated carbons</li><li>* Activated carbon fibers</li><li>* Metallurgical cokes</li><li>* Carbon blacks</li><li>* Intercalation materials</li><li>* Elastic carbons</li><li>* Fullerenes or "bucky-balls"</li><li>* Diamond-like films</li></ul> |
|--|--|

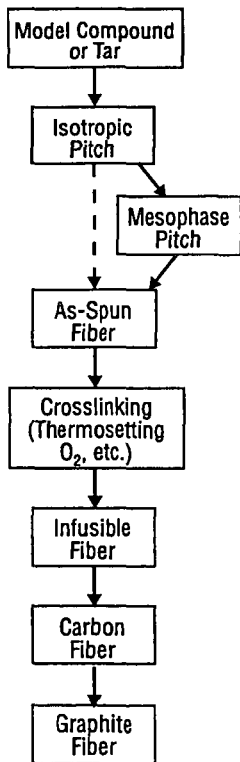


**Figure 1: Preparation of isotropic and mesophase pitch carbon fibers**